J. Bruce Gemell

Studies of VHMS-related alteration: geochemical and mineralogical vectors to ore

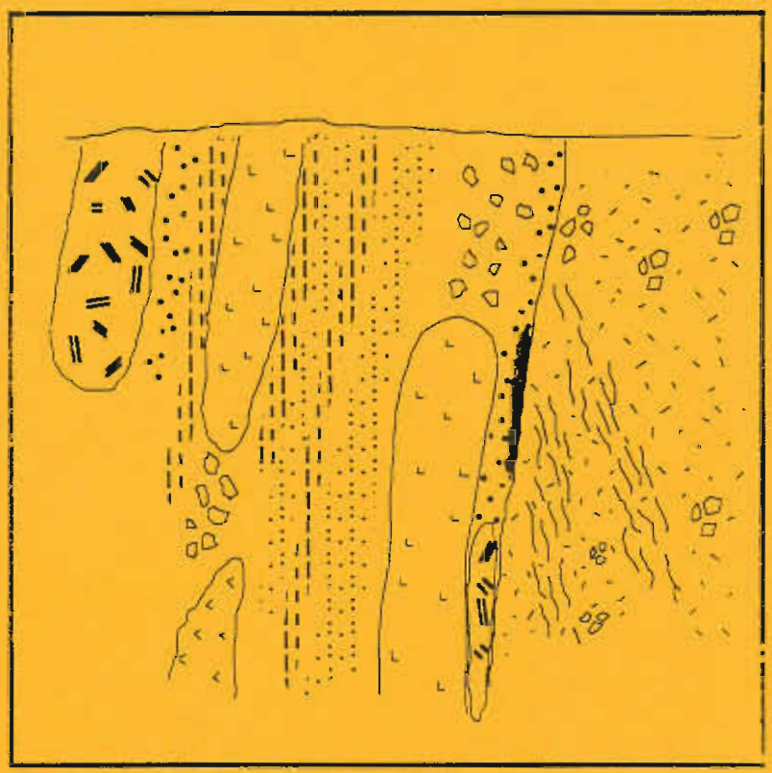

AMIRA/ARC project P439

Report 2
May 1996

Centre for Ore Deposit and Exploration Studies
University of Tasmania

Studies of VHMS-related alteration: geochemical and mineralogical vectors to ore

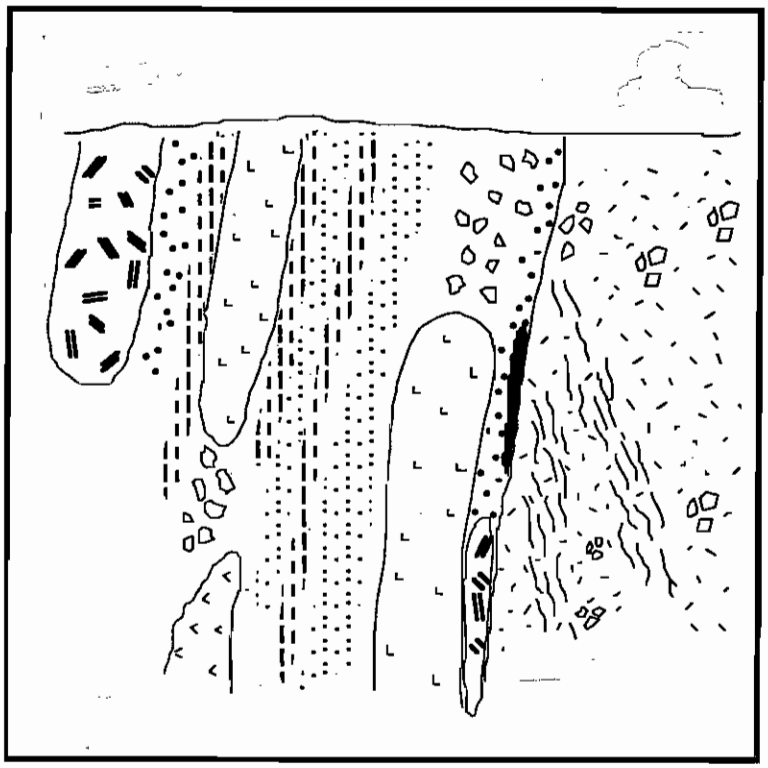

AMIRA/ARC project P439

Report 2
May 1996

Centre for Ore Deposit and Exploration Studies
University of Tasmania

Contents

Structure and management of the project

INTRODUCTION

Volcanic-hosted massive sulphide deposits (VHMS) provide a significant contribution to the total zinc, copper, lead, silver and gold production in Australia and continue to be a major target for most base metal explorers. However, due to the geological complexity of ancient submarine volcanic terrains, new VHMS deposits are becoming extremely difficult to discover, especially deposits that are buried more than a few tens of metres below the surface. To complement the conventional multidisciplinary approach utilising geology, geophysics and geochemistry, a new attack to the problem is proposed here which involves the integration of volcanic facies analysis with alteration geochemical and mineral chemical studies to develop a set of vectors to guide explorers toward ore-grade mineralisation. The research will concentrate on three productive submarine volcanic belts in Australia: the Mount Read Volcanics (MRV) in western Tasmania, the Mount Windsor Volcanics (MWV) in northern Queensland, and the Archean Murchison volcanic province in western Australia.

PROJECT OBJECTIVES

1. To characterise the mineralogy and geochemistry for the various styles of hydrothermal alteration throughout the Mount Read Volcanics (MRV) and the Mount Windsor Volcanics (MWV). This will be based on mapping supported by whole-rock and trace element geochemistry, mineral chemistry, REE and stable isotope geochemistry.

2. To determine the relationship between geochemical alteration patterns and sub-volcanic intrusions that are coeval with VHMS formation.

3. To undertake case studies of alteration halos related to specific VHMS deposits with particular emphasis on hangingwall alteration, and the relationship between alteration patterns and volcanic facies.

4. To develop a set of vectors towards ore, based on the regional studies and ore deposit specific studies, that can be applied in the exploration for VHMS deposits in submarine volcanic sequences throughout Australia. The vector matrix will include whole-rock, trace element, mineral chemistry, REE, isotope and volcanic facies factors.

RESEARCH FRAMEWORK

As there has been considerable research on alteration mineralogy and geochemistry of VHMS systems, our research is not to repeat previous work but to break new ground, utilising a multi-disciplinary approach at both the regional volcanic belt scale and selected ore deposit scale, with emphasis on selective geochemical techniques.

The project consists of three research modules as outlined on page vi.

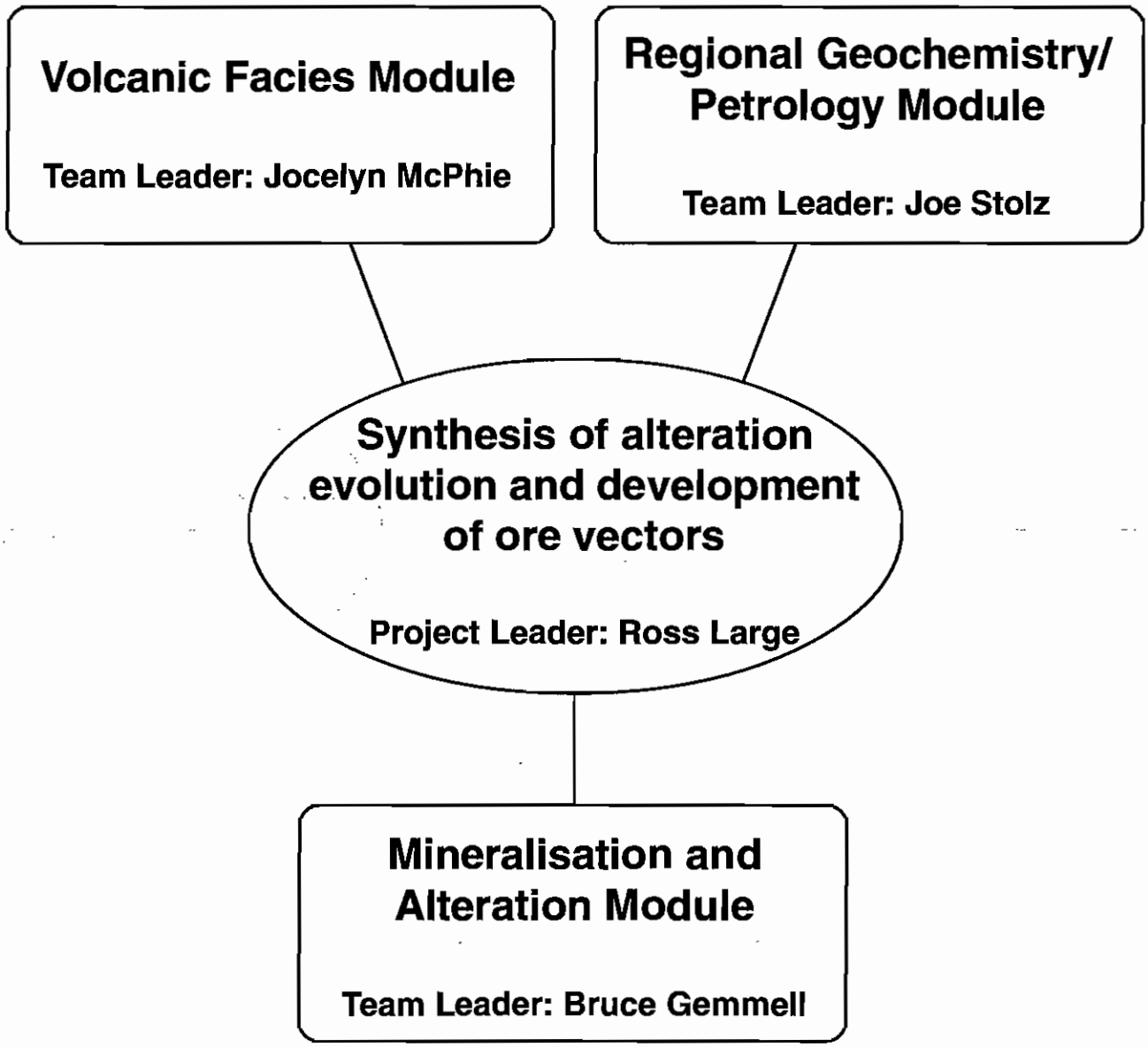
Volcanic Facies Module
Team Leader: Jocelyn McPhie
Regional Geochemistry/ Petrology Module
Team Leader: Joe Stolz
Synthesis of alteration evolution and development of ore vectors
Project Leader: Ross Large
Mineralisation and Alteration Module
Team Leader: Bruce Gemmell

THIS REPORT

This is the second major report on the project, coming twelve months after the commencement of the project in May 1995. Major advances over the last six months have occurred in the following areas:

Regional volcanic facies, alteration and geochemistry in the MRV

Mapping and sample collection took place along three major east-west traverses selected to provide exposure to a range of volcanic facies and alteration styles:

- Mt Black to Murchison Gorge
- Halls Rivulet Canal – Hercules–Red Hills–Anthony Dam
- Jukes Road across CVC and EQP sequences

Reports on the preliminary results are given for each traverse. Detailed petrography, alteration mineralogy, geochemistry and volcanic facies analysis will proceed over the next six months. This data will form an important base line for the MRV database.

Ore deposit case studies

Progress reports for the case studies at Hellyer, Rosebery, Thalanga and Gossan Hill are presented in this report. All these studies are at an early stage of development and represent MSc and PhD research by three students, supported by Bruce Gemmell, Rod Allen and Jocelyn McPhie.

Geochemical database for MRV

The MRV database is partially completed, and a preliminary assessment of the primary geochemistry and alteration geochemistry are presented. A series of alteration vectors are presented and discussed, however, considerably more research is required to refine these vectors by including the regional traverses and ore deposit case studies into the database.

ACKNOWLEDGMENTS

We wish to acknowledge the support of the companies who have provided access to their deposits and exploration areas for the purposes of this project.

Ross R. Large
Director

Summaries

Mount Black to the Murchison Gorge: Preliminary volcanic facies analysis and alteration styles—C.C. Gifkins, R.L. Allen, A.J. Stolz and N. Duhig

During this traverse across the northern Mount Read Volcanics outcrops of the Mount Black Volcanics, Sterling Valley Volcanics, Farrell Slates, Murchison Volcanics and the Murchison Granite were examined. The aim was to determine the primary volcanic facies, the alteration stages, primary and secondary controls on the alteration and to eventually identify the alteration processes which have modified the rocks. The transect is bisected by the major Henty Fault across which no units could be correlated.

To the west of the Henty Fault are the Sterling Valley Volcanics and the Mount Black Volcanics. The Sterling Valley Volcanics are a thick sequence of monomictic and polymictic dacitic to basaltic mass-flow breccias and dacitic to basaltic lavas and sills. Conformably overlying these to the west is the Mount Black Volcanics. The Mount Black Volcanics are a package of feldspar-phyric massive, flowbanded and flow brecciated lavas and sills of generally dacitic composition with minor volcaniclastic sediments.

To the east of the Henty Fault are the Murchison Volcanics. The Murchison Volcanics comprise of a pile of quartz-phyric rhyolitic lava domes and sills which have been emplaced into pyroclastic deposits of a similar composition. These deposits have been invaded by a swarm of rhyolite porphyry sills and the Murchison Granite towards the eastern margin. Unconformably overlying the Murchison Volcanics are the Farrell Slates. They are an interbedded package of grey to black siltstones with abundant interbedded feldspar-quartz-mica sandstone turbidites and towards the base interbedded thick pumiceous to crystal-rich rhyolitic mass-flow units which probably represent waning stages of the silicic eruption of the Murchison Volcanics.

All the units have been variably modified and the complex alteration patterns reflect primary and secondary porosity, compositional contrasts in the rocks and the combined effects of different alteration stages. The most common alteration stages within the volcanics were; silicification, domainal quartz-feldspar, domainal sericite-chlorite and sericite-quartz-chlorite, weak fine grained disseminated sericite±quartz, fine grained disseminated carbonate, and patchy, selective and pervasive chlorite alteration. Alteration within and adjacent to the Murchison Granite was dominated by K-feldspar–chlorite alteration and this was surrounded by an alteration halo of feldspar–chlorite–epidote and sericite–chlorite alteration. Overprinting alteration stages have produced a variety of pseudoclastic and apparently polymict textures in both the coherent and clastic units.

Hall Rivulet Canal–Hercules–Mount Read–Red Hills–Anthony Dam—Jocelyn McPhie

1. Along Hall Rivulet Canal, the White Spur Formation and Central Volcanic Complex are conformable, although alteration is more intense in the CVC than in the White Spur Formation.

2. The Mount Black Volcanics and Red Hills Volcanics are dominated by coherent lithofacies in contrast to the White Spur Formation, Hercules footwall and Hercules hangingwall, all of which include both volcaniclastic and non-volcanic sedimentary lithofacies.

3. Conglomerate in the Tyndall Group at Anthony Dam contains abundant Cambrian granitoid and hematite clasts. The granitoid clasts are texturally dissimilar from the nearby Murchison Granite.

4. An unconformity between the Tyndall Group and the Owen Conglomerate is exposed at Anthony Dam.

5. A strongly deformed metasedimentary block that could be Precambrian basement occurs near the Anthony Dam.

Jukes Road: Preliminary volcanic facies analysis and alteration petrography—Bill Wyman, Rod Allen and Nathan Duhig

Preliminary textural and mineralogical data support paragenetic and geochemical relationships about both regional and hydrothermal alteration styles. Research to date suggests that hydrothermal mineral assemblages can be distinguished from regional assemblages. Hydrothermal mineral assemblages identified along the Jukes Rd. include: sericite, K-feldspar, chlorite (2 phases), silica, and carbonate. Of the five styles, sericite, chlorite and K-feldspar are the most common and most easily identified. Carbonate and silica alteration are minor. Regional alteration styles identified include sericite, chlorite and possibly K-feldspar or albite.

A system for characterising alteration in the field was required prior to the start of detailed field work. Reviews of alteration literature and discussions with various industry geologists led to the system used and presented. The system is based on the application of an arbitrary scale for alteration from 1 to 10, with 1 being the least and 10 being the most altered. The scale also includes a scale for textural destruction(TD). Degrees of textural destruction are critical in correctly characterising alteration.

Volcanic facies along the Jukes Rd are described. The two dominant volcanic facies in the CVC are a thick columnar jointed feldspar phyric rhyolite and a thick sequence of volcaniclastic and mass flow deposits. Sedimentary facies are minor. The columnar jointed rhyolite is the host rock for the Jukes Prospect and its associated hydrothermal alteration and mineralisation.

Report 1: Exhalite geochemistry. A preliminary geochemical documentation of two barren ferruginous chert bodies in the Mount Windsor Volcanics—G.J. Davidson, A.J. Stolz & S.M. Eggins

Previously obtained geochemistry from two barren ironstones in the Mount Windsor Volcanic Belt is the starting point for defining geochemical changes in ironstone approaching massive sulphide deposits. Broad features of the data set are described here, including spatial trends in REE, variation in Fe/Si ratio, and consistent differences in Ti/Zr between the hostrock and overlying chemical sediment.

Mineral chemistry of the hangingwall alteration zone at the Hellyer mine, western Tasmania—Russell Fulton

The purpose of this project is to study the mineral chemistry of the hangingwall alteration at the Hellyer mine. The primary focus is to attempt to discriminate between the mineralogy and mineral chemistry related to Cambrian hydrothermal alteration and the mineralogy and mineral chemistry related to Devonian regional metamorphism. Later, the inter-relationship between mineral chemistry and whole rock geochemistry of the hangingwall will also be considered. No study of the alteration mineralogy of the hangingwall has previously been undertaken apart from a small amount of work which formed part of a MSc project (Jack, 1989).

At this stage enough research has been undertaken to indicate that there is substantial preservation of primary hydrothermal alteration features in the hangingwall alteration at Hellyer. Two distinct chlorite chemistries are apparent, and unusual chromian chlorites with up to 1.9 wt% Cr_2O_3 have been analysed. Only one fuchsite has been analysed, however not many good analyses of white mica have been obtained at this stage. The majority of feldspars analysed have been albites. There is a wide variation in the texture and chemistry of carbonates providing scope for more detailed work.

Rosebery alteration study—Rodney Allen, Nathan Duhig and Ross Large

The Rosebery site study was started up in February. The aims of the project are to determine the distribution, physical character, timing relationships and geochemistry of carbonate alteration around A-B lens and K lens at Rosebery Mine. The alteration, and geological context of the alteration, will be studied in the footwall, hangingwall, ore zone and along strike in order to interpret physical, geochemical and isotopic vectors to ore. Whole rock and selected trace element geochemistry and mineral chemistry will also be studied in order to relate trends in the carbonate alteration to whole rock trends. The AB-K lens area of the mine was chosen because it is the simplest to study (least deformation and Devonian granite-related hydrothermal overprint), sufficient drill core is available, and the area is of special interest to the Rosebery mine staff because the area is currently being developed for mining and further exploration.

The first seven drill holes in a proposed progragm of 22 holes was logged for volcanic facies, alteration and mineralisation. One hundred and seventy-nine samples were collected for petrography and geochemical analysis. At least two generations and several styles of carbonate alteration were recognised in the drill core. The relationship between carbonate and sericite/chlorite alteration is discussed in terms of diagenesis, ore formation and deformation.

The Darwin Granite-Slate Spur area: Geology, volcanic facies analysis and alteration petrography—Bill Wyman

The Darwin granite is a highly fractionated granite of the magnetite series. A well documented close association exists between magnetite series granites and Cu-Au mineralisation. Alteration assemblages, in and around the Darwin granite, resemble alteration assemblages found in other granite related hydrothermal systems throughout the world. Alteration assemblages are dominated by K-feldspar, chlorite, silica and sericite in various combinations and intensities. Accessory minerals include pyrite, magnetite, tourmaline, barite and chalcopyrite. Alteration assemblages appear to be most intense and widespread in the cupola region of the granite, and appear to drop off rapidly along the sides. Mineralisation and alteration appear to be related to the late stage intrusion of the white equagranular granite and the porphyritic white granite phase. Magnetite and tourmaline veining also appears to be related to this phase of granitic intrusion. Hydrofracturing of the cupola region, above the granite, resulted in emplacement of the alteration assemblages, veins and mineralisation.

Volcanic facies relationships and hydrothermal modification of primary volcanic textures, Thalanga—Anthea P. Hill

The abundance of coherent volcanics and their associated volcaniclastic facies underlying and overlying the Thalanga massive sulphide deposit, and absence of coherent units in the hangingwall along strike (~500 m west), is interpreted as evidence that the massive sulphide lenses are located within a volcanic centre. Crystal-rich, polymict breccias, containing distinctive large, blue quartz crystals (known as the quartz 'eye' volcaniclastic unit: QEV), are concentrated within the ore horizon where they overly and are partly replaced by sulphides. The abundant quartz and feldspar crystals in the QEV could have been liberated by either explosive eruption or intense quench fragmentation of a highly porphyritic magma. The site of eruption of the crystal-rich component is not known, but was probably not in the immediate vicinity of Thalanga. However, the quartz-feldspar porphyry clasts within the polymict breccia are interpreted to be part of the peperitic margins of syn-volcanic quartz-feldspar porphyry sills that are present within the ore horizon in East Thalanga.

At Thalanga, the rhyolitic footwall is composed of variably quartz ± sericite ± chlorite ± pyrite altered, perlitic feldspar-quartz phyric rhyolite, with volcaniclastic facies common in western and eastern parts of the deposit. Feldspar phenocrysts are destroyed and the perlitic fractures are replaced by sericite in the most altered parts of the rhyolite underlying the massive sulphide deposit. Such intense hydrothermal alteration results in kernels of recrystallised quartz isolated in pervasive sericite.

Facies architecture, alteration and metamorphism of the volcanic host rock sequence at the Thalanga massive sulphide deposit, north Queensland, Australia—Holger Paulick

This project combines volcanological, geochemical and petrological studies on the host rock sequence of the Ordovician VHMS deposit at Thalanga (north Queensland). The volcano-sedimentary host rocks experienced variable degrees of hydrothermal alteration associated with base metal mineralisation and subsequently upper greenschist facies metamorphism. In order to investigate the relationships between volcanic facies and alteration facies mineralised and strongly altered cross sections through the Thalanga host rock sequence will be compared with unmineralised and less altered cross sections. This comparison may reveal vectors to mineralisation in terms of volcanic facies association, metamorphic mineral assemblages, mineral phase composition or oxygen isotope content.

Field work commenced in June 1996, and 18 diamond drill holes selected from three cross sections through the western part of the deposit have been examined. The ore hosting favourable horizon is sandwiched between rhyolitic volcanics in the footwall (Mount Windsor Formation) and a volcano-sedimentary succession in the hangingwall dominated by coherent dacites and dacitic volcaniclastic deposits (Trooper Creek Formation). Occurrences of quartz-feldspar crystal-rich sandstones and coarse, quartz-rich rhyolite in the hangingwall may be important for exploration targeting as similar rock types from the favourable horizon have been interpreted to be genetically related with mineralisation. However, Ti/Zr ratios of coarse, quartz-rich rhyolite from the hanging wall and the favourable horizon are very distinct, suggesting that these are petrogenetically unrelated.

Five alteration types have been defined (phyllosilicate-rich assemblages, 'white silica flooding', green staining (epidote alteration), red staining (albite? alteration) and carbonate-calcsilicate assemblages) and their distribution in the footwall rhyolites and hangingwall dacites has been studied. Compositional differences between phyllosilicate-rich assemblages and white silica alteration in the footwall rhyolites suggest that silica enrichment is an independent process and not related to the loss of sodium and increase in iron and sulphur which characterises zones of intense footwall alteration at Thalanga.

Gossan Hill alteration: Styles and distribution—Robina Sharpe

The Gossan Hill deposit is a Cu-Zn VHMS deposit of Archean age. Mineralisation straddles three stratigraphic members of the Golden Grove Formation. Cu-rich pyrite–magnetite mineralisation has the form of an anastomosing stringer zone and is hosted by the GG4 Member. Massive sphalerite–pyrite mineralisation is hosted by the GG6 Member. Separating the two mineralised zones is the GG5 Member which is unmineralised. Alteration enveloping mineralised zones show intense development with a stratabound alteration zonation developed. Quartz crystal-rich sandstones of the GG4 Member are ubiquitously chlorite altered and thinly bedded siltstones and sandstones of the GG6 Member are intensely silicified. Strong lithological controls on the spatial distribution of hydrothermal alteration are indicated.

Alteration textural styles include, silica alteration, chlorite alteration, carbonate nodular alteration, silica nodular alteration and andalusite-chloritoid alteration. Textural alteration styles are variably developed within specific host units of the volcaniclastic stratigraphy. The style and intensity of alteration styles may be partially related to compositional variations of the original lithology. Broadly, however, alteration zonation recognised at Gossan Hill is comparable to that reported in the classification of Mattabi-style mineralisation of Morton and Franklin (1981).

PIMA-II Spectral analysis of alteration associated with the Hellyer VHMS deposit: Preliminary results—Kai Yang, J. Bruce Gemmell and Russell Fulton

AMIRA project P435 "Mineral Mapping with Field Spectroscopy for Exploration" (Project leader Jon Hunnington) is a multi-disciplinary research project focusing on the development of new, operational, field spectroscopic techniques for mapping mineral, soil and rock composition during exploration. The field portable spectrometer (PIMA-II) has brought the opportunity of applying this technology routinely to exploration programs. For example, the PIMA-II can easily map, in situ, hematite, geothite, smectite varieties, kaolinite, dickite, halloysite, sericite/illite varieties, gibbsite, jarosite, alunite, gypsum, pyrophyllite, amphiboles, opaline silica, carbonate species, epidote, talc, tremolite, chlorite varieties, phlogopite, and biotite.

As part of this project P435 several case histories of well documented alteration zones around selected mineral deposits are being undertaken. One of these case histories is the Hellyer VHMS deposit in Tasmania as the footwall alteration zonation (Gemmell and Large, 1992) and the hangingwall alteration (Jack, 1989) is well developed and preserved. AMIRA projects P435 and P439 started at roughly the same time and several companies are sponsors of both projects. These companies suggested that as the alteration at Hellyer was being investigated by both projects that we should collaborate. Both sponsor groups were approached and it was decided to combine research efforts to compare the spectral data from the PIMA-II generated from P435 with the detailed mineral chemistry and whole rock chemistry obtained from P439. From March 27–30 Kai Yang visited CODES and worked with Bruce Gemmell and Russell Fulton to obtain spectral data from selected drill core and rock pulps, previously used for whole rock analyses, from Hellyer. This paper reports some preliminary results from the study of the Hellyer material.

Progress report on the utilisation of the Mount Read Violcanics database — J. Stolz, R. Large and N. Duhig

A preliminary examination of the MRV database has been undertaken to assess the gross chemical variability in the data set and the likely causes of this variability. Comparisons with a large database for modern unaltered volcanics from both oceanic and continental margin arc settings provides useful constraints on the likely variability in the MRV database that could be due to primary magmatic compositions. The modern unaltered volcanics display a very limited range of values for the traditional Alteration Index (20–50) compared with the MRV database. Samples with A.I. values <20 appear to be characterised by albitic alteration, whereas the Ca and Na depletion which accompanies feldspar breakdown and development of sericite and chlorite results in the characteristic high A.I. values (>80). Samples with substantial carbonate alteration commonly have values for the A.I. in the range of unaltered volcanics. Minimum Na_2O contents of about 2 wt.% prior to alteration typify most arc volcanics except for unusual K-rich alkaline varieties. The unaltered island arc suites also indicate the very restricted ranges expected for base metal concentrations over a range of whole-rock compositions.

Preliminary assessment ofMRV geochemical database in terms of possible vectors to ore — R. Large, J. Stolz and N. Duhig

Preliminary assessment of the MRV geochemical database allows a division of the CVC and Que–Hellyer volcanics into three groups based on Na_2O content; "altered" (Na_2O < 1.5 wt %), "unaltered" (Na_2O = 1.5–5.0 wt %), and "albitised" (Na_2O > 5.0 wt%). Using these three groups, and the Ishikawa alteration index, it is possible to plot a series of diagrams to show the relationship between the major alteration mineral endmembers (sericite, chlorite, K-feldspar, dolomite and albite) and the alteration index variation. Two new indices have been developed and tested on the database; a chlorite index and a Mn–carbonate index. The latter index shows potential for use as a vector to VHMS mineralisation, however, considerable more work is required to evaluate, refine and test the index. By combining the three indices in various graphs, it is possible to obtain a rapid visual estimate of the spread of alteration mineral assemblages in the MRV database.

Mount Black to the Murchison Gorge: Preliminary volcanic facies analysis and alteration styles

C.C. Gifkins, R.L. Allen, A.J. Stolz and N. Duhig
Centre for Ore Deposit and Exploration Studies, University of Tasmania

INTRODUCTION

This regional geological traverse of the Mount Read Volcanics, western Tasmania, examined outcrops of the Central Volcanic Complex (CVC) and Eastern Sequence between the "Mount Black Fault" near Rosebery and the upper Owen Conglomerate at Murchison Dam. The path of the traverse (Fig. 1) was designed to maximise the use of outcrop along the Murchison Highway and Murchison Dam Road and to compliment previous structural cross sections by Ron Berry (1993).

The aim of this current work was to better understand the alteration processes which have variably modified the volcanic facies within the northern Mount Read Volcanics. To interpret the alteration processes correctly it is critical that we firstly understand the volcanic architecture. This requires unravelling both the complex geometry and character of the volcanic facies and the overprinting alteration assemblages.

In March 1996, four members of the AMIRA project (Cathryn Gifkins, Rod Allen, Joe Stolz and Nathan Duhig) spent four days examining outcrops of the Murchison Granite and the Murchison Volcanics along the Murchison Gorge and the Tullah end of Anthony Road. A further day was spent on the western side of the Mount Black along a 4WD track which leads to the summit. Data and samples collected during this period have been collated with mapping in the Mount Black Volcanics and the Sterling Valley Volcanics by the first author. Forty-six samples (MB1–MB46) were collected to supplement those already examined in the authors current Phd collection. The samples have been submitted for sectioning and geochemical analysis, however at the time of this report no petrological or geochemical data is available. In this paper descriptions of the volcanic facies and textures, alteration assemblages and textures based on the results of detailed field examinations are presented.

Previous work in the Mount Black Volcanics and Sterling Valley Volcanics has been limited and is reported by Allen (1994, 1995), Anderson (1972), Brathwaite (1969), Gifkins (1995), Green (1983), Lees (1987) and Warmeant (1990). Work on the Farrell Slates, Murchison Volcanics and Murchison Granite has been reported by Allen (1995), Large et al. (1996) and McNeill and Corbett (1987).

REGIONAL STRUCTURE AND STRATIGRAPHY OF THE TRAVERSE

The traverse contains four main NNE-striking stratigraphic units from west to east. These are: Mount Black Volcanics, Sterling Valley Volcanics, Farrell Slate, and Murchison Volcanics. The Rosebery–Hercules sequence which unconformably underlies the Mount Black Volcanics to the west of this traverse hosts both the Rosebery and Hercules orebodies and was not examined in detail during this traverse. Rod Allen will examine this sequence during a study into the carbonate alteration associated with the north Rosebery ore lenses. The Rosebery–Hercules sequence dips and faces towards the east. The Mount Black Volcanics also dip and face east at their western margin, however towards the east they dip and face west. The Sterling Valley volcanics, Farrell Slates and Murchison Volcanics all dip steeply west, and also face west.

These changes in structural orientation are

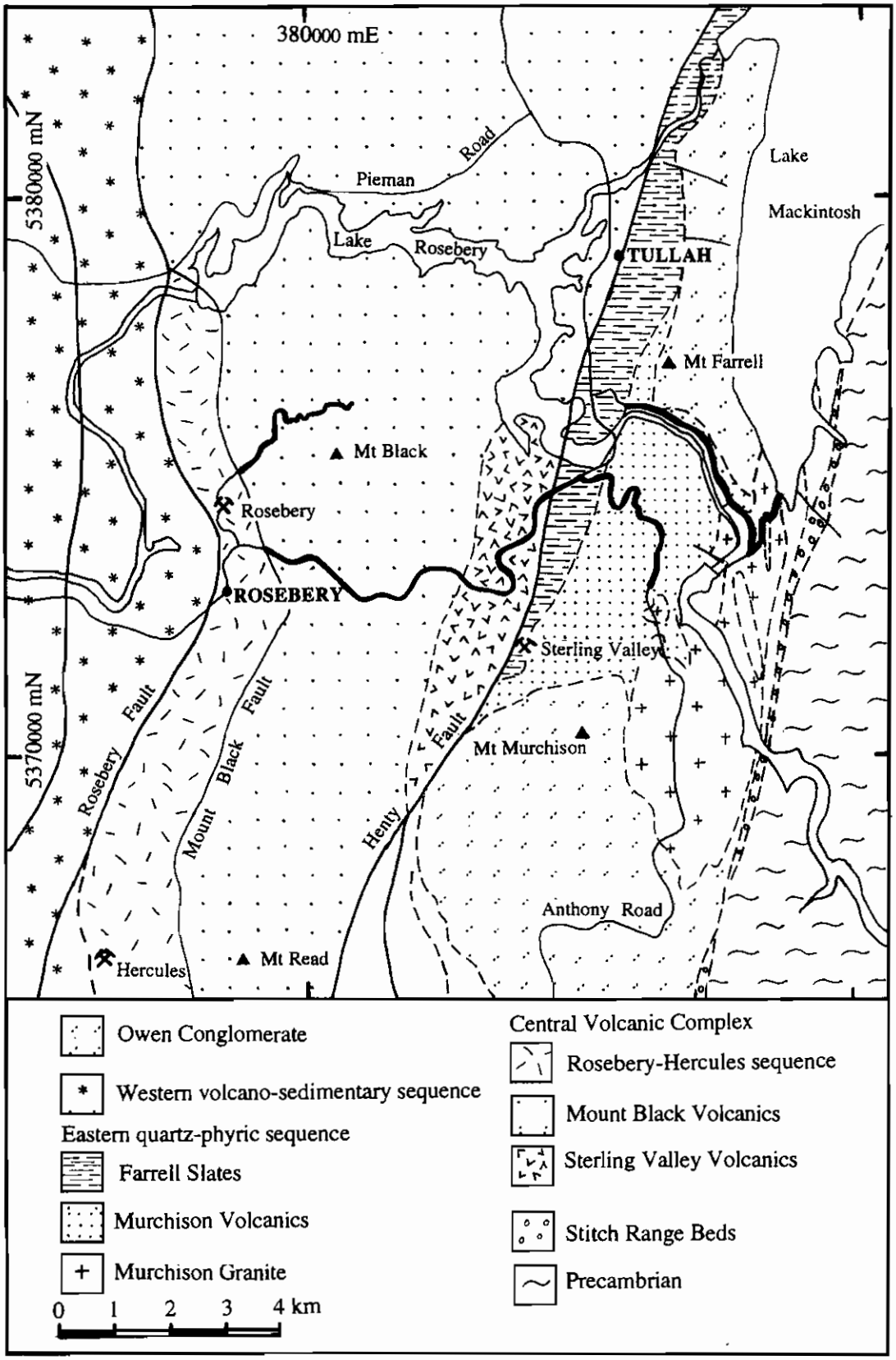

Figure 1: Geological map of the northern Mount Read Volcanics belt (adapted from Corbett and McNeill, 1988). Showing the distribution of the major rock associations in the Central Volcanic Complex and the Eastern sequence. The heavy lines mark the path of the Mount Black to Murchison Gorge traverse.

interpreted to indicate that the Rosebery sequence and western Mount Black Volcanics are the eastern limb of a NNE trending regional anticline which extends for 20 km from Hercules in the south to Pinnacles in the north. The Mount Black Volcanics represent a large open syncline. The Sterling Valley Volcanics occur in the core and on the western limb of a regional anticline which extends from the north of Mount Block and is truncated to the south by the Henty Fault. This suggests that the Sterling Valley Volcanics are the lowest exposed stratigraphic component of the CVC.

Faults are common throughout the package, but three appear the most important; the Mount Black Fault, the Henty Fault and the Murchison Fault. The Mount Black Fault can be seen in drill core at Rosebery, but is not exposed along the traverse. It is a brittle thrust fault forming the contact between the quartz-phyric volcaniclastic mass-flow units of the Rosebery–Hercules Hangingwall and the feldspar-phyric Mount Black Volcanics. A 2–10 m zone of intense ductile shearing and silicification exists either side of the brittle fault. The Henty Fault is a complex relatively brittle fault forming the contact between the Sterling Valley Volcanics and the Farrell Slates. It is a major reverse fault dipping westward under the Sterling Valley Volcanics and comprises several metres of intensely broken and sheared, quartz veined rock within a strong zone of silicification. The fault is slightly oblique to bedding in both cross section and map view. In map view this discordance is reflected in the southward truncation of both the Farrell Slates and Sterling Valley Volcanics. This structural discordance and change in facies either side of the fault indicate that there has been major displacement on the Henty Fault. The original stratigraphic relationship between the Sterling Valley Volcanics to the west and Farrell Slates to the east is uncertain. The Murchison Fault is a more ductile shear on the contact of the Farrell Slates and the Murchison Volcanics.

From previous work by Allen (1988), Allen (1995), Gifkins (1995) and Corbett and Lees (1987), the following regional stratigraphy for the traverse is interpreted (Table 1).

To the west of the Henty Fault the traverse included the Mount Black Volcanics and the Sterling Valley Volcanics. The Mount Black Volcanics are a several kilometre thick package of feldspar-phyric massive, flowbanded and flow-brecciated lavas and sills of generally dacitic composition with minor rhyolite and andesite. Variable proportions of pumiceous material are interbedded in the sequence and the entire package has been intruded by a series of mafic dykes. Conformably underlying the Mount Black Volcanics to the east is a package of basalts to

Table 1

	west of the Henty Fault (Western Sequence & CVC)	east of the Henty Fault (Eastern Sequence & Precambrian)
u	White Spur Formation	
p	*Rosebery Fault and conformable*	
	Rosebery–Hercules Hangingwall	*fault*
f	*conformable*	Farrel Slate
a	Rosebery–Hercules Footwall	*Murchison Fault*
c	*Mount Black Fault*	Murchison Volcanics
i	Mount Black Volcanics	*????*
n	*conformable*	Sticht Range Beds & Precambrian
g	Sterling Valley Volcanics	
	fault	

andesites, locally known as the Sterling Valley Volcanics. These are composed of numerous monomict and polymict basaltic and andesitic mass-flow breccias, basaltic to dacitic lavas and sills and rare tuffaceous siltstones. The Sterling Valley Volcanics and Mount Black Volcanics are in stratigraphic contact and appear to petrographically and chemically related.

Immediately to the east of the Henty Fault is the Farrell Slates. They comprise of grey to black siltstones with abundant thin to thick interbedded, feldspar–quartz–mica sandstone turbidites and rhyolitic pumiceous to crystal-rich mass-flow deposits.

To the east, the Farrell Slates unconformably overlie the Murchison Volcanics. The major stratigraphic units inspected in the Murchison Volcnaics comprise of quartz-phyric rhyolitic lava domes, sills and pyroclastic deposits which are invaded by a swarm of rhyolite porphyry sills and the Murchison Granite.

PRIMARY FACIES

The main facies observed during this traverse are reported here. The distribution of the facies can be seen in Figure 2, which is a log of the facies and alteration styles from west to east. This log is not a stratigraphic log. Structural complications have not been removed and so this represents a ground log of the outcrops. A schematic stratigraphic log of the volcanic facies for the Mount Black and Sterling Valley Volcanics is depicted in Figure 3 and for the Murchison Volcanics in Figure 4. It is important to note that in many areas pervasive alteration has obscured and destroyed primary textures and petrology and geochemistry will need to be employed to help determine the primary lithology.

The Mount Black Volcanics

The western side of Mount Black is dominated by flowbanded rhyolites intruded by thick feldspar–hornblende porphyritic dacitic sills. Conversely the eastern side of Mount Black is dominated by massive red-brown to grey feldspar–hornblende porphyritic dacitic to andesitic lavas and sills with minor rhyolite. Minor interbedded pumiceous breccias, sandstones and volcaniclastic siltstones are also present throughout the Mount Black Volcanics.

The *feldspar-phyric rhyolites* in the Mount Black Volcanics are commonly flowbanded and flow-brecciated. The rhyolites typically have 3–10% euhedral feldspar phenocrysts of 1–2 mm in diameter which often form glomeroporphyritic aggregates in a siliceous groundmass. Groundmass textures include snowflake texture, spherulites and perlitic fractures. Large spherulites (0.5–2 cm) are commonly elongated and aligned in the direction of flow. Vesicles are mostly filled with chlorite, calcite and quartz. The margins of units may be marked by peperite textures, rare inclusions of fine grained buff coloured siltstone which have mixed with the lava as it flowed over or intruded into wet sediment. Clasts of flowbanded and vesicular lava are also rarely included within the feldspar-phyric rhyolite bodies.

Feldspar-phyric rhyolitic autobreccias and hyaloclastite are syn-eruptive volcaniclastic deposits. Autobreccias are the product of non-explosive flow fragmentation. As parts of lavas that are cooler or more viscous flow, they are subjected to locally higher strain rates (McPhie et al., 1993). They may respond to the stress created by strain gradients by plastically deforming and/or by brittle fragmentation (Cas and Wright, 1987). Hyaloclastite is produced when a hot coherent magma body suddenly comes into contact with cold water or water saturated sediment. As quenching occurs thermal stresses cause contraction of the magama and this may in turn fragment the magma body producing clasts with distinctive curviplanar margins. Aggregates of quench-fragmented debris are often called hyaloclastite (Pichler, 1965; Cas and Wright, 1987; McPhie et al, 1993). The blocks produced by flow brecciation and quenching may be enclosed within the non-fragmented magma, deposited on the flanks of a moving flow, or are free to be redeposited by sedimentary processes.

The feldspar-phyric rhyolitic autobreccias and hyaloclastite deposits in the Mount Black Volcanics are dominated by non-vesicular massive to flow-banded clasts and pumiceous lava clasts. The pumiceous clasts are commonly streaky sericitic fragments. The deposits are typically massive, poorly sorted and vary from matrix supported aggregates of rotated clasts to clast supported breccias with jigsaw fit textures. Locally the deposits can be very coarse with 1–2m blocks.

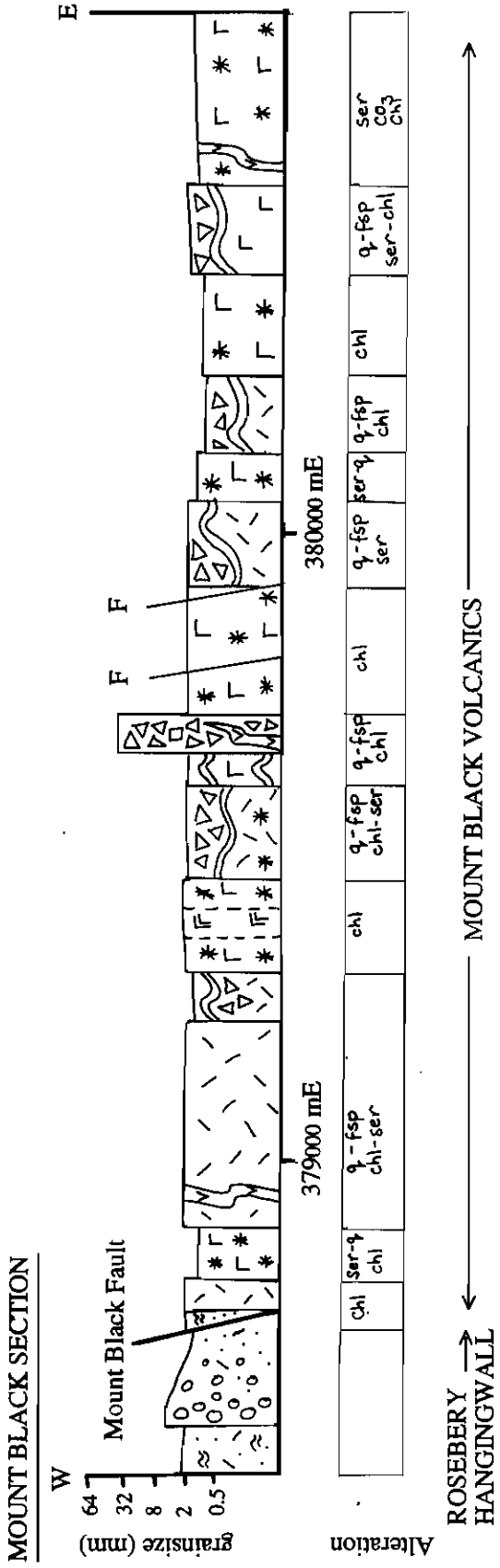

Figure 2a: Graphic log of the distribution of facies and alteration styles from west to east along the Mount Black traverse. The log is not a stratigraphic reconstruction. Structural complications have not been removed and so it represent a ground log of the outcrops along the path of the traverse. A key to the facies symbols and alteration terms are included on the following page.


Rhyolite/crystal-rich rhyolite


Dacite/crystal-rich dacite


Andesite/crystal-rich andesite


Basalt


Granite


Siltstone


Crystal-rich sandstone


Crystal-pumice sandstone


Pumice breccia


Monomict lithic breccia


Conglomerate


Flowbanding


Dense lithic clasts


Pumice clasts


Siltstone clasts


Spherulites


Feldspar-phyric volcaniclastic


Crystal-rich feldspar-phyric volcaniclastic


Quartz-phyric volcaniclastic


Crystal-rich quartz-phyric volcaniclastic

Fault

Key term	**Alteration assemblage**
sil	silicification
q-fsp	quartz-feldspar
ser	sericite
ser-q	sericite-quartz
ser-q-chl±CO3	sericite-quartz-chlorite±carbonate
ser-chl	sericite-chlorite
CO3	carbonate
chl	chlorite
chl-CO3±ser	chlorite-carbonate±sericite
fsp-chl±ep	feldspar-chlorite±epidote
K-fsp-chl	K-feldspar-chlorite
py	pyrite

Key to figures 2, 3 and 4: volcanic facies symbols and alteration terms.

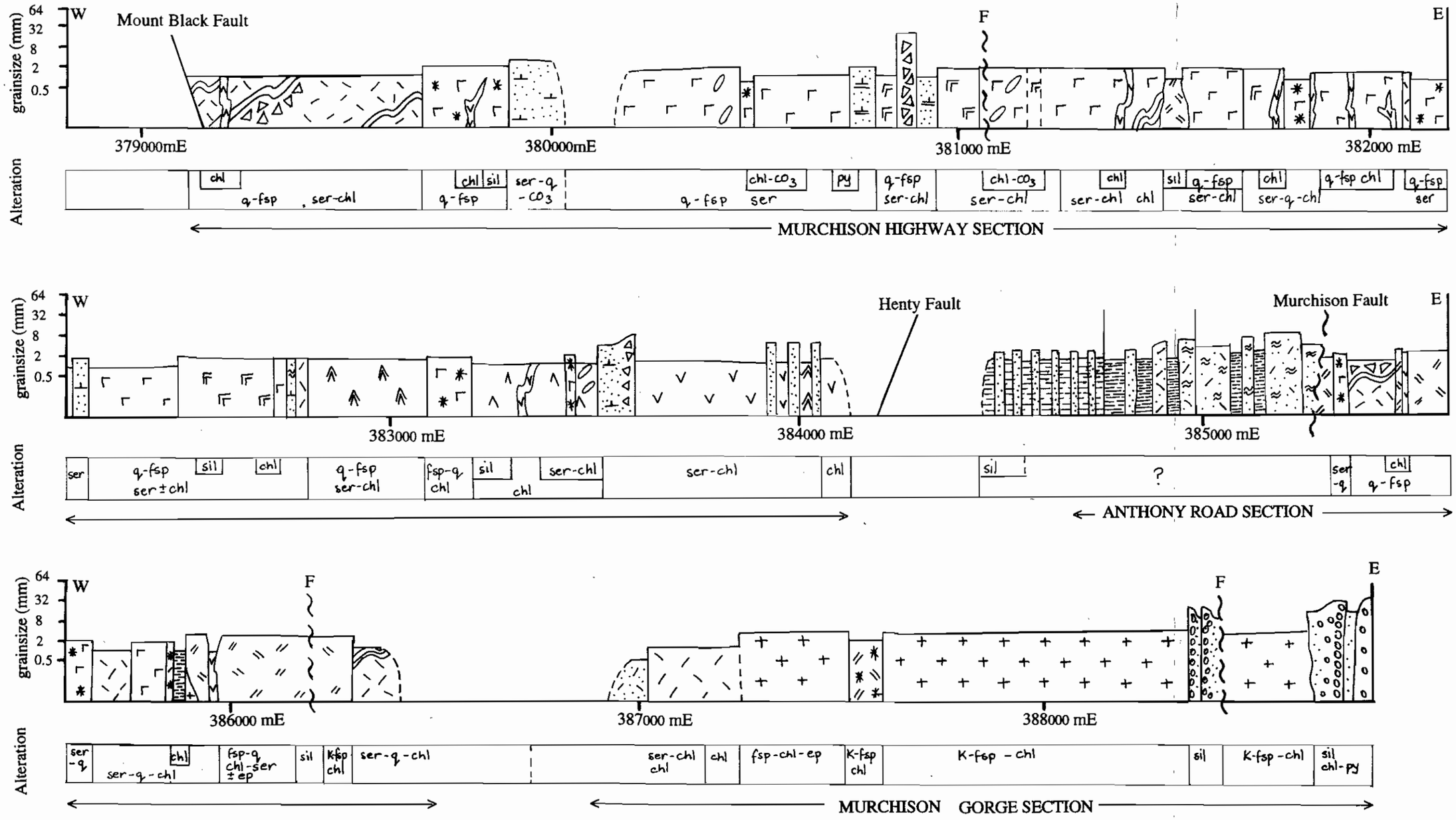

Figure 2b: Graphic log of the distribution of facies and alteration styles from west to east along the Mount Black to Murchison Gorge traverse. This log includes outcrops along the Murchison Highway, Anthony Road and the Lake Mackintosh Dam Road.

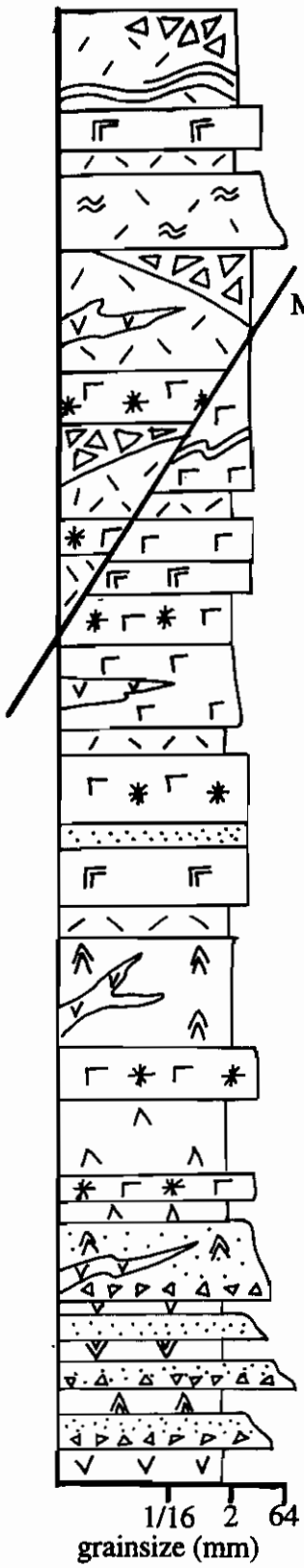

Mount Black Volcanics:
Abundant flowbanded and brecciated, feldspar porphyritic rhyolitic lavas and sills intruded by thick, massive spherulitic feldspar-hornblende phyric dacitic sills. Mass-flow deposits composed of blocky to vesicular feldspar porphyritic lava clasts. Rare pumice breccias, tuffaceous siltstones and crystal-rich sandstones.

Thick massive to spherulitic, feldspar-hornblende porphyritic dacites, rare flowbanded rhyolites and andesitic sills. Occasional lenses of tuffaceous siltstone, pumiceous sandstone and crystal-rich dacitic sandstones.

Sterling Valley Volcanics:
Monomict and polymict basaltic and andesitic mass-flow deposits, dacitic-basaltic lavas and sills and rare tuffaceous siltstones. Abundant fine grained basaltic intrusions of the Henty Dyke Swarm.

Figure 3: A schematic stratigraphic log of the volcanic facies and relationships for the traverse **west** of the Henty Fault Zone. Included are the Sterling Valley Volcanics and the conformably overlying Mount Black Volcanics. The total thickness of the section illustrated here is ~ 3000 m.

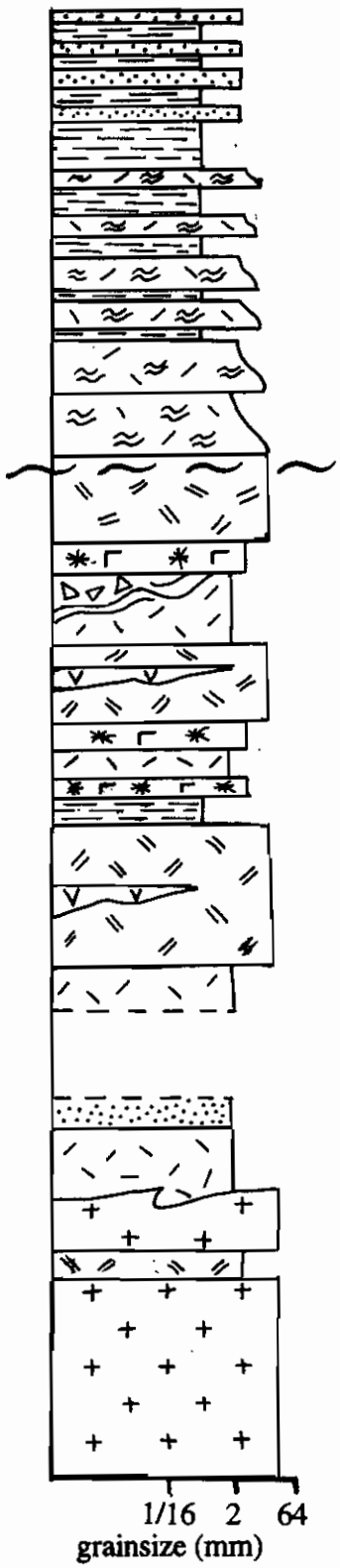

Farrell Slates:
Grey to black siltstones with abundant interbedded, feldspar-quartz-mica sandstones and thick rhyolitic pumiceous to crystal-rich mass flow deposits.

Murchison Volcanics:
Quartz porphyritic, massive to flowbanded rhyolite lavas and quartz-phyric siltstones and sandstones, intruded by abundant quartz-feldspar porphyritic sills, spherulitic dacitic sills and rare basaltic dykes.

Murchison Granite:
Quartz- plagioclase- K-feldspar- hornblende- biotite± magnetite microgranodiorite intruding into the Murchison Volcanics

Figure 4: A schematic stratigraphic log of the volcanic facies and relationships for the traverse **east** of the Henty Fault Zone. Included are the Murchison Granite, Murchison Volcanics and the Farrell Slates. The total thickness of the section illustrated here is ~ 2500 m.

Polyphase domainal alteration within the autobreccias and hyaloclastites has enhanced the matrix component and highlighted the fine flow laminations in the clasts. The result is pseudo-fiamme in non-explosively derived autobreccias and hyaloclastite.

Feldspar-hornblende phyric, spherulitic, dacitic sills are massive, blocky, medium brown with 5–7%, 1–2 mm euhedral feldspar phenocrysts and 2–3%, 2 mm prismatic hornblende crystals. The hornblende phenocrysts are commonly replaced by chlorite and form 2–6 mm aggregate intergrowths with feldspar crystals. The groundmass has a fine sandy texture reflecting the high density of micro spherulites. The feldspar–hornblende phyric dacite sills are occasionally flowbanded and often have sharp intrusive contacts.

Massive, feldspar–hornblende phyric dacites to andesites compose the majority of the exposed volume of the Mount Black Volcanics. The dacites–andesites are thick, massive, textureless and red-brown to grey in colour. They typically contain 1–3 mm euhedral feldspar phenocrysts and 2 mm hornblende laths which often form glomeroporphyritic aggregates in the siliceous groundmass.

Pumiceous, feldspar-phyric, mass-flow breccias vary in composition from rhyolitic to dacitic. They contain dark lenticular patches, 1–5 cm long aligned roughly in the plane of regional bedding. The lenses comprise of compacted pumice and resemble fiamme in welded ignimbrites. These phyllosilicate-rich (chlorite–sericite) lenses are set in paler quartz-feldspar altered pumice. In the quartz-feldspar rich domains unflattened tube pumice clasts can be observed with the aid of a handlens. Other components are; broken and euhedral feldspar and quartz crystals and fine grained blocky flowbanded to massive porphyritic lava clasts. On an outcrop scale the deposits are normally graded with sharp bases and finely stratified tops.

Tuffaceous siltstones are commonly siliceous, pale grey to buff coloured and weakly laminated or cross bedded. Sedimentary structures within the siltstones are typical of turbidite deposits and indicate the below wave base environment of deposition for many parts of the Mount Black Volcanics.

The Sterling Valley Volcanics

The Sterling Valley Volcanics are a 1 km package of normally graded, basaltic to dacitic mass-flow units, minor siltstone, and numerous basaltic to dacitic lavas and sills.

Andesitic to basaltic lavas and sills are fine grained, blue-green and massive, with hornblende and feldspar phenocrysts. The hornblende is largely replaced by biotite and chlorite. The groundmass is variably altered and occasionally perliticly fractured. There are a minor number of dacite and rhyolite sills identical to those in the Mount Black Volcanics.

The ***mass-flow deposits*** vary from monomictic to polymictic and comprise of angular, feldspar-hornblende porphyritic lava clasts ranging from basaltic to dacitic in composition. The clasts range in texture from highly vesicular or pumiceous to dense quenched lava clasts and coarsely porphyritic mafic clasts. These deposits also contain abundant angular and broken feldspar crystals in a chlorite-rich matrix.

Both the Mount Black Volcanics and the Sterling Valley Volcanics have been intruded by abundant basaltic dykes of the ***Henty Dyke Swarm***. The dykes are fine grained, massive and often form irregular branching dark green bodies. They commonly contain calcite–chlorite–quartz filled amygdales and are rarely more than one metre wide. The dykes and sills have very irregular disruptive intrusive contacts and their distribution appears random although the frequency decreases away from the Henty Fault.

The Farrell Slates

The Farrell slates are a package of interbedded grey siltstones, quartz–feldspar–muscovite sandstones and rhyolitic, pumice- crystal- rich sandstones and breccias. The entire formation is composed of volcaniclastic and clastic sediments which were deposited in a below wave base environment as the result of turbidity currents and mass-flows during the end of a major rhyolitic eruptive stage, possibly the end of the emplacement of the Murchison Volcanics.

The Murchison Volcanics

The Murchison Volcanics are dominated by quartz–feldspar porphyritic rhyolite lavas and sills. These have been extruded and intruded into a rhyolitic volcaniclastic succession and have in turn been

intruded by a series of feldspar-phyric dacite sills. The host volcaniclastic succession was not observed during this traverse so only the rhyolite and dacite lavas and sills will be discussed in detail.

Quartz-feldspar porphyritic rhyolite lavas and sills. These contain 2 distinctive sizes of clear volcanic quartz phenocrysts, large 2 mm euhedral to subhedral crystals with moderately developed embayments and smaller 1 mm round crystals. The feldspar phenocrysts are generally smaller (1–1.5 mm) and the total crystal content is approximately 10%. The lavas are dominantly massive but locally contain flowbanding, perlite, spherulites and hyaloclastite. Pseudo-clastic textures are developed in the coherent lavas as a result of the anastomosing cleavage stretching and dismembering the perlitic and hyaloclastite textures.

Crystal-rich, quartz-feldspar phyric, rhyolite porphyry sills are common particularly in the eastern half of the Murchison Volcanics, towards the Murchison Granite. They contain large 2 mm euhedral quartz phenocrysts and larger (>2 mm) zoned feldspars similar to those in the Murchison Granite. The total crystal content of the porphyries varies from 10–25% in a white, sericitised, fine grained groundmass. The porphyries have textural and mineralogical similarities to the feldspar–quartz–biotite–hornblende Murchison Granite, which underlies and intrudes them in the eastern half of the Murchison Volcanics. It is likely that these are genetically and temporally related to the granite. The sills may represent a precursor, high level sill swarm, that grades from volcanic in texture at the top (the quartz-feldspar porphyritic rhyolite lavas and sills), to granophyric subgranitic at deeper levels (quartz-feldspar phyric rhyolite prophyries), and which was subsequently intruded by the Murchison Granite.

Feldspar porphyritic, rhyolite/dacite sills and dykes are massive, grey to pink-brown, with 5–10%, 2 mm feldspar phenocrysts in a fine grained siliceous densely spherulitic groundmass. Glomeroporphyritic clusters of feldspar and chlorite are common. The feldspar porphyritic dacites are generally strongly foliated and weak to moderately altered.

Rare ***mafic dykes*** have intruded into the Murchison Volcanics. These dykes are similar to those of the Henty Dyke Swarm which invaded the Sterling Valley Volcanics and the Mount Black Volcanics to the west of the Henty Fault. The dykes are fine grained, moderately foliated, dark green with intense sericite+chlorite±pyrite alteration and have strong magnetic signatures.

The Murchison Granite

Petrologically the Murchison Granite has similarities to the crystal-rich quartz-feldspar rhyolite porphyries of the Murchison Volcanics. It is a quartz–plagioclase–K-feldspar–hornblende–biotite ± magnetite microgranodiorite which underlies and intrudes into the eastern half of the Murchison Volcanics. The margin of the granite is porphyritic with large zoned plagioclase phenocrysts which predate the pink K-feldspars crystals. Away from the margins the granite is equigranular and variably altered and recrystallised.

Owen Conglomerate

The Owen Conglomerate is a thick sequence of silicic, hematite altered, interbedded quartz sandstones and pebble conglomerates which contain rounded clasts of quartzite and vein quartz in a pink siliceous sandy matrix. A silicified contact zone is exposed at the Lake Mackintosh Dam where lobate flames of deformed microgranodiorite intrude into the overlying pink hematite altered Owen quartzite. Other contacts between the Owen and Murchison Granite are exposed along the Lake Mackintosh Dam road and are both faulted and bedding parallel intrusive ?

VOLCANIC ARCHITECTURE

No units could be correlated across the Henty Fault and the stratigraphic relationship between the Sterling Valley Volcanics in the west and the Farrell Slates in the east is uncertain. Thus the volcanic architecture for the traverse has been reconstructed for both sides of the Henty Fault separately.

The oldest package to the west of the Henty Fault is the Sterling Valley Volcanics. They are a thick succession of mass-flow deposits, extrusive lavas and intrusive shallow sills which record the eruptive history and erosional events of one or more mafic volcanic centres. The volcanic centre was predominantly basaltic but also produced more fractionated magmas which were extruded into the submarine environment. Quenching of the hot lava during extrusion brecciated the basaltic magma and

this debris was redeposited down slope by mass-flow events. The quenched lava clasts indicate that part of the source volcano was subaqueous or that lava flowed into the sea from a summit that emerged above sea level. The base of the volcano has been removed by displacement along the Henty Fault. The regional significance of the Sterling Valley Volcanics is that they are the structural relic of the medial facies association of a large marine mafic volcano that was active early in the eruptive history of the CVC.

The mafic to intermediate activity of the Sterling Valley Volcanics was followed by the emplacement of the basal succession of the Mount Black Volcanics, a period of complex extrusion and shallow intrusion of coherent felsic lavas and sills coeval with the deposition of felsic pumiceous mass-flow units. The felsic lavas and shallow intrusions were commonly autobrecciated during emplacement and quench fragmented as they came into contact with seawater. Clastic debris derived from the coherent lavas remained in-situ, was deposited on the flanks of the moving flow or redeposited by mass-flow forming poorly sorted, normally graded breccias. The best evidence for the environment of emplacment of the Mount Black Volcanics and Sterling Valley Volcanics is the presence of facies and sedimentary structures typical of a subaqueous setting. Finely laminated and cross-bedded tuffaceous siltstones have been deposited by turbidites in below wave base conditions. Rare mudstones also indicate that background conditions to the volcanic activity were relatively quiet marine.

The most voluminous event in the Mount Black Volcanics was the emplacement of a thick pile of intermediate lavas and sills. These feldspar-hornblende porphyritic dacites post dated the more felsic lavas and pumiceous debris into which they are emplaced and may represent a period of intermediate lava dome or cryptodome formation. The margins of the sills and lavas are commonly autobrecciated, but little redeposition of this autoclastic material has occurred. Late in the development of this phase densely spherulitic, massive to faintly flowbanded, feldspar-hornblende phyric dacite sills swarmed throughout the felsic and intermediate Mount Black succession and into the upper part of the Sterling Valley Volcanics.

The final volcanic event recorded to the west of the Henty Fault in the CVC was the intrusion of a series of mafic dykes and sills which are part of the Henty Dyke Swarm.

To the east of the Henty Fault the oldest rocks are the rhyolitic volcaniclastic sediments, lavas and high-level sills of the Murchison Volcanics. Early phases of eruption were explosive, generating a succession of pumiceous volcaniclastic deposits. The volcaniclastic sediments are interpreted as reworked pyroclastic debris which has been deposited subaqueously by mass-flow events (Allen, 1995). These were subsequently invaded by passive intrusion of rhyolitic lava domes and sills, and by a series of spherulitic, feldspar-phyric dacitic sills and dykes. The Murchison Volcanics were intruded by the Murchison Granite and a number of apprently related quartz-feldspar porphyry sills.

Finally, the Farrell Slate sediments were deposited in a below wave base subaqueous environment. The volcaniclastic beds are syn-eruptive to post-eruptive subaqueous mass-flow units and the grey feldspar-quartz-mica sandstones are turbidites. The gradation from abundant pumiceous rhyolitic mass flow units at the base of the Farrell Slates to abundant polymict reworked sandstones at the top, suggests that the Farrell Slates record the end of a major rhyolitic eruptive stage in the submarine basin. The textural, mineralogical and facies characteristics of the pumice–crystal mass flow units of the Farrell Slate are similar to the pumice–crystal mass flow units in the top of the Murchison Volcanics (Allen, 1995). It is therefore suggested that the Farrell Slates record the waning stages of the eruption of the Murchison Volcanics.

ALTERATION

All the units discussed in this report appear variably modified. The present alteration assemblages reflect the combined effects of different post-depositional processes on the primary mineralogies and textures. Devitrification, hydration, hydrothermal and diagenetic alteration, diagenetic compaction and metamorphism have acted to modify the primary facies. Each process is influenced by the existing deposit texture but also overprints and modifies this texture. Thus the texture of the volcanic facies evolves by a series of steps, however the steps are not

necessarily discrete and many overlap making the recognition of individual phases complicated. The result of this series of alteration processes operating is often a complex pattern of two or more phase alteration assemblages which may enhance primary or devitrification textures in the volcanic rock.

The characteristics of each of the alteration stages are currently not satisfactorily understood to make any conclusions in this report. No attempt to distinguish between diagenetic alteration, regional metamorphism and hydrothermal alteration will be made as it is felt by the authors that based on field characteristics alone we have insufficient proof of the timing of the alteration assemblages. However, the characteristics of each alteration phase will be discussed below with a comment on the distribution of alteration assemblages compared with volcanic facies. This information is also presented graphically in the series of geological logs (Fig. 2) which show the distribution of volcanic facies and textures and the alteration mineralogy.

Silicification is widespread and pervasive occurring most notably within the high level intrusions (dacitic sills) of the Mount Black and Sterling Valley Volcanics and in the quartz-rich sandstones and conglomerates of the Owen Conglomerate. Silicification is also associated with major faults and shear zones throughout the sequence.

Quartz-feldspar alteration appears to be the most common throughout the transect and has also been reported extensively during the two other AMIRA traverses (Mt Read and Jukes Road) and by numerous workers in the Rosebery–Hercules sequence. It is regionally extensive and significant. It is characterised by a pink colouration due to the presence of albite and varies in intensity and texture. It may be selective, albite replacing primary feldspar phenocrysts or domainal in character, forming pink quartz-feldspar rich zones. It is commonly associated with chlorite–sericite or sericite alteration producing a distinctive pink and green mottled pattern. This occurs in both coherent and volcaniclastic deposits. In the massive, coherent units pink-green alteration is patchy, forming a contrasting green and pink mottled pattern on a scale of 2–20 cm, while in the flowbanded units the pink and green alteration is confined to individual bands where sericite-chlorite defines the originally glassy flowbands and quartz-feldspar the spherulitic flowbands. False clastic and polymictic textures are often developed in the coherent flowbanded units by this 2 phase alteration and primary clastic textures in the volcaniclastic units are enhanced. In many of the autobreccias and hyaloclastite quartz-feldspar alteration forms pink halos or rinds around lithic clasts set in a green sericite–chlorite groundmass. The pumice-rich units are also pink-green altered, with original pumice textures being preserved in the pale quartz-feldspar altered domains while in the sericite–chlorite domains only the porphyritic nature of the original pumice clasts can be determined. Quartz-feldspar is also a very common vein assemblage, particularly on the western side of Mount Black and in the Murchison Volcanics.

Sericite alteration. Fine grained sericite rims feldspar phenocrysts and is scattered as disseminated grains throughout the recrystallised quartz-felspathic groundmass of many of the coherent units, giving a green-grey colouration to the Mount Black dacites. Although this alteration phase is widespread in the Mount Black and Sterling Valley Volcanics it is rarely strong enough to mask primary volcanic features although it can partially or completely replace phenocrysts. Pale green sericite also commonly forms along cleavage and fracture surfaces.

Sericite–quartz alteration is a common weak pervasive alteration style in many of the massive, feldspar-phyric, coherent lavas and sills. It imparts a pale green siliceous appearance to many of the Mount Black dacites and the quartz-feldspar porphyritic rhyolites of the Murchison Volcanics.

Sericite–quartz–chlorite±carbonate alteration occurs in coherent flowbanded lavas and sills, autobreccias, hyaloclastite and pumiceous breccias. Pale green variably silicified and chloritised, it is often non-homogenous alteration producing patches or lenses of dark green chlorite–sericite in a paler quartz-rich composition. These dark lenses typically form in pumiceous debris with carbonate–sericite altered feldspar phenocrysts but they can also form in individual flowbands of a coherent unit or the flowbanded clasts of autoclastic deposits. This is common in the Mount Black rhyolites and also in the quartz-feldspar porphyritic rhyolites of the Murchison Volcanics where weak pervasive sericite–quartz–chlorite alteration overprints an earlier feldspar–chlorite±epidote phase.

Sericite–chlorite alteration is pervasive in the dacitic to basaltic coherent units. Weak pervasive chlorite–sericite±magnetite alteration occurs in the groundmass of feldspar–hornblende dacites of the Mount Black Volcanics while more intense chlorite–sericite alteration is common in the mafic dykes of the Henty Dyke Swarm. Partial to complete pseudomorphing of the ferromagnesian phases by chlorite is also common. In the more rhyolitic units sericite–chlorite alteration tends to be patchy set in quartz-feldspar rich domains. Within the chlorite–sericite rich domains the phenocrysts are preserved but other primary volcanic textures are largely destroyed.

Carbonate alteration is fine grained, either disseminated, replacing or rimming feldspar phenocrysts as well as occurring as vein and vesicle fill material. Carbonate alteration is generally weak, however more intense carbonate alteration often masks the presence of primary phenocrysts leaving a fine grained massive homogenous pale grey rock. It is often observed to be moderately strong in mafic dykes and decrease in strength in the wallrock away from the dyke.

Chlorite alteration has more than one recognisable phase. In outcrop at least two types of chlorite can be determined. A dark (hydrothermal) chlorite and paler green (metamorphic) chlorite. Chlorite alteration is very widespread occurring in almost all units in a number of different forms. Most commonly as patchy to pervasive disseminated fine grained aggregates in the groundmass of the basalts to dacites of the Sterling Valley Volcanics and the spherulitic dacite sills of Mount Black Volcanics. It occurs in the pumice-rich volcaniclastics as styolitic textures parallel to the compaction foliation, it pseudomorphs hornblende in the Sterling Valley andesites and the Murchison Volcanic dacites, and as weak to intense pervasive alteration in the Murchison Granite. Chlorite alteration of the granite is accompanied by pyrite and tourmaline and where intense masks the feldspar phenocrysts so only the quartz crystals can be recognised. Chlorite alteration halos are also associated with mafic dykes and sills and with brittle fractures and faults throughout the region.

Chlorite–carbonate±sericite alteration is most common as vesicle fill, hydraulic fracture or vein assemblages. It also occurs as fine grained rims around feldspar phenocrysts in the Mount Black rhyolites and dacites and particularly as moderately strong pervasive alteration in the basaltic lavas, sills and dykes of the Sterling Valley Volcanics and the Henty Dyke Swarm.

Feldspar–chlorite ± epidote alteration is largely associated with the alteration halo surrounding the Murchison Granite and with the more basic rocks of the Sterling Valley Volcanics. Adjacent to the Murchison Granite quartz-phyric rhyolite lavas are moderately feldspar–chlorite–epidote altered, with a blotchy orange and green appearance. The feldspar–chlorite–epidote is also a common vein assemblage forming a fine vein network in areas of strong albitisation.

K-feldspar–chlorite alteration has a fairly limited extent occurring within the Murchison Granite and extending out into the surrounding Murchison Volcanics where it is pervasive and occurs as veins. The originally quartz-felspathic groundmass of the granite has been recrystallised, silicified and partially replaced by K-feldspar. This is associated with disseminated chlorite–epidote–pyrite imparting a mottled pink-green alteration similar to the pink-green quartz–feldspar and sericite–chlorite alteration which is widespread throughout the Mount Read Volcanics. The strong K-feldspar–chlorite–epidote alteration which occurs over an extensive area within the Murchison Volcanics, appears to be spatially associated with the Murchison Granite and an extensive swarm of thick rhyolite porphyry sills. Overprinting this within the granite are areas of intense chlorite alteration.

ALTERATION TEXTURES AND THEIR CONTROLS

The original composition of the volcanic units has exerted strong control on the alteration assemblage and textures formed. There are large variations in alteration textures observed within the rhyolites and dacites and these appear typical of devitrified, hydrothermally altered, subaqueous lavas. The alteration of the andesites and basalts is more uniformly pervasive although varying in intensity. Despite the effect of the primary composition on the alteration style the patterns of permeability and

compositional contrasts formed by primary volcanic processes, quenching, hydration, and devitrification have had a far more striking effect on the final appearance of the rocks. Most notably there is a significant difference between the style of alteration in coherent lavas and sills compared with the alteration textures developed in volcaniclastic deposits. Alteration is strongly controlled by fluid pathways, in the coherent facies it is controlled by the fractures which are generally produced by quenching and flow, perlitic fractures and the distribution of spherulites and flowbanding. Alteration in clastic facies is controlled by the distribution of matrix to clasts.

Many of the coherent lavas and shallow intrusions observed during this traverse displayed two or more superimposed alteration phases. The different alteration phases within the same rock result from different alteration stages, even though the time between stages may be very short. Within flowbanded and spherulitic lavas and sills the quartz-feldspar-rich bands, nodules and devitrification textures (spherulites) have been recrystallised and replaced by feldspar or quartz-feldspar during alteration. In contrast the glassy domains have been replaced by phyllosilicate assemblages dominated by sericite and chlorite. The phenocrysts are more prominent in these darker phyllosilicate-rich bands and give the false impression that the darker domains are more phenocryst-rich than the paler quartz-feldspar domains. The alternating pink and green altered flowbands can resemble folded, thinly bedded, volcaniclastic rocks with crystal-rich phyllosilicate layers and crystal-poor siliceous layers. Spherulites often resemble rounded to sub-rounded volcanic clasts in many of the flowbanded lavas and in densely spherulitic lavas and sills they impart a sandy texture similar to the granular texture of a volcaniclastic sandstone.

In the more massive lavas and sills alteration is controlled by the fluid pathways and has progressed as fronts moving outward from the primary fractures, perlitic fractures and chilled margins towards the unaltered domains. In less altered examples perlitic fractures have been highlighted by phyllosilicate alteration and the enclosed core has been altered by paler quartz–feldspar ± sericite. The alteration has enhanced the fractures creating a contrast in composition and colour between the fractures and the areas that they enclose, resulting in a pseudoclastic texture. The more advanced that the prominent fracture controlled alteration the more matrix supported the resulting alteration texture.

False clastic textures have also produced apparent polymictic appearance where two or more alteration phases exist. The apparent polymictic character can be due to a number of features; phenocrysts in the dark phyllosilicate domains can appear more prominent than those in the quartz-feldspar altered domains; differences in the intensity of alteration and hence colour within individual units; and overprinting alteration assemblages in the same unit. In summary it appears that the alteration in glassy coherent lavas and sills evolves towards matrix supported monomict and polymict textures typical of volcaniclastic massflow deposits. With increasing alteration the false clastic textures converge to produce textures similar to those of welded pyroclastic deposits (Allen, 1988).

In autobreccias and hyaloclastite alteration is also commonly polyphase and the preservation of pre-existing textures is controlled by the intensity of the alteration phases. In weak to moderately altered deposits the primary clastic texture is enhanced by the alteration stages and this often imparts a polymictic appearance. The alteration is matrix and fracture controlled in a similar manner to the fracture controlled alteration in coherent lavas and sills. In more intensely altered units the primary nature of the unit becomes obscured.

In the pumice-rich deposits pumice and shards have been patchily replaced by phyllosilicates and quartz-feldspar domains. The quartz-feldspar domains contain relic uncompacted tube pumice indicating that the deposits were originally unwelded and that the feldspar alteration occurred very early, prior to compaction. The phyllosilicate altered domains have been flattened by compaction producing fiamme-like textures in which only the primary phenocrysts can still be recognised. In areas of strong deformation the flattened tube pumices become stretched and transposed in the cleavage resulting in a foliated fabric which resembles eutaxitic texture in welded primary pyroclastic deposits (Allen, 1988). Hence the results of alteration such as the formation of mechanically weak phyllosilicate mineral assemblages and strong quartz-feldspar in turn

influences subsequent compaction, deformation and metamorphism.

SUMMARY

During this traverse across the northern Mount Read Volcanics outcrops of the Mount Black Volcanics, Sterling Valley Volcanics, Farrell Slates, Murchison Volcanics and the Murchison Granite were examined. The aim was to determine the primary volcanic facies, the alteration stages, primary and secondary controls on the alteration and to eventually identify the alteration processes which have modified the rocks. The transect is bisected by the major Henty Fault across which no units could be correlated.

To the west of the Henty Fault are the Sterling Valley Volcanics and the Mount Black Volcanics. The Sterling Valley Volcanics are a thick sequence of monomictic and polymictic dacitic to basaltic mass-flow breccias and dacitic to basaltic lavas and sills. Conformably overlying these to the west is the Mount Black Volcanics. The Mount Black Volcanics are a package of feldspar-phyric massive, flowbanded and flow brecciated lavas and sills of generally dacitic composition with minor volcaniclastic sediments.

To the east of the Henty Fault are the Murchison Volcanics. The Murchison Volcanics comprise of a pile of quartz-phyric rhyolitic lava domes and sills which have been emplaced into pyroclastic deposits of a similar composition. These deposits have been invaded by a swarm of rhyolite porphyry sills and the Murchison Granite towards the eastern margin. Unconformably overlying the Murchison Volcanics are the Farrell Slates. They are an interbedded package of grey to black siltstones with abundant interbedded feldspar-quartz-mica sandstone turbidites and towards the base interbedded thick pumiceous to crystal-rich rhyolitic mass-flow units which probably represent waning stages of the silicic eruption of the Murchison Volcanics.

All the units have been variably modified and the complex alteration patterns reflect primary and secondary porosity, compositional contrasts in the rocks and the combined effects of different alteration stages. The most common alteration stages within the volcanics were; silicification, domainal quartz-feldspar, domainal sericite-chlorite and sericite-quartz-chlorite, weak fine grained disseminated sericite±quartz, fine grained disseminated carbonate, and patchy, selective and pervasive chlorite alteration. Alteration within and adjacent to the Murchison Granite was dominated by K-feldspar–chlorite alteration and this was surrounded by an alteration halo of feldspar–chlorite–epidote and sericite–chlorite alteration. Overprinting alteration stages have produced a variety of pseudoclastic and apparently polymict textures in both the coherent and clastic units.

REFERENCES

Allen, R.L., 1995. Geological Transect across the Sterling Valley and Murchison Volcanics, Tasmania. Unpubl Pasminco Exploration Rep.

Allen, R.L., 1994. Volcanic Facies analysis indicates large pyroclastic eruptions, sill complexes, synvolcanic grabens, and subtle thrusts in the Cambrian "Central Volcanic Complex" volcanic centre, western Tasmania. Contentious issues in Tasmanian geology. Ed by Cooke, D.R. and Kitto, P.A. in Geol Soc of Aust Abstracts 39, 31–34.

Allen, R.L., 1988. False pyroclastic textures in altered silicic lavas, with implications for volcanic-associated mineralisation. Econ. Geol. 83: 1424–1446.

Anderson, W.B., 1972. The Mount Read Volcanics in the Rosebery–Tullah area, petrology, geochemistry, and possible tectonic significance. Unpub Hons Thesis, University of Tasmania.

Berry, R.F., 1993. Structure and Mineralisation of Western Tasmania. AMIRA Project P291 Final Report.

Brathwaite, R.L., 1969. The geology of the Rosebery ore deposit. Unpubl. Phd Thesis. University of Tasmania.

Cas, R.A.F. and Wright, J.V., 1987. *VOLCANIC SUCCESSIONS: MODERN AND ANCIENT: A GEOLOGICAL APPROACH TO PROCESSES, PRODUCTS AND SUCCESSIONS.* Allen and Unwin: 487 pp.

Corbett, K.D. and Lees, T.C., 1987. Stratigraphic and structural relationships and evidence of the Cambrian deformation at the western margin of the Mt Read Volcanics, Tasmania, Australia. *Aust. J. Earth Sci.* 34: 45–69.

Gifkins, C.C., 1995. Subaqueous silicic volcanism in the Mount Black Volcanics, western Tasmania. AMIRA Project P439 Report 1.

Green, G.R., 1983. The geological setting and formation of the Rosebery volcanic-hosted massive sulphide orebody, Tasmania. Unpubl. PhD thesis, Univ. Tasmania.

Large, R., Doyle, M., Raymond, O., Cooke, D., Jones, A. and Heasman, L., 1996. Evaluation of the role of Cambrian granites in the genesis of world-class VHMS deposits in Tasmania. *Ore Geology Reviews.*

Lees, T.C., 1987. Geology and mineralisation of the Rosebery–Hercules area, Tasmania. Unpubl. MSc thesis. University of Tasmania.

McNeill, A.W. and Corbett, K.D., 1989. Geology of the Tullah–Mt Block area. Mt Read Volcanics Project Geological Report 2.

McPhie, J., Doyle, M. and Allen, R.L., 1993. Volcanic Textures: a guide to the interpretation of textures in volcanic rocks: 198.

Pichler, H., 1965. Acid hyaloclastites. *Bull. Volcanol.* 28, 293–310.
Warmeant, P.J., 1990. The Geology, Geochemistry and Mineralisation of the Mount Black Volcanics. Unpubl. Hons. thesis. University of Tasmania.

Hall Rivulet Canal–Hercules–Mount Read–Red Hills–Anthony Dam

Jocelyn McPhie
Centre for Ore Deposit and Exploration Studies, University of Tasmania

INTRODUCTION

The Hall Rivulet Canal–Hercules Mount Read–Red Hills–Anthony Dam traverse was the first of the planned series of six regional traverses across the Mount Read Volcanics. The traverse involved team members from the three modules (volcanic facies, geochemistry and alteration) and about 15 days in the field. Data from a total of 118 observation and sampling locations were collected. At each, the following information was recorded: lithology, lithofacies, contact relationships; alteration mineralogy, style, distribution and intensity; bedding, cleavage, any other conspicuous structural features; magnetic susceptibility. This integrated approach was deliberately chosen so that interpretation of alteration processes and patterns could be constrained by the stratigraphic, lithofacies and structural context.

The traverse is oriented approximately SW–NE (Fig. 1) and about 20 km long. It was completed in four stages, beginning in the southwest. This report summarises observations regarding the lithofacies associations and alteration present in each of the principal lithostratigraphic units (Corbett 1992) crossed by the traverse:

1. Hall Rivulet Canal: White Spur Formation and Central Volcanic Complex (CVC), including exposure of the contact between these two units.
2. Hercules–Mount Read: Central Volcanic Complex, including the mineralisation at Hercules and the Mount Black Volcanics on Mount Read.
3. Red Hills: Henty Fault, Tyndall Group and Central Volcanic Complex.
4. Anthony Dam: Owen Conglomerate and Tyndall Group.

HALL RIVULET CANAL

This section of the traverse made use of the continuous fresh exposures in the Hydro-Electric Commission canal excavations. The traverse began at the western end of the canal close to the gradational contact between the White Spur Formation (basal part of the Dundas Group) and the rest of the Dundas Group. The western two-thirds of the section is composed of the White Spur Formation and the eastern one-third comprises CVC.

White Spur Formation

Folds and faults are present in the western end of the section but overall, the stratigraphy is younging to the west and for much of the eastern end, also dipping to the west. The formation comprises several very thick units of quartz-bearing volcaniclastic mass-flow breccia and sandstone interbedded with non-volcanic or mixed provenance sandstone turbidites and black mudstone (Fig. 2).

Volcanic lithofacies: Pumice breccia, pumice-lithic breccia, crystal-rich sandstone, pumiceous sandstone, mud-matrix pumice breccia, volcanolithic sandstone (Figs 2, 3).

These lithofacies occur in graded units several to 10s m thick and are composed of variable proportions of relict pumice, crystals (quartz, feldspar), lithic clasts and mudstone clasts. The lower parts of some units (HRC 96-4, HRC 96-8) have very dark grey, very fine chloritic matrix and commonly contain abundant large plastically deformed mudstone clasts. The matrix is most probably mud-rich and derived from disintegration of poorly consolidated mud intraclasts eroded from the underlying substrate and incorporated in the volcaniclastic mass flow. One example

(HRC 96-25B) contains rounded quartz-phyric rhyolite and sparse granitoid clasts.

Non-volcanic lithofacies: Black mudstone, micaceous and lithic sandstone, pebbly sandstone, grey siltstone.

Black mudstone and grey siltstone are laminated to thinly bedded, and interbedded with very thin and thin beds of lithic sandstone. Micaceous lithic sandstone and pebbly sandstone occur in graded and massive medium to thick beds (e.g. HRC 96-11). Conspicuous components are muscovite, biotite, quartz, feldspar and metamorphic rock fragments.

Central Volcanic Complex

Grading and bedding in pumice breccia in the CVC near the contact with the White Spur Formation indicate that this part youngs and dips to the west. The CVC comprises very thick units of feldspar-phyric pumice breccia and sandstone, syn-volcanic felsic intrusions and felsic lavas (Fig. 4). Non-volcanic lithofacies are very minor.

Volcanic lithofacies: Feldspar-phyric pumice breccia and sandstone; tuffaceous mudstone; quartz-phyric rhyolite?, feldspar>>quartz-phyric dacite?, feldspar-phyric dacite, rhyolitic breccia, dacitic breccia.

Pumice breccia units are graded to massive and very thick (several to 10s m). The tops of graded units are composed of diffusely stratified pumiceous sandstone and mudstone. In weakly altered samples, closely packed tube pumice clasts and sparse lithic clasts can be recognised. Sills of feldspar + quartz + hornblende–phyric rhyolite (?) and feldspar + hornblende >> quartz–phyric dacite (?) intrude the top of the CVC (Fig. 4) and have peperitic contacts. Feldspar-phyric rhyolite (?) and monomict rhyolitic breccia occur lower in the CVC.

Non-volcanic lithofacies: Black laminated to very thinly bedded mudstone.

Summary of alteration facies

White Spur Formation: In general, alteration is weak to moderate, and pervasive or else blotchy and mottled or banded. Black and dark grey mudstone are commonly pyritic, with the pyrite (py) being both disseminated and concentrated in laminae (e.g. 96-24). Carbonate (co) occurs in the very thin beds of fine to coarse sandstone (e.g. 96-10B) that are interbedded with mudstone. Some medium to thick beds of coarse sandstone and pebbly sandstone are strongly carbonate altered, in some cases with a zonation from carbonate in the centre of the bed to quartz–sericite–pyrite (q–ser–py) at the margins (e.g. 96-15). Interbedded feldspar>>quartz crystal-rich sandstone and black mudstone at the base of the White Spur Formation (e.g. 96-28) show pronounced alteration. An assemblage of ser?–co ± py occurs in the crystal-rich sandstone beds whereas the black mudstone contains ser ± chl ± py.

Fiamme in pumice breccia units are dark green and composed of chlorite and/or sericite. Feldspar phenocrysts in pumice clasts and feldspar crystal fragments are variably altered to co-ser. Pumiceous and crystal-rich matrices of sandstone and pumice breccia units contain a variety of alteration assemblages: chl–ser, ser–chl–co, ser–co, ser–q, ser–q ± pyrophyllite, q–co. Units that have mud-rich matrix (e.g. 96-4, Fig. 2) are strongly chloritic. Parts of a very thick interval of graded feldspar-crystal rich sandstone (Fig. 2) are distinctly though diffusely banded (e.g. 96-13). The banding comprises pinkish f > chl–ep layers alternating with green chl±ep layers and is bedding parallel but not obviously defined by primary grain size variations. The upper part of a thinner unit that occurs stratigraphically higher (96-7) also shows banding. In this case, the bands comprise grey q–py versus green q > chl layers.

Central Volcanic Complex: In general, the alteration in the pumice breccia is moderate to strong and pervasive or strongly domainal, either banded or mottled and patchy. The principal alteration assemblages are ser–co, ser–chl, f–chl–epid–leuc–mag. Feldspar phenocrysts in pumice clasts are commonly cp-altered. Intervals of coherent rhyolite and dacite are weakly altered, involving chl–ser, ser–q±co and f>>chl–mg assemblages. Fiamme in pumice breccia units are composed of ser and ser–chl assemblages.

Black mudstone is weakly pyritic and ser–q-altered.

White Spur Formation–Central Volcanic Complex contact

The contact is very well exposed along Hall Rivulet Canal and is both conformable and gradational. Interbedded mudstone and feldspar crystal-rich sandstone and pumiceous sandstone at the base of the White Spur Formation overlie graded feldspar-phyric pumice breccia units of the CVC. Although

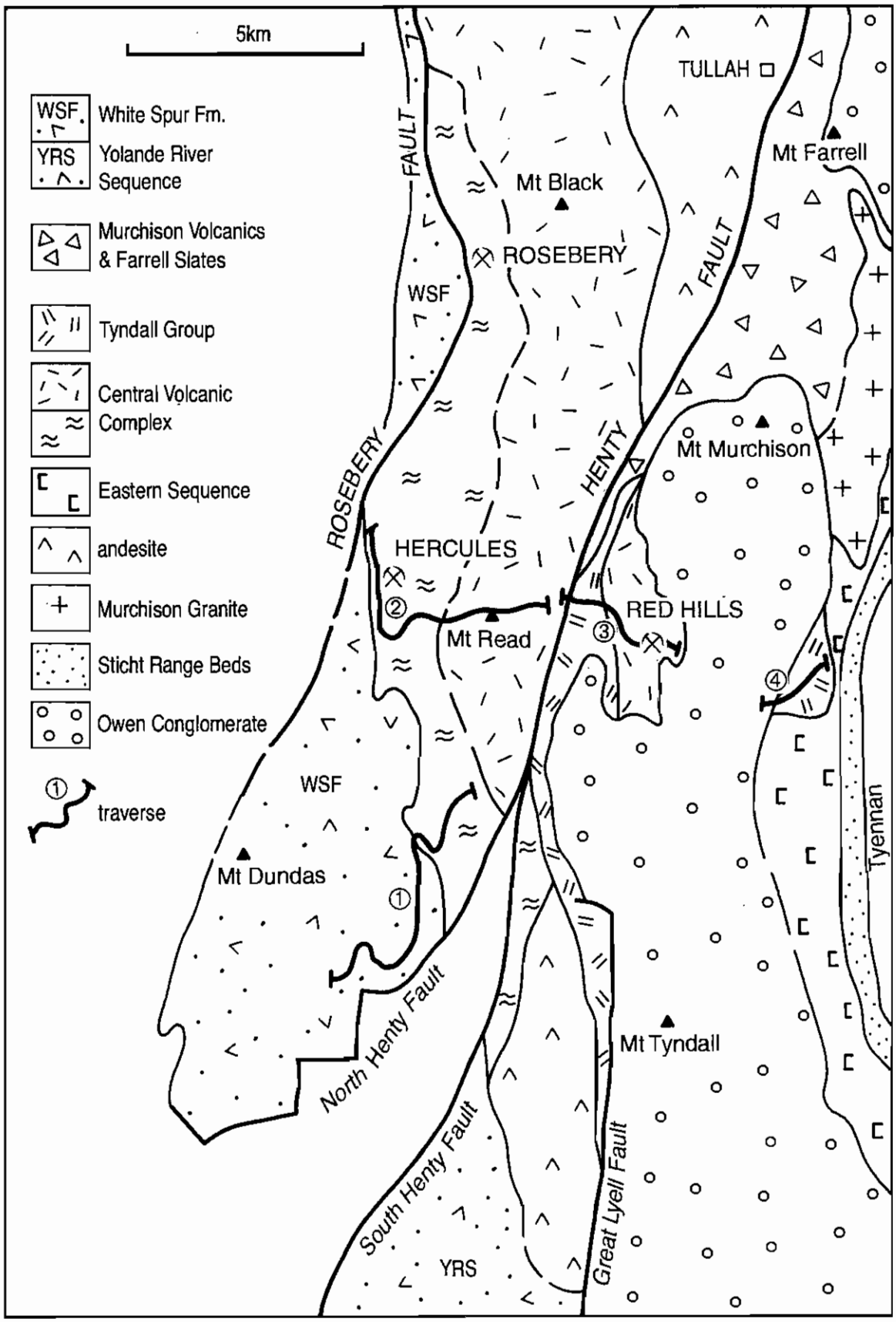
5km
WSF White Spur Fm.
YRS Yolande River Sequence
Murchison Volcanics & Farrell Slates
Tyndall Group
Central Volcanic Complex
Eastern Sequence
andesite
Murchison Granite
Sticht Range Beds
Owen Conglomerate
① traverse
TULLAH
Mt Farrell
Mt Black
ROSEBERY
FAULT
WSF
HENTY
Mt Murchison
ROSEBERY
HERCULES
RED HILLS
Mt Read
Tyenman
WSF
Mt Dundas
North Henty Fault
Mt Tyndall
South Henty Fault
Great Lyell Fault
YRS

Figure 1

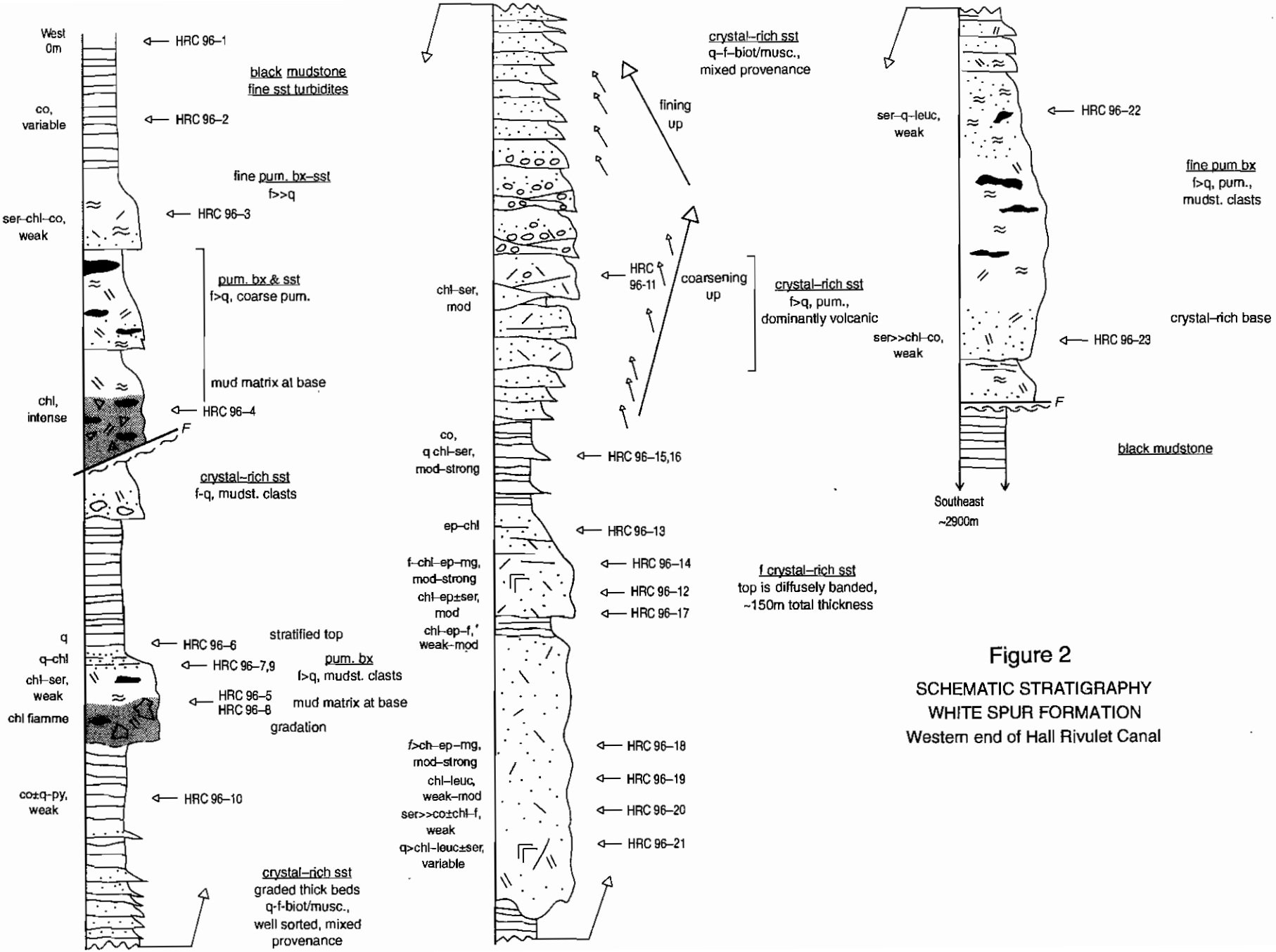

Figure 2

SCHEMATIC STRATIGRAPHY
WHITE SPUR FORMATION
Western end of Hall Rivulet Canal

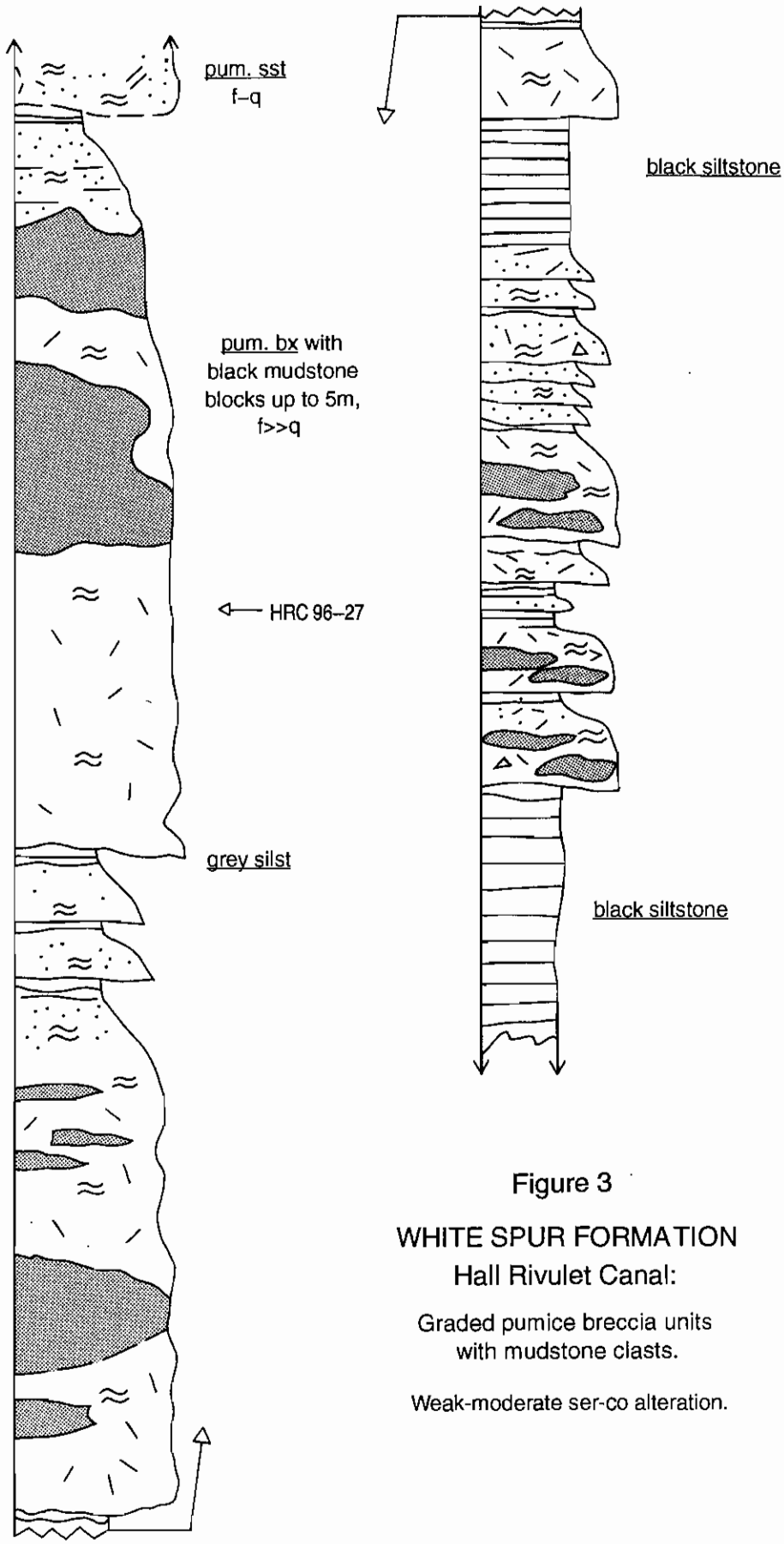

Figure 3

WHITE SPUR FORMATION
Hall Rivulet Canal:

Graded pumice breccia units
with mudstone clasts.

Weak-moderate ser-co alteration.

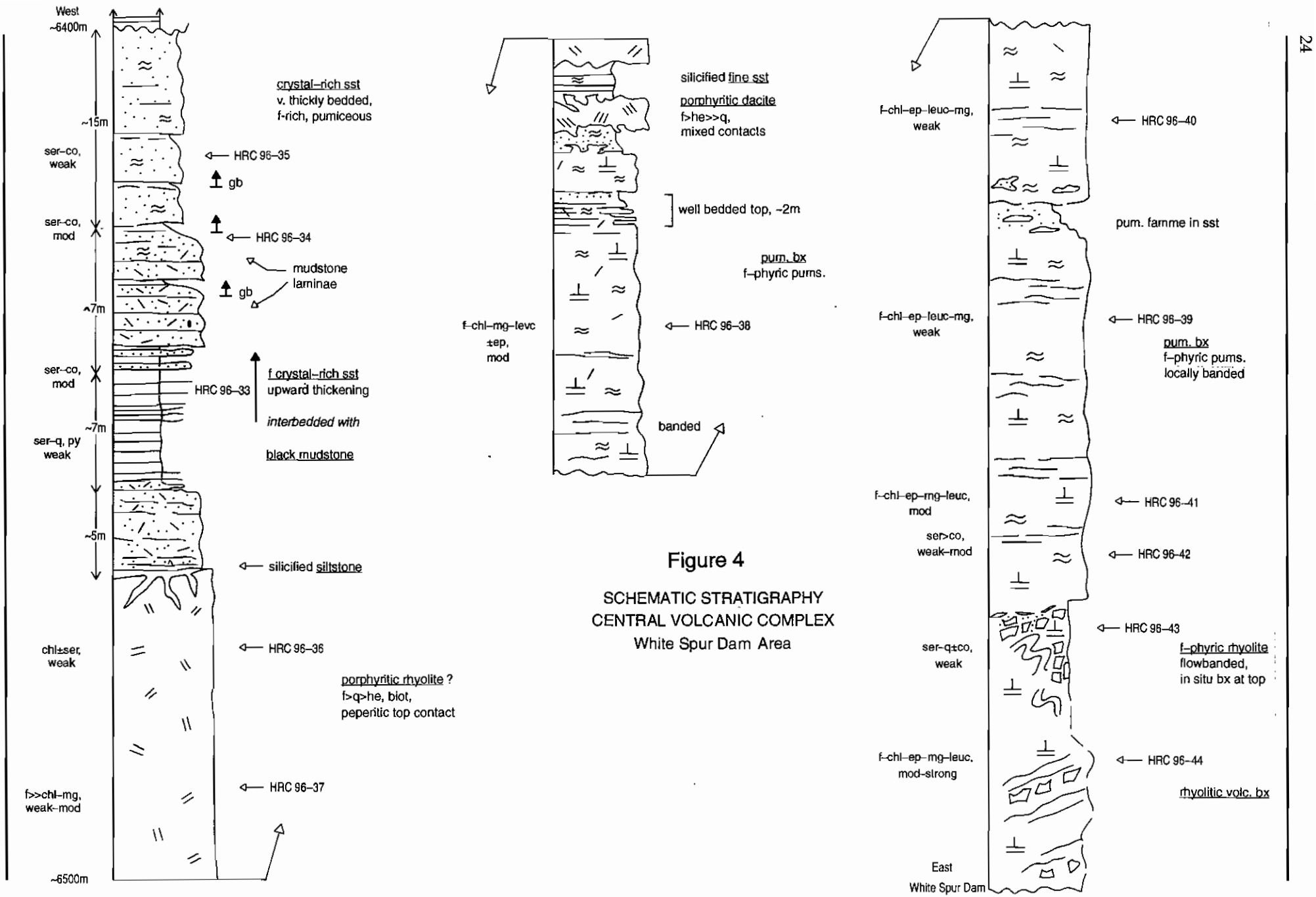

Figure 4

SCHEMATIC STRATIGRAPHY
CENTRAL VOLCANIC COMPLEX
White Spur Dam Area

conformable and gradational, the contact marks changes in alteration intensity, composition and the dominant lithofacies: in the CVC, alteration varies from moderate to strong, whereas alteration is very weak to moderate in the White Spur Formation; volcaniclastic units in the CVC are feldspar-phyric whereas most units in the White Spur Formation have both quartz and feldspar; the CVC includes both volcaniclastic and coherent lithofacies whereas the White Spur Formation comprises substantial sections of mixed provenance (partly Precambrian basement derived) and non-volcanic sedimentary lithofacies.

Sills that intrude the finer, stratified pumiceous sandstone and mudstone top of the CVC pumice breccia are somewhat less altered than the host CVC, though clearly syn-volcanic in having peperitic contacts.

HERCULES–MOUNT READ

This traverse includes the footwall to the Hercules massive sulfide deposit, the Hercules mineralisation, the hangingwall and the Mount Black Volcanics on Mount Read (Fig. 1), all of which are part of the CVC. Natural outcrop, road and mining excavations are abundant although discontinuous and some contact relationships were not established. The hangingwall includes intervals in which the lithologies are very similar to those in the footwall and may in fact be sections of the footwall repeated by thrust faults (Allen, unpublished). That complication aside, overall the section appears to young and dip to the east; however, many parts yielded only scant bedding data. The CVC is again dominated by volcanic lithofacies. The footwall comprises very thick units of pumice breccia and the hangingwall is composed of a varied section of volcaniclastic sandstone and breccia overlain by coherent rhyolite and rhyolitic breccia (Mount Black Volcanics).

Hercules footwall and massive sulfide mineralisation

The footwall comprises very thick (10s m to >100 m) massive to graded feldspar-phyric pumice breccia units. Pumice clasts have tube vesicle texture at random orientations, indicating that the pumice breccia was originally non-welded. Sparse lithic clasts are present and some units are characterised by distinctive lithic cast populations. Allen (unpublished) recognised that the pumice breccia has a diagenetic compaction foliation delineated by lenticular phyllosilicate-rich domains (fiamme) subparallel to bedding and overprinted by the steeply dipping regional cleavage (e.g. MR-48).

The Hercules massive sulfide mineralisation occurs near the top of a very thick interval of pumice breccia that is overlain by interbedded black mudstone and crystal-rich sandstone. The top of the footwall is composed of stratified fine pumice breccia, pumiceous sandstone and siltstone (e.g. MR 96-56).

Hercules hangingwall

The hangingwall section includes graded quartz and felspar, crystal-rich pumiceous breccia and sandstone units interbedded with thin intervals of mudstone. Some of the volcaniclastic units contain large mudstone clasts. In addition, possibly fault-bounded sections of feldspar-phyric pumice breccia occur in the hangingwall (e.g. MR 96-60). These intervals are compositionally and texturally very similar to the footwall pumice breccia and also have similar alteration assemblages and style.

Mount Black Volcanics

The Mount Black Volcanics are dominated by feldspar-phyric flow banded and massive rhyolite and monomict rhyolitic volcanic breccia (e.g. MR 96-66), interbedded with thin intervals of laminated to thinly bedded grey siltstone and sandstone (eg. MR 96-67B). Quartz-phyric and feldspar-phyric rhyolitic intrusions also occur (e.g. MR 96-68, MR 96-71). Near the eastern end of the traverse (MR 96-73), the section includes a thin (<2 m) but complex association of thinly bedded rhyolitic siltstone and sandstone with thick beds of coarse rhyolitic lava and pumice breccia.

Summary of alteration facies

Footwall feldspar-phyric pumice breccia and similar pumice breccia in the hangingwall are affected by weak to intense alteration, comprising assemblages of: ser–co, ser–q–co, ser–f–co, q–ser±co. Dark green fiamme are composed of sericite and chlorite. Feldspar crystals are altered to co–ser and co. At the mineralisation, alteration is intense, pervasive and

poddy comprising ser–co, ($MnCO_3$), q–ser and chl-dominated assemblages.

Alteration in the hangingwall (apart from the feldspar-phyric pumice breccia interval) is generally weak to moderate, involving chl>ser, f–chl, chl>ser–co, ser–f–co, ser–q–co, f–ser–chl–co and ser±co.

Comparison with CVC on Hall Rivulet Canal

The footwall to the Hercules mineralisation strongly resembles the topmost section through the CVC exposed along Hall Rivulet Canal in terms of lithofacies, composition and alteration style and intensity. A second point of comparison between the two traverses is the transition from feldspar-only volcaniclastic units (CVC on Hall Rivulet Canal and the footwall to Hercules) to a quartz-bearing volcaniclastic succession (White Spur Formation on Hall Rivulet Canal and the hangingwall to Hercules).

RED HILLS

This section of the traverse began in mafic intrusions? just west of the Henty Fault and continued eastward through porphyritic rhyolite regarded as Tyndall Group (Corbett 1992) and CVC at Red Hills, to a point just west of the cover of Owen Conglomerate at the eastern end (Figs 1, 5). The traverse used track exposures and natural outcrops which are very good at Red Hills. Both the Tyndall Group and CVC sections are dominated by felsic porphyritic rocks that include coherent and clastic facies. One narrow interval of bedded black mudstone occurs in the CVC. Bedding and facing data are very limited in the thick porphyritic units, and relationships between and within the main lithostratigraphic units are poorly known.

Principal lithofacies

The Tyndall Group occupies the western end of the section and is composed dominantly of quartz + feldspar–phyric rhyolite, including flow banded and in situ brecciated facies. Neither non-volcanic nor volcaniclastic lithofacies were encountered. At least three texturally distinct rhyolite intervals are present. The Red Hills are made of massive to locally flow banded and brecciated feldspar-phyric rhyolite or dacite, together with one narrow interval of strongly cleaved, weakly pyritic black mudstone (MR 96-93). Quartz+feldspar-phyric rhyolite occurs at the eastern end of the traverse (MR 96-103). In most cases, contacts between the units are not exposed.

Alteration facies

Alteration in the quartz-phyric rhyolite units ranges from weak to moderate, involving assemblages of ser–q, f–chl, q–ser±chl, f–chl>co±ser, and locally more intense chloritic alteration (e.g. MR 96-88). On the western flank of the Red Hills (MR 96-89 to 96-92), alteration has in places generated apparent fiamme defined by ser–chl lenses, and patchy to mottled pink-green f–chl assemblages. The most intense alteration mainly occurs across the crest of the Red Hills (MR 96-94, MR 96-95, MR 96-96 to 96-101). The assemblages recognised are:- q–ser–py, chl–q, f–chl±q–py, f>chl and f–chl±q. Farther east, alteration is generally weak to moderate and the dominant assemblages are f–q–chl and q–f>>chl.

ANTHONY DAM

This section of the traverse began east of the end of the Red Hills section where the Mount Read Volcanics once again emerge from intervening cover of Owen Conglomerate (Fig 1). The western end of the section is evidently within the Tyndall Group (Corbett 1992) and includes exposure of the Owen Conglomerate–Tyndall Group contact. The eastern end of the section may extend into the Eastern Sequence. Uncertainty arises because of the difficulty of distinguishing between the Tyndall Group and the Eastern Sequence in places where contact relationships are not exposed. Very good exposures are available around the Anthony Dam but outcrop at the eastern end is limited to patchy excavations along tracks.

Tyndall Group–Owen Conglomerate contact and Tyndall Group lithofacies

The western end of the section begins in the Owen Conglomerate which comprises very thickly bedded, westerly dipping cobble conglomerate. Clasts are well rounded and the predominant clast type is quartzite. The Owen Conglomerate is in contact to the east with weathered porphyritic dacite (?) that has a phenocryst

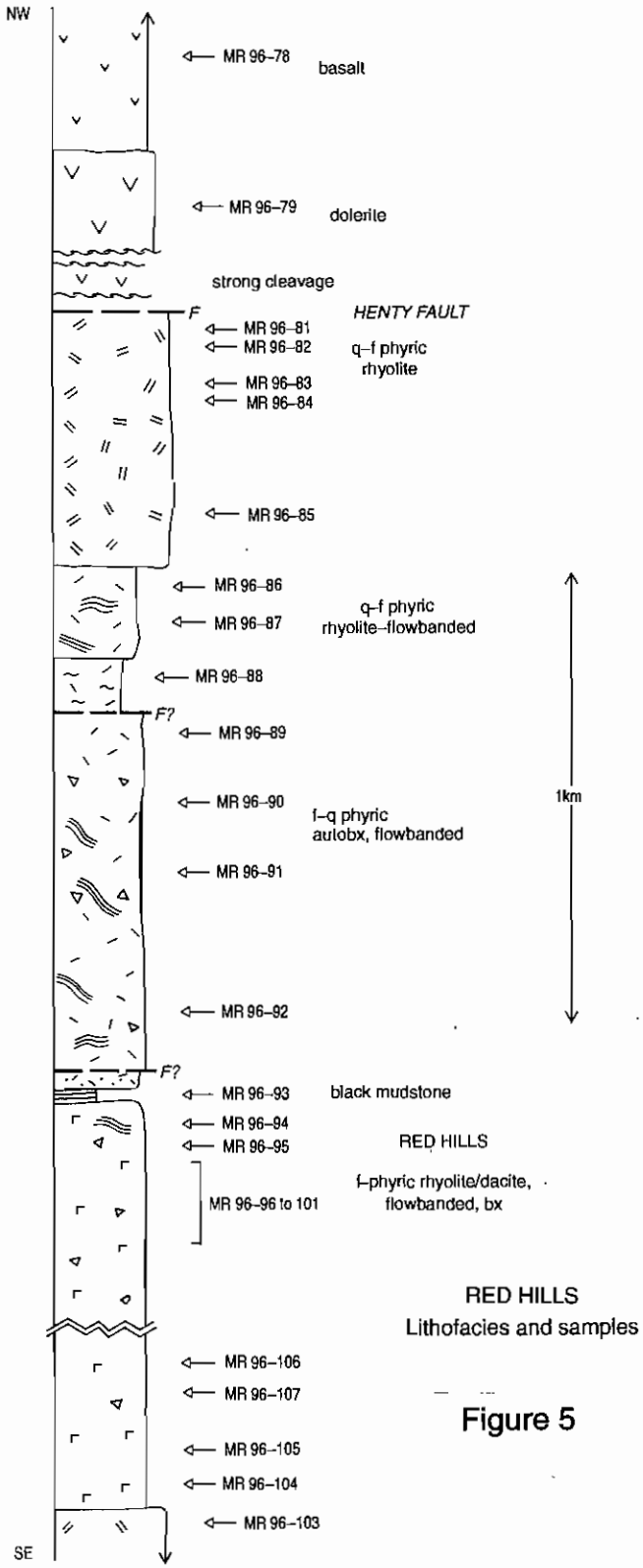

RED HILLS
Lithofacies and samples

Figure 5

assemblage of biotite >> hornblende, quartz and feldspar. The contact is unsheared and interpreted to be an unconformity that is oriented subparallel to bedding the Owen Conglomerate.

Outcrop of the dacite continues about 20 m to the east and its eastern contact with diffusely stratified pebble to boulder polymict conglomerate (Tyndall Group, MR 96-108) is not exposed. The clast population in the polymict conglomerate includes quartz ± feldspar – phyric rhyolite, quartz + feldspar > biotite – phyric rhyolitic porphyry, medium to coarse porphyritic granite, fine even-grained granite, hematite and quartz–hematite. The granitoid clasts are the largest (up to 1 m) and well rounded. Rhyolite clasts are also well rounded. Hematite clasts range up to 10 cm across and are moderately rounded. The matrix comprises coarse, volcanolithic sandstone. Pebbly sandstone, pebble and cobble conglomerate farther east contain a similar range of clast lithologies although the granitoid and hematite clasts decrease in size and abundance (e.g. MR 96-112), and are dominated instead by rhyolitic clasts.

Coherent porphyritic lithofacies (e.g. MR 96-113, 114, 116) are interleaved with the volcanogenic sedimentary lithofacies at the eastern end of the section. The principal lithofacies are feldspar-phyric rhyolite, quartz-phyric porphyritic microgranite and quartz+feldspar-phyric rhyolite. Contacts are not exposed and locally intense cleavage has modified the coherent textures, generating psuedoclastic textures (e.g. MR 96-117).

Strongly deformed quartzite block

At MR 96-109, strongly cleaved, fine grained quartzite outcrops although no contacts are expected. In addition to the strong cleavage, brittle fractures and zones of intense shearing occur. The degree of deformation and the lithofacies are different from those typical of the Mount Read Volcanics. One possibility is that this block is a previously unrecognised fault bounded and structurally emplaced block of Precambrian (Tyennan?) basement.

Alteration facies

Volcanic clasts in the polymict conglomerate lithofacies show patchy hematite (he) alteration whereas the granitoid clasts are pervasively sericite-altered. The matrix of the Conglomerate is typically weakly ser- or he- altered. Chlorite alteration is locally strong and pervasive (e.g. MR 96-118).

The coherent porphyritic lithofacies are affected by alteration that ranges from weak to moderate, ser–chl–q, f–chl–ser and chl–ser–ep assemblage to strong patchy chl- or mg- alteration.

The strongly deformed Precambrian (?) block has disseminations, patches and veins of magnetite.

ON-GOING INVESTIGATIONS

Samples are currently being sectioned and analysed. On-going studies involve petrography and analysis of the whole rock and probe data in order to refine and constrain the field observations. In addition, the traverse data is being converted to cross-sections and graphic stratigraphic logs upon which details of the alteration facies will also be recorded.

SUMMARY OF IMPORTANT RESULTS

1. Along Hall Rivulet Canal, the White Spur Formation and Central Volcanic Complex are conformable, although alteration is more intense in the CVC than in the White Spur Formation.

2. The Mount Black Volcanics and Red Hills Volcanics are dominated by coherent lithofacies in contrast to the White Spur Formation, Hercules footwall and Hercules hangingwall, all of which include both volcaniclastic and non-volcanic sedimentary lithofacies.

3. Conglomerate in the Tyndall Group at Anthony Dam contains abundant Cambrian granitoid and hematite clasts. The granitoid clasts are texturally dissimilar from the nearby Murchison Granite.

4. An unconformity between the Tyndall Group and the Owen Conglomerate is exposed at Anthony Dam.

5. A strongly deformed metasedimentary block that could be Precambrian basement occurs near the Anthony Dam.

Jukes Road: Preliminary volcanic facies analysis and alteration petrography

Bill Wyman, Rod Allen and Nathan Duhig
Centre for OreDeposit and Exploration Studies, University of Tasmania

INTRODUCTION

Jukes Road is located approximately 9 km south of Queenstown and cuts through sections of the Western Sequence (Yolande River Sequence), Central Volcanic Complex (CVC) and Eastern Sequence (Eastern Quartz Phyric Sequence (EQP) and Tyndall Group) (Fig. 1). The Jukes Pty. Cu–Au prospect is located along the and has been the subject of research by others most recently being Doyle (1990) and White (1975). Road cuttings along Jukes Road provide an excellent opportunity to examine a variety of alteration assemblages in Central Volcanic Complex rocks as well as alteration associated with the Jukes Prospect.

As part of AMIRA project P.439, over 100 ten-metre long chip samples were collected along a 5.7 km traverse along the Jukes Road in early 1995. Rock chip and whole rock samples were collected at 500 m intervals outside the Jukes prospect and at 10 m intervals within the prospect. In March 1996, the authors spent three days on the Jukes Road examining the volcanic facies and regionally developed alteration assemblages in the CVC and EQP rocks. During the 1995 traverse, 87 selected chip samples and 32 selected hand specimens were collected and analysed, and 65 thin sections were prepared. During the March 1996 traverse an additional 15 rocks were collected and are in the process of being prepared for thin section petrography and whole rock geochemistry.

Descriptions of volcanic facies and alteration assemblages presented in this paper are based on the results of detailed field and petrographic examinations. Details of the facies descriptions and regional alteration features are the result of the 3 days work in March 1996. Detailed descriptions of alteration styles at the Jukes prospect are the result of previous work by Bill Wyman. Where appropriate, geochemical data that supports some of the interpretations is presented.

GEOLOGY OF THE JUKES ROAD

Rocks of the Western Sequence (Yolande River Sequence), Central Volcanic Complex (CVC) and Eastern Sequence (Eastern Quartz Phyric Sequence and Tyndall Group) are all well exposed along Jukes Road. For the purposes of this traverse, rocks of the Western sequence were not examined, and rocks of the Tyndall Group were only briefly examined and not sampled. Neither unit will be described in this paper. Figure 1 shows a simplified geological map of the Jukes Road area and sample locations for samples to be studied as part of this study. A graphic log depicting the more detailed geology of both the entire Jukes Road as well as the Jukes Prospect is shown as Figure 2a, b. The Eastern Quartz-Phyric Sequence (EQP) lies between Tyndall Group volcaniclastic rocks to the east, and CVC rocks to the west. The dominant facies in the EQP is quartz-feldspar phyric volcaniclastics, with subordinate quartz-feldspar phyric lavas. The eastern contact between the EQP and the Tyndall Group is not exposed. The western contact between the EQP and the CVC rocks is a major fault visible on the ground and on aerial photographs. Rocks of the CVC appear to interfinger with rocks of the Yolande River Sequence to the west in an apparently conformable contact. Rocks of the CVC along Jukes Road are dominantly feldspar-phyric lavas and pumiceous volcaniclastics and mass-flow deposits with a minor tuffaceous/sedimentary facies. In the following sections, facies of the EQP and CVC will be discussed in more detail.

Eastern Quartz-Phyric Sequence (EQP)

Quartz-Feldspar-Phyric Rhyolite (Dacite?)

Quartz-feldspar-phyric rhyolite is the dominant lithology in the EQP. It is exposed along Jukes Road for over 1 km, in an area between CVC and Tyndall Group rocks. Quartz-feldspar-phyric rhyolites have well developed tectonic cleavage and contain up to 30% feldspar and quartz phenocrysts. Average crystal size is 0.5 to 1 mm. The groundmass has a sandy texture. Lithic clasts of quartz-feldspar-phyric volcanic rocks are common. The rhyolites are altered to sericite with minor potassium feldspar (K-feldspar) chlorite, pyrite, and carbonate. Chip sample geochemistry suggests that some of the rocks may be dacitic in composition (Fig. 3). This unit is interpreted to be a massive moderately crystal rich volcaniclastic sediment or mass flow.

Quartz-Feldspar Porphyry

The quartz-feldspar porphyry facies of the EQP is only exposed for a short distance along Jukes Road where it is in fault contact with the CVC (Fig. 1).

The quartz-feldspar porphyry facies is interpreted to be coherent lava. Quartz and feldspar crystals are 1–3 mm in size and comprise 10% of the porphyry. Quartz crystals are strongly embayed. The groundmass is fine grained. The unit contains a few scattered spherulitic rhyolite clasts.. Tectonic cleavage is well developed and has dismembered many crystals. Alteration is dominated by sericite with subordinate K-feldspar and chlorite.

Central Volcanic Complex (CVC)

Columnar Jointed Feldspar-Phyric Rhyolite

Columnar jointed feldspar-phyric rhyolite is the primary host unit to the Jukes prospect and is in fault contact with the Eastern Quartz-Phyric Sequence. This unit is exposed for over 2 km along Jukes Road and dips to the north. The rocks are locally spherulitic, and contains 5–7% feldspar crystals in a fine grained groundmass. Locally small amygdales, lithophysae and tuff/ash inclusions can be found. Well developed columnar joints are common (Plate 1A). Actual tops and bottoms of individual sills or flows have not yet been identified, however it is believed that this unit is probably a stack of sills or flows. Regional cleavage is poorly developed in unaltered rocks but is well developed in rocks with chlorite alteration.

Alteration assemblages that occur vary along the road, with sericite ± chlorite alteration dominant in the west. Alteration becomes more chloritic and K-feldspar dominant near numerous quartz-feldspar ± biotite porphyry dykes in the Jukes Prospect area. Chlorite has overprinted K-feldspar and K-feldspar has overprinted chlorite indicating multiple stages of overprinting alteration assemblages. Most of the samples contain varying amounts of magnetite, with the highest abundances in the more chloritically altered rocks. Magnetite also occurs as veins in the matrix of several breccia bodies that are described below.

Tuffaceous-Ash/Sandstone Facies

The tuffaceous-ash/sandstone facies includes thin tuffaceous-ash horizons interbedded with thin tuffaceous-sandstone and pumiceous volcaniclastic horizons. The unit as a whole is approximately 230 m thick. Graded bedding is preserved in some of the thin sandstone horizons and facing directions can be interpreted. Regional cleavage is well developed in this unit and is subparallel or slightly oblique to bedding. Cleavage is best developed in the more sericitic or chloritic units.

This facies is most altered to sericite, with only local chlorite alteration. Silicification is weak in most samples, however in some of the more tuffaceous horizons, silicification has produced light pink or light green cherts.

Feldspar-Phyric Rhyolitic Volcaniclastics and Mass-Flow Deposits

Feldspar-phyric rhyolitic volcaniclastics and mass-flow deposits are restricted to the western part of the CVC, between the sedimentary section described above and the Yolande River Sequence to the west. Plate 1B shows an outstanding example of a mass flow deposit. More typical volcaniclastic rocks contain 10–20% feldspar crystals up to 1–2 mm in diameter. Relict feldspar-phyric pumice clasts formed well developed fiamme-like lenses. Undeformed pumice textures are rare.

One horizon in this unit is distinct from all of the others. It contains excellent tube pumice breccia

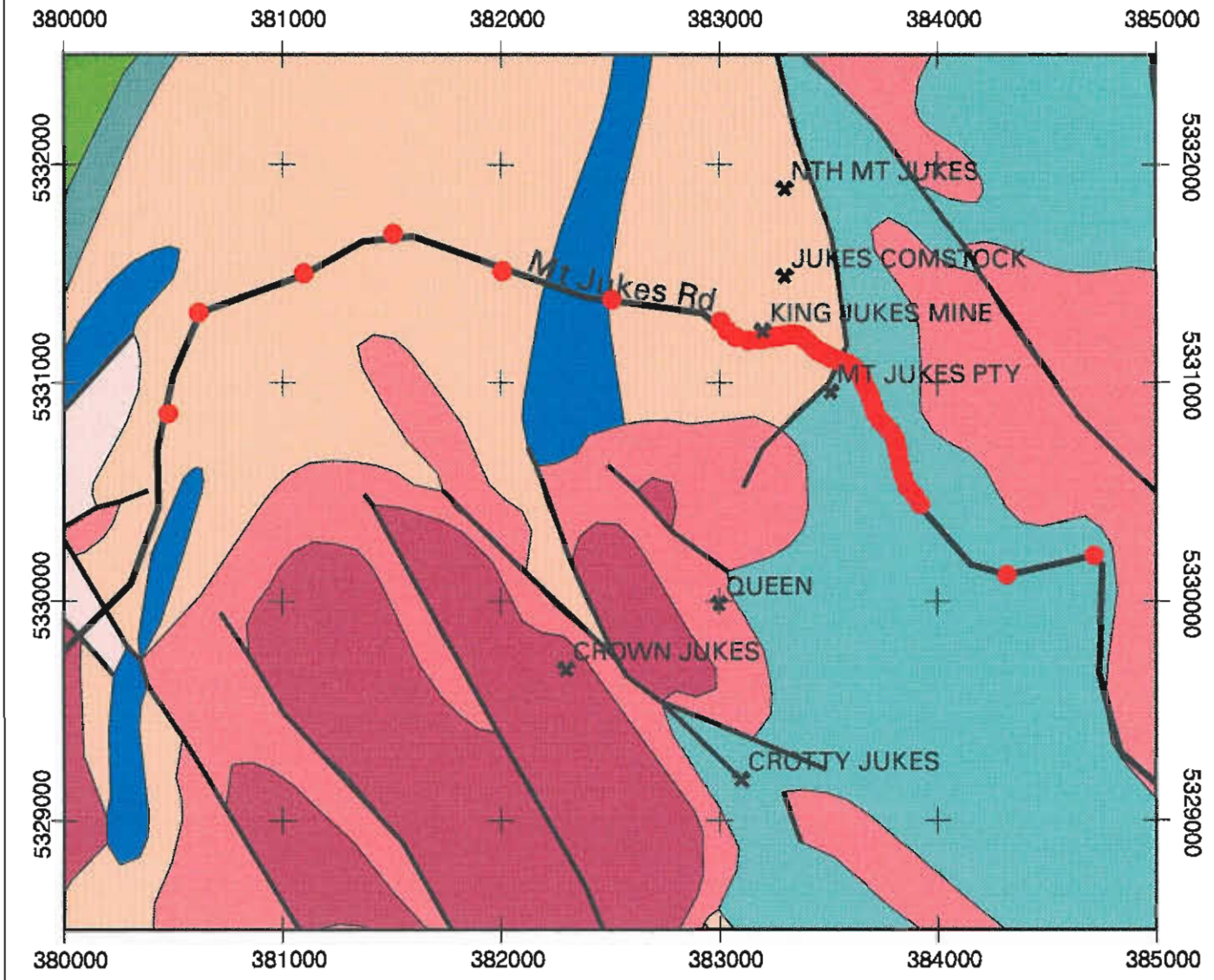

Figure 1

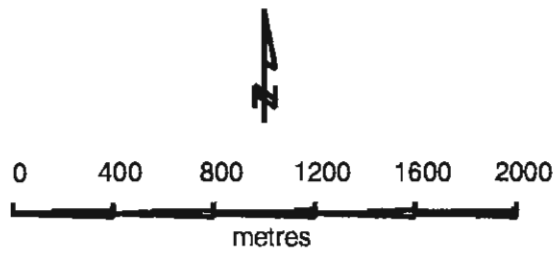

Grid: Australian Map Grid, Zone 55.

JUKES AREA
Simplified Geology & Sample Location Map

- Owen Conglomerate upper sandstone
- Owen Conglomerate (undiff.)
- Tyndall Group
- CVC feldspar-phyric volcanics
- CVC sedimentary rocks
- Western sequence volcanics & volcaniclastics
- felsic porphyry

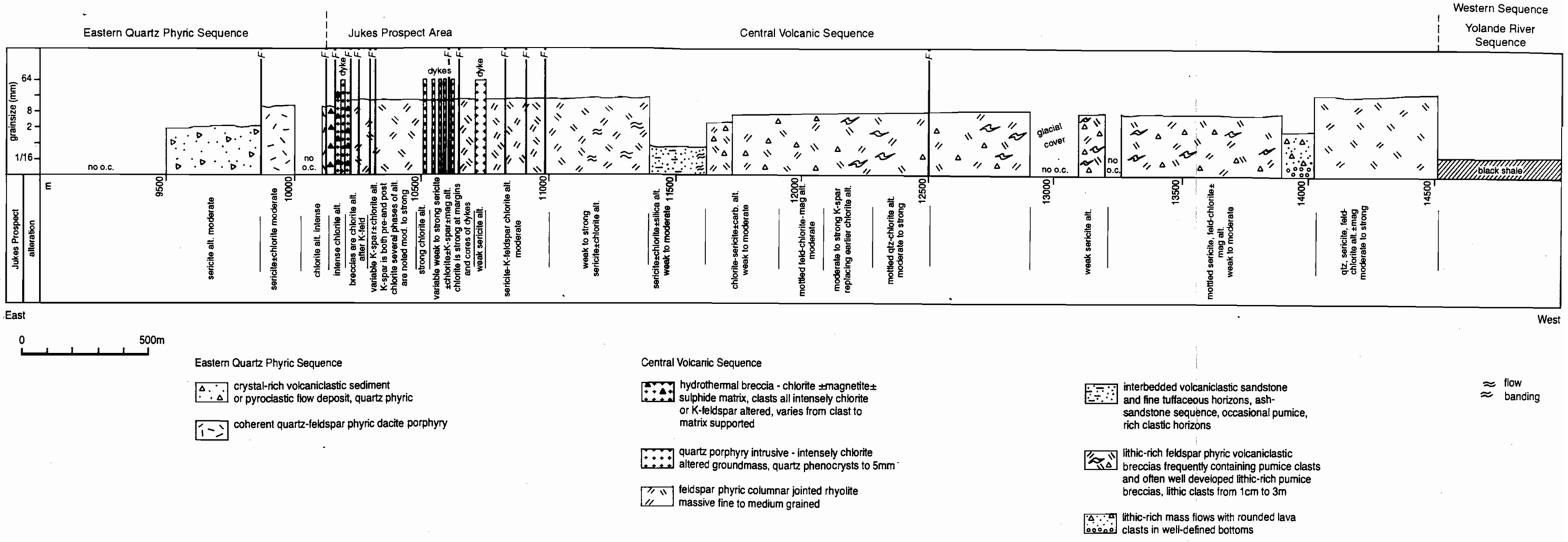

Figure 2a: Graphic presentation of the geology and alteration along the Jukes Road

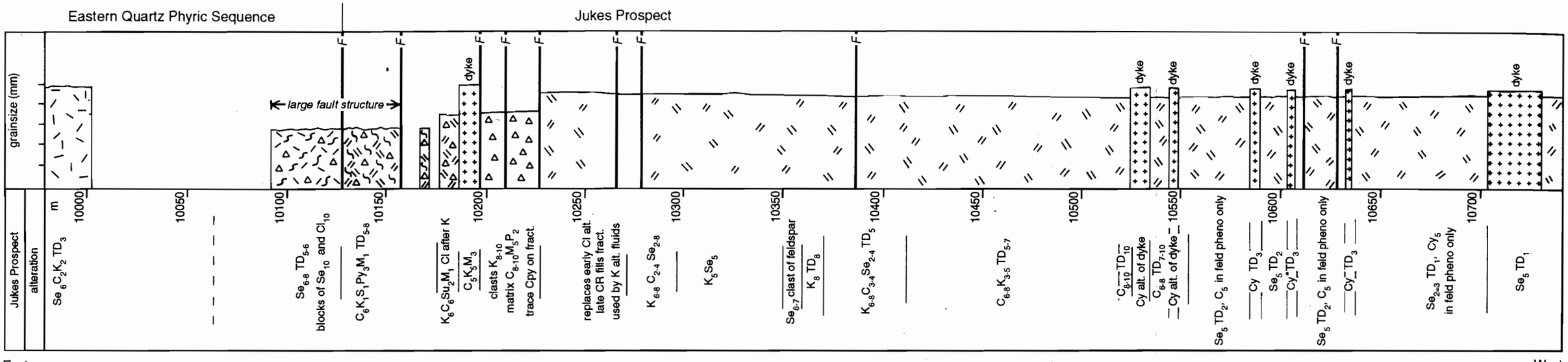

Eastern Quartz Phyric Sequence

- coherent quartz-feldspar dacite porphyry
- brecciated and sheared quartz-feldspar dacite porphyry, alteration varies from Se_{5-10} to Cl_{5-10}

Central Volcanic Sequence

- brecciated, sheared feldspar phyric rhyolite
- brecciated, feld-phyric rhyolite breccia contains rounded clasts of quartz porphyry dyke rx
- quartz ± feld porphyry dyke

- probable polylithic hydrothermal breccia matrix to clast supported clasts almost always K_{8-10}, matrix usually $Cl_{8-10}M_5P_2$, clasts angular, little transport
- feldspar phyric (± quartz) rhyolite columnar jointing well developed in least altered areas

Figure 2b: Graphic presentation of the geology and alteration at the Jukes Prospect

textures and altered pumice and lithic clasts in a matrix of 5–10% orange feldspar ± quartz. This unit looks similar to the Rosebery–Hercules feldspar-phyric pumice breccia, except for the presence of more lithic clasts. Pumice lithic clasts are generally large and have a pink alteration mineral (K-feldspar or albite ?).

Regional cleavage is well developed in the facies due to the pervasive sericite and chlorite alteration. Chlorite/K-feldspar alteration is well developed, and in one area forms distinct pink and green banding characteristic of diagenetic alteration seen elsewhere in the CVC (White, 1996). In some areas, pink K-feldspar occurs as rims around green chlorite cores in lithic clasts, suggesting that K-feldspar formed after the chlorite alteration. The pink feldspar is most likely albite, as described by Allen and Cas (1990). Magnetite is most abundant in the chloritically altered samples and is absent in the sericitic and K-feldspar altered phases. This chlorite–magnetite association is common along Jukes Road but geochemically is highly unusual, as chlorite formation should be destructive to magnetite (D. Cooke, per. comm.).

Quartz-Feldspar ± Biotite Porphyry Dykes

Dykes of quartz-feldspar porphyry crosscut the columnar jointed feldspar-phyric rhyolite at numerous localities. Seven dykes have been mapped along Jukes Road. The contacts with feldspar-phyric rhyolite are sharp and have been intensely chloritised. One large dyke has columnar joints that are oblique to the columnar jointing developed in the feldspar-phyric rhyolite. The rocks contains 5–10% of 2–3 mm quartz and 5–10% of 2–3 mm feldspar phenocrysts in a dark chloritically and/or sericitically altered matrix. Feldspars have mostly been altered to chlorite. Locally, some quartz phenocrysts show superb cauliflower resorbed margins.

Three of the dykes have an intensely chlorite-altered groundmass, and local chlorite altered feldspar phenocrysts. Dyke margins are intensely chloritised, and chlorite alteration extends out into the feldspar-phyric rhyolite, suggesting that fluid movement was controlled by the dyke margins. Four of the dykes show only regional sericite/chlorite alteration. K-feldspar alteration has not been recognised within the quartz-feldspar porphyry dykes.

Breccia Bodies

At the Jukes Prospect, a large breccia body has been identified that appears to be of hydrothermal origin. The breccia was previously identified by Doyle (1990) as a pseudobreccia developed by chlorite alteration overprinting K-feldspar alteration. We now interpret the breccia to have formed by a subsurface phreatic explosion. The breccia occurs on both sides of a chloritically altered quartz-feldspar porphyry dyke. Rounded clasts of the porphyry dyke are found in the breccia, indicating that they were disrupted and transported during breccia formation. Clasts in the breccia are dominated by angular blocks of intensely K-feldspar altered feldspar-phyric rhyolite. Chloritically altered blocks of feldspar-phyric rhyolite are also present. Clasts are set in a matrix containing various amounts of chlorite or chlorite ± magnetite/hematite ± tourmaline as shown in Plate 1C. Fragments vary in size from <1 mm to > 20 cm. The breccia varies from a fine network of fractures near the margins to chlorite-matrix supported breccia in the core of the breccia body. The matrix of the breccia appears to contain increasing amounts of magnetite/hematite ± tourmaline near the margins. The breccia is cut by several faults but clearly predates fault-related tectonic fracturing.

Disseminated pyrite ± chalcopyrite mineralisation occurs throughout the breccia. Best grades of chalcopyrite mineralisation are found in the post-breccia faults, most likely as a result of later re-mobilization and concentration.

ALTERATION

Alteration Intensity

Altered volcanic rocks are exposed over the entire length of Jukes Road, in the Central Volcanic Complex, Yolande River Sequence and Eastern-Quartz-Phyric Sequence. Characterising the effects of hydrothermal alteration in a manner useful to field geologists has presented a distinct challenge. Previous workers have attempted to describe alteration as weak, moderate, strong or intense. Due to complexities involved in overlapping alteration mineralogies and intensities, this simple subjective terminology does not appear adequate for more complex situations. That some

PLATE 1

A: Columnar Jointed Rhyolite at the Jukes Prospect. Well preserved columns at the top of the photo. Notice orange/pinkish color from moderate to intense K-feldspar alteration.

B: Volcaniclastic mass flow deposit along the western part of Jukes Road. Notice large clast size (several meters).

C: Hydrothermal Breccia body. Notice angular K-feldspar altered clasts in a matrix if chlorite ± magnetite.

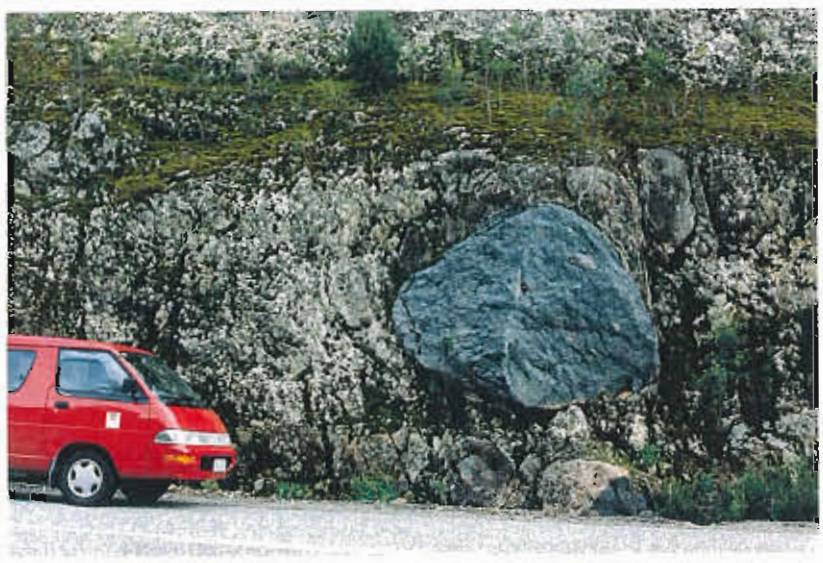


CENTIMETER

subjectivity is used cannot be eliminated. The question is simply how to control and direct subjective judgments to produce useful informative observations. At the same time, any system must be simple and quick or field geologists simply won't use it. At the beginning of this project, it became obvious that a method of characterising alteration in the field would be required as a mapping tool and would be useful to later readers who wished to examine the various rocks in the field. Reviews of alteration texts by Taylor (1992) and discussions with various industry geologists led to the system used by the author on this project. The system is based on the application of an arbitrary scale for alteration from 1 to 10, with 1 being the least and 10 being the most altered. The scale also includes a scale for textural destruction (TD). Degrees of textural destruction are critical in correctly characterising alteration, and are often but not always related to intensity. In general, the weaker the degree of alteration, the less the degree of textural destruction, and the greater the degree of alteration, the greater the degree of textural destruction. This applies only to the rocks mapped along the Jukes Road and is not universally applicable. As Titley (1982) points out, alteration can have the effect of enhancing some primary rock textures under some circumstances. Syn, or post-alteration tectonism movement can also result in destruction of primary rock textures.

The alteration scale used by the authors in characterising alteration and textural destruction is shown in Table 1. In addition to the alteration descriptions given, it is easy to add abbreviated rock names and attach them to the end of the alteration string. Examples are shown at the bottom of Table 1.

Several other critical observations must be made to accurately characterise the alteration style and distribution. These observations are kept in field notes and become the basis for later descriptions.

- **How was the host rock altered on a mineral by mineral basis?** Is alteration confined to the phenocrysts only?, the groundmass only?, ferromagnesian minerals only? etc.
- **How did the fluids gain access? (Channelway Identification)** This may require careful examination of the entire outcrop and may be inconclusive. Frequently a search for channelways will reveal several overlapping styles of alteration and data about the alteration paragenesis.
- **Were elements added or subtracted?** This is often subjective unless alteration is intense. The possibility of apparent enrichment of some elements as a result of depletion in other elements can not be overlooked. The best way to answer this question is to conduct detailed whole-rock or mineral geochemistry and that is the subject of later work on this project.

STYLES AND DISTRIBUTION OF ALTERATION ALONG JUKES ROAD

Distinguishing between diagenetic alteration, regional metamorphic alteration and hydrothermal alteration is difficult under the best of circumstances. It is possible for identical alteration assemblages to be produced by all three alteration processes. The use of detailed petrographic and geochemical techniques must be employed to sift through complex overprinting relationships. Work to date along the Jukes Road has involved only limited petrography and whole rock geochemistry. Interpretations presented here are, therefor mostly based on hand specimen examination, geologic mapping and supported by the limited petrography and geochemical analyses completed to date. Later fluid inclusion work will be critical in removing the metamorphic effects on the alteration assemblages.

Five styles of alteration have been identified along the Jukes Road. Each of these can be considered to be an end member, and the alteration assemblages seen at any one locality is almost always a combination of two or more styles. The five styles are: Sericitic (S), Chloritic (C), Potassium feldspar (K or K-feldspar), Carbonate (CO_3) and silicification (Si). Of the five styles, sericite, chlorite and K-feldspar are the most common and most easily identified. Carbonate and silica alteration are minor. Carbonate alteration is difficult to distinguish in hand specimen, and can typically only be identified through the use of 50% HCl solution.

Accessory minerals include pyrite, magnetite, tourmaline, hematite, goethite, chalcopyrite and rarely apatite. Magnetite and pyrite are, by far, the most abundant accessory phases.

Table 1 Alteration Scale

Scale	Alteration Intensity	Textures
1	**Trace:** Just visible, often confined to just groundmass or phenocrysts	Clearly visible, virtually no textural destruction
2	**Weak:** Feldspars or mafic minerals show the effects of alteration first, Quartz unaffected	Most clearly visible, zoning in feldspars, wispy flow banding and small textures begin to disappear
3	**Weak:** Phenocrysts of feldspar may show moderate replacement, Mafic minerals begin to show chlorite-sericite alt. Magnetite present as traces with chlorite.	Some fine groundmass textures destroyed such as weak flow banding and zoning
4	**Moderate:** Mafic minerals almost totally replaced, feldspars show extensive replacement, Quartz unaffected, Magnetite present with chlorite.	Fine groundmass textures destroyed but the medium to coarser rock textures are still identifiable
5	**Moderate:** Feldspars strongly replaced but pseudomorphs are still visible. Mafic minerals strongly replaced. Quartz showing weak to no effects, Magnetite present with chlorite.	medium grained groundmass textures destroyed coarse textures affected. Textures still defined by quartz in the groundmass
6	**Moderate:** Quartz in the groundmass is being replaced. Almost total replacement of other minerals unless coarse grained. Phenocryst pseudomorphs visible.	Coarse textures weakly visible, some destroyed dependent on grainsize and quartz content
7	**Strong:** Quartz phenocrysts showing weak replacement, finer quartz in groundmass is almost all replaced Feldspar replacement is total unless phenocrysts are extremely large. Magnetite is abundant in chloritic rocks.	Groundmass textures are almost totally destroyed regardless of grain size. Porphyritic textures all show strong effects of alteration
8	**Strong:** All medium to coarse mineralogy is replaced by alteration minerals	All groundmass textures are totally destroyed. . Coarse pseudomorphs of phenocrysts may be visible but replacement is total.
9	**Intense: :** All original rock mineralogy is replaced by alteration mineral assemblages	Virtually all original rock textures are destroyed. only weak pseudomorphic shapes of coarse phenocrysts may be visible. Quartz is destroyed.

Combinations of alteration mineralogies and intensities are possible. Textural destruction is also ranked.

Examples:

- $Se_2C_3K_1\ TD_2$ Qfpv — is a quartz-feldspar-phyric (Qfpv) volcanic rock with weak sericite (Se_2), weak chlorite (C_3) and a trace of K-feldspar (K_1) alteration. Metasomatism has resulted in weak textural destruction (TD_2).
- $K_7C_5\ M_2\ TD_6$ Fpv — is a feldspar-phyric volcanic (Fpv) rock with strong K-feldspar(K_7) and moderate chlorite (C_5) alteration. The rock contains about 2% magnetite and has undergone moderate textural destruction (TD_6)

Accessory minerals are identified and their relative percent in the rock is estimated.
Pyrite (Py) e.g. Py_3 is pyrite 3%.
Magnetite (M) e.g. M_2 is magnetite 2%
Tourmaline (T) e.g. T_5 is tourmaline 5%

Sericitic Alteration

Sericite or white mica alteration is the most common alteration assemblage found in rocks along the Jukes Road. It occurs in all sequences from the Eastern Quartz-Phyric through to the Yolande River Sequence.

All of the rocks in the Mount Read Volcanics south of Queenstown have been described as being of greenschist metamorphic grade. Sericite(fine grained muscovite) is a common but not indicative mineral of greenschist metamorphic grade, and is common in rocks of rhyolitic to dacitic composition. Since sericite is widespread throughout the Mt. Read volcanic belt, it is likely that most of the sericite is of metamorphic origin. In areas of weak sericite alteration, proof of hydrothermal origin will most likely involve detailed geochemical techniques. The type of sericite (white mica) present can vary widely in hydrothermal alteration assemblages. Currently all white to light green fine-grained mica is classified as sericite alteration. Later mineral separate and XRD analysis will attempt to be more specific as to the mineralogical composition of white mica alteration.

Sericite Alteration in the Eastern Quartz Phyric Sequence (EQP)

Sericite in the EQP is well-developed as the pervasive alteration assemblage of moderate to strong intensity. Sericite has replaced the fine grained groundmass, that was originally composed of feldspars and quartz. In volcaniclastic rocks, sericite occurs in both the lithic clasts and host rock with equal intensity, indicating that they were equally reactive. Mafic minerals and quartz appear to have been unaffected by weak sericite alteration, but mafic minerals were destroyed during the formation of the intense alteration assemblage. Feldspar phenocrysts in feldspar-phyric rocks vary from unaltered to almost total replacement by light green sericite. Many phenocrysts are only weakly altered whereas the groundmass can have been almost totally replaced. Other rocks contain feldspar phenocrysts that have been almost totally replaced by sericite. In the EQP, sericite is rarely accompanied by accessory minerals, and textures are generally well-preserved. Alteration minerals associated with sericite in lesser amounts include chlorite, K-feldspar and carbonate. Sericite alteration occurs in association with weak silicification and weak K-feldspar alteration near the faulted contact between the EQP and the CVC.

Geochemically, the EQP rocks plot on sericite alteration trends as defined by Barrett and MacLean (1994) (Figs 3, 4).

Sericite Alteration in the Central Volcanic Complex (CVC)

Sericite alteration is well-developed in all lithologies and facies found in the CVC sequence exposed along the Jukes Road. This widespread occurrence is consistent with a diagenetic and/or metamorphic origin. Unlike EQP rocks, sericite is well-developed as pervasive alteration of weak to moderate intensity. Sericite is well developed in finer grained groundmasses originally composed of fine grained feldspars and quartz. Quartz appears to have been unaffected by weak sericite alteration. Feldspar phenocrysts in feldspar phyric rocks range from unaltered to totally replaced by light green sericite. The groundmasses typically show almost total sericite replacement. In the CVC, sericite is typically accompanied by at least one additional alteration phase. Other alteration assemblages found with sericite include weak chlorite, weak K-feldspar and weak carbonate alteration. Textures are generally well-preserved.

CVC rocks plot on the sericite alteration trends as defined by Barrett and MacLean (1994) (Figs 3, 4), in the same area as sericitic rocks of the EQP.

Sericite at the Jukes Prospect area occurs in the same manner as elsewhere in the CVC sequence along Jukes Road. It is, however more intensely developed and texturally destructive. Intensity and textural destruction are taken as evidence of a hydrothermal origin for at least some of the sericite in the prospect area. Sericite alteration is locally intense, replacing virtually all of the feldspar leaving only pseudomorphed crystal shapes. The groundmass of rocks with this style of alteration are typically weakly to moderately chloritic or weakly K-feldspar altered. Textural destruction of the groundmass is typically moderate. Rocks within the Jukes prospect with visible sericite alteration tend to be hard and have probably undergone minor silica alteration.

Geochemically, intensely sericitised rocks from the Jukes Prospect area show a clear trend of potassium enrichment in relation to weakly regionally sericitised rocks. Intense sericite altered rocks trend toward the K-feldspar alteration line shown on Figures 4 and 5 (Barrett and MacLean, 1994).

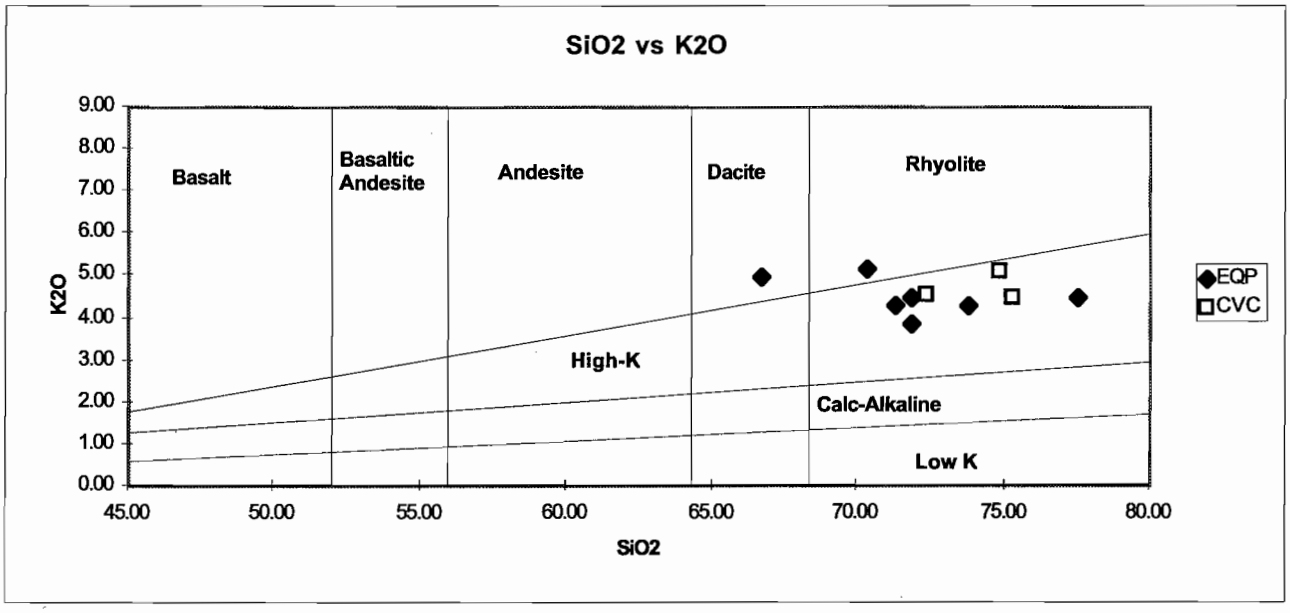

Figure 3: SiO_2 vs. K_2O plot showing the high-K affinities of both EQP and CVC rhyolites.

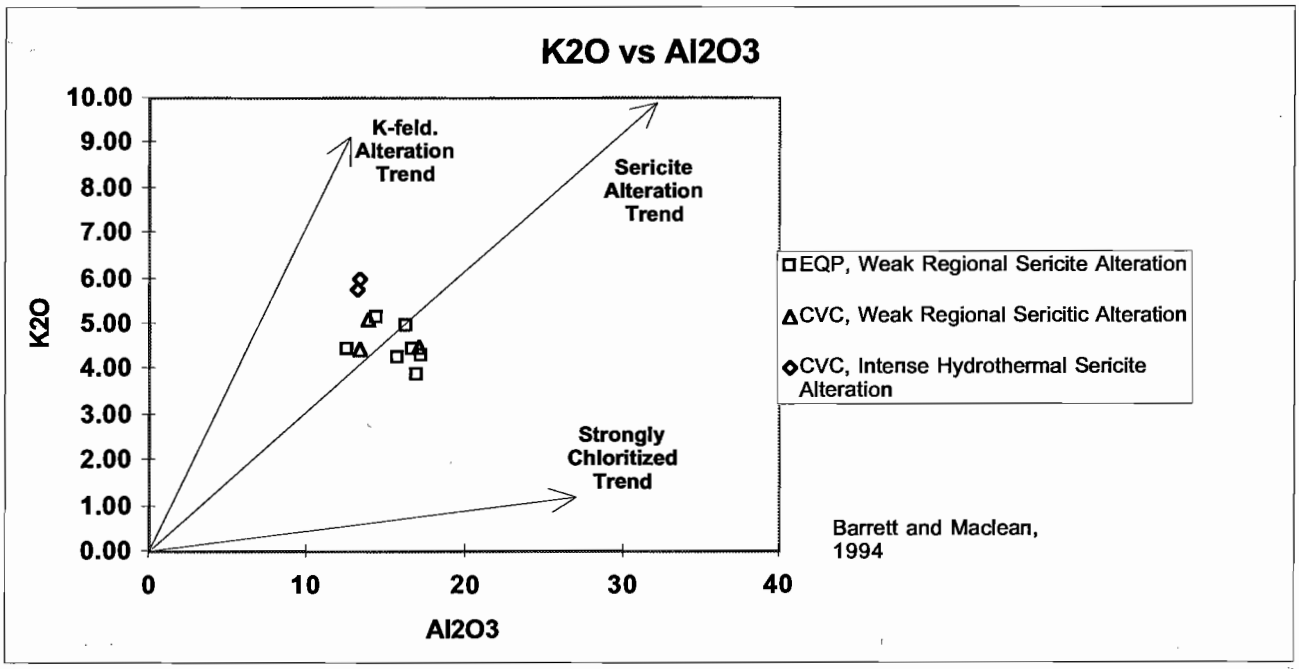

Figure 4: K_2O vs. Al_2O_3 diagram showing how regionally sericitised rocks of both the EQP and CVC plot on the sericite alteration trend, but intense hydrothermal sericite altered rocks in the CVC tend to shift toward the K-feldspar alteration trend.

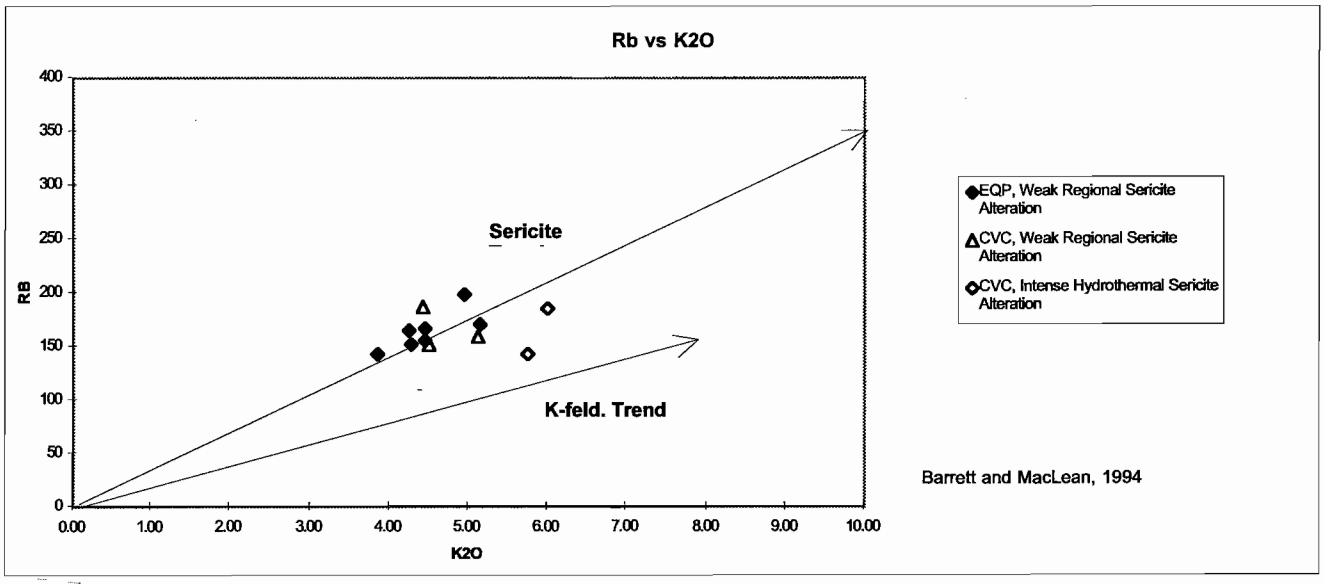

Figure 5: Rb vs. K_2O diagram showing similar trends to Figure 4.

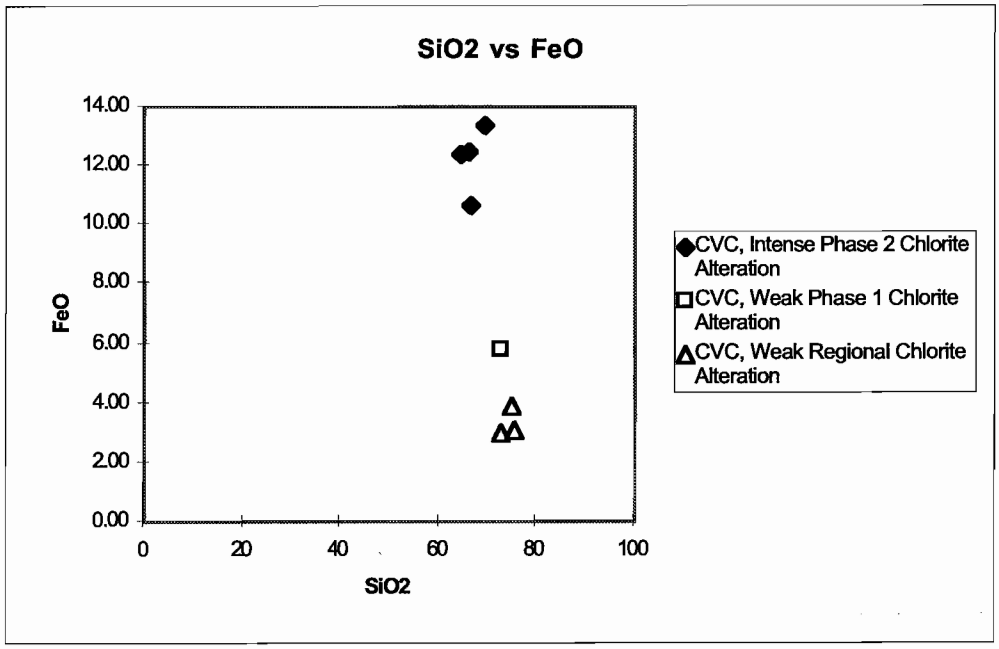

Figure 6: SiO_2 vs. FeO plot showing three populations of chlorite altered CVC rocks. Note that both the Phase 1 and Phase 2 chlorites are differentiated from regional chlorite on the basis of their iron content.

Chlorite Alteration

Chlorite alteration is perhaps the most texturally destructive style of alteration developed along Jukes Road. Rocks that contain only weakly developed chloritic alteration assemblages exhibit well developed regional cleavage (Devonian) and locally intense fault-related cleavages. Chlorite alteration occurs throughout the CVC, but is only locally developed in the EQP. Since chlorite is another common greenschist facies, mineral the following criteria have been used to distinguish between metamorphic, diagenetic and hydrothermal chlorite.

- Association or lack of association with clinozoisite (Fe-rich epidote). This assemblage is a key indicator of greenschist facies metamorphism.
- Occurrence of accessory minerals indicating either mass gain or mass loss. Accessory minerals include pyrite, chalcopyrite, tourmaline or large amounts of magnetite/hematite
- Intensity of chlorite alteration given that the host rocks are rhyolites and dacites.
- Widespread occurrence. A widespread occurrence of weak alteration strongly suggests a diagenetic or metamorphic origin.
- Degree of textural destruction. Rocks with weakly moderate or greater degrees of non-tectonic textural destruction generally show the effects of hydrothermal alteration.
- Association with quartz-feldspar porphyry dykes.

Mineral chemistry coupled with detailed petrography will be useful later in the study.

Chlorite Alteration in the Eastern Quartz Phyric Sequence

Chlorite alteration is only weakly developed in most of the EQP rocks. Chlorite typically occurs with moderate sericite alteration, and is typically confined to weak groundmass alteration in the coherent quartz-feldspar-phyric rhyolite/dacite facies. This chlorite alteration is probably metamorphic in origin. Strong chlorite alteration within the EQP only occurs within the fault zone that separates the EQP from the CVC. Chlorite alteration can vary from weak to intense and be totally texturally destructive in the fault zone. Blocks of EQP rocks in the fault breccias are set in a chlorite matrix and show the entire range of alteration styles from weak sericite alteration to intense chlorite alteration.

Regional Chlorite Alteration in the Central Volcanic Complex

Chlorite in the CVC is expressed in varying degrees throughout almost all facies mapped. Chlorite alteration typically occurs with weak to moderate sericite alteration and occasionally with weak to moderate K-feldspar alteration. Chlorite alteration is almost always accompanied by magnetite in amounts directly proportional to the degree of chlorite alteration.

Chlorite alteration is well developed in all volcaniclastic and mass flow deposits along the western margin of the CVC. Chloritically altered tube pumice breccias around 12500 appear to be overprinted by weak to moderate K-feldspar alteration due to the presence of green chlorite cores in the pumiceous breccia clasts. This "pink/green" mottled chlorite/K-feldspar alteration appears to be always conformable to bedding, and is believed to be diagenetic or metamorphic in origin. At other locations within the CVC, the pink feldspar mineral has been shown to be albite. Chlorite alteration in other volcaniclastic and mass flow deposits is typically weak to moderate and is best developed in rocks with well developed regional cleavage. Shears and faults are typically associated with intense, texturally destructive chlorite development.

Weak regional chlorite alteration does not appear to show effects of added iron or magnesium. Figures 6 and 7 show the relationship of FeO and MgO to SiO_2 for both regional chlorite alteration and hydrothermal chlorite alteration discussed below.

Chlorite alteration is typically weak to absent, and is only a minor component of the alteration in the 230 m long section of tuffaceous sandstones and volcano-sedimentary rocks along Jukes Road. Chlorite in this section is developed only along cleavage surfaces, or within a few thin pumiceous volcaniclastic horizons. Chlorite alteration in this unit is almost always subordinate to more intense sericite or silica alteration.

Chlorite alteration within the large feldspar phyric columnar jointed rhyolite unit occurs in two fashions. Regional weak chlorite alteration is well developed in all rocks. Hydrothermal chlorite alteration is also well developed and is discussed in the next section. The regional chlorite alteration is associated with weak to moderate sericite alteration throughout the entire unit. This alteration is not texturally destructive, and

is believed to be of metamorphic or diagenetic origin. Chlorite alteration is confined to the groundmass probably as a result of ferromagnesian mineral destruction. The intensity of chlorite alteration development in this type of alteration is controlled by fluid/rock ratios and by the original ferromagnesian mineral contents of the rocks.

Hydrothermal Chlorite Alteration in the CVC

Hydrothermal chlorite development in the feldspar phyric rhyolite unit is associated with a corresponding increase in total iron and manganese in the rocks (Figs 5, 6). Three major phases of chlorite alteration have been identified at the Jukes prospect. The coarse euhedral chlorite that occurs with quartz in cross-cutting veins of obvious Devonian age will not be discussed further. The other two chlorite assemblages are discussed in more detail below.

Phase One: Doyle (1990) identified two phases of chlorite alteration at the Jukes Pty Prospect. A pervasive light green chlorite contains submicron grains of residual quartz and K-feldspar Dark to pale green chlorite is also generally pervasive in nature. Doyles's first phase of chlorite alteration (pale green) is probably part of the regional pervasive alteration seen throughout the CVC, and is not part of the hydrothermal story. Doyle's second phase of chlorite alteration (dark green) is probably part of the Phase One chlorite alteration of hydrothermal origin discussed here.

Phase One hydrothermal chlorite alteration is here defined as: pre K-feldspar alteration that is generally associated with only one accessory mineral, magnetite. Evidence for this early phase of hydrothermal chlorite alteration includes:

- Chlorite veins that have cut sericite/chlorite altered rhyolites (Plate 2A). These veins show diffuse chlorite alteration boundaries with chlorite replacing sericite/chlorite altered volcanics. Generally these veins occur on the centimeter scale with the diffuse boundary being limited to a few centimeters.
- Chlorite replacement of feldspars and the moderate occurrence with sericite in the groundmass of the feldspar phyric rhyolite. This is informally referred to as "chlorite disease" because of the dark green spotted nature of the rocks (Plate 2B). A zone of this alteration occurs at approximately 10350 m within an intensely K-feldspar altered zone. Controls on this alteration appear to be fracture density. Textures are generally well preserved and columnar jointing is still present.
- This phase of alteration involves the addition of iron but not magnesium and is shown of Figures 6 and 7.

Phase Two: There are two diagnostic features of this chlorite alteration phase: (1) Chlorite is post K-feldspar timing. (2) The presence of sulfides, magnetite and traces of tourmaline. Pyrite is the principal sulfide, but chalcopytite occurs in minor amounts and has locally been significantly remobilised and concentrated in post-mineral faults.

Fluids infiltration during phase of alteration appears to have been associated with hydrothermal and phreatic brecciation, with transport and rounding of lithic clasts. New fracture systems were formed and old fracture systems were reopened. Chlorite occurs as both matrix (along with varying amounts of magnetite) and fracture fillings. Chlorite in the matrix surrounds angular blocks of strong to intensely K-feldspar altered volcanic clasts and rounded to sub-rounded clasts of chloritically altered quartz-feldspar porphyry and feldspar-phyric rhyolite. Sulfide accessory minerals are common.

In strong to intensely K-feldspar altered zones, fractures that were clearly used by K-feldspar altering fluids are now filled with chlorite ± pyrite, and may show diffuse boundaries.

Phase two chlorite alteration occurs in and around several quartz-feldspar porphyry dykes that crosscut the feldspar-phyric rhyolite. Chlorite alteration is locally texturally destructive and is intensely developed in the rhyolitic rocks near the margins of the dykes. Chlorite alteration within the dykes can be of moderate to strong intensities, and in dykes proximal to the Jukes prospect may be texturally destructive to all but the largest quartz phenocrysts. This alteration phase is clearly syn or post-dyke emplacement.

Geochemically, phase 2 chlorite involved additional mass of both magnesium and iron as is shown of Figures 6 and 7.

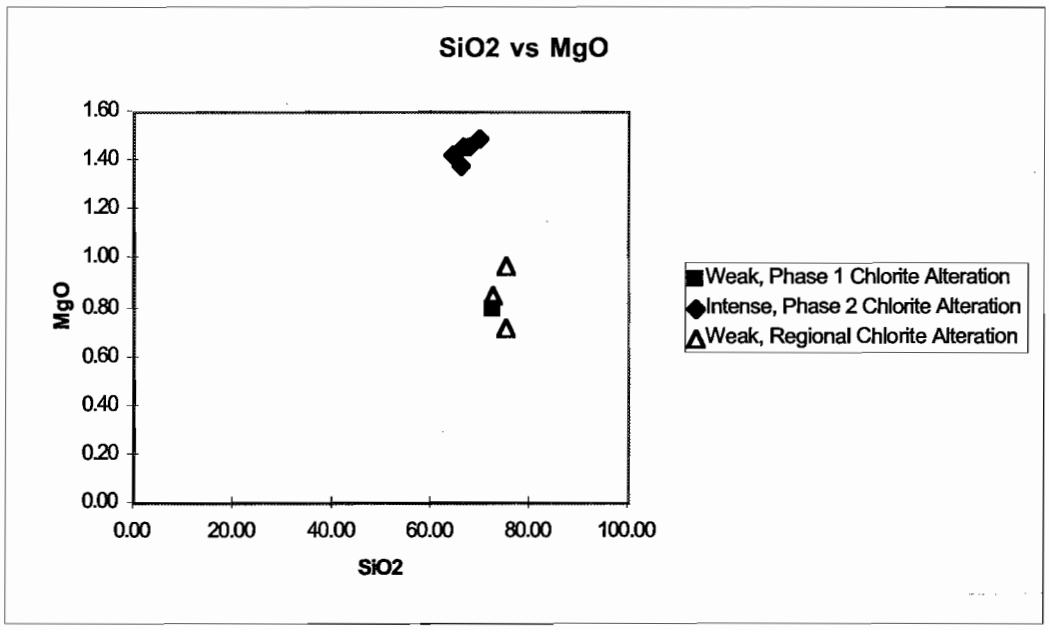

Figure 7: SiO_2 vs. MgO plot showing two populations of chlorite altered CVC rocks. Note that Phase 1 chlorite altered rocks and regionally chlorite altered rocks appear to have similar MgO contents, while the Phase 2 chlorites show an apparent increase in MgO.

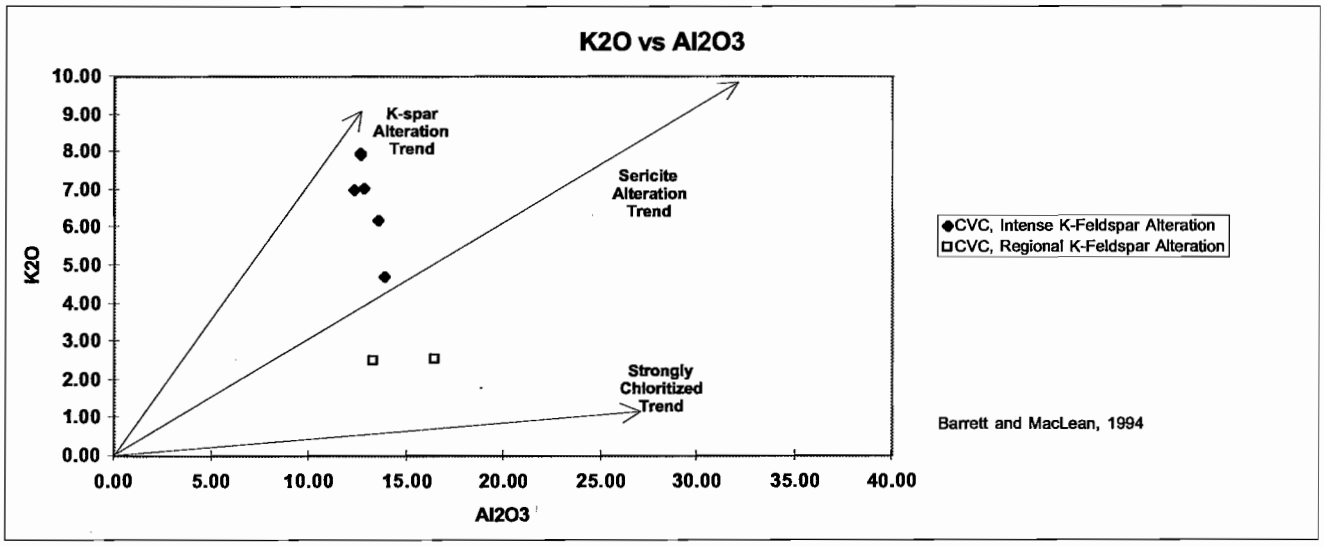

Figure 8: K_2O vs. Al_2O_3 plot showing the trend of intensely K-feldspar altered rocks toward the K-feldspar altered line. Note the low K_2O content of the regionally altered rocks, possibly due to albite alteration instead of K-feldspar alteration.

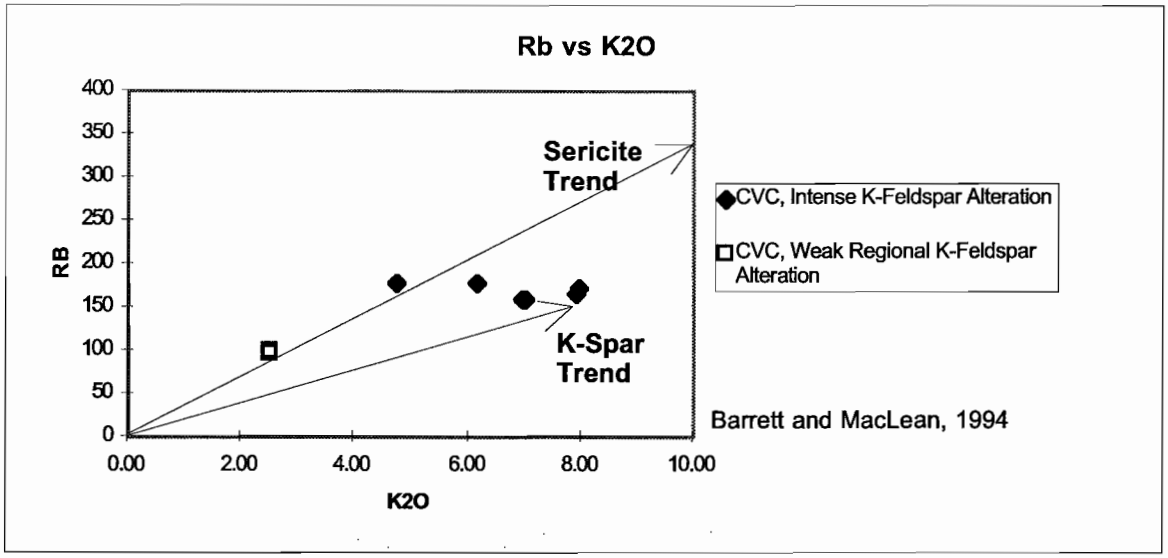

Figure 9: Rb vs. K_2O plot showing similar trends to Figure 8.

K-Feldspar Alteration

Potassium feldspar alteration varies from weak to intense along the Jukes Road. K-feldspar of probable diagenetic, metamorphic and/or hydrothermal origins are present. Hydrothermal K-feldspar appears to be confined to the area near Jukes Prospect and is typically moderate to intense and texturally destructive. Weak K-feldspar(or albite) alteration is generally not texturally destructive, and is believed to be diagenetic or metamorphic in origin. This regional style of alteration would have intensities controlled by fluid/rock ratios during diagenesis or metamorphism.

K-feldspar Alteration in the Eastern Quartz Phyric Sequence

K-feldspar alteration in EQP rocks along Jukes Road is weakly developed in association with moderate sericite alteration. K-feldspar is always subordinate to sericite alteration. K-feldspar is light pink to fleshy in color, and fine grained and spotty in nature. K-feldspar alteration in the EQP is rare, and appears to only have affected the groundmass feldspar and mafic minerals; phenocrysts are unaffected.

Regional K-feldspar Alteration in the Central Volcanic Complex

K-feldspar alteration is widely developed in CVC rocks. In the western part of the sequence, this alteration assemblage is weak, whereas in the eastern part of the sequence the K-feldspar assemblage is dominated by alteration at the Jukes prospect. K-feldspar alteration is always associated with weak chlorite alteration. In the pink/green mottled rocks at 12500, weak K-feldspar alteration appears to have overprinted earlier weak chlorite alteration. Evidence includes chloritic cores in K-feldspar altered pumice clasts. Along Jukes Road, outcrops of tube pumice breccias around 12500 are the best exposures of alteration believed to be pink diagenetic K-feldspar (or albite) (Plate 2C). K-feldspar has replaced both the groundmass and lithic clasts, and appears to be conformable to bedding. K-feldspar alteration is always minor(except at 12500) relative to the degree of sericite and chlorite alteration in CVC rocks.

Geochemically the regional K-feldspar alteration does not appear to have involved addition of potassium when compared to other hydrothermally altered rocks from the Jukes prospect. (Figs 8, 9).

K-feldspar ± silica alteration appear to be weakly developed in the tuffaceous sandstone sedimentary horizons. Fine grained tuffaceous horizons appear as light pinkish green cherts. Coarser volcaniclastics within this unit do not appear to have developed K-feldspar alteration.

Hydrothermal K-feldspar Alteration in the CVC: K-feldspar alteration is widespread in most rocks within the immediate Jukes prospect area. K-feldspar varies in intensity from weak to intense depending on the accompanying minerals. K-feldspar alteration only occurs without other alteration assemblages in

PLATE 2

A: Phase 1 chlorite veins crosscutting weak sericite alteration in CVC rhyolites at the Jukes Prospect.

B: "Chlorite Disease" : Phase I chlorite selectively replacing feldspar phenocrysts in feldspar-phyric rhyolites. Notice light greenish/gray coloration of the groundmass due to weak sericite and chlorite alteration.

C: Pink/green mottled rocks at 12500. The pink alteration mineral is believed to be pink diagenetic K-feldspar or albite. Weak pink K-feldspar alteration appears to have overprinted earlier weak chlorite alteration. Evidence includes chloritic cores in K-feldspar altered pumice clasts.

the most intensely altered rocks. The most common accessory alteration assemblages found in association with K-feldspar alteration in order of abundance are chlorite, sericite and silica. Sulfides are only found in post K-feldspar alteration fractures in the presence of chlorite.

K-feldspar alteration is clearly post phase one chlorite alteration. Fractures within chloritically altered feldspar-phyric rhyolites exhibiting chlorite disease are filled with K-feldspar. This alteration extends outward with decreasing intensity away from the fractures. Commonly, total textural destruction is observed within 5 cm of the fractures while 15 cm from the fracture, chlorite-replaced phenocrysts are still preserved.

K-feldspar altered rocks do not appear to be magnetic unless accompanied by chlorite. Since K-feldspar alteration was clearly post phase one chlorite development, and chlorite alteration produced minor magnetite, K-feldspar alteration must have been destructive to magnetite as well as chlorite. All K-feldspar alteration at Jukes occurs within a zone surrounded by rocks containing dominantly chlorite alteration.

Strong to intense K-feldspar alteration has caused replacement of primary quartz and as feldspar phenocrysts, and destruction of all primary textures. Intensely altered rocks appear as a fine grained pinkish orange rock with a sandy texture.

Silica Alteration

Silica alteration in the form of silicification occurs to a limited extent in the CVC and EQP sequences. Silicification is typically weak and appears to always be accompanied by weak K-feldspar alteration. K-feldspar alteration, conversely, is not always accompanied by silicification. Silica alteration is only a minor phase of alteration along Jukes Road. It is significant only in localized areas at Jukes Prospect, where it occurs with K-feldspar alteration in weak to moderate intensities. Silicification has resulted in flooding of the groundmass by silica. Typically, the groundmass is light pink to light green, slightly translucent and dense and hard. Silica alteration is texturally destructive to the groundmass mineralogy.

Carbonate alteration

Carbonate alteration occurs along the Jukes Road, but its extent is not well documented due to difficulties in recognizing it. It typically occurs as weakly disseminated blebs and patches in sericite or chlorite altered rocks. Coarser carbonate occurrences also are found in late crosscutting veins with quartz ± chlorite. These veins may be Devonian. Carbonates identified to date are calcite, dolomite (Doyle, 1990), ankerite ($CaFe(CO_3)_2$) and siderite ($FeCO_3$). A better understanding of the distribution of carbonate alteration is planned as part of the ongoing work.

DISCUSSION

The textural and mineralogical data outlined above is preliminary and detailed information on paragenetic and geochemical relationships will be provided in a later report. Work to date suggests that hydrothermal mineral assemblages can be distinguished from regional assemblages on the basis of five observations:

1. Association or lack of association with clinozoisite(Fe-rich epidote). This
2. Widespread occurrence. Widespread occurrence of weak alteration strongly suggests a diagenetic or metamorphic origin.
3. The presence or absence of accessory minerals such as pyrite, chalcopyrite, tourmaline or large amounts of magnetite/hematite.
4. Intensity of alteration assemblages. Distinguishing weak hydrothermal alteration from weak diagenetic alteration will require the use of detailed mineral or whole-rock geochemistry. Moderately to intensely altered rocks with mass loss or mass gain appear to be easily distinguished.
5. Degree of textural destruction. Rocks with weakly moderate or greater textural destruction, in general, clearly show the effects of hydrothermal alteration. Complexities arise when textural destruction from hydrothermal alteration is overprinted by textural destruction caused by later, tectonically-related events.

Along the Jukes Road, two facies of the CVC have clearly been altered by hydrothermal solutions. The feldspar-phyric rhyolite and the quartz-feldspar

porphyry both show varying hydrothermal alteration effects. The quartz-feldspar porphyry is only altered by chlorite alteration and not by K-feldspar alteration. This may suggest a genetic link or close timing relationship. The fact that the hydrothermal breccia follows the apparent boundary of a quartz-feldspar porphyry dyke also may suggest a relationship to phase 2 chlorite alteration.

Further work will examine implications for Cambrian Cu–Au mineralisation being related to the phase 2 event. Limited fluid inclusion and stable isotope studies will be undertaken to gather information about fluids involved in hydrothermal, diagenetic and metamorphic processes. Polished section petrography, microprobe analysis, XRD and mineral separate geochemistry are planned. Results will be presented in later reports.

REFERENCES

Allen, R.L. and Cas, R.A.F., 1990. The Rosebery Controversy: distinguishing prospective submarine ignimbrite in the Rosebery–Hercules Zn–Cu–Pb massive sulphide district, Tasmania. Geological Society of Australia Abstracts 25: 31–32

Barrett, T.J. and MacLean, W.H., 1994. Chemostratigraphy and Hydrothermal Alteration in Exploration for VHMS Deposits in Greenstones and Younger Volcanic Rocks. *In* Lentz, D. R., ed., Alteration and Alteration Processes associated with Ore-forming Systems. Geological Society of Canada, Short Course Notes 11: 433–467.

Doyle, M. G., 1990. The geology of the Jukes Proprietary prospect, Mt. Read Volcanics: Unpubl. Honours Thesis, Univ. Tas., 114p.

Eastoe, C.J., Solomon, M., and Walshe, J.L. 1987. District-scale alteration associated with massive sulfide deposits in the Mount Read Volcanics, western Tasmania. Econ. Geol. 82(5): 1239–1258.

Polya, D. A., 1981. The geology of Murchison Gorge. Unpubl. BSc (Honours) thesis, University of Tasmania

Taylor, R. G., 1992, Ore Textures, Recognition and Interpretation: Volume 1, Infill Textures. Series produced by the Key Centre in Economic Geology in conjunction with the Economic Geology Resource/Research Unit at James Cook University of North Queensland

Taylor, R. G., 1992, Ore Textures, Recognition and Interpretation: Volume 2, Alteration Textures. Series Produced by the Key Centre in Economic Geology in conjunction with the Economic Geology Resource/Research Unit at James Cook University of North Queensland

Titley, S. R., 1982. The Style and Progress of Mineralization and Alteration in Porphyry Copper Systems: American Southwest. *In* Titley, S.R. (ed.) Advances in Geology of the Porphyry Copper deposits: Southwestern North America. Univ. Ariz. Press.

White, M., 1996. Volcanic facies correlations in the Tyndall Group. Unpubl. PhD thesis, Univ. Tas.

Report 1
Exhalite geochemistry. A preliminary geochemical documentation of two barren ferruginous chert bodies in the Mount Windsor Volcanics

G.J. Davidson, A.J. Stolz & S.M. Eggins
CODES, University of Tasmania; and Research School of Earth Sciences, ANU

ABSTRACT

Previously obtained geochemistry from two barren ironstones in the Mount Windsor Volcanic Belt is the starting point for defining geochemical changes in ironstone approaching massive sulphide deposits. Broad features of the data set are described here, including spatial trends in REE, variation in Fe/Si ratio, and consistent differences in Ti/Zr between the hostrock and overlying chemical sediment.

INTRODUCTION

Most previous studies of exhalite geochemistry have focussed on the broad composition of exhalites in volcanic belts without determining the variability within lenses, or the spatial controls on any variation. The fundamental approach of the current research effort is to document the geochemistry of exhalite bodies in far more detail than has been practiced in the past. This will provide explorationists with basic information needed to determine the level of sampling required to satisfactorily characterise an exhalite body. If sampled systematically, it will also provide basic information to determine the formative controls on the development of exhalite deposits, and aid understanding of their evolution towards VHMS deposits. Finally, a systematic study of the variation within and between those lenses that show a gradtion towards VHMS mineralisation (e.g. exhibiting increasing Ba and/or Pb+Zn) will provide a framework for the use of exhalite geochemistry as a halo tool for exploration.

Previous work in the Mount Windsor Volcanic Belt by Duhig et al. (1992a,b) has shown that hematite-rich cherts are common, and show a relationship to VHMS deposits. This work laid the groundwork for further investigations. These studies discovered that microbial organisms played a fundamental role in the accumulation of iron in the cherts, and that deposits discovered to date formed largely as chemical precipitates at a sediment–water interface, mainly free of clastic detritus. Ferruginous cherts are particularly numerous around the Thalanga VHMS deposit, where they display distinctive geochemistry compared to chert away from mineralisation (+Eu/chondrite anomaly, Ba–Pb–Zn enrichment, higher Fe contents). One of the aims of this project is to test whether this argument for distinctive geochemistry adjacent to ore is valid.

This report documents a preliminary assessment of the geochemistry of two "barren" but extensive ferruginous cherts to the east of Thalanga within the Trooper Creek Formation (Fig. 1), discovered by Joe Stolz during previous mapping. On Figure 1 they are SS71A (FJ = Flat Jaspilite) and SS38A (SJ = Steep Jaspilite). This geochemistry was obtained in a previous study funded by an ARC Small Grant from the University of Tasmania. The aim was to obtain very detailed geological, geochemical and geophysical information on these lenses.

METHODS

Both chert lenses were selected because they occur in an area of moderately low metamorphic grade, were extensive compared to other examples in the belt (strikelength of 100–250 m), and contained microbial textures. Each deposit was mapped in detail, and sampled at 20 m intervals at surface; no drilling data

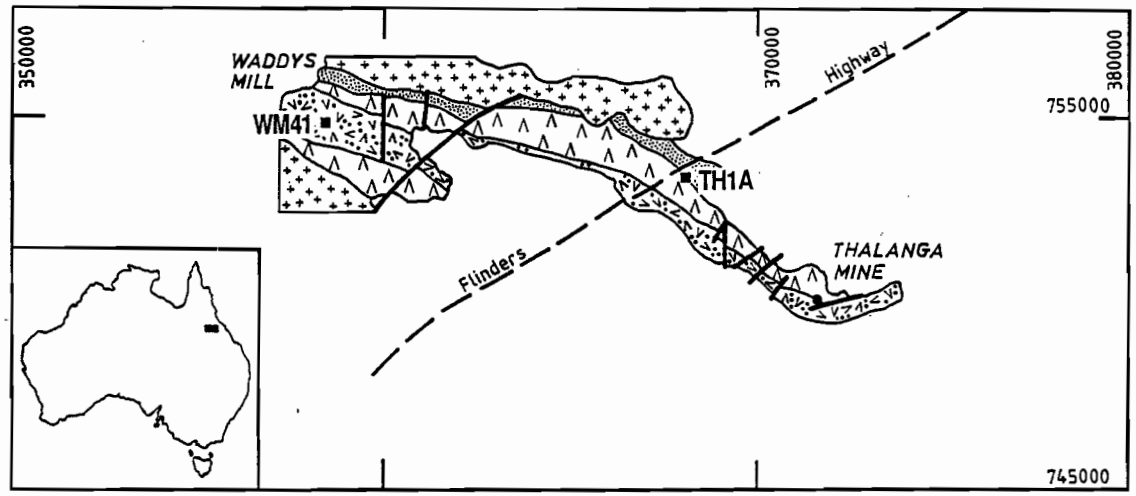

TERTIARY–TRIASSIC

Younger cover rocks; sands, grits, gravels

DEVONIAN–ORDOVICIAN

Granitoids of the Lolworth–Ravenswood batholith

ORDOVICIAN–CAMBRIAN

Rollston Range Formation — siltstone, greywacke, minor volcaniclastics and dacitic volcanics

Trooper Creek Formation — Rhyolitic, dacitic and andesitic volcanics and volcaniclastics; psammitic, pelitic and calcareous rocks, minor doleritic intrusives

Mt Windsor Formation — Rhyolitic volcanics and volcaniclastics

CAMBRIAN

Puddler Creek Formation — Greywacke, siltstones, andesitic volcanics and intrusives

Figure 1 Geology and sample location, Mount Windsor Volcanic Belt.

is available. Sulphides were present in some samples. However, ex-sulphide pits in other samples indicate that some leaching of sulphides has occurred during weathering. Samples were obtained from approximately the same stratigraphic level along-strike, although it was not possible to be precise, because of the broken rubbly character of outcrops. Magnetic susceptibility measurements were obtained at 5 m intervals along outcrops using a handheld instrument. Samples were subsequently analysed by XRF (CODES) for major elements, and by ICP-MS (RSES)for a wide range of trace elements, including REE. The hematite–quartz-rich mineralogy was ideal for dissolution and preparation of ICP-MS solutions; dissolution occurred rapidly, without leaving residual phases. A suite of samples was also prepared by A.J. Stolz for Nd–Sm and Sr-isotope analysis, but results of this work will be discussed at a subsequent meeting.

RESULTS

Geology—FJ & SJ lenses

The geology of FJ lens at the top of the Trooper Creek Formation, is presented in Fig. 2, with ironstone sample locations, although sample locations of footwall samples are not presented. The ironstone outcrops occur over a large area, dipping gently westward above an altered andesitic hyaloclastite package. It is overlain by Ralston Range Formation sediments, which outcrop poorly, and were only sampled ~ 40 m above the chert lens (FJ21; Fig. 2). FJ lens may attain a maximum thickness of ~ 20m at its eastern end, but most of the body is 5–10 m thick. It is characteristically massive with a hackly fracture pattern, although several thin banded zones occur at the top of the body (Fig. 2). The eastern outcrops contain annular veins ~ 10 cm in diameter that are interpreted as paleo-chimney-infill structures. They are also more complexly veined than the rest of the lens, although fine anastomosing veining is characteristic of the entire outcrop. The immediate footwall is only exposed at the eastern end of the lens, where carbonate–chlorite alteration ± pyrite occurs, transected by sinuous 5 cm wide quartz veins. On the basis of geology, the eastern end of the lens was identified as being most proximal to an underlying feeder channel system.

SJ lens (not figured in report) is an east–west trending, steeply dipping lens intermittently outcropping over ~150m, with an average thickness of < 3m. It also occurs at the contact between Ralston Range sediments and Trooper Creek Formation, but here the footwall is tuffaceous siltstone, 10 m above coherent rhyolite. The jaspilite is in places more shaly than the FJ lens, suggesting a higher component of clastic silt. Some sections have prominent pits after coarse cubes of pyrite, whereas others are massive, or contain rare clasts of volcanic material.

Geochemistry

Samples have total Fe(as Fe_2O_3) contents < 25 wt. %, very high SiO_2 contents, and less than ~1% for other major elements. Zr contents are ≤14 ppm, indicating a very low clastic detrital component to the chemical sediment (Fig. 3). Ti/Zr values within the FJ lens ironstones lie between 0–20, distinct from footwall andesite samples of 65–72 (Fig. 4), suggesting that provided the principle of immobility is valid in this system, the ironstone does not contain abundant unmodified footwall andesite detritus, or hangingwall sediment detritus. Ti contents at FJ lens show a covariance with Mg, tentatively interpreted as the effect of increasing accommodation of Ti within chlorite (Fig. 4). Chlorite variation may therefore account for the wide Ti/Zr variation in ironstone. A higher Fe zone is defined in the centre of the existing outcrop by $Fe_2O_3/SiO_2+Fe_2O_3$ ratios> ~0.10 (Fig. 6). Some high Ba values of ~1000 ppm occur, but much higher Ba occurs in the immediate footwall alteration at FJ lens (up to 7600 ppm).

REE element abundances and patterns show a subtle spatial zoning. From east to west, possibly from more veined to less veined material and hence trending away from a hydrothermal upflow zone, the following changes are observed at FJ lens.∑REE increase from east to west, or low sample number to high sample number, from <10X chondritic abundances to >100X chondritic abundances (Fig. 7). No +Eu anomaly is present in any sample— all samples have –Eu anomalies, despite elevated Ba contents. A weak –Ce anomaly characterises some samples that are most distal to the most veined zone (e.g. FJ11,

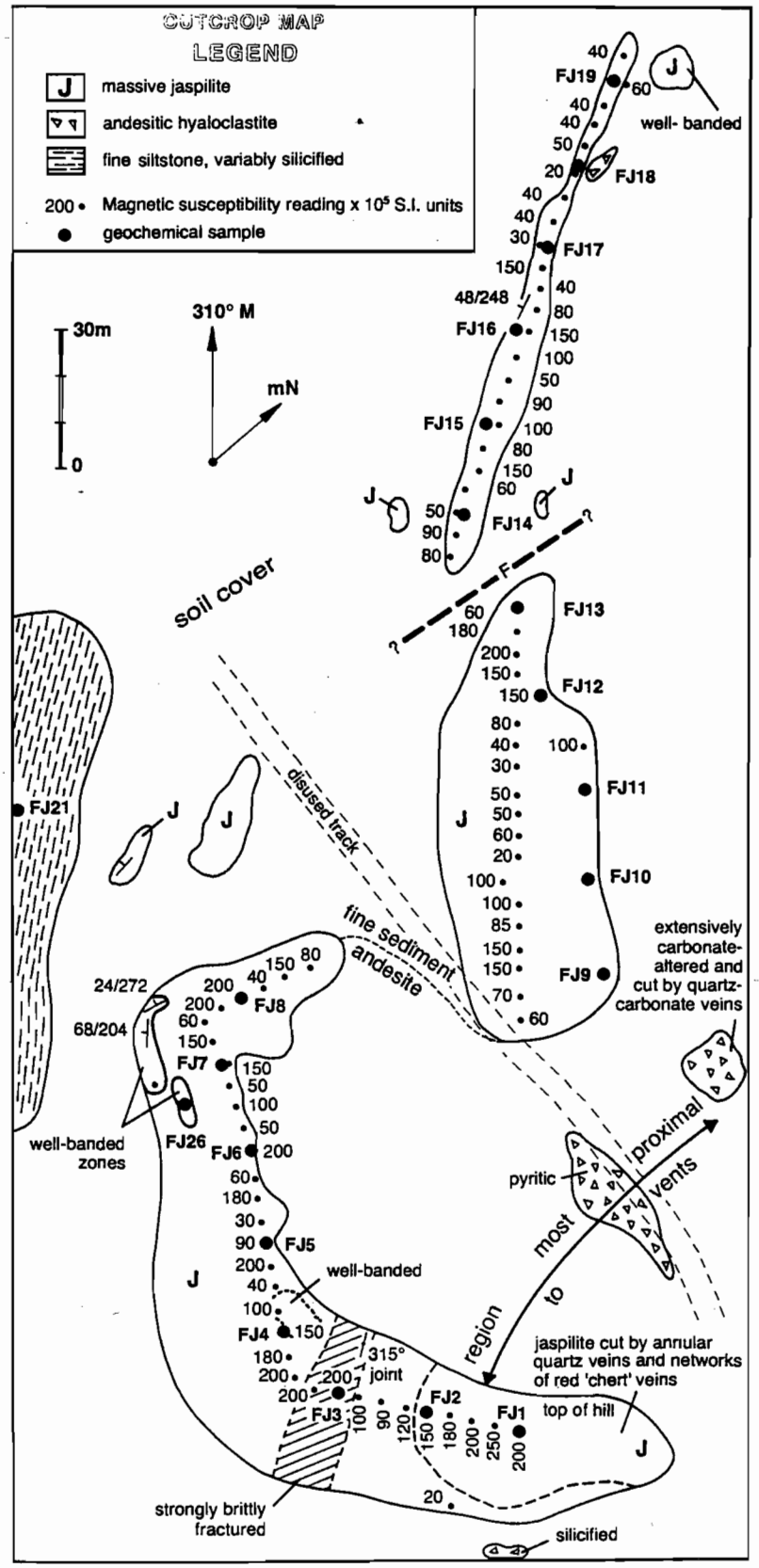

Figure 2 Geology of FJ lens.

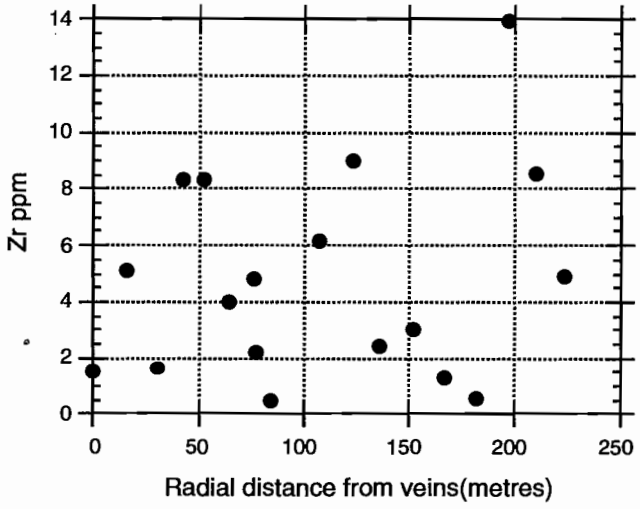

Figure 3 Zr versus radial distance from the most veined section at the east of theFJ lens.

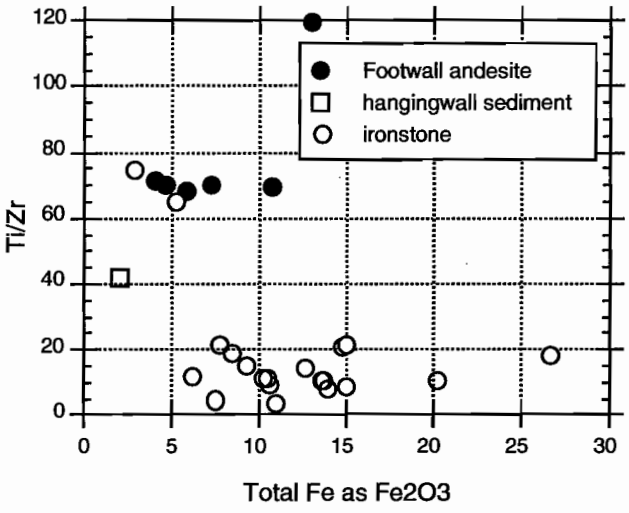

Figure 4 Ti//Zr versus Fe content (wholerock) for all lithologies, illustrating that ironstones do not share the geochemical provenance of the footwall.

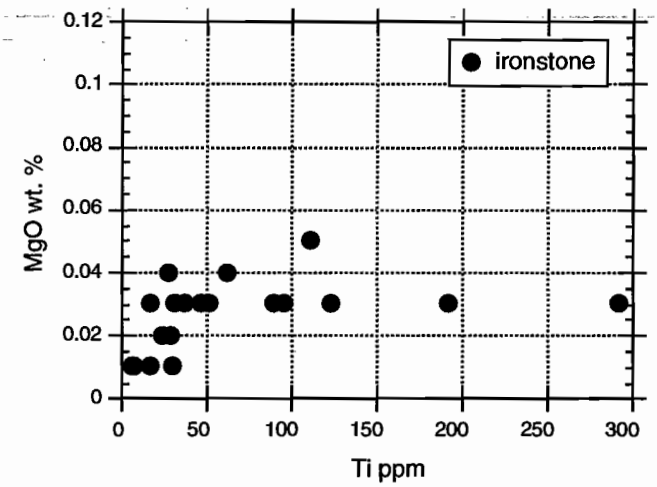

Figure 5 MgO versus TiO_2 content in FJ lens ironstones.

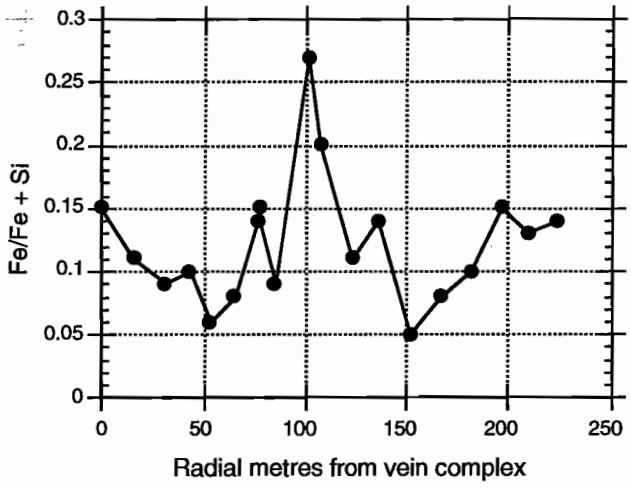

Figure 6 $Fe_2O_3/SiO_2+Fe_2O_3$ versus radial distance from the most veined section at the east of theFJ lens.

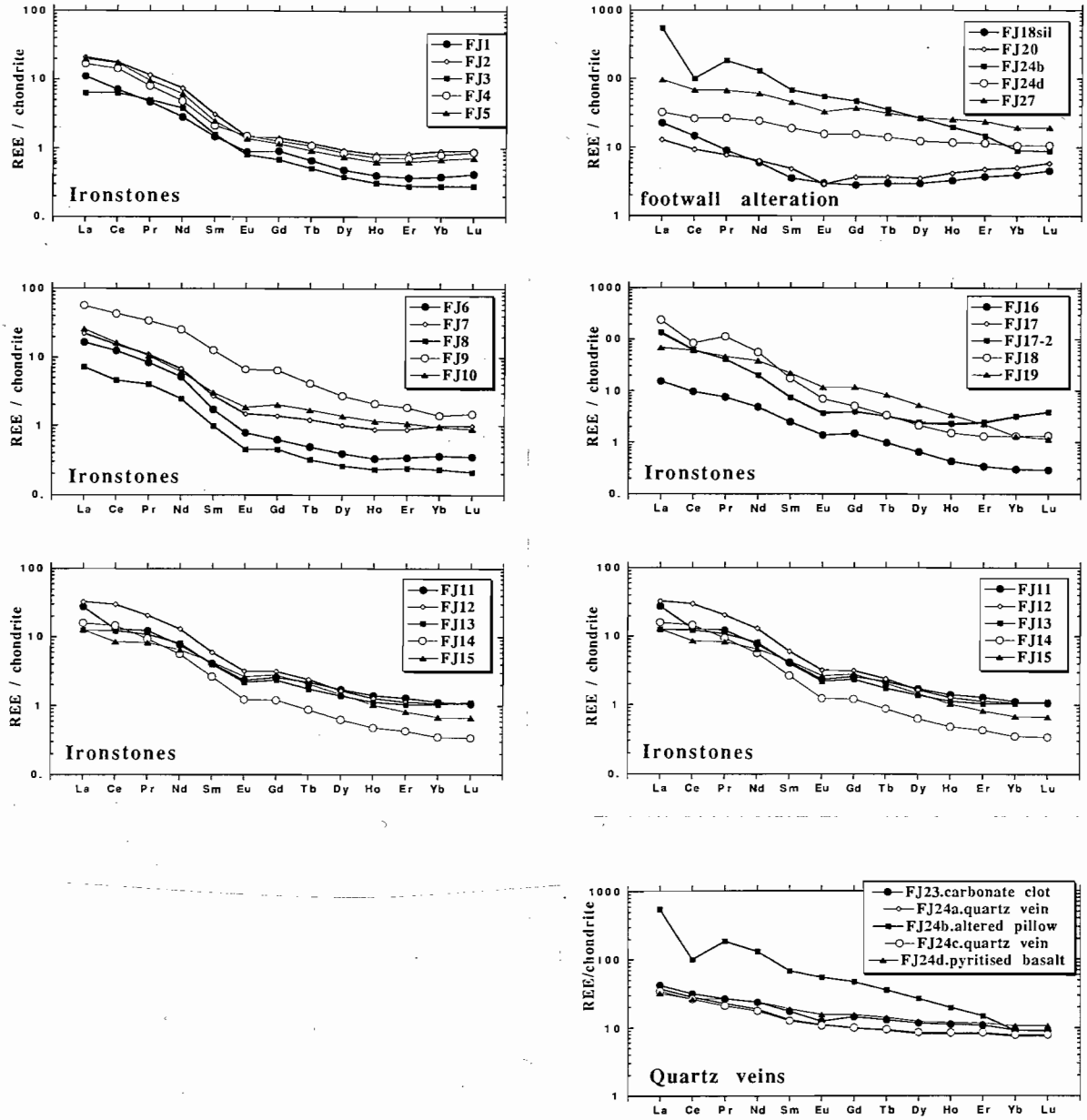

Figure 7 Ironstone and footwall REE patterns/chondrite at FJ lens.

FJ15, FJ18), and this is very pronounced in some altered footwall andesite samples (e.g. FJ24b). Quartz vein samples from the footwall have similar REE patterns to some footwall alteration, and together with high Ti and Zr contents, this suggests contamination although care was taken to obtain pure samples of vein feeder quartz.

REE analyses from the SJ lens (Fig. 8) display more pronounced –Ce anomalies and HREE enrichment than FJ lens, suggesting a greater component of seawater REE addition. The REE will be important for further analysis of the abundance of clastic material in the jaspilites, and defining the sources of geochemical components in general.

REE at both of the ironstone lenses is markedly different from REE patterns of ironstones adjacent to Thalanga, which exhibit strong LREE enrichment and +Eu anomalies (Duhig et al. 1992b).This work indicates strong potential for using REE as a screening tool for VHMS exploration.

FUTURE WORK

In the 1996 field season Ba–Pb–Zn-rich ironstones will be sampled to assess detailed geochemical changes approaching ores, following extensive consultation with company representatives to identify the best sample locations. Analysis of ironstones from the Henty Au deposit, provided by RGC, are in progress. Results of radiogenic isotope analysis at FJ and SJ lenses will be complete for the November meeting.

REFERENCES

Duhig, N.C., Davidson, G.J. and Stolz, J., 1992a. Microbial involvement in the formation of Cambrian sea-floor silica-iron oxide deposits, Australia. *Geology* 20: 511-514.

Duhig, N.C., Stolz, J., Davidson, G.J. and Large, R.R., 1992b. Cambrian microbial and silica gel textures in silica iron exhalites from the Mount Windsor Volcanic Belt, Australia: Their petrography, chemistry, and origin. *Economic Geology* 87: 764-784.

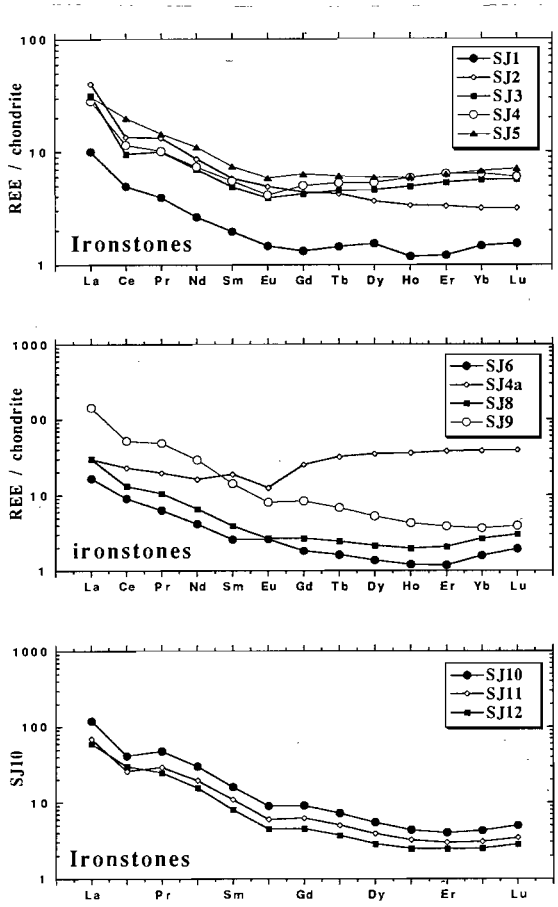

Figure 8 Ironstone REE patterns/chondrite at SJ lens.

Mineral chemistry of the hangingwall alteration zone at the Hellyer mine, western Tasmania

Russell Fulton
Centre for Ore Deposit and Exploration Studies, Geology Department, University of Tasmania

INTRODUCTION

The purpose of this project is to study the mineral chemistry of the hangingwall alteration at the Hellyer mine. The primary focus is to attempt to discriminate between the mineralogy and mineral chemistry related to Cambrian hydrothermal alteration and the mineralogy and mineral chemistry related to Devonian regional metamorphism. Later, the inter-relationship between mineral chemistry and whole rock geochemistry of the hangingwall will also be considered. No study of the alteration mineralogy of the hangingwall has previously been undertaken apart from a small amount of work which formed part of a MSc project (Jack, 1989).

PREVIOUS WORK

Volcanic facies of the hangingwall basalt

The hangingwall basalt is the uppermost of four informal subunits which make up the Que–Hellyer Volcanics, a unit of the Mount Charter Group (Corbett, 1992) (Fig. 1). The hangingwall basalt or Hellyer basalt (pillow lava sequence or PLS in mine terminology) has been subdivided into three major primary volcanic facies which grade into each other both vertically and laterally (Waters and Wallace, 1992). Laterally, the sequence shows complex variation and in some areas consists of andesitic lavas (Corbett and Komyshan, 1989; Waters and Wallace, 1992). The descriptions below are summarised from Waters and Wallace (1992).

Massive basaltic lava facies

This facies consists of massive, sheetlike flows of up to tens of metres thickness with minor sediment or lava breccias occurring between individual flow units. The basalts are mostly porphyritic and non-vesicular to weakly vesicular (5–10%). Mineralogically, the least altered of the basalts, away from the ore body, are composed of phenocrysts or glomerocrysts of augite (15–20%), plagioclase (up to 15%) and a chlorite± calcite altered pseudomorph after olivine (Crawford et al., 1992). The ground mass consists of feldspar microlites, distinctive reddish-brown chromite and opaques. The massive basaltic lava facies becomes increasingly predominant to the south of the deposit.

Pillow lava facies

This facies consists of pillow lavas with interpillow mud- to silt-sized sediments and hyaloclastic breccias. Pillows vary in cross-sectional width from 0.25 to 2 m and commonly have chilled rims. Vesicularity of the pillows increases from ≈2% at the cores to ≈10% at the rims, although a few rims have considerably higher vesicularity. Vesicles range in size from 2 to 5 mm at the cores, to 30 to 50 mm at the rims and are filled with chlorite, chlorite–carbonate or quartz. The interpillow hyaloclastites are fine grained and interpreted to have been derived from the margins of pillows whilst the sediments, which can contain up to 20% authigenic(?) pyrite are considered to be an indicator of extrusion of the lavas into black shales, similar to the overlying Que River Shale. Near the contact with the Que River Shale a characteristic peperitic texture has developed within the Hellyer basalt. The pillow lava facies becomes more predominant to the north of the deposit.

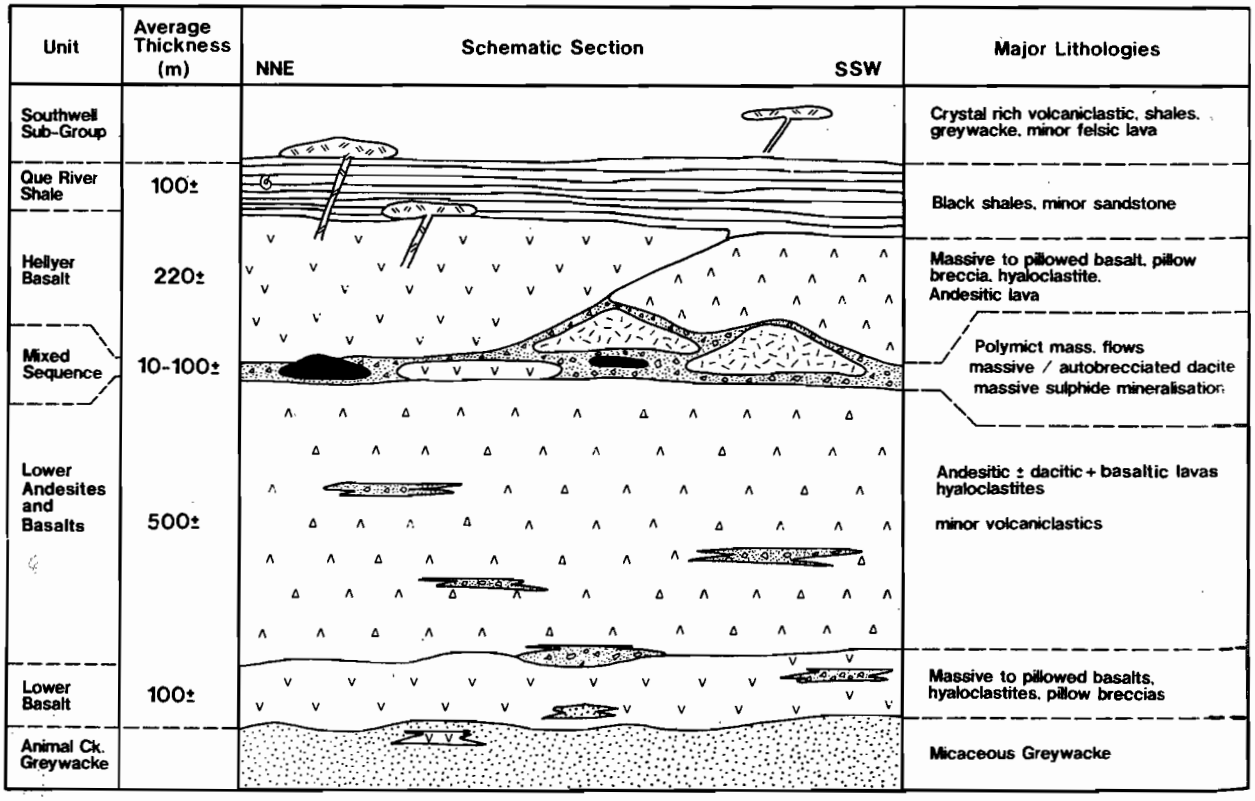

Figure 1. Stratigraphy of the Que–Hellyer Volcanics (from Waters and Wallace, 1992)

Brecciated basaltic lava facies

This facies consists of poorly sorted, angular fragments: porphyritic fragments of the first two basalt facies ranging in size from a few millimetres up to tens of centimetres, and aphyric, totally chloritised fragments of what are interpreted to have been chilled juvenile glassy fragments, ranging in size from 4 to 6 cm. Vesicularity ranges from 0 to 20% in both fragment types. The breccias range from closed framework jigsaw-fit to open framework with up to 50% mud matrix and are considered to be the product of quench fragmentation. This facies occurs throughout the Hellyer basalt and represents 10 to 15% of the unit.

As well as the above three facies some areas of the hangingwall are predominantly andesitic lavas. These lavas consist of plagioclase phenocrysts and glomerocrysts (10–15%), altered totally to albite± sericite ± carbonate and a feldspar/ glass groundmass extensively altered to chlorite, sericite, silica and carbonate.

At the base of the Hellyer basalt there is a thin unit of poorly sorted breccia intercalated with a fine grained bedded volcaniclastic which onlaps the ore body and is known as the the Hellyer hangingwall volcaniclastic suite (HVS).

Geochemistry

Geochemically, the Hellyer basalt has been assigned to Suite III of the five major geochemical suites defined by Crawford et al. (1992). Suite III basalts and andesites have a distinctive and variable chemistry. They range from rocks with low TiO_2 (0.5%), low P_2O_5 (0.1%) and Ti/Zr values of 30–40, to rocks with low TiO_2 (0.4–0.8%), high P_2O_5 (0.4–1%), light REE enriched and Ti/Zr ranging from 19 to 25. The former have affinities with transitional medium to high K calc-alkaline lavas from modern arcs such as Sunda, whilst the latter have been described as "remarkably P_2O_5 and REE-enriched shoshonites with no compositional equivalents in the Andes or modern arc systems." (Crawford et al., 1992). A whole rock geochemistry database was set up by Jack (1989) and the majority of analyses are in the Ti/Zr range of 30–40, with a minor number of analyses down in the 20–30 range. A more primitive core lava, with higher MgO, Cr, Ni,

and Ti/Zr of ≈53, has been identified (Jack, 1989) and occurs immediately above the Hellyer ore body.

Metamorphism and alteration

In the Que–Hellyer area of western Tasmania, Cambrian hydrothermal alteration associated with mineralisation has been overprinted by regional Devonian prehnite–pumpellyite facies metamorphism (Jack, 1989). This has been expressed by the formation of epidote, pumpellyite and prehnite in the footwall andesites at Hellyer, but only rarely are these minerals developed within the Hellyer basalt. The grade of regional metamorphism in this part of the Mt Read Volcanics is lower than that further south where greenschist facies metamorphism is recorded at Mt Lyell (Walshe and Solomon, 1981) and Rosebery/Hercules (Jack, 1989). It has been argued that despite significant textural modification related to deformation, the chemistry of the alteration assemblage formed by hydrothermal processes operating during mineralisation at Mt Lyell has been preserved (op. cit.). McLeod and Stanton (1989) have suggested, with respect to VHMS deposits of southeastern Australia, that regional metamorphism has simply perfected crystal structures and coarsened grain sizes. At Que River, Offler and Whitford (1992) have suggested that the extent of metamorphic recrystallisation has been less than further south, and that preservation of hydrothermal textures and mineral chemistries within the alteration halo is common. At Hellyer, the ore body is substantially less deformed than the ore body at Que River (McArthur, 1986). It would therefore seems likely that substantial preservation of primary hydrothermal minerals and textures has occurred. Offler and Whitford (1992) have outlined textural criteria for discriminating between hydrothermal alteration and metamorphic overprinting and these are outlined below:

Hydrothermal origin

1. Minerals occur in sheaf like, spherulitic, atoll-like, botryoidal, colloform or radiating habit, similar to modern seafloor hot spring deposit mineral textures or the textures observed in the Kuroko VHMS deposits.
2. Exhibit primary depositional features, eg growth banding.
3. Exhibit non-preferred orientation and pleochroism distinctive from their metamorphic counterparts.
4. Are wrapped around by any schistosity present.
5. Are euhedral and associated with other minerals lacking a preferred orientation.
6. Display a void-filling habit.

Metamorphic origin

1. Have a strong preferred orientation
2. Commonly exhibit a fibrous growth habit and occur in extension fractures or pressure shadows.
3. Exhibit annealing or dynamic recrystallisation textures.

Minerals with a burial metamorphic origin, such as plagioclase altered to white mica and/or carbonates, may be difficult to distinguish from the same minerals formed through hydrothermal processes.

At Hellyer, there is an intense green alteration plume immediately above the ore body consisting of pervasive fuchsite–carbonate, some Fe-chlorite, calcite veins and greater amounts of interpillow pyrite than in other areas (Jack, 1989).

RESULTS TO DATE

A. In order to ascertain whether or not alteration zones can be defined around the ore body from drill core logging work already completed, the following exercise is being undertaken. To date, a complete map of the hangingwall alteration at Hellyer has not been produced. Using Datamine software twenty eight east–west cross-sections have been generated for the length of the ore body, from 10150N to 11000N using the Hellyer drill core log database. These cross-sections contain drill hole traces and are annotated with lithologies and colours corresponding to an alteration assemblage type, as determined during core logging. The Hellyer core logging system allows for up to four basic alteration types to be allocated for each core log entry made; the entry "FuCOSePy", for instance, indicates a piece of core which exhibits fuchsite + carbonate + sericite + pyrite alteration. There are 365 different combinations of alteration assemblage in the database, so these have been amalgamated to form 13 alteration assemblage types

(Table 1), based on frequency of occurrence and on importance as determined by the mine experience of Aberfoyle's geologists at Burnie. Work on this exercise is progressing currently. The aim of this portion of the project is to map out the hangingwall alteration in both section and plan.

B. Electron probe microanalyses of carbonates, chlorites, white micas, feldspars and clinopyroxenes have been performed on drill core samples taken from a hole (HL28) within the fuchsite–carbonate alteration zone directly above the ore body, and from another hole (HL14) outside the fuchsite–carbonate alteration plume (Fig. 2). Thin sections were taken at regular intervals down each hole from where they pass into the Hellyer basalt from the Que River Shale to where they pass out of the basalt into the underlying hangingwall volcaniclastic sequence or the ore body (Table 2). The material used was originally put together for a MSc project (Jack, 1989).

Petrography of the Hellyer basalt

The intensity of alteration is variable throughout the basalt. The alteration does not increase in intensity progressively down-hole towards the ore body, and so may be controlled by lithology and/or geochemistry as well as hydrothermal fluids. Samples investigated so far have been dominated by the alteration assemblage carbonate + chlorite + quartz ± white mica ± albite ± pyrite.

Preservation of hydrothermal textures is very common, whereas obvious metamorphic textures such as preferred orientation of minerals, fibrous growth habits and dynamic recrystallisation or annealing are uncommon. Common hydrothermal features are spherulites; ellipsoidal or lobate structures sometimes ringed by pyrite; atoll-like structures ringed with fine grained Ti-rich opaques; growth banded mineral aggregates; colloform or botryoidal textures; and euhedral quartz, pyrite.

Fresh clinopyroxene was found in three samples: 333973, 333974 and 334201. In other samples, clinopyroxene is replaced by carbonate plus varying amounts of quartz and/or chlorite.

Chlorite occurs in very fine grained intergrowths with varying amounts of quartz, carbonate, white mica and albite; at the centre of ellipsoidal, spheroidal or lobate structures and displaying a radiating habit or rimming these structures when they contain quartz or carbonate; in colloform growth with white mica, quartz and carbonate. Occasionally, chlorite exhibits

Table 1. Hellyer alteration assemblages.

Type	Alteration assemblage	Colour code
1	Fu, FuCO, FuCO+..., COFu, COFu+...	56
2	FuSe, FuSe+..., SeFu, SeFu+...	54
3	Cl, FuCl, FuCl+..., ClPy, ClPy+...	47
4	ClSe, ClSe+..., SeCl, SeCl+...	51
5	Se	49
6	SeCO, SeCO+..., COSe, COSe+...	50
7	CO, COCl, COCl+..., COSi, COSi+..., ClCO, ClCO+...	31
8	AbSi, AbSi+...(except Cl), Si, SiAb, SiAb+...(except Cl)	28
9	Ab, Ab+...(except Si, Fu)	29
10	AbSiCl, ClAb, ClAb+..., ClSi, ClSi+..., SiAbCl, SiAbCl+...	36
11	AbFu, AbFuCl, FuAb, FuAb+...	13
12	Si+...(except Ab, Ep)	4
13	Ep, Ep+..., SiEp, SiEp+...	8

Al = albite, Cl = chlorite, CO = carbonate, Ep = epidote, Fu = fuchsite, Py = pyrite, Se = sericite, Si = silica.
Explanatory note:
FuCO = fuchsite + carbonate alteration
FuCO+.. = fuchsite + carbonate + one or two other alteration types eg FuCOSe, FuCOClSe etc
AbSi+...(except Cl) = Albite + silica + one or two other alteration types but not AbSiCl or AbSiClFu etc.

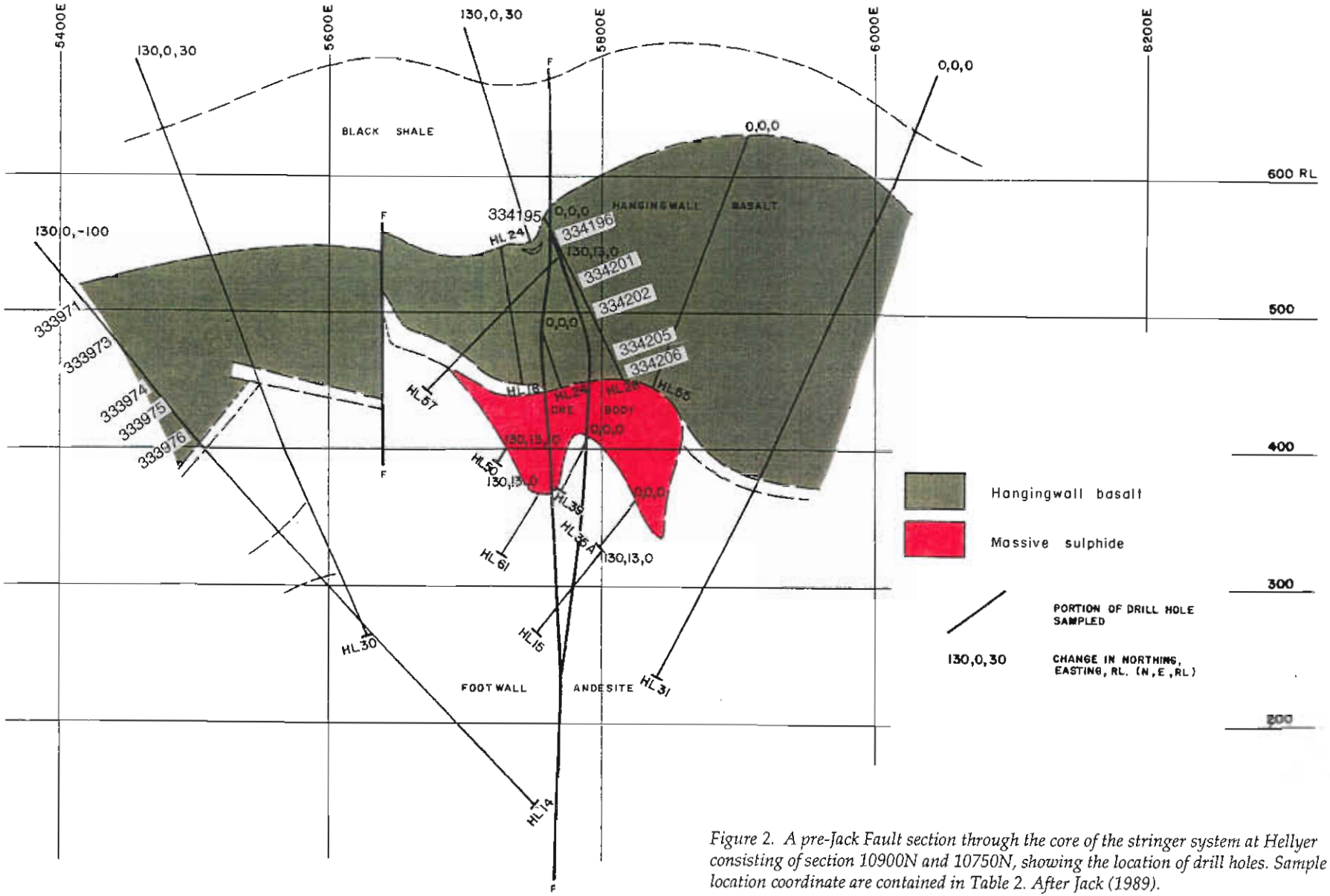

Figure 2. A pre-Jack Fault section through the core of the stringer system at Hellyer consisting of section 10900N and 10750N, showing the location of drill holes. Sample location coordinate are contained in Table 2. After Jack (1989).

Table 2. Details of samples from Hellyer basalt. Pl= pillow lava; l = massive lava; basalt (4) = basalt, alteration intensity (visual estimation) of 4, from Jack (1989).

Hole #	sample #	Northing	Easting	R.L.	Description
HL14	333970	10500	5382	629	black shale (2)
HL14	333971	10500	5419	605	basalt (5)
HL14	333972	?	?	?	basalt (5)
HL14	333973	10498	5439	580	basalt (5)
HL14	333974	10496	5463	550	basalt-pl (5)
HL14	333975	10495	5477	534	basalt-pl (5)
HL14	333976	10493	5495	514	basalt-pl (5)
HL14	333977	10493	5495	513	hangingwall volcaniclastic (9)
HL14	333978	10495	5500	507	lava (9)
HL14	333979	10490	5524	480	albite porphyritic andesite (10)
HL28	334224	10902	5759	566	black shale (2)
HL28	334195	10901	5760	563	basalt-pl (4)
HL28	334196	10901	5763	557	basalt-pl (3)
HL28	334197	10900	5768	546	basalt-pl (3)
HL28	334198	10899	5773	536	basalt-pl (4)
HL28	334199	10899	5774	535	basalt-pl (4)
HL28	334200	10899	5775	533	basalt-pl (4)
HL28	334201	10898	5781	520	basalt-pl (4)
HL28	334202	10896	5790	501	basalt-pl (4)
HL28	334203	10894	5799	483	basalt-l (4)
HL28	334204	10894	5802	478	basalt-pl (4)
HL28	334205	10892	5809	465	basalt-pl (4)
HL28	334206	10891	5816	451	basalt-pl, fuchsite altered (4)

a preferred orientation and fibrous growth habit.

Carbonates occur as irregular aggregates; in spheroidal or ellipsoidal structures rimmed by quartz and/or chlorite, or rimming quartz and/or chlorite; in colloform growths; and in veins. It can display either a sheaflike habit within large spherulites or ellipsoids, or be a optically continuous clear grains up to 10mm across. In one sample (334201) was there a strong preferred orientation of carbonate grains and veins with fibrous growth habit. Carbonate occurs in very fine grained intergrowths with varying amounts of chlorite, quartz, white mica and albite

Quartz occurs in very fine grained intergrowths with varying amounts of chlorite, carbonate, white mica and albite; filling small to large ellipsoidal, spheroidal or lobate structures, usually being coarse grained at the centre and finer grained at the rims; as euhedral crystal in carbonate filled amygdules; as irregular aggregates. A minor amount of fibrous quartz in the pressure shadow of pyrite.

White mica occurs mostly in very fine grained intergrowths with varying amounts of chlorite, carbonate, quartz and albite. In one sample (333972) much coarser white mica occurred in a colloform intergrowths with chlorite.

Albite is mainly distributed throughout the groundmass, intergrown with other minerals and displaying a very fine grained habit, occasionally coarsening up to small lathes. In sample 334196 albite phenocrysts and glomerocrysts up to 1mm across were observed.

Pyrite occurs as discrete euhedral crystals; partially or completely rimming spheroidal, ellipsoidal or lobate structures; in veins; finely disseminated.

Mineral chemistry

The mineral analyses were carried out on a CAMECA SX50 electron microprobe by wavelength dispersive methods using an accelerating voltage of 15kV and beam currents of 20nA for clinopyroxenes, 15nA for

feldspars and 10nA for chlorites, micas and carbonates. The structural formulae were calculated on the basis of 28 oxygens for chlorite, 22 oxygens for white micas, 8 oxygens for feldspars and 6 oxygens for clinopyroxenes.

The majority of chlorites analysed have similar chemistries (Table 3, see end of this report) and are classified as ferro-clinochores (Fig. 3) (Bayliss, 1975). The chlorites from outside the fuchsite–carbonate plume are remarkably similar with Mg/Mg + Fe values ranging from ≈63 to 70. Chlorites from within the fuchsite–carbonate plume have a greater range of Mg/Mg + Fe values, from ≈42 to 81. The low Mg/Mg + Fe chlorites form a distinctive group and are from the most intensely fuchsite–carbonate altered core sample in drill hole HL28, immediately above the ore body (although there are more intensely altered samples still to be analysed). These low Mg/Mg + Fe chlorites are magnesio-chamosites, previously identified as Fe-chlorites. A small group of chlorites have lower Al and higher Mg/Mg + Fe and also contain significant amounts of Cr, up to 1.91 wt % Cr_2O_3. These Cr bearing chlorites were found in two samples in HL28, 334195 and 334202. A total of five analyses of chlorites had more than 1 wt % Cr_2O_3. The chlorites from the most intensely fuchsite–carbonate altered sample, 334206, had a maximum of only 0.11 wt % Cr_2O_3.

Analyses of white micas are presented in Table 4 (see end of this report). Good analyses of white micas have proved difficult to obtain due to their fine grained nature. Many analyses have been rejected due to impurities from accidental inclusion of the edges of neighbouring minerals, (e.g. analysis r5mica1, sample 334202 in Table 4 probably represents a partial analysis of albite with white mica). This problem should be solved when the number of samples analysed increases. White mica analyses from the most intensely fuchsite–carbonate altered core sample in drill hole HL28 (sample 334206), show there is very little Cr enrichment. The nomenclature of chrome micas is not entirely clear – the term fuchsite is defined as a chromian muscovite containing more than 1 wt % Cr_2O_3 (Deer et al., 1962), and having a Si to tetrahedral Al ratio of 6:2, whilst the term mariposite has been used for Cr bearing micas which have a ratio of Si to tetrahedral Al of 7:1 and may have lower Cr contents (Heinrich, 1965). Bailey (1984) suggested that varietal

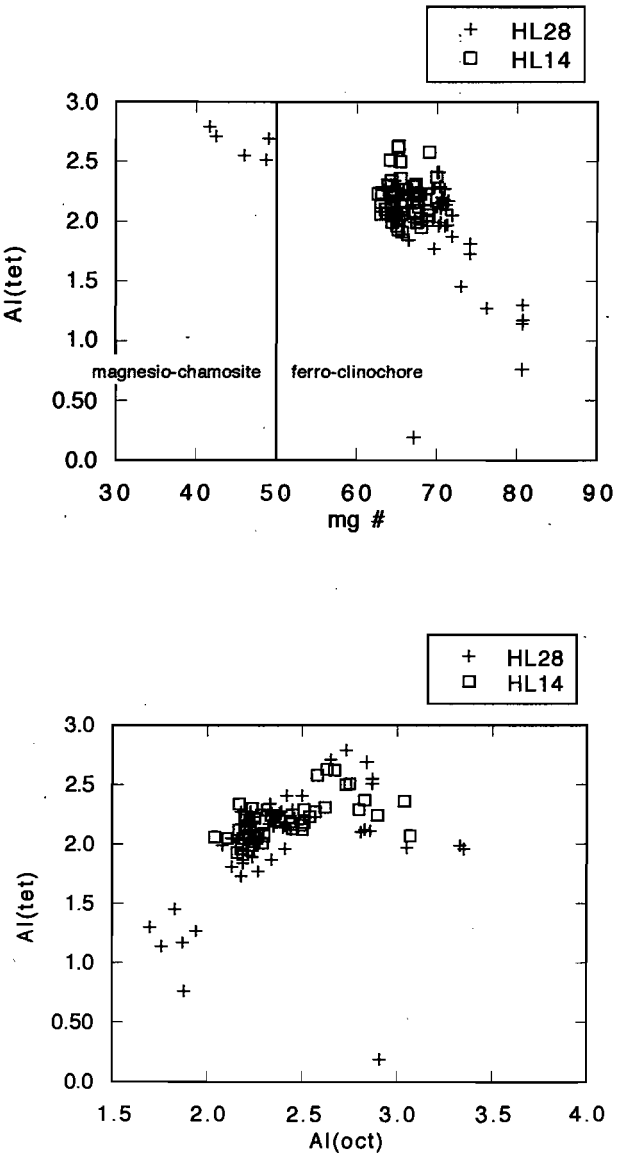

Figure 3. Composition of chlorites in terms of (a) Tetrahedral Al and mg# (Mg/Mg + Fe), and (b) Tetrahedral Al and octahedral Al.

names such as fuchsite and mariposite be abandoned in favour of the use of adjectival modifiers with ideal end members, e.g. chromian muscovite for fuchsite and chromian phengite for mariposite. However the term fuchsite is well established in the Mt Read Volcanics for "bright green mica" and so use of that name will be made here as per the definition of Deer et al. (1962). On that basis, only one analysis from sample 334206 is a fuchsite, (1.11 wt % Cr_2O_3), and this was a mica which was immediately adjacent to a large euhedral chromite. The two other micas with significant Cr (0.66 and 0.47 wt % Cr_2O_3) were also adjacent to chromites. Micas not adjacent to chromites had a range of 0.00 to 0.30 wt % Cr_2O_3. Other workers have recorded high Cr content in white micas at Hellyer (Jack, 1989), and at Que River (Offler and Whitford, 1992). Jack (1989) analysed several white micas from the intensely fuchsite–carbonate alteration plume and recorded up to 1.0 wt % Cr_2O_3, and used the term fuchsite to indicate mica that is light-chrome green macroscopically.

It seems unlikely that the source of Cr in the white micas and chlorites is from chromites except where the micas or chlorites are immediately adjacent, and even then the source may be disseminated chromite. At Hellyer, a more likely source is probably the breakdown of Cr rich clinopyroxene. Clinopyroxenes in the Hellyer basalt have a high Cr_2O_3 content, up to 1.3 wt % Cr_2O_3 (Table 5, see end of this report), and have been completely replaced by carbonate ± quartz ± carbonate in the samples where high Cr content chlorites occur.

The carbonates analysed in the Hellyer hanging-wall alteration are calcites, ferroan dolomites and ankerites (Figure 4; Table 6, see end of this report). The dolomites and ankerites containing the greatest amounts of Mg and Fe are found furthest away from the zone of intense fuchsite–carbonate alteration, and carry up to ≈6 wt % $MnCO_3$. Petrographically these carbonates are "dirty" in appearance, but give good analysis totals. Clear, recrystallised grains, adjacent to the dolomitic and ankeritic carbonates are calcites. The carbonates from the zone of intense fuchsite–carbonate alteration have Mn and Fe > Mg. Most of the vein carbonates are calcites with the exception of some small veins which have up to ≈4.5 wt % $MnCO_3$ and one ankeritic vein. The chemistry of the carbonates is quite variable and there appears to have been more than one phase of carbonate alteration.

Of the feldspars analysed (Table 7, see end of this report), the majority have been albites. Only a few of the feldspars, discounting the bad analyses which indicate contamination with quartz or white mica, contain significant amounts of anorthite, e.g. up 19%.

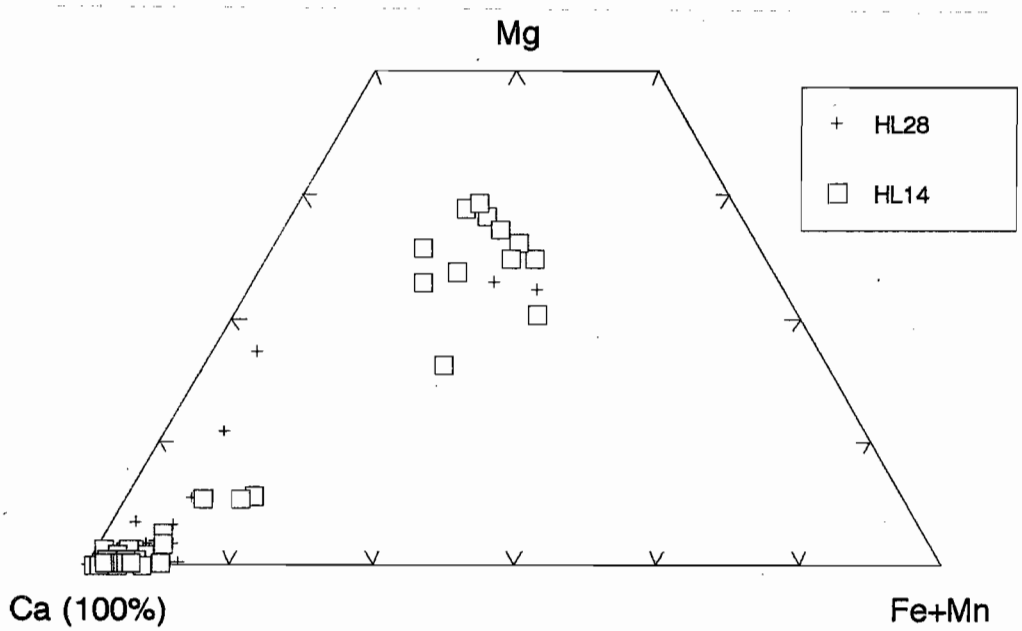

Figure 4. Analyses of carbonates in terms of atomic Ca, Mg, Fe +Mn.

CONCLUSIONS

At this stage enough research has been undertaken to indicate that there is substantial preservation of primary hydrothermal alteration features in the hangingwall alteration at Hellyer. Two distinct chlorite chemistries are apparent, and unusual chromian chlorites with up to 1.9 wt% Cr_2O_3 have been analysed. Only one fuchsite has been analysed, however not many good analyses of white mica have been obtained at this stage. The majority of feldspars analysed have been albites. There is a wide variation in the texture and chemistry of carbonates providing scope for more detailed work.

FUTURE WORK PROGRAM

1. Analysis of minerals using the electron microprobe will continue, with an emphasis on characterising the amount and nature of Cr enrichment in both chlorites and white micas in the hangingwall alteration zone, and identifying the different phases of carbonate alteration and their textures.

2. To map out the hangingwall alteration in section and plan and compare the alteration zonation generated from core logging with alteration zonation defined by electron microprobe analysis of minerals.

REFERENCES

Bailey, S.W. 1984. Classification and structures of the micas. *In* Bailey, S.W. (ed): *REVIEWS IN MINERALOGY 13.* Mineralogical Society of America.

Bayliss, P. 1975. Nomenclature of the trioctahedral chlorites. *Canadian Mineralogist* 13:178–180.

Corbett, K.D., 1992. Stratigraphic-volcanic setting of massive sulfide deposits in the Cambrian Mount Read Volcanics, Tasmania. *Economic Geology* 87: 564–586.

Corbett, K.D. and Komyshan, P. 1989. Geology of the Hellyer–Mt Charter area. Tasmania Department of Mines, Mt Read Volcanics Project Geology Report 1: 48 pp.

Crawford, A.J., Corbett, K.D., and Everard, J.L. 1992. Geochemistry of the Cambrian volcanic-hosted massive sulfide-rich Mount Read Volcanics. *Economic Geology* 87: 597–619.

Deer, W.A., Howie, R.A. and Zussman, J. 1962. *ROCK FORMING MINERALS 3: SHEET SILICATES.* Longmans: 371pp.

Heinrich, E.W. 1965. Further information on the geology of chromian muscovites. *American Mineralogist.* 50: 758–765.

Jack, D.J., 1989. Hellyer Host Rock Alteration. Unpubl. MSc thesis, University of Tasmania: 182 pp.

Offler, R., Hand, M. and Whitford, D.J. 1987. A study of white micas in "fuchsite–carbonate" rocks adjacent to mineralisation, Que River, Tasmania. CSIRO Division of Mineral Physics and Mineralogy, Restricted Report 1684R: 11 pp.

Offler, R. and Whitford, D.J. 1992. Wall–rock alteration and metamorphism of a volcanic-hosted massive sulfide deposit at Que River, Tasmania: petrology and mineralogy. *Economic Geology* 87: 686–705.

McLeod, R.L. and Stanton, R.L. 1984. Phyllosilicates and associated minerals in some Palaeozoic stratiform sulfide deposits of southeastern Australia. *Economic Geology* 79: 1–22.

Walshe, J.L. and Solomon, M. 1981. An investigation into the environment of formation of the volcanic-hosted Mt Lyell copper deposits using geology, mineralogy, stable isotopes and a six-component chlorite solid solution model. *Economic Geology* 76: 246–284.

Waters, J.C. and Wallace, D.B., 1992. Volcanology and sedimentology of the host succession to the Hellyer and Que River volcanic-hosted massive sulfide deposits, western Tasmania. *Economic Geology* 87: 650–666.

Table 3. Electron microprobe analyses of chlorites and structural formulae (28 oxygens.)

Hole	HL14	HL14	HL14	HL14	HL14	HL14	HL14	HL14	HL14	HL14	HL14	HL14	HL14	HL14	HL14	HL14
sample #	333971	333971	333971	333971	333971	333971	333971	333971	333971	333971	333971	333971	333971	333972	333972	333972
analysis #	R2CHL1	R2CHL2	R3CHL1	R3CHL2	R3CHL3	R4CHL2	R4CHL3	R4CHL4	R4CHLE5	R5CHL1	R5CHL1	R5CHL1	R5CHL4	R2CHL1	R2CHL2	R2CHL3
SiO2	26.33	27.11	28.22	28.34	28.33	26.65	26.58	28.38	27.16	29.61	29.90	29.81	29.03	29.77	30.07	29.98
TiO2	0.02	0.01	0.01	0.03	0.07	0.04	0.00	0.00	0.00	0.00	0.03	0.00	0.00	0.02	0.03	0.05
Al2O3	21.28	22.04	22.06	23.05	20.30	22.28	22.11	21.48	21.89	17.94	17.44	17.54	19.24	18.01	18.28	22.07
FeO	16.71	19.05	15.99	17.76	18.35	18.94	18.88	17.24	18.53	18.11	18.01	18.42	18.96	17.71	17.66	16.19
MnO	0.11	0.20	0.07	0.12	0.11	0.14	0.17	0.18	0.05	0.00	0.06	0.06	0.09	0.23	0.16	0.15
MgO	20.89	19.20	20.90	18.90	20.09	19.88	19.88	19.97	19.67	21.58	21.51	21.48	20.15	22.12	21.80	18.69
CaO	0.10	0.29	0.04	0.09	0.08	0.35	0.27	0.09	0.10	0.11	0.12	0.11	0.09	0.23	0.21	0.09
Na2O	0.00	0.00	0.01	0.00	0.07	0.00	0.00	0.00	0.02	0.03	0.03	0.00	0.02	0.01	0.00	0.03
K2O	0.00	0.00	0.00	0.04	0.02	0.01	0.00	0.03	0.00	0.03	0.00	0.00	0.01	0.04	0.04	1.08
Cr2O3	•	•	•	•	•	•	•	•	•	•	•	•	•	•	•	•
Cl	0.00	0.02	0.01	0.00	0.00	0.02	0.01	0.00	0.01	0.03	0.01	0.01	0.02	0.01	0.01	0.00
F	0.22	0.03	0.06	0.01	0.10	0.00	0.34	0.01	0.10	0.09	0.15	0.34	0.19	0.26	0.15	0.12
CalcTotal	85.66	87.94	87.36	88.37	87.53	88.39	88.12	87.44	87.57	87.49	87.25	87.66	87.75	88.36	88.42	88.42
Si	5.42	5.49	5.64	5.64	5.73	5.38	5.37	5.71	5.50	5.98	6.05	6.01	5.87	5.95	6.00	5.93
Al(tet)	2.58	2.51	2.37	2.36	2.27	2.62	2.63	2.29	2.50	2.02	1.95	1.99	2.13	2.05	2.01	2.07
Al(oct)	2.58	2.75	2.83	3.04	2.57	2.67	2.63	2.80	2.73	2.25	2.22	2.18	2.45	2.19	2.29	3.07
Fe2	2.88	3.23	2.67	2.96	3.10	3.20	3.19	2.90	3.14	3.06	3.05	3.11	3.21	2.96	2.94	2.68
Mg	6.41	5.79	6.22	5.60	6.06	5.98	5.98	5.99	5.94	6.50	6.49	6.46	6.07	6.59	6.48	5.51
Ca	0.02	0.06	0.01	0.02	0.02	0.08	0.06	0.02	0.02	0.02	0.03	0.02	0.02	0.05	0.05	0.02
Na	0.00	0.00	0.01	0.00	0.03	0.00	0.00	0.00	0.01	0.01	0.01	0.00	0.01	0.00	0.00	0.01
K	0.00	0.00	0.00	0.01	0.01	0.00	0.00	0.01	0.00	0.01	0.00	0.00	0.00	0.01	0.01	0.27
Ti	0.00	0.00	0.00	0.00	0.01	0.01	0.00	0.00	0.00	0.00	0.00	0.00	0.00	0.00	0.00	0.01
Mn	0.02	0.04	0.01	0.02	0.02	0.03	0.03	0.03	0.01	0.00	0.01	0.01	0.02	0.04	0.03	0.03
F	0.14	0.02	0.04	0.01	0.07	0.00	0.22	0.01	0.07	0.06	0.10	0.22	0.12	0.17	0.09	0.07
Cl	0.00	0.01	0.01	0.00	0.00	0.01	0.00	0.00	0.00	0.01	0.00	0.00	0.01	0.00	0.00	0.00
Zn	0.01	0.00	0.00	0.00	0.01	0.01	0.00	0.01	0.01	0.00	0.01	0.00	0.00	0.01	0.01	0.00
mg#	69.03	64.24	69.96	65.48	66.13	65.17	65.24	67.37	65.42	67.99	68.04	67.53	65.45	69.00	68.76	67.29
Total Cation	20.07	19.90	19.79	19.67	19.89	19.97	20.11	19.76	19.92	19.93	19.92	20.01	19.91	20.02	19.91	19.67
Ox Equiv	28.00	28.00	28.00	28.00	28.00	28.00	28.00	28.00	28.00	28.00	28.00	28.00	28.00	28.00	28.00	28.00

Table 3. cont

Hole	HL14	HL14	HL14	HL14	HL14	HL14	HL14	HL14	HL14	HL14	HL14	HL14	HL14	HL14	HL14	HL14
sample #	333972	333972	333972	333972	333972	333972	333972	333972	333972	333972	333973	333973	333973	333973	333973	333973
analysis #	R2CHL4	R2CHL5	R2CHL6	R2CHL7	R3CHL1	R3CHL2	R4CHL1	R4CHL2	R4CHL3	R4CHL4	R1CHL1	R1CHL2	R1CHL3	R1CHL4	R2CHL1	R2CHL2
SiO2	28.95	29.55	28.75	28.77	28.90	28.72	29.05	28.94	28.35	28.21	28.48	29.81	29.23	29.41	29.53	29.90
TIO2	0.00	0.01	0.00	0.09	0.04	0.02	0.04	0.03	0.01	0.05	0.00	0.00	0.00	0.00	0.05	0.04
Al2O3	19.65	18.61	19.49	21.75	19.70	20.15	19.38	19.58	20.20	20.73	16.90	17.09	17.99	17.55	17.15	17.07
FeO	17.82	17.48	17.96	16.74	17.14	17.67	17.54	18.26	18.15	17.65	19.09	19.19	20.56	19.84	19.39	19.06
MnO	0.16	0.21	0.07	0.11	0.13	0.12	0.19	0.08	0.15	0.07	0.31	0.36	0.40	0.22	0.35	0.27
MgO	20.74	21.65	21.29	19.43	20.96	20.67	20.59	20.79	20.72	20.46	19.31	20.17	19.65	20.17	20.25	20.42
CaO	0.20	0.40	0.25	0.18	0.19	0.22	0.16	0.16	0.11	0.10	1.65	0.69	0.36	0.27	0.44	0.49
Na2O	0.02	0.01	0.02	0.03	0.03	0.00	0.04	0.03	0.01	0.00	0.03	0.00	0.00	0.01	0.03	0.05
K2O	0.02	0.03	0.03	0.63	0.14	0.20	0.11	0.12	0.05	0.08	0.08	0.10	0.06	0.06	0.05	0.10
Cr2O3	•	•	•	•	•	•	•	•	•	•	•	•	•	•	•	•
Cl	0.00	0.00	0.00	0.01	0.00	0.03	0.02	0.02	0.02	0.01	0.00	0.00	0.00	0.00	0.02	0.01
F	0.01	0.24	0.30	0.00	0.13	0.11	0.06	0.18	0.03	0.08	0.21	0.31	0.16	0.01	0.09	0.06
CalcTotal	87.62	88.10	88.03	87.73	87.34	87.96	87.15	88.12	87.87	87.43	86.01	87.68	88.35	87.53	87.32	87.48
Si	5.84	5.91	5.77	5.76	5.83	5.77	5.88	5.81	5.72	5.69	5.95	6.07	5.94	6.01	6.04	6.09
Al(tet)	2.16	2.09	2.23	2.24	2.18	2.23	2.12	2.19	2.29	2.31	2.05	1.93	2.06	1.99	1.96	1.91
Al(oct)	2.50	2.30	2.38	2.90	2.51	2.54	2.50	2.44	2.51	2.62	2.11	2.16	2.25	2.24	2.18	2.19
Fe2	3.01	2.93	3.01	2.80	2.89	2.97	2.97	3.07	3.06	2.98	3.33	3.27	3.50	3.39	3.32	3.25
Mg	6.23	6.46	6.37	5.80	6.30	6.19	6.21	6.22	6.23	6.15	6.01	6.12	5.95	6.14	6.18	6.20
Ca	0.04	0.09	0.05	0.04	0.04	0.05	0.04	0.04	0.02	0.02	0.37	0.15	0.08	0.06	0.10	0.11
Na	0.01	0.00	0.01	0.01	0.01	0.00	0.01	0.01	0.00	0.00	0.01	0.00	0.00	0.01	0.01	0.02
K	0.00	0.01	0.01	0.16	0.04	0.05	0.03	0.03	0.01	0.02	0.02	0.03	0.02	0.02	0.01	0.03
Ti	0.00	0.00	0.00	0.01	0.01	0.00	0.01	0.00	0.00	0.01	0.00	0.00	0.00	0.00	0.01	0.01
Mn	0.03	0.04	0.01	0.02	0.02	0.02	0.03	0.01	0.03	0.01	0.06	0.06	0.07	0.04	0.06	0.05
F	0.01	0.15	0.19	0.00	0.08	0.07	0.04	0.12	0.02	0.05	0.14	0.20	0.10	0.01	0.06	0.04
Cl	0.00	0.00	0.00	0.00	0.00	0.01	0.01	0.01	0.01	0.00	0.00	0.00	0.00	0.00	0.01	0.00
Zn	0.01	0.00	0.00	0.00	0.01	0.01	0.00	0.00	0.01	0.00	0.00	0.01	0.00	0.00	0.00	0.01
mg#	67.48	68.82	67.88	67.41	68.55	67.58	67.67	67.00	67.04	67.39	64.33	65.20	63.01	64.43	65.06	65.63
Total Cation	19.84	19.97	20.03	19.75	19.89	19.91	19.85	19.95	19.91	19.87	20.06	20.00	19.97	19.89	19.93	19.89
Ox Equiv	28.00	28.00	28.00	28.00	28.00	28.00	28.00	28.00	28.00	28.00	28.00	28.00	28.00	28.00	28.00	28.00

Table 3. cont

Hole	HL14	HL14	HL14	HL14	HL14	HL14	HL14	HL14	HL14	HL14	HL14	HL14	HL14	HL14	HL14	HL14
sample #	333973	333973	333973	333973	333973	333975	333975	333975	333975	333975	333975	333975	333975	333975	333975	333975
analysis #	R3CHL1	R3CHL2	R3CHL3	R4CHL1	R4CHL2	R3CHL1	R3CHL2	R3CHL3	R3CHL4	R4CHL1	R4CHL2	R4CHL3	R4CHL4	R5CHL1	R5CHL2	R5CHL3
SIO2	28.53	28.80	29.00	28.55	28.73	28.20	28.24	27.67	28.15	29.42	28.85	28.65	27.57	28.32	28.64	29.26
TIO2	0.00	0.00	0.00	0.00	0.08	0.03	0.05	0.00	0.06	0.00	0.00	0.05	0.04	0.02	0.00	0.02
AI2O3	17.99	17.78	18.04	17.83	17.60	19.02	18.57	18.68	18.33	17.49	17.47	18.18	18.63	19.08	18.15	17.14
FeO	20.33	20.19	20.02	19.68	19.33	20.47	20.20	20.26	21.06	19.64	19.51	20.19	20.25	19.88	20.20	19.97
MnO	0.28	0.34	0.42	0.41	0.28	0.28	0.08	0.23	0.15	0.21	0.22	0.15	0.29	0.25	0.27	0.33
MgO	19.46	19.82	19.86	19.39	19.82	19.70	20.33	20.14	19.89	20.67	20.25	20.43	20.51	20.24	20.49	21.39
CaO	0.93	0.53	0.31	0.27	0.40	0.09	0.12	0.07	0.08	0.14	0.18	0.07	0.01	0.15	0.12	0.02
Na2O	0.02	0.02	0.00	0.04	0.03	0.02	0.02	0.01	0.01	0.02	0.04	0.01	0.01	0.03	0.02	0.01
K2O	0.02	0.07	0.06	0.08	0.06	0.03	0.02	0.00	0.00	0.00	0.02	0.00	0.00	0.02	0.01	0.00
Cr2O3	•	•	•	•	•	•	•	•	•	•	•	•	•	•	•	•
Cl	0.00	0.00	0.00	0.00	0.02	0.02	0.03	0.01	0.03	0.00	0.00	0.00	0.02	0.00	0.00	0.02
F	0.00	0.13	0.02	0.00	0.23	0.09	0.00	0.14	0.19	0.16	0.11	0.17	0.25	0.00	0.09	0.12
CalcTotal	87.56	87.69	87.73	86.24	86.49	87.91	87.71	87.21	87.92	87.68	86.60	87.85	87.49	88.02	87.94	88.27
SI	5.87	5.90	5.93	5.93	5.94	5.76	5.78	5.70	5.77	5.99	5.95	5.84	5.66	5.76	5.84	5.94
Al(te1)	2.13	2.10	2.07	2.07	2.07	2.24	2.22	2.30	2.23	2.01	2.05	2.16	2.34	2.24	2.16	2.06
Al(oct)	2.23	2.20	2.27	2.30	2.22	2.34	2.25	2.24	2.20	2.18	2.20	2.21	2.17	2.34	2.20	2.04
Fe2	3.50	3.46	3.42	3.42	3.34	3.50	3.46	3.49	3.61	3.34	3.37	3.44	3.48	3.38	3.45	3.39
Mg	5.97	6.06	6.05	6.01	6.10	6.00	6.20	6.19	6.08	6.27	6.23	6.21	6.28	6.14	6.23	6.47
Ca	0.21	0.12	0.07	0.06	0.09	0.02	0.03	0.02	0.02	0.03	0.04	0.02	0.00	0.03	0.03	0.00
Na	0.01	0.01	0.00	0.02	0.01	0.01	0.01	0.01	0.01	0.01	0.01	0.01	0.00	0.01	0.01	0.00
K	0.00	0.02	0.02	0.02	0.02	0.01	0.01	0.00	0.00	0.00	0.01	0.00	0.00	0.00	0.00	0.00
TI	0.00	0.00	0.00	0.00	0.01	0.00	0.01	0.00	0.01	0.00	0.00	0.01	0.01	0.00	0.00	0.00
Mn	0.05	0.06	0.07	0.07	0.05	0.05	0.01	0.04	0.03	0.04	0.04	0.03	0.05	0.04	0.05	0.06
F	0.00	0.08	0.02	0.00	0.15	0.06	0.00	0.09	0.12	0.10	0.07	0.11	0.16	0.00	0.06	0.08
Cl	0.00	0.00	0.00	0.00	0.01	0.01	0.01	0.01	0.01	0.00	0.00	0.00	0.01	0.00	0.00	0.01
Zn	0.00	0.01	0.00	0.00	0.00	0.00	0.01	0.01	0.01	0.00	0.00	0.00	0.01	0.01	0.00	0.01
mg#	63.05	63.63	63.88	63.72	64.63	63.18	64.21	63.94	62.73	65.23	64.92	64.33	64.36	64.48	64.39	65.62
Total Cation	19.96	20.01	19.92	19.90	20.00	19.99	19.99	20.08	20.08	19.97	19.97	20.03	20.16	19.96	20.01	20.06
Ox Equiv	28.00	28.00	28.00	28.00	28.00	28.00	28.00	28.00	28.00	28.00	28.00	28.00	28.00	28.00	28.00	28.00

Table 3. cont

Hole	HL14	HL28	HL28	HL28	HL28	HL28	HL28	HL28	HL28	HL28	HL28	HL28	HL28	HL28	HL28	HL28
sample #	333975	334195	334195	334195	334195	334195	334195	334195	334195	334195	334195	334195	334196	334196	334196	334196
analysis #	R5CHL4	R1CHL1	R1CHL2	R1CHL2	R1 CHL3	R1CHL4	R4CHL1	R4CHL2	R5CHL1	R5CHL2	R5CHL3	R5CHL4	R1CHL1	R1CHL2	R2CHL1	R3CHL1
SiO2	28.93	30.77	30.55	30.81	29.74	30.71	29.27	30.17	31.30	31.15	30.01	30.06	28.68	28.65	28.91	28.30
TiO2	0.00	0.03	0.03	0.00	0.05	0.00	0.02	0.01	0.05	0.01	0.06	0.05	0.12	0.03	0.03	0.01
Al2O3	17.90	16.26	17.76	16.65	18.23	21.71	19.22	21.30	23.32	23.40	21.41	21.49	18.57	19.77	19.14	18.60
FeO	20.30	14.05	15.17	14.68	15.87	14.39	15.90	15.20	14.33	14.30	15.78	15.52	19.63	19.54	18.92	18.95
MnO	0.29	0.00	0.02	0.07	0.10	0.05	0.11	0.11	0.10	0.08	0.09	0.13	0.15	0.17	0.14	0.11
MgO	20.61	22.55	21.77	23.60	21.78	20.03	21.97	21.00	18.96	19.09	20.67	20.79	20.80	20.52	20.94	21.25
CaO	0.20	0.19	0.19	0.18	0.19	0.25	0.42	0.46	0.28	0.25	0.25	0.31	0.17	0.13	0.13	0.12
Na2O	0.01	0.00	0.00	0.03	0.03	0.01	0.05	0.02	0.12	0.03	0.03	0.03	0.08	0.09	0.07	0.04
K2O	0.00	0.00	0.00	0.01	0.02	0.40	0.05	0.11	0.47	0.72	0.14	0.21	0.01	0.00	0.00	0.00
Cr2O3	•	1.18	1.27	•	•	•	•	•	•	•	•	•	•	•	•	•
Cl	0.00	0.01	0.03	0.02	0.00	0.03	0.03	0.00	0.00	0.00	0.01	0.00	0.00	0.02	0.01	0.00
F	0.00	•	•	0.34	0.00	0.23	0.36	0.28	0.07	0.12	0.23	0.02	0.00	0.26	0.00	0.28
CalcTotal	88.32	85.04	86.78	86.23	86.01	87.70	87.25	88.54	88.96	89.10	88.57	88.62	88.21	89.06	88.30	87.56
Si	5.88	6.27	6.14	6.19	6.04	6.03	5.86	5.90	6.04	6.01	5.88	5.89	5.81	5.73	5.82	5.75
Al(tet)	2.12	1.73	1.87	1.81	1.96	1.97	2.14	2.10	1.96	1.99	2.12	2.11	2.19	2.27	2.18	2.25
Al(oct)	2.17	2.18	2.34	2.13	2.41	3.05	2.40	2.81	3.35	3.33	2.83	2.86	2.25	2.39	2.36	2.21
Fe2	3.45	2.40	2.55	2.47	2.70	2.36	2.66	2.49	2.31	2.31	2.59	2.54	3.33	3.27	3.19	3.22
Mg	6.25	6.86	6.52	7.07	6.59	5.86	6.56	6.13	5.46	5.49	6.04	6.08	6.28	6.12	6.29	6.44
Ca	0.04	0.04	0.04	0.04	0.04	0.05	0.09	0.10	0.06	0.05	0.05	0.07	0.04	0.03	0.03	0.03
Na	0.01	0.00	0.00	0.01	0.01	0.01	0.02	0.01	0.05	0.01	0.01	0.01	0.03	0.03	0.03	0.02
K	0.00	0.00	0.00	0.00	0.01	0.10	0.01	0.03	0.12	0.18	0.04	0.05	0.00	0.00	0.00	0.00
Tl	0.00	0.01	0.00	0.00	0.01	0.00	0.00	0.00	0.01	0.00	0.01	0.01	0.02	0.00	0.01	0.00
Mn	0.05	0.00	0.00	0.01	0.02	0.01	0.02	0.02	0.02	0.01	0.02	0.02	0.03	0.03	0.03	0.02
F	0.00	0.00	0.00	0.21	0.00	0.15	0.23	0.17	0.04	0.07	0.14	0.01	0.00	0.17	0.00	0.18
Cl	0.00	0.00	0.01	0.01	0.00	0.01	0.01	0.00	0.00	0.00	0.00	0.00	0.00	0.01	0.01	0.00
Zn	0.01	0.19	0.20	0.00	0.00	0.00	0.00	0.00	0.00	0.00	0.00	0.00	0.00	0.00	0.00	0.00
mg#	64.42	74.10	71.90	74.13	70.99	71.28	71.12	71.12	70.23	70.42	70.01	70.48	65.38	65.18	66.36	66.66
Total Cation	19.98	19.68	19.66	19.95	19.78	19.59	20.00	19.74	19.40	19.46	19.73	19.66	19.97	20.04	19.92	20.12
Ox Equiv	28.00	28.00	28.00	28.00	28.00	28.00	28.00	28.00	28.00	28.00	28.00	28.00	28.00	28.00	28.00	28.00

Table 3. cont

Hole	HL28	HL28	HL28	HL28	HL28	HL28	HL28	HL28	HL28	HL28	HL28	HL28	HL28	HL28	HL28	HL28
sample #	334196	334196	334196	334196	334196	334196	334201	334201	334201	334201	334201	334201	334201	334201	334201	334201
analysis #	R3CHL2	R4CHL1	R4CHL2	R6CHL1	R6CHL2	R6CHL3	R2CHLve1	R2CHLve2	R2CHL1	R3 CHL2	R3CHL1	R3 CHL2	R4CHL1	R4CHL2	R5CHL2cpx	R5CHL4
SiO2	28.54	28.73	28.44	29.41	28.84	28.59	28.11	27.72	27.94	28.16	28.54	27.82	29.64	29.88	37.46	41.75
TiO2	0.00	0.01	0.00	0.03	0.03	0.00	0.00	0.02	0.01	0.00	0.02	0.02	0.03	0.00	0.00	0.00
Al2O3	19.08	19.02	19.50	19.36	19.81	19.47	19.12	19.44	18.74	18.71	18.28	18.91	17.01	16.55	11.59	14.04
FeO	19.30	18.78	19.15	18.73	19.49	19.06	20.05	19.53	19.14	19.16	20.11	20.11	18.91	18.57	11.13	16.04
MnO	0.11	0.20	0.14	0.20	0.10	0.12	0.47	0.63	0.46	0.44	0.50	0.46	0.23	0.35	0.14	0.34
MgO	20.75	20.75	20.73	20.59	20.16	20.58	20.36	20.12	19.86	19.39	20.15	19.55	21.75	20.67	25.99	18.40
CaO	0.17	0.10	0.11	0.05	0.04	0.07	0.22	0.28	0.15	0.16	0.53	0.18	0.15	0.06	0.85	0.18
Na2O	0.12	0.12	0.14	0.16	0.15	0.11	0.02	0.08	0.01	0.02	0.05	0.04	0.01	0.03	0.08	0.02
K2O	0.00	0.01	0.04	0.02	0.03	0.04	0.00	0.00	0.01	0.01	0.02	0.01	0.02	0.04	0.04	0.01
Cr2O3	•	•	•	•	•	•	•	•	0.00	0.12	•	•	•	0.00	•	•
Cl	0.00	0.02	0.02	0.01	0.03	0.00	0.00	0.01	0.00	0.00	0.02	0.00	0.00	0.00	0.00	0.00
F	0.22	0.16	0.06	0.12	0.21	0.29	0.00	0.07	•	•	0.10	0.00	0.00	•	0.19	0.01
CalcTotal	88.20	87.84	88.29	88.63	88.80	88.21	88.35	87.87	86.34	86.17	88.29	87.12	87.76	86.14	87.40	90.78
Si	5.76	5.81	5.74	5.88	5.78	5.76	5.71	5.66	5.79	5.84	5.81	5.74	6.01	6.16	7.24	7.81
Al(tet)	2.24	2.19	2.26	2.12	2.22	2.24	2.29	2.34	2.21	2.16	2.19	2.26	1.99	1.84	0.76	0.19
Al(oct)	2.31	2.35	2.38	2.44	2.46	2.38	2.29	2.33	2.36	2.41	2.20	2.34	2.08	2.19	1.88	2.91
Fe2	3.26	3.18	3.23	3.13	3.27	3.21	3.41	3.33	3.31	3.32	3.43	3.47	3.21	3.20	1.80	2.51
Mg	6.25	6.26	6.24	6.14	6.02	6.18	6.17	6.12	6.13	6.00	6.12	6.01	6.58	6.36	7.49	5.13
Ca	0.04	0.02	0.02	0.01	0.01	0.01	0.05	0.06	0.03	0.04	0.12	0.04	0.03	0.01	0.18	0.04
Na	0.05	0.05	0.05	0.06	0.06	0.04	0.01	0.03	0.01	0.01	0.02	0.02	0.00	0.01	0.03	0.01
K	0.00	0.00	0.01	0.01	0.01	0.01	0.00	0.00	0.00	0.00	0.01	0.00	0.00	0.01	0.01	0.00
Ti	0.00	0.00	0.00	0.00	0.01	0.00	0.00	0.00	0.00	0.00	0.00	0.00	0.01	0.00	0.00	0.00
Mn	0.02	0.04	0.03	0.03	0.02	0.02	0.08	0.11	0.08	0.08	0.09	0.08	0.04	0.06	0.02	0.05
F	0.14	0.10	0.04	0.08	0.13	0.18	0.00	0.04	0.00	0.00	0.07	0.00	0.00	0.00	0.12	0.01
Cl	0.00	0.01	0.01	0.00	0.01	0.00	0.00	0.01	0.00	0.00	0.01	0.00	0.00	0.00	0.00	0.00
Zn	0.00	0.00	0.00	0.00	0.00	0.00	0.00	0.00	0.00	0.02	0.00	0.00	0.00	0.00	0.00	0.00
mg#	65.72	66.33	65.87	66.21	64.84	65.81	64.41	64.74	64.91	64.34	64.10	63.41	67.22	66.49	80.63	67.16
Total Cation	20.06	20.00	20.00	19.91	19.98	20.05	20.00	20.04	19.93	19.87	20.04	19.97	19.95	19.84	19.52	18.65
Ox Equiv	28.00	28.00	28.00	28.00	28.00	28.00	28.00	28.00	28.00	28.00	28.00	28.00	28.00	28.00	28.00	28.00

Table 3. cont

Hole	HL28	HL28	HL28	HL28	HL28	HL28	HL28	HL28	HL28	HL28	HL28	HL28	HL28	HL28	HL28	HL28
sample #	334201	334201	334201	334202	334202	334202	334202	334202	334202	334202	334202	334202	334202	334202	334202	334202
analysis #	R5CHL5	R5CHL3cpx	R5CHL7	R1CHL1	R1CHL2	R2CHL1	r2chl2	r2chl3	R2CHL4	R2CHL5	R3CHL2	R3CHL3	R4CHL1cr	R4CHL2	R4CHL3rm	R4CHL4rm
SiO2	29.29	33.88	29.66	29.16	28.81	34.38	33.57	34.56	29.11	27.84	27.97	28.35	33.08	28.87	27.94	28.62
TiO2	0.00	0.02	0.00	0.01	0.00	0.04	0.00	0.03	0.00	0.00	0.00	0.00	0.00	0.00	0.00	0.02
Al2O3	17.45	13.70	17.05	18.04	18.79	12.31	12.74	13.03	18.49	19.59	20.50	19.38	14.08	18.68	20.83	19.12
FeO	19.58	13.48	18.86	15.68	16.73	10.82	11.18	10.83	16.90	16.23	16.91	17.20	16.05	17.01	16.62	17.73
MnO	0.44	0.19	0.38	0.29	0.21	0.03	0.06	0.00	0.22	0.29	0.27	0.15	0.10	0.28	0.37	0.51
MgO	20.99	24.22	20.23	22.49	21.94	25.32	26.22	25.51	22.72	21.64	22.34	22.17	24.42	22.89	21.78	22.52
CaO	0.17	0.46	0.14	0.10	0.05	0.53	0.29	0.39	0.07	0.07	0.03	0.07	0.25	0.09	0.21	0.04
Na2O	0.01	0.03	0.02	0.02	0.02	0.04	0.05	0.06	0.09	0.03	0.05	0.11	0.05	0.01	0.09	0.00
K2O	0.04	0.03	0.01	0.00	0.00	0.00	0.00	0.01	0.00	0.00	0.00	0.01	0.02	0.00	0.04	0.03
Cr2O3	•	0.69	0.09	0.01	0.01	1.91	1.46	1.54	•	0.00	•	•	•	•	•	•
Cl	0.00	0.02	0.00	0.00	0.01	0.06	0.00	0.00	0.02	0.01	0.01	0.00	0.01	0.00	0.00	0.01
F	0.09	•	•	•	•	•	•	•	0.14	•	0.09	0.03	0.09	0.00	0.20	0.00
CalcTotal	88.03	86.73	86.46	85.79	86.58	85.43	85.58	85.95	87.70	85.70	88.13	87.46	88.10	87.84	88.00	88.58
Si	5.95	6.73	6.11	5.95	5.85	6.86	6.70	6.83	5.84	5.71	5.59	5.72	6.55	5.80	5.59	5.73
Al(tet)	2.05	1.27	1.89	2.05	2.15	1.14	1.30	1.17	2.16	2.29	2.41	2.28	1.45	2.20	2.41	2.27
Al(oct)	2.13	1.94	2.24	2.29	2.35	1.76	1.70	1.87	2.22	2.45	2.42	2.33	1.83	2.22	2.50	2.23
Fe2	3.33	2.24	3.25	2.67	2.84	1.81	1.87	1.79	2.84	2.79	2.83	2.90	2.66	2.86	2.78	2.97
Mg	6.36	7.17	6.21	6.84	6.65	7.53	7.80	7.52	6.80	6.62	6.66	6.67	7.21	6.85	6.49	6.72
Ca	0.04	0.10	0.03	0.02	0.01	0.11	0.06	0.08	0.02	0.02	0.01	0.02	0.05	0.02	0.05	0.01
Na	0.00	0.01	0.01	0.01	0.01	0.02	0.02	0.02	0.04	0.01	0.02	0.04	0.02	0.01	0.03	0.00
K	0.01	0.01	0.00	0.00	0.00	0.00	0.00	0.00	0.00	0.00	0.00	0.00	0.00	0.00	0.01	0.01
Ti	0.00	0.00	0.00	0.00	0.00	0.01	0.00	0.00	0.00	0.00	0.00	0.00	0.00	0.00	0.00	0.00
Mn	0.08	0.03	0.07	0.05	0.04	0.01	0.01	0.00	0.04	0.05	0.05	0.03	0.02	0.05	0.06	0.09
F	0.06	0.00	0.00	0.00	0.00	0.00	0.00	0.00	0.09	0.00	0.06	0.02	0.06	0.00	0.13	0.00
Cl	0.00	0.01	0.00	0.00	0.00	0.02	0.00	0.00	0.01	0.00	0.01	0.00	0.00	0.00	0.00	0.00
Zn	0.00	0.11	0.02	0.00	0.00	0.30	0.23	0.24	0.00	0.00	0.00	0.00	0.00	0.00	0.00	0.00
mg#	65.65	76.21	65.66	71.89	70.04	80.67	80.70	80.77	70.56	70.38	70.20	69.67	73.06	70.58	70.02	69.36
Total Cation	20.00	19.62	19.82	19.88	19.90	19.55	19.70	19.54	20.03	19.93	20.04	20.01	19.85	20.00	20.05	20.02
Ox Equiv	28.00	28.00	28.00	28.00	28.00	28.00	28.00	28.00	28.00	28.00	28.00	28.00	28.00	28.00	28.00	28.00

Table 3. cont

Hole	HL28	HL28	HL28	HL28	HL28	HL28	HL28	HL28	HL28	HL28
sample #	334202	334202	334202	334202	334205	334206	334206	334206	334206	334206
analysis #	R5CHL1	R5CHL2	R6CHL1	R6CHL2	R3CHL1	R4CHL1	R4CHL2	R6CHL1	R4CHL2	R6 CHL2
SiO2	28.43	28.70	28.71	28.53	30.68	24.77	24.21	25.21	25.98	25.47
TiO2	0.00	0.00	0.02	0.01	0.05	0.02	0.02	0.04	0.07	0.14
Al2O3	18.76	18.80	19.29	18.74	16.85	21.32	21.77	22.23	21.61	21.48
FeO	16.87	16.03	16.13	17.90	16.45	29.89	29.85	25.77	25.65	26.57
MnO	0.23	0.35	0.30	0.26	0.08	0.19	0.17	0.23	0.20	0.19
MgO	23.11	22.44	22.00	22.00	21.18	12.41	11.98	13.95	13.68	12.74
CaO	0.05	0.03	0.08	0.05	0.20	0.05	0.13	0.26	0.14	0.09
Na2O	0.02	0.04	0.04	0.02	0.04	0.00	0.05	0.00	0.02	0.05
K2O	0.00	0.00	0.02	0.01	0.02	0.00	0.00	0.06	0.03	0.03
Cr2O3	•	0.01	0.00	•	0.72	•	•	•	0.03	0.11
Cl	0.00	0.02	0.00	0.00	0.03	0.00	0.00	0.03	0.00	0.03
F	0.08	•	•	0.06	•	0.12	0.00	0.09	•	•
CalcTotal	87.53	86.43	86.59	87.57	86.29	88.72	88.18	87.83	87.42	86.89
Si	5.73	5.83	5.82	5.77	6.24	5.29	5.21	5.32	5.49	5.45
Al(tet)	2.27	2.17	2.18	2.23	1.77	2.71	2.79	2.69	2.51	2.55
Al(oct)	2.18	2.33	2.42	2.24	2.27	2.65	2.73	2.84	2.87	2.87
Fe2	2.84	2.72	2.73	3.03	2.80	5.34	5.37	4.54	4.53	4.76
Mg	6.94	6.79	6.64	6.64	6.42	3.95	3.84	4.39	4.31	4.07
Ca	0.01	0.01	0.02	0.01	0.04	0.01	0.03	0.06	0.03	0.02
Na	0.01	0.02	0.01	0.01	0.02	0.00	0.02	0.00	0.01	0.02
K	0.00	0.00	0.01	0.00	0.01	0.00	0.00	0.02	0.01	0.01
Ti	0.00	0.00	0.00	0.00	0.01	0.00	0.00	0.01	0.01	0.02
Mn	0.04	0.06	0.05	0.05	0.01	0.04	0.03	0.04	0.04	0.03
F	0.05	0.00	0.00	0.04	0.00	0.08	0.00	0.06	0.00	0.00
Cl	0.00	0.01	0.00	0.00	0.01	0.00	0.00	0.01	0.00	0.01
Zn	0.00	0.00	0.00	0.00	0.12	0.00	0.00	0.00	0.01	0.02
mg#	70.94	71.39	70.85	68.66	69.65	42.53	41.71	49.11	48.75	46.09
Total Cation	20.08	19.93	19.89	20.01	19.70	20.07	20.03	19.96	19.81	19.83
Ox Equiv	28.00	28.00	28.00	28.00	28.00	28.00	28.00	28.00	28.00	28.00

Table 4. Electron microprobe analyses of white micas and structural formulae (22 oxygens).

Hole	HL14	HL14	HL14	HL14	HL14	HL14	HL14	HL14	HL14	HL14	HL14	HL28	HL28	HL28
sample #	333972	333972	333972	333972	333972	333972	333973	333973	333973	333973	333973	334195	334195	334196
analysis #	r1mica1	r1mica2	r2mica1	r2mica2	r2mica3	r2mica4	r3mica1	r3mica2	r4mica1	r4mica2	r4mica3	r1mica2	r5mica1	r6mica1
SiO2	50.44	51.16	50.99	50.96	50.87	51.40	56.03	57.32	56.32	56.29	55.90	49.42	46.15	48.55
TiO2	0.26	0.19	0.31	0.22	0.32	0.24	0.12	0.28	0.39	0.43	0.34	0.07	0.09	0.02
Al2O3	27.45	27.91	28.28	28.25	27.86	28.31	19.96	18.68	19.93	18.90	19.11	31.74	29.31	32.47
FeO	1.43	1.56	1.39	1.37	1.82	1.35	0.63	0.95	0.66	0.78	0.99	1.05	3.19	1.10
MnO	0.00	0.00	0.00	0.00	0.00	0.00	0.07	0.00	0.04	0.01	0.00	0.00	0.00	0.00
MgO	3.13	3.27	3.16	3.28	3.40	3.16	0.43	0.48	0.39	0.56	0.51	2.60	4.95	1.10
CaO	0.22	0.16	0.18	0.21	0.16	0.15	0.70	0.63	0.83	0.95	0.96	0.07	0.41	0.03
Na2O	0.12	0.08	0.04	0.04	0.10	0.08	0.63	0.78	0.56	1.59	0.36	0.07	0.07	0.41
K2O	9.63	9.64	9.98	9.70	9.79	10.09	13.00	12.84	13.16	11.69	13.40	9.94	8.78	9.97
Cr2O3												•	•	•
Cl	0.04	0.01	0.00	0.02	0.01	0.02	0.02	0.00	0.03	0.01	0.03	0.01	0.01	0.00
F	0.22	0.04	0.15	0.07	0.11	0.35	0.10	0.00	0.17	0.10	0.00	0.25	0.21	0.00
CalcTotal	92.84	94.00	94.42	94.09	94.39	94.99	91.64	91.97	92.39	91.26	91.60	95.13	93.08	93.64
Si	6.83	6.84	6.79	6.80	6.79	6.80	7.77	7.92	7.76	7.82	7.80	6.52	6.32	6.52
Al(tet)	1.17	1.16	1.21	1.20	1.21	1.20	0.23	0.08	0.24	0.18	0.20	1.48	1.68	1.48
Al(oct)	3.21	3.24	3.23	3.25	3.18	3.21	3.04	2.96	2.99	2.92	2.95	3.46	3.04	3.66
Fe2	0.16	0.18	0.16	0.15	0.20	0.15	0.07	0.11	0.08	0.09	0.12	0.12	0.37	0.12
Mg	0.63	0.65	0.63	0.65	0.68	0.62	0.09	0.10	0.08	0.12	0.11	0.51	1.01	0.22
Ca	0.03	0.02	0.03	0.03	0.02	0.02	0.10	0.09	0.12	0.14	0.14	0.01	0.06	0.00
Na	0.03	0.02	0.01	0.01	0.03	0.02	0.17	0.21	0.15	0.43	0.10	0.02	0.02	0.11
K	1.66	1.64	1.70	1.65	1.67	1.70	2.30	2.26	2.31	2.07	2.39	1.67	1.53	1.71
Ti	0.03	0.02	0.03	0.02	0.03	0.02	0.01	0.03	0.04	0.05	0.04	0.01	0.01	0.00
Mn	0.00	0.00	0.00	0.00	0.00	0.00	0.01	0.00	0.00	0.00	0.00	0.00	0.00	0.00
F	0.09	0.02	0.06	0.03	0.05	0.15	0.04	0.00	0.07	0.04	0.00	0.11	0.09	0.00
Cl	0.01	0.00	0.00	0.00	0.00	0.01	0.00	0.00	0.01	0.00	0.01	0.00	0.00	0.00
Cr												0.00	0.00	0.00
mg	79.56	78.85	80.20	81.01	76.92	80.67	55.20	47.49	51.74	56.09	48.14	81.50	73.43	64.08
Total Cation	13.85	13.79	13.84	13.80	13.86	13.91	13.84	13.77	13.86	13.86	13.84	13.90	14.13	13.82
Ox Equiv	22.00	22.00	22.00	22.00	22.00	22.00	22.00	22.00	22.00	22.00	22.00	22.00	22.00	22.00

Table 4 cont

Hole	HL28	HL28	HL28	HL28	HL28	HL28	HL28	HL28	HL28	HL28	HL28	HL28	HL28	HL28
sample #	334196	334201	334202	334202	334205	334205	334205	334206	334206	334206	334206	334206	334206	334206
analysis #	r6mica2	r1mica3	r5mica1	r5mica1	r2mica1	r2mica2	r2mica3	r1mica1	r1mica2	r2mica1	r2mica2	r2mica3	r3mica1	r3mica2
SiO2	49.69	47.72	48.95	55.02	48.40	46.51	46.69	49.30	49.36	51.67	53.00	52.49	48.71	46.01
TiO2	0.00	0.01	0.01	0.01	0.03	0.00	0.01	0.90	0.12	0.06	0.11	0.01	2.10	0.17
Al2O3	31.82	34.95	31.07	26.37	31.34	31.94	31.85	30.99	31.34	29.10	29.65	30.06	30.17	31.53
FeO	1.02	1.32	2.82	2.07	2.65	2.92	2.71	1.30	1.37	1.51	1.59	1.36	1.43	2.43
MnO	0.00	0.10	0.06	0.01	0.07	0.00	0.00	0.03	0.00	0.00	0.00	0.01	0.00	0.02
MgO	1.37	0.46	1.55	1.95	2.13	2.14	2.15	1.51	1.50	2.03	2.05	1.91	1.60	1.72
CaO	0.00	0.08	0.16	0.34	0.41	0.10	0.09	0.26	0.09	0.16	0.15	0.21	0.40	0.22
Na2O	0.76	0.26	0.58	4.09	0.14	0.21	0.23	0.34	0.23	0.14	0.20	0.24	0.31	0.21
K2O	9.68	9.90	9.10	5.61	8.90	8.33	8.21	8.35	8.73	7.20	7.67	8.17	8.51	8.98
Cr2O3	•	0.01	0.00	0.00	0.02	0.02	0.00	0.05	0.09	0.05	0.08	0.00	0.20	0.30
Cl	0.00	0.00	0.00	0.00	0.00	0.00	0.00	0.04	0.00	0.01	0.02	0.07	0.00	0.02
F	0.11	•	•	•	•	•	•	•	•	•	•	•	•	•
CalcTotal	94.41	94.79	94.30	95.46	94.10	92.18	91.94	93.06	92.82	91.94	94.50	94.50	93.42	91.62
Si	6.60	6.33	6.56	7.15	6.49	6.36	6.39	6.61	6.64	6.93	6.93	6.88	6.54	6.36
Al(tet)	1.40	1.67	1.44	0.85	1.51	1.64	1.61	1.39	1.37	1.07	1.07	1.12	1.46	1.64
Al(oct)	3.58	3.80	3.47	3.19	3.45	3.52	3.53	3.50	3.60	3.52	3.50	3.52	3.31	3.50
Fe2	0.11	0.15	0.32	0.23	0.30	0.33	0.31	0.15	0.15	0.17	0.17	0.15	0.16	0.28
Mg	0.27	0.09	0.31	0.38	0.43	0.44	0.44	0.30	0.30	0.41	0.40	0.37	0.32	0.35
Ca	0.00	0.01	0.02	0.05	0.06	0.02	0.01	0.04	0.01	0.02	0.02	0.03	0.06	0.03
Na	0.20	0.07	0.15	1.03	0.04	0.06	0.06	0.09	0.06	0.04	0.05	0.06	0.08	0.06
K	1.64	1.68	1.56	0.93	1.52	1.45	1.43	1.43	1.50	1.23	1.28	1.37	1.46	1.58
Ti	0.00	0.00	0.00	0.00	0.00	0.00	0.00	0.09	0.01	0.01	0.01	0.00	0.21	0.02
Mn	0.00	0.01	0.01	0.00	0.01	0.00	0.00	0.00	0.00	0.00	0.00	0.00	0.00	0.00
F	0.05	0.00	0.00	0.00	0.00	0.00	0.00	0.00	0.00	0.00	0.00	0.00	0.00	0.00
Cl	0.00	0.00	0.00	0.00	0.00	0.00	0.00	0.01	0.00	0.00	0.01	0.02	0.00	0.01
Cr	0.00	0.00	0.00	0.00	0.00	0.00	0.00	0.01	0.01	0.01	0.01	0.00	0.02	0.03
mg	70.57	38.22	49.46	62.61	58.85	56.68	58.55	67.43	66.08	70.49	69.70	71.49	66.56	55.73
Total Cation	13.85	13.80	13.84	13.81	13.81	13.81	13.79	13.61	13.65	13.40	13.44	13.52	13.62	13.86
Ox Equiv	22.00	22.00	22.00	22.00	22.00	22.00	22.00	22.00	22.00	22.00	22.00	22.00	22.00	22.00

Table 4 cont

Hole	HL28	HL28	HL28	HL28	HL28	HL28	HL28	HL28	HL28	HL28	HL28	HL28
sample #	334206	334206	334206	334206	334206	334206	334206	334206	334206	334206	334206	334206
analysis #	r3mica3	r4mica1	r4mica2	r4mica3	r4mica4	r5mica1dk	r5mica3dk	r6mica1sp	r6mica2=sp	r6mica3=sp	r6mica4	r6mica5
SiO2	48.31	47.27	49.04	48.40	49.34	49.20	49.87	51.01	50.58	49.91	42.60	47.89
TiO2	0.10	1.28	0.80	0.27	0.25	0.17	0.14	1.92	0.18	1.61	13.31	0.77
Al2O3	30.56	29.12	31.04	31.85	30.73	30.88	31.30	30.90	32.09	30.68	27.45	31.28
FeO	1.52	1.36	1.73	1.62	1.37	2.04	1.85	1.83	1.51	1.38	1.37	1.76
MnO	0.00	0.00	0.00	0.05	0.04	0.03	0.00	0.00	0.01	0.03	0.03	0.00
MgO	1.56	1.65	1.50	1.55	1.66	1.70	1.68	1.70	1.63	1.62	1.35	1.55
CaO	0.15	2.75	0.14	0.25	0.89	0.38	0.26	0.28	0.12	0.81	0.22	0.19
Na2O	0.26	0.34	0.31	0.25	0.33	0.32	0.33	0.24	0.35	0.42	0.35	0.32
K2O	8.71	8.09	8.92	8.91	8.67	8.48	8.76	8.02	8.60	8.07	7.42	8.97
Cr2O3	0.18	0.11	0.15	0.06	0.08	0.07	0.19	1.11	0.47	0.66	0.16	0.17
Cl	0.03	0.05	0.04	0.00	0.02	0.03	0.02	0.09	0.03	0.07	0.02	0.02
F	.	.	.	.	.	.	.	.	.	.	.	.
CalcTotal	91.37	92.00	93.66	93.21	93.38	93.28	94.39	97.08	95.55	95.24	94.28	92.91
Si	6.62	6.49	6.57	6.51	6.62	6.61	6.62	6.58	6.61	6.56	5.77	6.48
Al(tet)	1.38	1.51	1.43	1.49	1.38	1.39	1.38	1.42	1.39	1.44	2.23	1.52
Al(oct)	3.55	3.21	3.47	3.56	3.48	3.50	3.51	3.27	3.55	3.32	2.15	3.48
Fe2	0.18	0.16	0.19	0.18	0.15	0.23	0.21	0.20	0.17	0.15	0.16	0.20
Mg	0.32	0.34	0.30	0.31	0.33	0.34	0.33	0.33	0.32	0.32	0.27	0.31
Ca	0.02	0.40	0.02	0.04	0.13	0.06	0.04	0.04	0.02	0.11	0.03	0.03
Na	0.07	0.09	0.08	0.07	0.09	0.08	0.09	0.06	0.09	0.11	0.09	0.08
K	1.52	1.42	1.53	1.53	1.48	1.45	1.48	1.32	1.43	1.35	1.28	1.55
Ti	0.01	0.13	0.08	0.03	0.03	0.02	0.01	0.19	0.02	0.16	1.36	0.08
Mn	0.00	0.00	0.00	0.01	0.01	0.00	0.00	0.00	0.00	0.00	0.00	0.00
F	0.00	0.00	0.00	0.00	0.00	0.00	0.00	0.00	0.00	0.00	0.00	0.00
Cl	0.01	0.01	0.01	0.00	0.00	0.01	0.00	0.02	0.01	0.02	0.01	0.01
Cr	0.02	0.01	0.02	0.01	0.01	0.01	0.02	0.11	0.05	0.07	0.02	0.02
mg	64.66	68.35	60.60	63.16	68.45	59.79	61.91	62.46	65.81	67.66	63.69	61.03
Total Cation	13.69	13.77	13.70	13.73	13.71	13.70	13.70	13.53	13.64	13.61	13.37	13.75
Ox Equiv	22.00	22.00	22.00	22.00	22.00	22.00	22.00	22.00	22.00	22.00	22.00	22.00

Table 5. Electron microprobe analyses of clinopyroxenes and structural formulae (6 oxygens).

Hole	HL14	HL14	HL14	HL14	HL14	HL14	HL14	HL14	HL14	HL14	HL14	HL14	HL14	HL14
sample #	333973	333973	333973	333971	333971	333973	333973	333973	333974	333974	333974	333974	333974	333974
analysis #	r1cpx1	r1cpx2cr	r1cpx2rim	r1cpx3cr	r1cpx3rim	r3cpx1rim	r3cpx1cr	r5cpx1	r4cpx1	r4cpx2	r4cpx 3	r4cpx4cr	r4cpx4rim	r1cpx1
SiO2	53.78	51.11	49.66	53.17	50.84	52.62	43.05	51.36	52.81	53.31	53.22	53.35	52.67	53.01
TiO2	0.19	0.38	0.79	0.14	0.29	0.24	12.31	0.30	0.11	0.13	0.21	0.20	0.27	0.17
Al2O3	1.09	3.34	5.43	1.41	3.15	2.29	4.00	2.31	1.59	1.88	1.10	1.32	1.83	1.57
FeO	4.67	6.09	6.98	3.73	6.21	5.00	3.55	4.66	3.09	3.46	4.73	4.94	4.37	3.87
MnO	0.22	0.24	0.24	0.04	0.19	0.11	0.00	0.13	0.20	0.11	0.28	0.20	0.16	0.11
MgO	18.23	17.57	15.60	17.94	17.28	17.44	10.12	17.25	17.99	18.21	18.25	18.39	17.56	18.32
CaO	21.14	19.71	20.82	22.34	20.07	21.43	24.27	21.48	21.94	21.76	21.27	20.93	21.85	21.41
Na2O	0.09	0.13	0.13	0.12	0.12	0.11	0.16	0.13	0.15	0.15	0.12	0.08	0.13	0.13
K2O	0.00	0.02	0.00	0.00	0.01	0.00	0.07	0.02	0.00	0.00	0.02	0.00	0.00	0.00
P2O5	0.35	0.30	0.37	0.34	0.40	0.33	0.32	0.30	0.38	0.37	0.32	0.32	0.42	0.34
Cl	0.00	0.00	0.01	0.00	0.00	0.02	0.09	0.01	0.00	0.00	0.02	0.00	0.00	0.01
Cr2O3	0.21	0.17	0.02	0.74	0.37	0.31	0.41	0.56	1.15	1.34	0.31	0.38	0.48	0.77
NiO	0.06	0.09	0.00	0.04	0.00	0.04	0.03	0.03	0.05	0.01	0.03	0.07	0.00	0.04
CalcTotal	100.04	99.17	100.05	100.00	98.94	99.94	98.34	98.53	99.46	100.74	99.87	100.20	99.76	99.74
Si	1.96	1.89	1.84	1.94	1.89	1.93	1.65	1.91	1.94	1.93	1.95	1.95	1.93	1.94
Al	0.05	0.15	0.24	0.06	0.14	0.10	0.18	0.10	0.07	0.08	0.05	0.06	0.08	0.07
Fe3	•	0.01	•	•	•	•	•	•	•	•	•	•	•	•
Fe2	0.14	0.18	0.22	0.11	0.19	0.15	0.11	0.15	0.10	0.11	0.15	0.15	0.13	0.12
Mg	0.99	0.97	0.86	0.98	0.96	0.95	0.58	0.96	0.98	0.98	1.00	1.00	0.96	1.00
Ca	0.81	0.77	0.81	0.86	0.78	0.83	0.98	0.84	0.84	0.83	0.82	0.80	0.84	0.82
Na	0.01	0.01	0.01	0.01	0.01	0.01	0.01	0.01	0.01	0.01	0.01	0.01	0.01	0.01
K	0.00	0.00	0.00	0.00	0.00	0.00	0.00	0.00	0.00	0.00	0.00	0.00	0.00	0.00
Ti	0.01	0.01	0.02	0.00	0.01	0.01	0.35	0.01	0.00	0.00	0.01	0.01	0.01	0.01
P	0.01	0.01	0.01	0.01	0.01	0.01	0.01	0.01	0.01	0.01	0.01	0.01	0.01	0.01
Mn	0.01	0.01	0.01	0.00	0.01	0.00	0.00	0.00	0.01	0.00	0.01	0.01	0.01	0.00
Cr	0.01	0.01	0.00	0.02	0.01	0.01	0.01	0.02	0.03	0.04	0.01	0.01	0.01	0.02
Ni	0.00	0.00	0.00	0.00	0.00	0.00	0.00	0.00	0.00	0.00	0.00	0.00	0.00	0.00
mg #	87.43	84.09	79.94	89.56	83.22	86.14	83.54	86.84	91.21	90.37	87.31	86.90	87.76	89.39
Total Cations	3.98	4.00	4.00	3.99	4.00	3.99	3.88	4.00	3.98	3.98	3.99	3.99	3.98	3.99
Ox Equiv	6.00	6.00	6.00	6.00	6.00	6.00	5.99	6.00	6.00	6.00	6.00	6.00	6.00	6.00
Enstatite	51.05	50.53	45.71	50.15	49.65	49.36	34.59	49.26	51.21	51.37	50.86	51.21	49.72	51.51
Ferrosilite	7.34	9.56	11.47	5.84	10.01	7.94	6.81	7.47	4.93	5.47	7.39	7.72	6.93	6.11
Wollastonite	41.61	39.91	42.82	44.01	40.35	42.70	58.60	43.27	43.85	43.16	41.74	41.07	43.34	42.38

Table 5 cont

Hole	HL14	HL14	HL28	HL28	HL28	HL28	HL28	HL28	HL28	HL28	HL28	HL28	HL28
sample #	333974	333974	334201	334201	334201	334201	334201	334201	334201	334201	334201	334201	334201
analysis #	r1cpx2	r1cpx3	r1cpx1rim	r1cpx1cr	r1cpx1	r3cpx1cr	r3cpx1rim	r4cpx1cr	r4cpx1rim	r4cpx2rim	r4cpx2in	r5cpx1	r5cpx2
SiO2	51.76	52.86	52.25	53.30	52.14	53.43	53.78	51.35	52.77	53.46	53.58	52.37	52.17
TiO2	0.39	0.16	0.26	0.15	0.25	0.14	0.17	0.34	0.24	0.16	0.16	0.23	0.25
Al2O3	2.50	1.13	2.82	1.64	2.90	1.74	1.55	3.74	2.58	1.71	1.55	2.33	3.06
FeO	5.30	5.22	5.17	4.56	6.15	4.72	4.99	5.98	4.81	4.77	4.90	4.30	4.65
MnO	0.24	0.22	0.21	0.19	0.23	0.15	0.24	0.15	0.26	0.10	0.21	0.13	0.21
MgO	17.24	17.75	17.44	17.99	17.81	18.18	18.00	17.21	17.52	18.26	18.39	17.49	16.81
CaO	21.13	21.34	21.09	21.38	20.38	21.55	21.45	20.41	21.53	21.16	20.82	21.89	21.82
Na2O	0.11	0.17	0.11	0.07	0.11	0.09	0.09	0.11	0.12	0.08	0.05	0.11	0.11
K2O	0.00	0.01	0.00	0.01	0.01	0.00	0.00	0.01	0.00	0.00	0.01	0.00	0.00
P2O5	0.33	0.28	0.36	0.39	0.33	0.34	0.38	0.32	0.38	0.32	0.35	0.36	0.39
Cl	0.02	0.00	0.02	0.00	0.00	0.02	0.00	0.00	0.00	0.00	0.00	0.00	0.00
Cr2O3	0.22	0.34	0.64	0.53	0.25	0.44	0.23	0.45	0.70	0.44	0.49	0.80	0.89
NiO	0.00	0.00	0.04	0.02	0.04	0.03	0.01	0.00	0.17	0.03	0.12	0.00	0.00
CalcTotal	99.24	99.48	100.42	100.23	100.58	100.84	100.90	100.08	101.07	100.49	100.63	100.00	100.39
Si	1.92	1.95	1.91	1.95	1.91	1.94	1.95	1.89	1.92	1.94	1.95	1.92	1.91
Al	0.11	0.05	0.12	0.07	0.13	0.08	0.07	0.16	0.11	0.07	0.07	0.10	0.13
Fe3	•	0.00	•	•	0.00	•	•	•	•	•	•	•	•
Fe2	0.16	0.16	0.16	0.14	0.19	0.14	0.15	0.18	0.15	0.15	0.15	0.13	0.14
Mg	0.95	0.98	0.95	0.98	0.97	0.98	0.97	0.94	0.95	0.99	1.00	0.96	0.92
Ca	0.82	0.83	0.81	0.82	0.78	0.82	0.81	0.79	0.82	0.81	0.79	0.84	0.84
Na	0.01	0.01	0.01	0.01	0.01	0.01	0.01	0.01	0.01	0.01	0.00	0.01	0.01
K	0.00	0.00	0.00	0.00	0.00	0.00	0.00	0.00	0.00	0.00	0.00	0.00	0.00
Ti	0.01	0.00	0.01	0.00	0.01	0.00	0.01	0.01	0.01	0.00	0.00	0.01	0.01
P	0.01	0.01	0.01	0.01	0.01	0.01	0.01	0.01	0.01	0.01	0.01	0.01	0.01
Mn	0.01	0.01	0.01	0.01	0.01	0.01	0.01	0.01	0.01	0.00	0.01	0.00	0.01
Cr	0.01	0.01	0.02	0.02	0.01	0.01	0.01	0.01	0.02	0.01	0.01	0.02	0.03
Ni	0.00	0.00	0.00	0.00	0.00	0.00	0.00	0.00	0.01	0.00	0.00	0.00	0.00
mg #	85.29	85.89	85.74	87.56	83.82	87.28	86.54	83.68	86.65	87.22	87.00	87.88	86.58
Total Cations	3.99	4.00	3.99	3.98	4.00	3.99	3.98	4.00	3.99	3.99	3.98	3.99	3.98
Ox Equiv	6.00	6.00	6.00	6.00	6.00	6.00	6.00	6.00	6.00	6.00	6.00	6.00	6.00
Enstatite	49.14	49.68	49.61	50.63	50.05	50.50	50.21	49.26	49.57	50.95	51.41	49.55	48.41
Ferrosilite	8.47	8.16	8.25	7.19	9.66	7.36	7.81	9.61	7.64	7.46	7.68	6.83	7.50
Wollastonite	42.39	42.17	42.14	42.18	40.29	42.14	41.98	41.13	42.79	41.59	40.91	43.62	44.09

Table 6. Electron microprobe analyses of carbonates.

Hole	HL14	HL14	HL14	HL14	HL14	HL14	HL14	HL14	HL14	HL14	HL14	HL14	HL14	HL14	HL14	HL14
sample #	333971	333971	333971	333971	333971	333971	333971	333971	333971	333971	333971	333971	333971	333971	333971	333971
analysis #	r1ca2	r2ca1cl	r2ca2cl	r3ca1cl	r3ca2dty	r4ca1dty	r4ca2dty	r4ca3dty	r4ca4dty	r5ca1dty	r5ca2dty	r5ca3dty	r5ca4	r5ca1cl	r5ca2cl	r5ca3cl
Mg(CO3)	0.00	0.39	0.43	1.34	7.29	35.92	29.40	36.52	37.21	32.75	34.91	34.12	32.43	0.43	0.70	0.56
Ca(CO3)	96.55	96.69	95.37	93.97	85.80	52.89	60.35	53.58	52.56	53.21	52.80	53.03	54.51	97.13	96.87	98.10
Mn(CO3)	0.19	0.65	0.64	0.81	0.73	5.08	3.91	5.95	5.43	1.74	2.99	2.42	1.93	0.49	0.89	0.51
Fe(CO3)	0.13	0.50	0.50	0.92	3.50	5.44	5.35	3.16	4.08	13.00	8.70	10.85	11.47	0.35	0.72	0.51
Zn(CO3)	0.05	0.00	0.00	0.01	0.06	0.00	0.00	0.04	0.02	0.01	0.00	0.00	0.04	0.00	0.00	0.00
Sr(CO3)	0.08	0.23	0.40	0.46	0.28	0.00	0.16	0.00	0.00	0.08	0.00	0.00	0.05	0.37	0.18	0.39
Ba(CO3)	0.00	0.00	0.00	0.00	0.00	0.00	0.00	0.03	0.00	0.00	0.00	0.03	0.00	0.02	0.00	0.01
Total	97.00	98.46	97.34	97.50	97.65	99.34	99.18	99.28	99.29	100.78	99.40	100.45	100.44	98.78	99.35	100.08

Hole	HL14	HL14	HL14	HL14	HL14	HL14	HL14	HL14	HL14	HL14	HL14	HL14	HL14	HL14	HL14	HL14
sample #	333972	333972	333972	333972	333972	333972	333972	333972	333972	333972	333972	333972	333972	333972	333972	333972
analysis #	r1ca1	r1ca3	r1ca5	r1ca6	r2ca1	r2ca2	r2ca4	r2ca5	r2ca6	r2ca7	r3ca1	r3ca3band	r3ca4band	r3ca5	r3ca6	r4ca1
Mg(CO3)	0.64	1.87	3.35	2.33	30.88	32.83	0.18	0.01	0.19	0.15	7.52	21.94	27.27	0.76	7.31	0.36
Ca(CO3)	94.83	93.35	90.17	90.97	57.77	58.36	95.94	95.85	96.65	96.92	82.40	64.65	56.20	94.34	83.57	96.25
Mn(CO3)	0.90	0.40	0.92	1.29	1.04	2.02	0.76	0.59	0.55	0.56	0.98	1.32	0.88	0.99	0.85	0.35
Fe(CO3)	1.06	1.64	2.23	2.22	9.79	6.09	0.41	0.22	0.37	0.24	6.05	12.14	16.25	1.12	5.48	0.40
Zn(CO3)	0.00	0.01	0.00	0.03	0.00	0.00	0.00	0.03	0.00	0.01	0.00	0.03	0.00	0.04	0.00	0.08
Sr(CO3)	0.16	0.17	0.29	0.35	0.13	0.09	0.32	0.28	0.34	0.25	0.31	0.11	0.11	0.10	0.27	0.16
Ba(CO3)	0.00	0.02	0.05	0.02	0.00	0.00	0.02	0.08	0.04	0.00	0.05	0.00	0.03	0.01	0.05	0.01
Total	97.78	97.45	97.02	97.20	99.61	99.39	97.61	97.06	98.15	98.14	97.32	100.18	100.73	97.35	97.53	97.61

Table 6 cont

Hole	HL14	HL14	HL14	HL14	HL14	HL14	HL14	HL14	HL14	HL14	HL14	HL14	HL14	HL14	HL14	HL14
sample #	333972	333973	333973	333973	333973	333973	333973	333973	333973	333973	333973	333973	333973	333973	333973	333973
analysis #	r4ca2	r1ca1	r1ca2	r1ca3	r1ca4	r2ca1	r2ca2	r2ca3	r2ca4	r3ca1	r3ca2	r4ca2	r4ca3	r4ca4	r4ca5	r5ca1
Mg(CO3)	0.57	0.12	0.42	0.41	0.66	0.83	0.36	0.21	0.12	0.80	1.28	0.51	0.46	0.19	0.00	1.92
Ca(CO3)	95.97	96.47	96.56	97.73	95.27	96.19	95.41	95.27	95.50	96.20	93.79	95.12	94.51	97.54	98.92	95.06
Mn(CO3)	0.25	0.72	0.78	0.52	0.69	1.06	1.36	1.04	0.94	0.81	0.77	0.74	0.68	0.60	0.19	0.54
Fe(CO3)	0.71	0.61	0.81	0.69	1.38	0.88	1.09	0.89	0.77	0.70	2.05	1.36	1.53	0.19	0.11	1.27
Zn(CO3)	0.00	0.02	0.00	0.02	0.00	0.09	0.00	0.00	0.00	0.01	0.00	0.00	0.04	0.00	0.03	0.06
Sr(CO3)	0.23	0.04	0.06	0.09	0.11	0.10	0.00	0.11	0.05	0.10	0.09	0.07	0.11	0.11	0.14	0.12
Ba(CO3)	0.05	0.00	0.00	0.00	0.04	0.00	0.01	0.00	0.00	0.00	0.00	0.00	0.00	0.00	0.01	0.00
Total	97.78	97.98	98.63	99.46	98.15	99.14	98.23	97.52	97.38	98.62	97.97	97.79	97.33	98.62	99.39	98.97

Hole	HL14	HL14	HL14	HL14	HL14	HL14	HL14	HL14	HL14	HL14	HL14	HL14	HL14	HL14	HL14	HL14
sample #	333973	333973	333973	333974	333974	333974	333974	333974	333974	333975	333975	333975	333975	333975	333975	333975
analysis #	r5ca2	r5ca3	r5ca4	r1ca1	r1ca2	r1ca3	r3ca1	r3ca3	r3ca4	r1ca1	r1ca3	r1ca4	r2ca1	r2ca2	r2ca3	r3ca1
Mg(CO3)	1.12	0.55	1.65	0.35	0.68	1.17	0.34	0.14	0.00	0.53	0.56	0.20	0.19	0.13	0.52	0.27
Ca(CO3)	95.67	96.12	95.87	96.17	96.67	95.55	92.99	95.26	97.31	96.01	94.69	95.85	98.38	95.31	95.91	95.57
Mn(CO3)	0.33	0.33	0.34	0.51	0.32	0.40	1.37	1.31	0.49	0.50	1.16	1.09	0.24	2.51	0.99	1.07
Fe(CO3)	0.94	0.67	0.01	0.85	0.71	0.98	2.70	1.76	0.20	0.43	1.37	0.62	0.66	0.51	1.04	1.13
Zn(CO3)	0.00	0.01	0.01	0.00	0.07	0.00	0.06	0.05	0.02	0.06	0.01	0.00	0.00	0.01	0.00	0.00
Sr(CO3)	0.15	0.08	0.21	0.10	0.13	0.14	0.04	0.02	0.05	0.06	0.05	0.06	0.06	0.02	0.05	0.06
Ba(CO3)	0.00	0.00	0.01	0.03	0.04	0.00	0.04	0.00	0.00	0.00	0.00	0.02	0.00	0.00	0.01	0.00
Total	98.22	97.76	98.11	98.01	98.63	98.24	97.54	98.54	98.06	97.59	97.83	97.84	99.54	98.48	98.51	98.10

Table 6 cont

Hole	HL14	HL14	HL14	HL14	HL14	HL28	HL28	HL28	HL28	HL28	HL28	HL28	HL28	HL28	HL28	HL28
sample #	333975	333975	333975	333975	333975	334195	334195	334195	334195	334195	334195	334195	334195	334195	334195	334195
analysis #	r3ca2	r3ca3	r5ca1	r5ca3	r5ca4	r1ca2rim	r1 ca3cr	r1ca4cr	r1ca5	r1ca6	r1ank1	r1ank12nd	r2ca1vn	r2ca2	r2ca3vn	r2ca4vn
Mg(CO3)	0.25	0.17	0.40	0.19	0.44	0.43	0.61	1.10	0.53	0.96	29.58	30.33	0.22	1.18	0.43	0.33
Ca(CO3)	95.71	95.95	95.23	95.68	94.53	95.99	97.44	94.24	96.36	95.81	54.60	57.03	94.48	95.09	97.06	94.42
Mn(CO3)	0.94	1.07	1.07	1.24	1.31	0.65	0.86	0.60	0.73	0.56	0.58	0.55	2.80	0.58	3.10	1.42
Fe(CO3)	0.81	0.74	0.83	0.87	0.99	0.83	1.06	1.30	0.62	0.89	15.52	12.91	0.42	1.52	0.46	0.45
Zn(CO3)	0.00	0.00	0.00	0.02	0.02	0.01	0.00	0.02	0.00	0.01	0.01	0.01	0.00	0.00	0.06	0.00
Sr(CO3)	0.05	0.05	0.11	0.02	0.07	0.13	0.08	0.08	0.13	0.14	0.11	0.14	0.10	0.11	0.13	0.14
Ba(CO3)	0.01	0.02	0.04	0.03	0.04	0.00	0.04	0.02	0.00	0.00	0.02	0.07	0.00	0.00	0.00	0.00
Total	97.77	98.01	97.67	98.04	97.40	98.04	100.08	97.35	98.36	98.37	100.41	101.03	98.02	98.47	101.25	96.76

Hole	HL28	HL28	HL28	HL28	HL28	HL28	HL28	HL28	HL28	HL28	HL28	HL28	HL28	HL28	HL28	HL28
sample #	334195	334195	334195	334195	334195	334195	334195	334195	334195	334195	334195	334195	334195	334195	334195	334195
analysis #	r2ca4	r2ca5rim	r2ca6in	r2ca7rim	r2ca8in	r2ca vn	r2ca9	r3ca1dty	r3ca2cl	r3ca4dty	r4ca5	r4ca5 rim	r3ca5in	r4vnrim	r4vnin	r4vnin
Mg(CO3)	1.14	0.54	0.50	0.44	0.49	0.40	0.37	0.98	1.74	1.41	22.66	4.59	14.66	0.35	0.41	0.39
Ca(CO3)	93.09	96.38	96.64	95.80	95.67	94.95	93.10	94.81	93.87	95.48	75.31	92.44	82.54	93.54	93.90	93.99
Mn(CO3)	2.22	0.81	0.72	0.82	0.71	3.01	3.49	0.79	0.77	0.75	0.41	0.38	1.67	3.74	2.39	3.87
Fe(CO3)	0.86	1.05	0.85	0.90	0.92	0.55	0.52	1.56	1.35	1.93	2.03	1.05	1.74	0.36	0.45	0.35
Zn(CO3)	0.04	0.01	0.00	0.02	0.07	0.07	0.00	0.07	0.00	0.00	0.00	0.09	0.12	0.02	0.00	0.01
Sr(CO3)	0.13	0.04	0.04	0.07	0.11	0.04	0.01	0.11	0.27	0.08	0.14	0.10	0.15	0.07	0.12	0.09
Ba(CO3)	0.07	0.00	0.00	0.00	0.00	0.00	0.00	0.02	0.00	0.00	0.02	0.00	0.07	0.00	0.03	0.00
Total	97.56	98.82	98.76	98.05	97.96	99.01	97.49	98.33	98.01	99.65	100.58	98.64	100.94	98.09	97.30	98.69

Table 6 cont

Hole	HL28	HL28	HL28	HL28	HL28	HL28	HL28	HL28	HL28	HL28	HL28	HL28	HL28	HL28	HL28	HL28
sample #	334195	334195	334195	334195	334195	334195	334195	334195	334195	334195	334196	334196	334196	334196	334196	334196
analysis #	r4vnrim	3r4ca1cl	r4ca2cl	r5vnrim	r5vnin	r5vninchl	r5vnmrim	r5ca1	r5 ca2strin	r5ca3	r1ca1	r1ca1rim	r1ca2in	r1ca3rim	r1ca3in	r2ca1rim
Mg(CO3)	0.33	0.79	0.60	1.04	0.87	0.90	1.19	0.76	0.64	0.79	0.15	0.26	0.26	0.50	0.31	0.12
Ca(CO3)	94.50	96.11	97.44	96.24	96.95	95.64	95.26	95.33	97.93	96.51	95.88	94.95	96.02	94.26	95.80	97.09
Mn(CO3)	3.76	0.65	0.76	0.22	0.43	0.82	0.51	0.84	0.39	0.94	0.87	1.22	1.41	1.65	1.43	1.26
Fe(CO3)	0.43	0.69	0.81	0.47	0.33	1.14	0.68	0.70	0.69	0.63	0.79	0.68	0.48	0.80	0.56	0.46
Zn(CO3)	0.00	0.00	0.05	0.00	0.02	0.00	0.01	0.00	0.03	0.00	0.00	0.00	0.00	0.01	0.08	0.00
Sr(CO3)	0.07	0.19	0.24	0.26	0.23	0.25	0.20	0.08	0.22	0.08	0.06	0.15	0.03	0.26	0.05	0.05
Ba(CO3)	0.00	0.04	0.01	0.06	0.02	0.05	0.02	0.00	0.00	0.02	0.00	0.00	0.06	0.00	0.00	0.04
Total	99.10	98.47	99.90	98.30	98.84	98.79	97.87	97.70	99.90	98.98	97.76	97.25	98.26	97.46	98.23	99.02

Hole	HL28	HL28	HL28	HL28	HL28	HL28	HL28	HL28	HL28	HL28	HL28	HL28	HL28	HL28	HL28	HL28
sample #	334196	334196	334196	334196	334196	334196	334196	334196	334196	334196	334196	334196	334196	334201	334201	334201
analysis #	r2 ca1in	r1ca1rim	r3ca1	r3ca2	r4ca1in	r4ca2in	r4ca2rim	r5ca1dty	r5ca2cl	r5ca2in	r6ca1	r6ca2	r6ca3	r1ca1cpx	r1ca1vn	r1ca2
Mg(CO3)	0.22	0.29	0.20	0.25	0.25	0.25	0.48	0.00	0.00	0.00	0.00	0.00	0.64	0.23	0.19	0.22
Ca(CO3)	95.46	95.46	96.00	95.42	95.98	95.50	94.70	97.36	96.33	96.75	99.87	99.33	97.78	98.25	96.80	97.89
Mn(CO3)	1.43	1.22	0.92	0.89	0.95	1.21	0.97	0.19	1.06	1.04	0.01	0.00	0.29	0.31	0.34	0.20
Fe(CO3)	0.48	0.57	0.87	0.76	0.57	0.51	0.77	0.15	0.23	0.19	0.00	0.08	0.08	0.18	0.11	0.13
Zn(CO3)	0.00	0.00	0.03	0.00	0.00	0.00	0.02	0.04	0.06	0.00	0.00	0.01	0.02	0.07	0.00	0.00
Sr(CO3)	0.03	0.07	0.02	0.07	0.04	0.07	0.05	0.19	0.01	0.00	0.08	0.21	0.13	0.11	0.10	0.10
Ba(CO3)	0.04	0.00	0.06	0.00	0.00	0.00	0.03	0.00	0.00	0.00	0.00	0.03	0.00	0.00	0.10	0.00
Total	97.66	97.62	98.09	97.40	97.79	97.54	97.02	97.92	97.68	97.98	99.95	99.66	98.94	99.14	97.65	98.54

Table 6 cont

Hole	HL28	HL28	HL28	HL28	HL28	HL28	HL28	HL28	HL28	HL28	HL28	HL28	HL28	HL28	HL28	HL28
sample #	334201	334201	334201	334201	334201	334201	334201	334201	334201	334201	334201	334201	334201	334201	334201	334201
analysis #	r1ca3	r2ca1vn	r2ca2	r2ca3	r2ca4vn	334201	r2c	334201r3ca1	r3ca3cpx	r3ca4	r4ca1	r5ca1=cpx	r5ca2	r5ca3	r5ca4vn	r5ca5	r5ca6
Mg(CO3)	0.00	1.83	2.55	0.08	0.98	0.61	2.40	1.61	0.58	0.09	0.00	0.46	0.02	0.00	0.00	0.69
Ca(CO3)	98.86	93.28	92.58	97.59	94.10	94.92	92.62	93.05	97.53	97.64	98.66	95.81	97.33	98.70	99.00	95.31
Mn(CO3)	0.18	0.32	0.47	1.36	3.23	1.65	0.41	0.48	0.25	0.31	0.27	0.47	0.36	0.40	0.31	0.43
Fe(CO3)	0.19	2.64	3.78	0.34	1.07	0.65	2.29	2.27	1.14	0.40	0.09	1.92	0.24	0.13	0.18	1.63
Zn(CO3)	0.00	0.00	0.02	0.00	0.01	0.02	0.01	0.02	0.07	0.00	0.03	0.00	0.04	0.00	0.00	0.03
Sr(CO3)	0.30	0.16	0.11	0.07	0.05	0.10	0.14	0.13	0.12	0.12	0.14	0.06	0.12	0.12	0.11	0.09
Ba(CO3)	0.01	0.00	0.00	0.07	0.00	0.00	0.03	0.01	0.00	0.03	0.01	0.00	0.01	0.01	0.00	0.02
Total	99.54	98.22	99.51	99.50	99.43	97.95	97.90	97.57	99.68	98.58	99.20	98.71	98.12	99.36	99.60	98.19

Hole	HL28	HL28	HL28	HL28	HL28	HL28	HL28	HL28	HL28	HL28	HL28	HL28	HL28	HL28	HL28	HL28
sample #	334202	334202	334202	334202	334205	334205	334205	334205	334205	334205	334205	334205	334205	334205	334205	334205
analysis #	r4ca1	r4ca2	r5ca1	r5ca3	r1ca1	r1ca2rim	r1ca2cr	r2ca1	r2ca2	r2ca3	r2ca4	r3ca1rim	r3ca2in	r4ca1	r4ca2	r5vnrim
Mg(CO3)	1.43	1.31	0.67	0.51	1.06	0.81	0.67	4.48	7.25	0.54	0.28	0.91	0.86	0.31	2.53	0.09
Ca(CO3)	94.63	95.53	94.24	96.45	94.52	95.56	98.06	89.26	86.89	97.61	96.73	95.17	95.38	97.12	91.47	95.13
Mn(CO3)	0.27	0.52	1.24	0.25	0.36	0.34	0.39	1.20	0.97	0.42	0.32	0.43	0.44	0.27	0.66	2.74
Fe(CO3)	1.08	0.92	0.60	0.78	1.19	0.89	0.91	2.32	2.81	0.79	0.47	0.92	0.91	0.54	2.32	0.71
Zn(CO3)	0.00	0.04	0.00	0.00	0.04	0.03	0.00	0.00	0.00	0.00	0.00	0.03	0.03	0.05	0.00	0.00
Sr(CO3)	0.07	0.08	0.08	0.08	0.10	0.08	0.06	0.12	0.17	0.10	0.08	0.11	0.13	0.11	0.09	0.02
Ba(CO3)	0.02	0.00	0.01	0.00	0.01	0.06	0.00	0.08	0.00	0.07	0.00	0.00	0.04	0.01	0.00	0.02
Total	97.49	98.40	96.83	98.07	97.28	97.77	100.08	97.45	98.09	99.52	97.87	97.56	97.79	98.40	97.08	98.70

Table 6 cont

Hole	HL28	HL28	HL28	HL28	HL28	HL28	HL28	HL28	HL28	HL28	HL28	HL28	HL28	HL28	HL28	HL28
sample #	334205	334205	334205	334205	334206	334206	334206	334206	334206	334206	334206	334206	334206	334206	334206	334206
analysis #	r5vnpyr	r5linvn	r5vntop	r6ca1	r1ca1	r1ca2	r1ca3	r2ca1	r2ca2	r2ca3	r3ca2	r4ca1	r4ca2	r4ca3	r5ca1dty	r5ca1dty
Mg(CO3)	0.17	0.07	0.38	0.67	0.55	0.84	0.36	0.36	0.24	0.38	0.36	0.80	0.28	0.55	0.33	0.38
Ca(CO3)	93.60	96.90	92.03	95.72	93.14	93.53	94.93	94.18	93.68	96.85	95.58	93.93	93.77	93.62	93.37	94.37
Mn(CO3)	3.04	0.48	4.44	0.39	1.15	1.67	2.34	1.20	1.82	1.67	1.28	1.17	1.56	1.57	2.72	2.08
Fe(CO3)	0.60	0.89	0.69	0.81	2.37	1.53	0.79	1.96	1.76	1.11	2.66	1.68	1.14	1.55	1.95	2.13
Zn(CO3)	0.00	0.07	0.00	0.00	0.00	0.00	0.02	0.03	0.00	0.01	0.00	0.07	0.03	0.09	0.00	0.03
Sr(CO3)	0.04	0.09	0.00	0.09	0.07	0.09	0.01	0.12	0.13	0.05	0.19	0.12	0.18	0.06	0.11	0.14
Ba(CO3)	0.00	0.00	0.00	0.00	0.03	0.03	0.00	0.02	0.01	0.02	0.02	0.00	0.00	0.00	0.05	0.02
Total	97.44	98.50	97.54	97.67	97.30	97.69	98.45	97.88	97.64	100.08	100.08	97.76	96.96	97.44	98.53	99.14

Hole	HL28	HL28	HL28
sample #	334206	334206	334206
analysis #	r5ca2grd	r5ca3grd	r6ca2
Mg(CO3)	2.11	0.37	0.26
Ca(CO3)	92.42	96.25	94.91
Mn(CO3)	1.32	2.46	2.11
Fe(CO3)	2.44	0.96	0.66
Zn(CO3)	0.00	0.00	0.04
Sr(CO3)	0.08	0.04	0.05
Ba(CO3)	0.05	0.01	0.00
Total	98.42	100.08	98.01

Table 7. Electron microprobe analyses of feldspars and structural formulae (8 oxygens).

Hole	HL14	HL14	HL14	HL14	HL14	HL14	HL14	HL14	HL14	HL14	HL28	HL28	HL28	HL28
Mineral	333973	333973	333973	333973	333973	333974	333974	333974	333975	333975	334195	334196	334196	334196
analysis #	r4fel1	r4 fel2	r4fel3	r4 fel4	r4fel5	r4fel1	r1fel1	r1fel2	r3fel2	r3fel3	r1fel1	r1fel1rim	r1fel2rim	r1fel2rim
SiO2	67.12	66.89	67.88	67.54	67.76	66.28	78.28	66.36	62.52	63.97	66.52	83.64	68.69	67.43
TiO2	0.02	0.03	0.00	0.00	0.00	0.04	0.55	0.04	0.02	0.04	0.00	0.02	0.02	0.00
Al2O3	19.36	19.41	19.24	19.64	19.03	19.50	11.56	19.61	19.88	19.43	19.55	10.36	19.68	20.48
FeO	0.15	0.05	0.06	0.15	0.04	0.39	0.55	0.65	0.87	0.57	0.10	0.25	0.18	0.09
MnO	0.00	0.02	0.05	0.03	0.03	0.00	0.09	0.01	0.01	0.00	0.00	0.01	0.03	0.00
MgO	0.10	0.03	0.00	0.00	0.00	0.15	0.13	0.32	0.66	0.42	0.01	0.10	0.08	0.02
CaO	0.44	0.43	0.06	0.34	0.06	1.04	1.55	1.04	4.14	4.03	1.87	0.37	0.28	0.24
Na2O	10.75	10.87	11.33	10.92	10.89	10.66	6.15	10.73	9.30	9.25	11.30	5.74	11.10	11.27
K2O	0.12	0.08	0.02	0.08	0.05	0.18	0.22	0.17	0.59	0.50	0.08	0.02	0.07	0.18
Cr2O3	0.00	0.00	0.00	0.03	0.00	0.11	0.00	0.01	0.03	0.01	0.01	0.00	0.00	0.01
SrO	·	·	·	·	·	·	·	·	0.34	0.36	0.25	0.34	0.27	0.36
BaO	·	·	·	·	·	·	·	·	0.04	0.06	0.00	0.01	0.04	0.03
CalcTotal	98.04	97.82	98.64	98.74	97.86	98.36	99.08	98.95	98.42	98.65	99.71	100.86	100.45	100.11
Si	2.99	2.98	3.00	2.99	3.01	2.96	3.36	2.95	2.84	2.89	2.94	3.48	2.99	2.95
Al	1.02	1.02	1.00	1.02	1.00	1.03	0.59	1.03	1.07	1.03	1.02	0.51	1.01	1.06
Fe2	0.01	0.00	0.00	0.01	0.00	0.02	0.02	0.02	0.03	0.02	0.00	0.01	0.01	0.00
Mg	0.01	0.00	0.00	0.00	0.00	0.01	0.01	0.02	0.05	0.03	0.00	0.01	0.01	0.00
Ca	0.02	0.02	0.00	0.02	0.00	0.05	0.07	0.05	0.20	0.20	0.09	0.02	0.01	0.01
Na	0.93	0.94	0.97	0.94	0.94	0.92	0.51	0.92	0.82	0.81	0.97	0.46	0.94	0.96
K	0.01	0.01	0.00	0.01	0.00	0.01	0.01	0.01	0.03	0.03	0.01	0.00	0.00	0.01
Ti	0.00	0.00	0.00	0.00	0.00	0.00	0.02	0.00	0.00	0.00	0.00	0.00	0.00	0.00
Mn	0.00	0.00	0.00	0.00	0.00	0.00	0.00	0.00	0.00	0.00	0.00	0.00	0.00	0.00
Cr	0.00	0.00	0.00	0.00	0.00	0.00	0.00	0.00	0.00	0.00	0.00	0.00	0.00	0.00
Sr	0.00	0.00	0.00	0.00	0.00	0.00	0.00	0.00	0.01	0.01	0.01	0.01	0.01	0.01
Ba	0.00	0.00	0.00	0.00	0.00	0.00	0.00	0.00	0.00	0.00	0.00	0.00	0.00	0.00
mg	54.31	52.61	0.00	0.00	0.00	41.00	30.28	46.90	57.75	56.91	20.63	40.93	45.14	32.16
Total Cat	4.97	4.98	4.98	4.97	4.96	4.99	4.59	5.00	5.05	5.02	5.04	4.50	4.98	5.00
Ox Equiv	8.00	8.00	8.00	8.00	8.00	8.00	8.00	8.00	8.00	8.00	8.00	8.00	8.00	8.00
Albite	97.13	97.36	99.61	97.82	99.39	93.90	86.01	93.99	77.62	78.35	91.23	96.33	98.24	97.85
Anorthite	2.18	2.15	0.28	1.70	0.30	5.07	11.98	5.02	19.11	18.87	8.34	3.46	1.36	1.14
Orthoclase	0.69	0.49	0.12	0.48	0.31	1.03	2.01	0.99	3.27	2.78	0.43	0.21	0.40	1.01

Table 7. cont

Hole	HL28	HL28	HL28	HL28	HL28	HL28	HL28	HL28	HL28	HL28	HL28	HL28	HL28	HL28
Mineral	334196	334196	334196	334196	334196	334196	334196	334196	334196	334196	334196	334196	334196	334196
analysis #	r1fel1in	r1fel1cr	r1fel4in	r1fel4rim	r2fel1	r2fel1ca	r2fel2in	r2fel2rim	r3fel1rim	r3fel1cr	r4fel1rim	r4fel1in	r4fel1in	r4fel1rim
SiO2	67.01	67.22	67.57	75.86	66.79	68.17	67.29	65.19	65.77	66.90	61.62	67.36	66.83	67.84
TiO2	0.02	0.00	0.00	0.00	0.00	0.02	0.00	0.00	0.03	0.01	0.02	0.02	0.02	0.00
Al2O3	21.06	20.85	20.42	15.03	21.14	20.16	21.15	22.51	21.74	21.26	24.56	20.68	20.59	20.60
FeO	0.02	0.10	0.01	0.65	0.20	0.05	0.12	0.17	0.10	0.07	0.45	0.09	0.03	0.13
MnO	0.00	0.04	0.02	0.00	0.07	0.00	0.01	0.00	0.02	0.00	0.06	0.04	0.01	0.00
MgO	0.04	0.02	0.01	0.59	0.07	0.03	0.11	0.22	0.09	0.03	0.35	0.03	0.01	0.02
CaO	0.19	0.33	0.31	0.17	0.39	0.38	0.26	0.16	0.28	0.26	0.24	0.22	0.43	0.43
Na2O	10.83	10.96	11.25	7.02	10.60	11.38	10.64	9.84	10.30	10.57	7.74	10.95	10.98	11.06
K2O	0.36	0.23	0.14	0.85	0.46	0.00	0.63	1.62	0.97	0.59	2.92	0.29	0.14	0.23
Cr2O3	0.01	0.03	0.02	0.00	0.00	0.00	0.00	0.04	0.01	0.01	0.04	0.01	0.03	0.00
SrO	0.32	0.34	0.33	0.34	0.38	0.28	0.33	0.27	0.33	0.37	0.30	0.34	0.40	0.32
BaO	0.02	0.03	0.01	0.06	0.08	0.00	0.02	0.08	0.05	0.07	0.06	0.02	0.02	0.00
CalcTotal	99.87	100.13	100.08	100.58	100.18	100.46	100.55	100.09	99.69	100.15	98.35	100.07	99.47	100.63
Si	2.94	2.94	2.96	3.24	2.93	2.97	2.94	2.87	2.90	2.93	2.78	2.95	2.94	2.95
Al	1.09	1.08	1.05	0.76	1.09	1.04	1.09	1.17	1.13	1.10	1.31	1.07	1.07	1.06
Fe2	0.00	0.00	0.00	0.02	0.01	0.00	0.00	0.01	0.00	0.00	0.02	0.00	0.00	0.01
Mg	0.00	0.00	0.00	0.04	0.00	0.00	0.01	0.01	0.01	0.00	0.02	0.00	0.00	0.00
Ca	0.01	0.02	0.01	0.01	0.02	0.02	0.01	0.01	0.01	0.01	0.01	0.01	0.02	0.02
Na	0.92	0.93	0.95	0.58	0.90	0.96	0.90	0.84	0.88	0.90	0.68	0.93	0.94	0.93
K	0.02	0.01	0.01	0.05	0.03	0.00	0.04	0.09	0.06	0.03	0.17	0.02	0.01	0.01
Ti	0.00	0.00	0.00	0.00	0.00	0.00	0.00	0.00	0.00	0.00	0.00	0.00	0.00	0.00
Mn	0.00	0.00	0.00	0.00	0.00	0.00	0.00	0.00	0.00	0.00	0.00	0.00	0.00	0.00
Cr	0.00	0.00	0.00	0.00	0.00	0.00	0.00	0.00	0.00	0.00	0.00	0.00	0.00	0.00
Sr	0.01	0.01	0.01	0.01	0.01	0.01	0.01	0.01	0.01	0.01	0.01	0.01	0.01	0.01
Ba	0.00	0.00	0.00	0.00	0.00	0.00	0.00	0.00	0.00	0.00	0.00	0.00	0.00	0.00
mg	77.16	23.99	61.31	61.88	37.74	54.04	63.25	69.60	61.63	43.87	58.01	37.80	27.64	24.34
Total Cat	4.99	4.99	5.00	4.70	4.99	4.99	4.99	5.01	5.00	4.99	4.99	4.99	4.99	4.99
Ox Equiv	8.00	8.00	8.00	8.00	8.00	8.00	8.00	8.00	8.00	8.00	8.00	8.00	8.00	8.00
Albite	96.95	97.08	97.73	91.50	95.37	98.18	95.05	89.49	92.84	95.21	79.06	97.23	97.10	96.63
Anorthite	0.92	1.60	1.48	1.22	1.92	1.79	1.27	0.81	1.41	1.31	1.33	1.08	2.08	2.06
Orthoclase	2.13	1.32	0.78	7.29	2.72	0.02	3.68	9.69	5.75	3.47	19.61	1.69	0.82	1.32

Table 7. cont

Hole	HL28	HL28	HL28	HL28	HL28	HL28	HL28	HL28
Mineral	334196	334196	334196	334196	334196	334196	334196	334196
analysis #	r5fel1in	r5fel1rim	r5fel1rim	r6fel1rim	r6fel1in	r6fel1rim	r6fel2	r6fel4
SiO2	66.56	65.44	69.63	66.59	67.97	66.86	61.99	68.08
TiO2	0.01	0.03	0.10	0.00	0.00	0.00	0.00	0.00
Al2O3	21.38	22.30	18.64	21.06	20.45	21.38	24.41	20.69
FeO	0.15	0.23	0.34	0.14	0.04	0.27	0.44	0.07
MnO	0.00	0.05	0.00	0.03	0.00	0.02	0.04	0.00
MgO	0.08	0.24	0.37	0.04	0.01	0.10	0.55	0.03
CaO	0.18	0.17	1.49	0.27	0.16	0.20	0.13	0.14
Na2O	10.30	9.76	6.87	10.88	11.30	10.73	7.56	11.38
K2O	0.77	1.43	1.85	0.43	0.16	0.68	3.38	0.24
Cr2O3	0.00	0.00	0.00	0.03	0.01	0.00	0.07	0.04
SrO	0.33	0.28	0.28	0.35	0.31	0.30	0.26	0.32
BaO	0.05	0.02	0.05	0.00	0.03	0.00	0.11	0.04
CalcTotal	99.81	99.96	99.61	99.81	100.44	100.55	98.96	101.03
Si	2.93	2.88	3.05	2.93	2.96	2.92	2.78	2.95
Al	1.11	1.16	0.96	1.09	1.05	1.10	1.29	1.06
Fe2	0.01	0.01	0.01	0.01	0.00	0.01	0.02	0.00
Mg	0.01	0.02	0.02	0.00	0.00	0.01	0.04	0.00
Ca	0.01	0.01	0.07	0.01	0.01	0.01	0.01	0.01
Na	0.88	0.83	0.58	0.93	0.96	0.91	0.66	0.96
K	0.04	0.08	0.10	0.02	0.01	0.04	0.19	0.01
Ti	0.00	0.00	0.00	0.00	0.00	0.00	0.00	0.00
Mn	0.00	0.00	0.00	0.00	0.00	0.00	0.00	0.00
Cr	0.00	0.00	0.00	0.00	0.00	0.00	0.00	0.00
Sr	0.01	0.01	0.01	0.01	0.01	0.01	0.01	0.01
Ba	0.00	0.00	0.00	0.00	0.00	0.00	0.00	0.00
mg	49.10	65.23	65.73	32.18	30.30	38.45	68.88	41.97
Total Cat	4.98	5.00	4.81	5.00	4.99	5.00	5.00	5.00
Ox Equiv	8.00	8.00	8.00	8.00	8.00	8.00	8.00	8.00
Albite	94.44	90.42	77.08	96.22	98.29	95.04	76.69	97.96
Anorthite	0.91	0.87	9.25	1.30	0.76	1.00	0.75	0.69
Orthoclase	4.65	8.71	13.67	2.48	0.95	3.96	22.56	1.35

Rosebery alteration study

Rodney Allen, Nathan Duhig and Ross Large
Volcanic Resources Limited, Stavanger, Norway; and Centre for Ore Deposit and Exploration Studies, University of Tasmania

Introduction

The Rosebery site study was started up in February. The aims of the project are to determine the distribution, physical character, timing relationships and geochemistry of carbonate alteration around A-B lens and K lens at Rosebery Mine. The alteration, and geological context of the alteration, will be studied in the footwall, hangingwall, ore zone and along strike in order to interpret physical, geochemical and isotopic vectors to ore. Whole rock and selected trace element geochemistry and mineral chemistry will also be studied in order to relate trends in the carbonate alteration to whole rock trends. The AB-K lens area of the mine was chosen because it is the simplest to study (least deformation and Devonian granite-related hydrothermal overprint), sufficient drill core is available, and the area is of special interest to the Rosebery mine staff because the area is currently being developed for mining and further exploration.

Work completed to date

One month was spent on site in February-March. With the help of geological staff at the Rosebery mine, an array of 22 drill cores has been chosen for study, and a longitudinal section and six cross sections have been designed to compile and display results (Fig. 1). The drill cores for study have been selected so that a three-dimensional data set can be built up from the centre of A-B lens and K lens (Fig. 1), to a distal position 800 m north of A-B lens and 600 m from K lens (hole 71R).

Each drill core will be carefully relogged for volcanic facies, stratigraphy, structure and alteration information, in order to provide the field geological context for petrographic and geochemical studies. The first seven drill cores were logged in this period and 179 samples were collected for further study (Table 1, Appendix). Examples of the drill core logging scheme are provided in Figure 2. The drill core samples are currently being processed at CODES for thin sections, polished thin sections for micoprobe study, and geochemical analysis.

Final conclusions from these first seven drill cores can not be made until the petrography and geochemistry have been completed. However, a list of important observations from the drill core logging is provided below.

Important observations of alteration and mineralization relationships from core logging and initial petrography

- There are at least two generations and several styles of carbonate alteration at Rosebery. Carbonates include: (1) Spotty white to pink, variably brown weathering carbonate not related to veins, and overprinted by S_2 cleavage. (2) Thin (1mm) white, sheeted, carbonate veins subparallel to S_2 cleavage in the hangingwall black slates. (3) White, thick, quartz-carbonate veins in the hangingwall black slates. (4) Cream- to brown-weathering carbonate veins with broad (up to 50 cm) bleached sericite-carbonate selvedges in hangingwall volcaniclastic facies. (5) Irregular zones of white carbonate matrix-impregnation within hangingwall mass flow facies. Overprinting relationships indicate that the various veins formed syn- to post-S_2 cleavage.

Table 1: Drill core logged to date in the Rosebery north-end alteration study

Drill hole	Detailed log of geology and alteration, Feb-Mar 1996	Detailed log of geology completed previously; alteration log still to do	Samples for alteration study
R4452	0-119 m		40
65R	2950-4271 ft		16
84R	528-905 m		18
109R	321-750 m		26
113RD1	668-995 m		25
120R	1050-1446 m		28
128R	844-1261 m		26
49R		0-1051 ft, R. Allen 1993	
71R		914-2357 ft, R. Allen 1990	
74R		752-1137 m, R. Allen 1991	
78R		650-955 m, R. Allen 1993	
120RD4		1000-1351 m, R. Allen 1993	
Total	7 holes, 2505 m	5 holes, 1989 m	179 samples

- First generation secondary feldspar alteration, chlorite alteration, sericite alteration, carbonate alteration and mineralization are all overprinted by, and therefore pre-date, the regional S_2 tectonic cleavage.

- Spotty carbonate alteration and strong silicification are spatially closely associated with ore or strong mineralization. In several cases, mineralization occurs within a silicified zone, which is partially enclosed by an irregular spotty carbonate zone.

- There are also at least two generations of chlorite and sericite alteration. Early chlorite and sericite are strongly S_2 cleaved and not vein-related, whereas a second generation of chlorite is less foliated and occurs in subplanar to variably folded syn- to post-S_2 veins that are most abundant in the hangingwall and increase in abundance toward the Mount Black Fault.

- Weak to moderate silicification is common within the hangingwall volcaniclastic mass flow facies.

- Diffuse zones of low grade disseminated sphalerite are common in the hangingwall volcaniclastic mass flow facies, many tens of metres above ore.

- Pumice textures are well preserved in many altered rocks, which indicates that an initial very competant alteration assemblage healed the rocks during early diagenesis.

- The earliest alteration assemblage identified so far is widespread secondary feldspar (albite, K-spar) ± chlorite-epidote-leucoxene. However, it is not proven that this assemblage was the first replacement of fresh glassy pumice or whether it replaces an earlier alteration assemblage.

- Secondary feldspar, carbonate and sulphide all initially preferentially nucleated on, or replaced, feldspar phenocrysts in the host pumiceous rocks.

- The secondary feldspar alteration is most intense in diffuse spots around igneous feldspar phenocrysts. Within these spots secondary feldspar has both filled the vesicles and replaced the framework of the pumice. It is inferred that the secondary feldspar nucleated on the igneous feldspar phenocrysts and grew out through the pumice.

- At more advanced stages of mineralization, sulphide forms extensive replacement of the pumice and matrix surrounding the feldspar

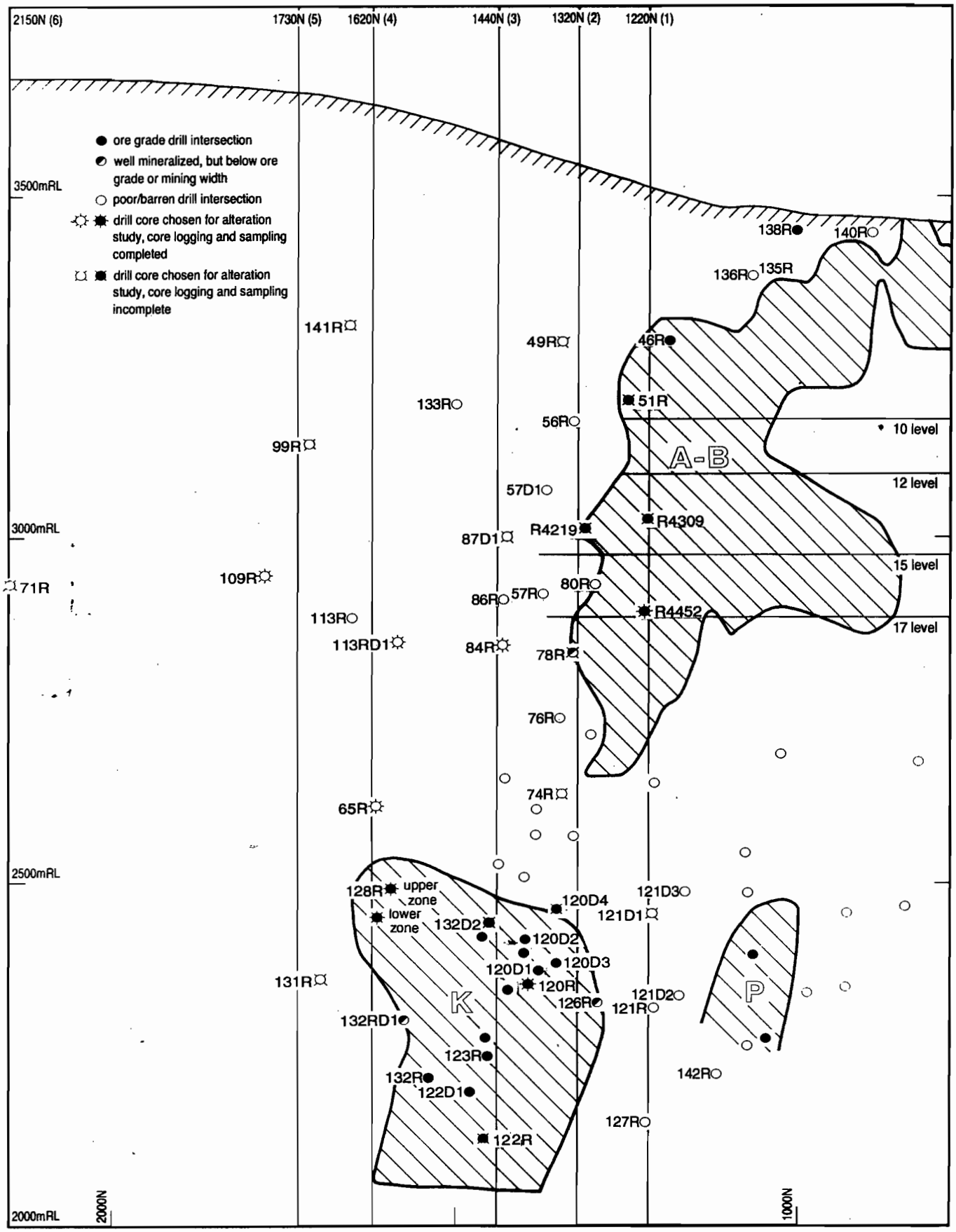

Figure 1: Longitudinal section of the north end of Rosebery mine showing the location of A-B, K and P ore lenses, drill core intersections of the ore stratigraphic position, drill cores selected for this study, and six cross sections designed to compile results (1220 mN, 1320 mN, 1440 mN, 1620 mN, 1730 mN and 2150 mN).

blank

phenocrysts, whereas the feldspar phenocrysts are replaced by quartz and occur as 0.5–3 mm quartz spots enclosed by sulphide.

- Primary features of the host volcaniclastic facies and tectonic fabrics can both be seen in low grade mineralization and the fringes of high grade ore. At these locations the mineralization occurs as bedding-parallel, stratabound impregnations and replacements that are overprinted by discordant to sub-parallel S_2 tectonic foliation.

- Spotty carbonate alteration is also at least locally stratabound, forming layers and spots along stratification, and overprinted by S_2 tectonic foliation (best observed on 4-level road at Hercules).

- Alteration veins are not more abundant near ore; if anything they are less abundant than above and below the ore zone.

- Chlorite and sericite alterations appear to overprint secondary feldspar alteration.

- The sericite- or chlorite-rich fiamme-like lenses in the footwall and hangingwall have more abundant feldspar (± quartz) phenocrysts than the rest of the rock that encloses them. This suggests that formation of the fiamme-like lenses was accompanied by volume reduction of the pumice matrix relative to the phenocryst component, either by compaction or dissolution or both.

- The fiamme-like lenses include: (1) True fiamme formed by compaction and sericite or chlorite alteration of large pumice clasts. (2) Stylolitic, bedding-parallel, S_1 foliation that comprises spaced, wavy, dissolution foliation marked by a concentration of sericite, chlorite and leucoxene (probably due to dissolution of quartz and feldspar).

- The true fiamme must have formed before or during the first introduction of competent alteration assemblages that healed the pumices (i.e. secondary feldspar, silicification or their precursor alterations). However, this relationship has not been proven petrographically yet.

- Stylolitic, pseudofiamme, S_1 foliation overprints and therefore post-dates secondary feldspar-leucoxene. However, the relationships of S_1 to silicification, carbonate spots and sulphide still remain to be proven. These are critical timing relationships to resolve.

- Ore-related alteration overprints the hangingwall quartz-feldspar-biotite porphyritic rhyolite sill at K and B lenses, and extends at least up to the black slates.

These field relationships indicate that the mineralization and ore-related alteration conform to one of the following two scenarios:

(1) Early stages of alteration and mineralization were synvolcanic. Subsequent deformation and cleavage development has resulted in strong deformation, transposition of ore shoots and bedding, and obliteration of most primary textures in mechanically weak alteration and mineralization assemblages (chlorite, sericite, sphalerite-galena ore), and less deformation and good preservation of primary textures in competent alteration and mineralization assemblages (secondary feldspar, silicification, pyrite-rich mineralization).

(2) Early competent alteration assemblages were synvolcanic and preserved primary pumice textures. However, a major or minor part of the mineralization occurred during a later stage, but before, or early during, S_2 cleavage development. Where new competent alteration assemblages related to the mineralizing event (silicification, carbonate) were superimposed on older competent alteration assemblages, primary textures continued to be pseudomorphed and relatively well preserved. Where new mechanically weak alteration assemblages formed, primary textures were destroyed during deformation.

Clearly, important relationships that must be determined in order to prove the timing of ore formation and ore-related alteration, including the spotty carbonate alteration, are the overprinting relations between S_1 foliation and spotty carbonate, silicification and mineralization. Finding these relationships would be a major breakthrough in resolving the debate over the origin of the Rosebery ore deposit, and would allow better interpretation of

the results of this alteration study. However, the documentation of alteration geometry, zoning, chemistry and textural relationships in this study is not dependent on those relationships.

Future plans

Ten drill cores remain to be logged for geology and alteration and sampled (51R, R4309, 121RD1, R4219, 87RD1, 132RD2, 122R, 141R, 99R, 131R), and five drill cores remain to be logged for alteration only and sampled (geological logs completed previously; 49R, 78R, 74R, 120RD4, 71R). This on-site drill core logging is planned to resume in November.

The petrographic and geochemical studies will commence during June-October.

Figure 2: Example drill core logs of surface drill hole 120R and underground drill hole R4452 showing the logging scheme used in this study.

GRAPHIC LOG
Volcanic Resources Ltd

Project: Mt Read Volcanics
Location: Rosebery Mine
Drill hole no.: 120R
Location no.:
Co-ords:
RL:
Scale: 1:200
Page: 1 of 8
Azim:
Incl:
Diam:
Logged by: Rod Allen
Date: 29.11.93, 15.3.96

m	Structure	Log with grainsize (mud 0.5 2 8 32 max mm)	Samples / TS results / Chemistry	Rock / facies description	Alteration
1050				grey f-mg granular, massive 10% 1mm feld-phyric dacite?	grey weak-moderate ser-chl-q
	fault			1052.0	
				1053.5 Mt Black Fault: intense foliation, lesser brittle clast- to matrix-supported tectonic bx. Q-fluorite ± mag-chl/biot veining parallel to cleav.	
	fault bx layers + foliation 80°			Normal graded, feld >> q xtal-lithic pumice bx subaqueous mass flow unit	1055 buff, bleached, (only minor dk brown weathering) weak-moderate q-CO_3-ser alteration, pervasive not distinctly associated with increase in q-CO_3 veining intensity
1060				Matrix-supported bx at base, polymict lithic assemblage, in order decreasing abundance:	
	increased S_2 cleavage intensity toward fault & increased hydraulic brecciation (tectonic)			(1) a) grey, white, brown fg poorly phyric felsic lava	
			10	grey fg siliceous lava lithic b) moderately f>q phyric felsic lava 5-15% 1-2mm phenos	
1070			1068.5		1070 grey > cream, mottled blotchy siliceous q> ser-chl-leucox alteration with many diffuse patches fine disseminated (1-2%) sp pyrh, especially replacing feld xtals + rimming lithics. Blotchy texture due to preferential cream q-rich alteration rimming lithics, and irreg alteration of pumice. Moderate intensity q >> CO_3 >> py sp syntectonic veining.
				(2) a) black mud ripups	
				b) f-mg feld xtal-pumice sandst	
				c) vcg xtal-rich q-f porphyry	
				d) buff, fg, amyg mafic lava	
				e) vcg xtal-rich q-f phyric pumice	
1080				Pumice-rich, moderately xtal-rich matrix above 1095m (25% 1.5mm feld, feld:q 95:5). Feld xtal-rich (xtals up to 50%, q 2%) below 1095m. Distinctly less q xtals than unit below (1104-1178m)	
	gb		1083.7		
				irreg black mudst	
	cleav 35°		250		
1090	f 62°		90	green-grey 15-20% 1.5mm f>q rhyolite	
			1094.5		
					1098 cream/white, strong pervasive CO_3 impreg in matrix
1100			40	buff fg granular amyg mafic	

104

GRAPHIC LOG

Volcanic Resources Ltd

Project	Mt Read Volcanics	Drill hole no.	120R
Location	Rosebery Mine	Location no.	
Co-ords		RL	Scale 1:200
Azim	Incl	Diam	Logged by Rod Allen

Page 2 of 8

Date 29.11.93 15.3.96

m	Structure	Log with grainsize mud 0.5 2 8 32 max mm	Samples TS results Chemistry	Rock / facies description	Alteration
1100		75	1100.3	grey fg felsic lava	+ abundant q-CO_3 syntectonic veins CO_3 content of veins greater than in adjacent intervals Minor dissem pyth sp
	contact approx 70° →			1104 faint sharp conformable	
				granular pumice-shred sandst with 1-3% 0.5mm q xtals < feld xtals	pale greenish grey, weak q-ser > chl-leucox (2-3%). Trace Sp dusting of feld xtals.
1110	mod-strong S2 44° →				Moderate network q >> CO_3 syntectonic veining cuts moderate network chl-q veining
			1115.9		
1120					
				increase grainsize due to 2mm av. fibrous pumice shreds = normal density grading, reverse size grading Possibly also cryptic boundary between mass flow pulses. ↑	
1130				← q xtals 3% 0.6mm	
1140	normal grading (gb) ↑				1040 green-grey, weak-moderate, pervasive ser-q-chl-white CO_3 ± epid, + moderate syntect veining of sub-planar CO_3 ≥ q veins with green chl selvedges.
			1147.8		
1150					

GRAPHIC LOG Volcanic Resources Ltd	Project Mt Read Volcanics Location Rosebery Mine	✓ Drill hole no. 120R Location no.	
Co-ords	RL	Scale 1:200	Page 3 of 8
Azim	Incl / Diam / Logged by Rod Allen		Date 30.11.93 15.3.96

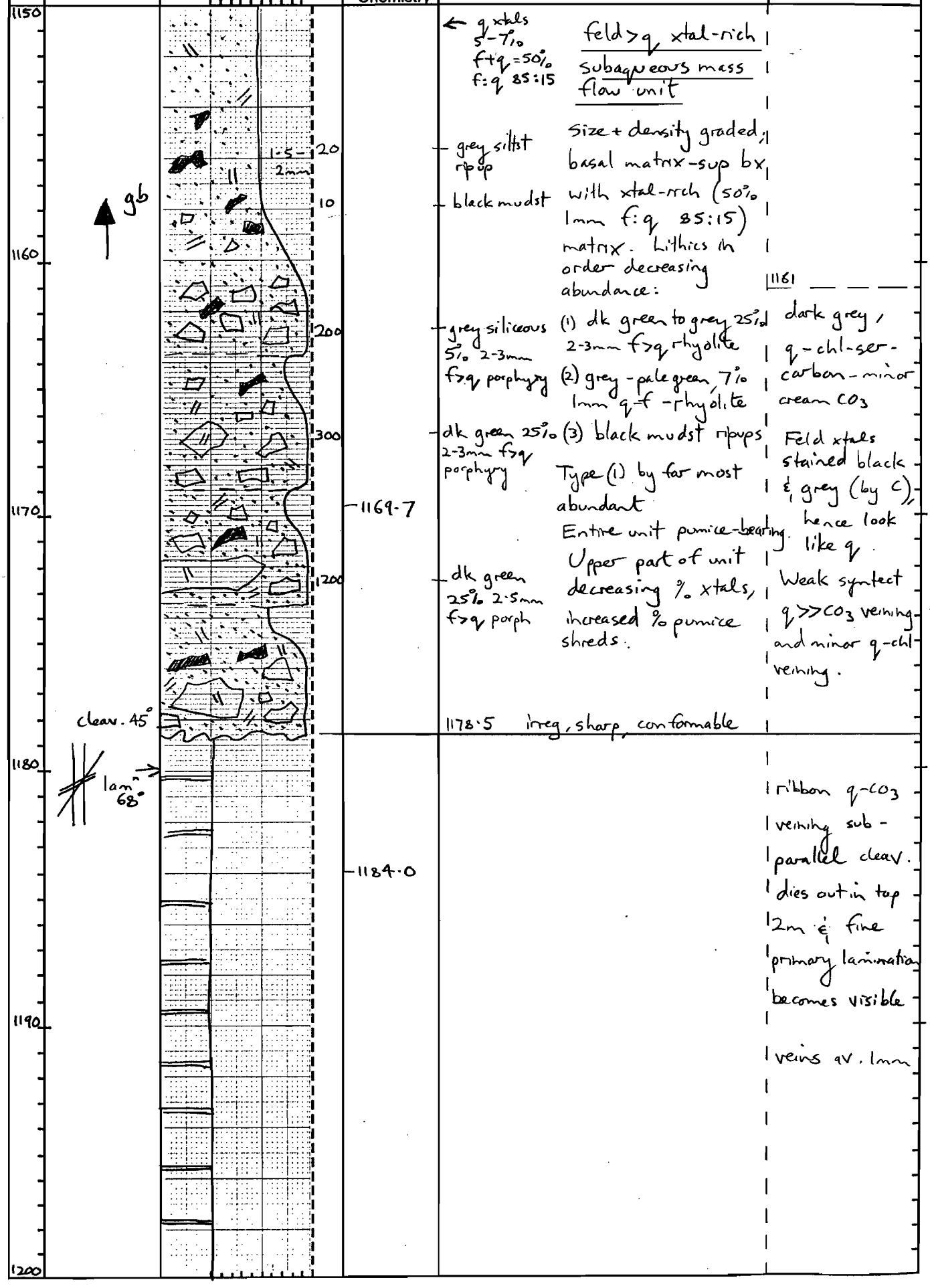

106 **GRAPHIC LOG**
Volcanic Resources Ltd

Project / Location	Mt Read Volcanics / Rosebery Mine	Drill hole no. / Location no.	120 R
Co-ords		RL	Scale 1:200
Page	4 of 8		
Azim	Incl	Diam	Logged by Rod Allen
Date	30.11.93 / 15.3.96		

Log with grainsize: mud 0.5 2 8 32 max mm

Samples / TS results / Chemistry

m | Structure | Rock / facies description | Alteration

1200

1m broken core in slightly stronger cleaved interval

Black slate with rare f>q xtal volc sandst beds

1210

cleav 64°
b 73°

← 1cm sandst beds

1220

b/cl relation gives overturned facing
cl 66°
b 84°

gb

1230

1229.3 ← 30cm overturned f>q xtal sandst turbidite (q 5-10%)

strong graphitic cleav 56°

F

sharp, sheared buckled q-veined faulted contact 1233.6m

Fault 10° late, brittle post-S_2 F

Planar stratified, feld xtal-rich volcanic sandst

Similar to 1259-78m. No q xtals. Sandst beds mainly close-packed well sorted feld xtals (60-80%). Lithic assemblage seems monomict fg lava type

grey, weak-moderate ser-q-py-pyrth (1-3%)

Local white CO_3 impregnation patches, and moderate intensity white q ≥ CO_3 syntect veining

1240

10cm sheared zone

10

1237.2 — subrounded to angular monomict grey-brown finely pyritic fg lava lithics

10

b 66°
cleav 57°

1241.8 — 20 — grey siltst riplap

3cm sub-mylonitic foln
37°
cleav 50°

gb

7 — grey brown fg lava lithic 3% <0.5mm feld phenos

1248.6 rapid gradational

1250

GRAPHIC LOG
Volcanic Resources Ltd

Project: Mt Read Volcanics
Location: Rosebery Mine

Drill hole no. 120R
Location no.

Co-ords | RL | Scale 1:200 | Page 5 of 8

Azim | Incl | Diam | Logged by Rod Allan | Date 30.11.93 15.3.96

m	Structure	Log with grainsize (mud 0.5 2 8 32 max mm)	Samples TS results Chemistry	Rock / facies description	Alteration
1250				Sandst turbidites similar to sandst at base overlying unit.	abundant white q-CO_3 veinlets subparallel S_2 and folded about S_2
				Black slate, minor thin (<15cm) feld>>lithic volc sandst turbidites. Minor q xtals at 1255.5 only.	
			1256.0		
	S_2 brittle post- F 15° cl 59°	F			
				1258.7 sharp fault contact	
1260				**Planar stratified, feld xtal-rich, tuffac. volcanic sandst & siltst.**	grey, weak-moderate ser-q-py pvrh (1-2%)-CO_3
		8		siliceous fg grey brown lava lithics with 3% 0.4mm feld laths. Q xtals rare/absent	
	?gb		1265.5		ser-q is pervasive, but white CO_3 as patchy impregnation in matrix
		10		as above. below 1278m: feld xtal-rich volc sandst turbidites (with normal grading + siltst ripups) interbedded with grey laminated siltst-fg sandst	
1270					
	cl 60° b 78°	15		as above. above 1278m: planar stratified, mod-well sorted, feld xtal > lithic volc sandst. Arranged in crude graded beds with internal planar stratificat. due to grainsize variation on 0.5-10cm scale. Lithics almost entirely angular, grey brown, commonly finely pyritic ?mafic/felsic lava clasts with 3% 0.4 mm feld lath/needle phenos. Bed form indicates traction deposition at base of low concentration, pulsating mass flows (turbidites)	Moderate syntectonic $CO_3 \geq q$ veining
	small normal faults along cl.		1278m		
1280	gb				
	cl 55° b 80°				
	gb	30		grey siltst ripups in bed with feld xtal base & sericite pumiceous top	
	cl 50° b 80° gives uphole facing				
	gb				
1290			1290.5		1289.5
	lam^n 80°	100	1291.8	irreg grey mod. siliceous siltst inclusions. irreg, sharp, mixed, intrusive (peperitic) contact. Unit appears more xtal-rich at top (35-40% 2.5mm xtals) q 10-15%	pale grey, mod-strong ser-q-py (1-2%) straddles intrusive contact. Local white CO_3 impregnation. pseudo granular sandy.
		2.5 mm			
1300					

GRAPHIC LOG — Volcanic Resources Ltd

Project: Mt Read Volcanics | Location: Rosebery mine | Drill hole no. 120R | Location no.

Co-ords | RL | Scale 1:200 | Page 6 of 8

Azim | Incl | Diam | Logged by Rod Allen | Date 30.11.93, 15.3.96

m	Structure	Log with grainsize (mud 0.5 2 8 32 max mm)	Samples / TS results / Chemistry	Rock / facies description	Alteration
1300				Massive, cg, feld > q > biot xtal-rich rhyolite porphyry sill	1302
				30% 2·5mm xtals. Feld 20-25% 2mm, q 7-10% 2·5mm, biot 2% 1·5mm. Xtals up to 6mm. Q phenos distinct sub- to well rounded, strongly embayed shapes, and have tiny white inclusions →	mainly medium buff-grey; weak ser-q-trace sulphide
1310		130	granular mg feld-sandst inclusions		Moderate q-CO_3 syntectonic veining
		140			
			1315·4		
1320				Variation in alteration comp and intensity & consequently foliation, results in variable preservation of phenos. Biot commonly not visible (well preserved at 1325·0m), locally only q phenos visible, locally only feld.	
				Groundmass finely granular, probably spherulitic in fresher parts. Local faint flow banding parallel to bedding.	
1330		150	granular mg feld sandst	Abundant irregular inclusions of feld-xtal rich sandst, interpreted as relics of the fg top of fw pumice bx/sandst that the sill intruded into.	1335 — dark grey relatively unaltered; q-ser-chl groundmass
1340			irreg grey mg well sorted feld xtal sandst	Thin irreg intrusive peperite contacts at top and base indicate unit is intrusive into unlithified volc sandst-siltst. Thin mixed contact and paucity hyaloclastite suggests unit was viscous &/or host partially dewatered at time of intrusion. No break in alteration at contacts suggests unit is pre-alteration + mineralization	Moderate syn-tectonic q-CO_3 veining
1350					1349

GRAPHIC LOG

Volcanic Resources Ltd

Project: Mt Read Volcanics
Location: Rosebery Mine

Drill hole no. 120R 109
Location no.

Co-ords | RL | Scale 1:200 | Page 7 of 8

Azim | Incl | Diam | Logged by Rod Allen | Date 30.11.93 15.3.96

m	Structure	Log with grainsize (mud 0.5 2 8 32 max mm)	Samples / TS results / Chemistry	Rock / facies description	Alteration
1350	fb 70°; S_2 52°		1353·8	← faint cm-scale planar flow banding	cream, moderate q-ser-trace py
				Sharp, mixed, non-faulted (peperitic) contact	1355 pale grey, mod-strong ser-q >> CO_3 - 1% py with thin intervals spotty CO_3 & intense dissem pysp>gn as shown
	Strong S_2 50°		1356·9 ?		
1360			1358·2	← 1358·2m superb relict pumice bx (5mm) texture	1358·4 semi massive spotty pink-cream CO_3 with ser matrix. Weak dissem + veinlet py sp. Mod CO_3-q syntectonic veining
	py elongation in S_2; S_2 45°; 55° S_1		1361·4	← 1361·5 relict 15% f-phyric ser rock (after pumice bx)	
			1364·4	Massive feld-phyric felsic pumice breccia with thin sandy, normal graded top. Contains strongly zoned alteration + mineralization: Spotty CO_3 (with superb concentric + radiating internal structures) above sulphide zone in ser-q schist; underlain in turn by chl-ser-minor CO_3 and ser-q-CO_3	
			1365·4		
			1366·0		1366 semi massive to locally massive py sp > gn in ser-q & chl-ser schist sulph pre-cleav but locally remobilized
	S_1 in spotty CO_3 indicates CO_3 pre-S_1				1369·2 syn-/post S_2 pale grey q-ser schist
1370	strong cleav 66°				1371 mod dissem sppy
					green chl-ser schist with strong streaky dissem sp > py qy > gn
	Mineralized, altered rocks strong foliated except for competant CO_3 or q rich parts				1374 intense ser, intense dissem/streaky sp >
	strong anastomosing cl. 78°		1378·3		1375·7 gn py
1380	foliation increases to 1369m			Mineralized interval 1366-1390m has lower intensity (weak) syntectonic q ± CO_3 veining than adjacent intervals	green-grey strong chl-ser (± sec. biot?) - 1-2% py > sp with CO_3 blotches increasing in abundance down hole
	S_2 77°; fiamme 90°		1386·5	Pumice bx contains prominent fiamme below 1378m, and anastomosing cleavage that crenulates the fiamme foliation.	? Second generation bright apple green chl/biot appears post S_2 & ?overprints translucent bright pale to dark green pre-cleav chl-ser
1390				Matrix pumice textures mainly obscured by alteration. Feld extensively obliterated, but locally visible as CO_3-ser pseudomorphs.	Dissem + veinlet sp (brown) becomes abundant toward top of interval
	stretch lin. pitches 90° down cleav.; cleav 75°; f 85°				1399
1400					

110 **RAPHIC LOG** — Volcanic Resources Ltd

Project: Mt Read Volcanics
Location: Rosebery Mine

Drill hole no. 120R
Location no.

Co-ords | RL | Scale 1:200 | Page 8 of 8

Azim | Incl | Diam | Logged by Rod Allen | Date 30.11.93 15.5.96

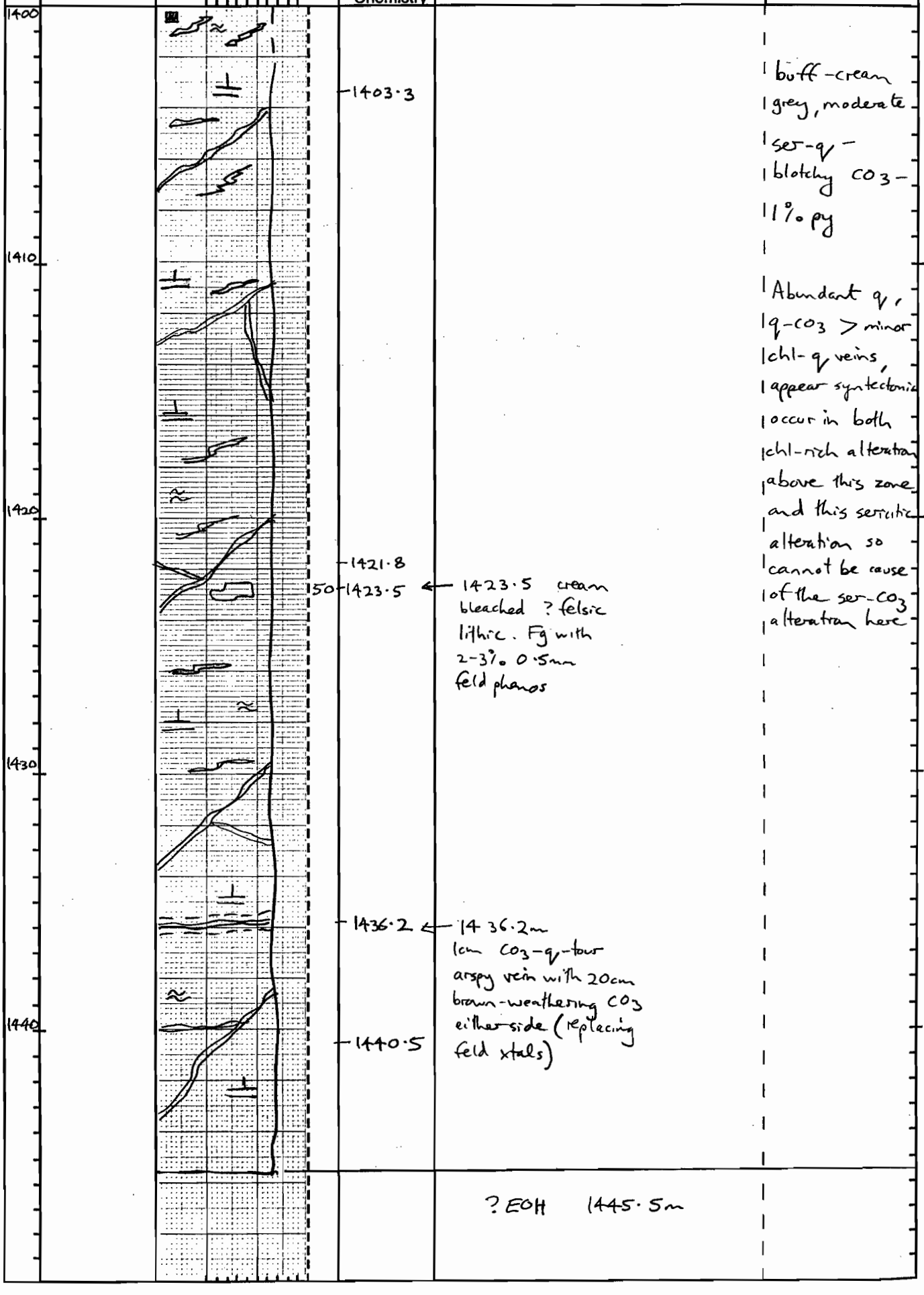

GRAPHIC LOG

Volcanic Resources Ltd

Project	Mt Read Volcanics	✓ Drill hole no.	R4452
Location	Rosebery Mine North end	Location no.	
Co-ords		RL	Scale 1:200
Page	1 of 3		
Azim	Incl	Diam	Logged by Rod Allen
Date	14.2.96		

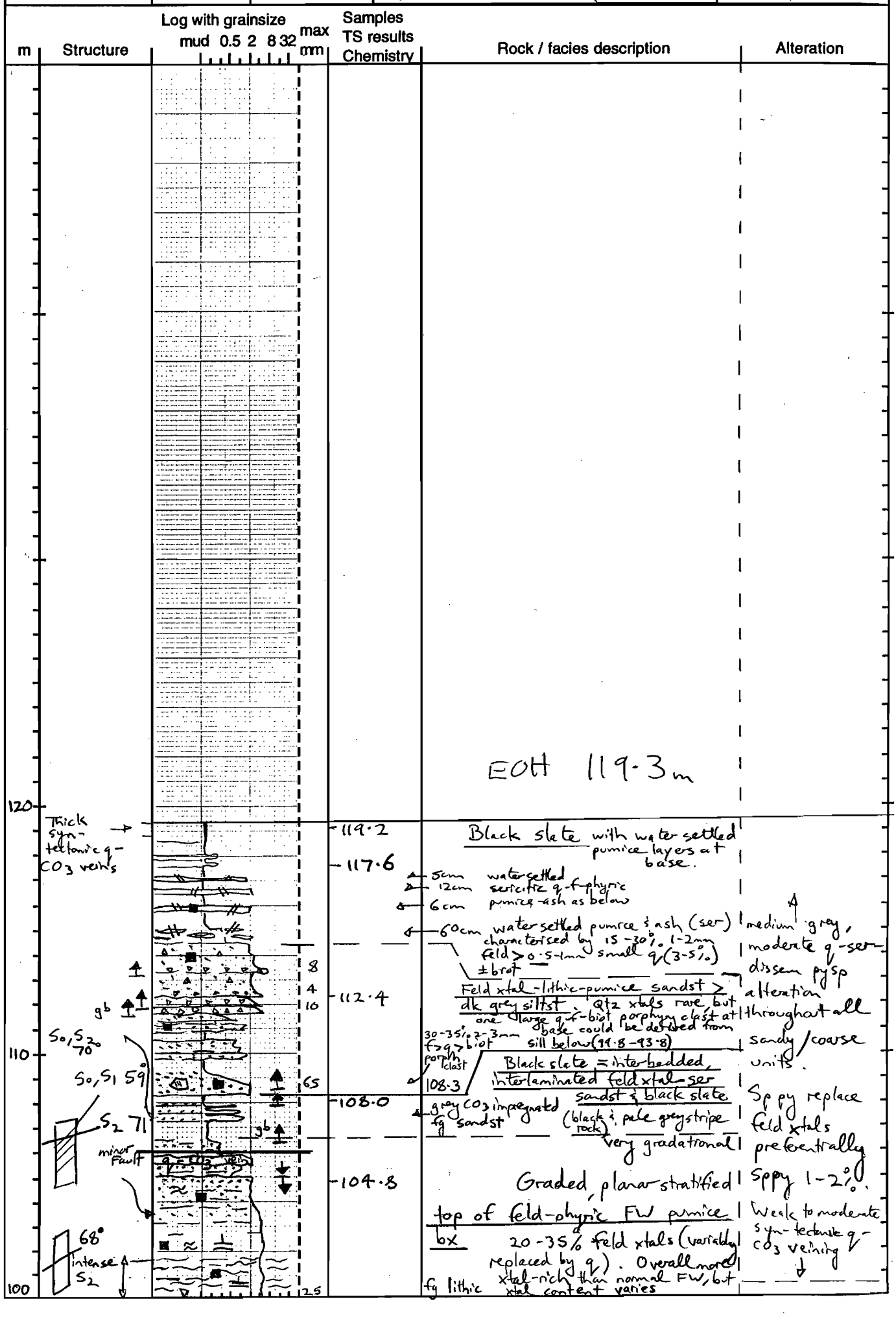

112 **RAPHIC LOG** Volcanic Resources Ltd	Project Mt Read Volcanics	✓ Drill hole no. R4452
	Location Rosebery Mine Northend	Location no.
Co-ords	RL	Scale 1:200	Page 2 of 3
Azim	Incl	Diam	Logged by Rod Allen	Date 13/14-2-96

m	Structure	Log with grainsize mud 0.5 2 8 32 max mm	Samples TS results Chemistry	Rock / facies description	Alteration
100				99.8m 35% 2-3mm f>q (10-15%) > biot (2-3%) rhyolite sill. Coherent except for intrusive peperitic top. Q phenos rounded to subhedral unbroken. Biot replaced by leucoxene.	pseudoclastic ser-chl-CO_3-q. ser-CO_3 → chl>ser (dark) minor dissem py.
	strike S_1 & S_2 almost ⊥.		96.0	93.8m	
	S_1+f 15°			← 25-30% 2mm f-phyric. Massive to ?diffuse stratified, 15-30% 2mm feld-phyric pumice bx. Extensive but variable destruction of primary textures due to alteration + mineraliz^n.	v. strong ser-CO_3 q. CO_3
	S_2 71		91.6	← good tube pumice	90.9m
90			90.8	← fiamme replaced by py	v. strong q-ser-py ≫ sp (1-7%)
			90.3		
			88.9		
	S_2 79		88.0	← py bands with S_1+S_2	88m py bands F_2 folded + D_3 x ≤ 10cm sp-gn bands ish intense q-ser
				strong py>sp-gn^ in feld xtal + pumice bearing rock. rapid gradational	
			85.8	B-lens Massive + semimassive sulphide. Commonly banded + F_2 folded. Increasing sp/py to top	semi-massive to massive py-sp, banded. Gangue chl at base, q-ser top.
	S_1+f 21°		84.1		semi-massive py in chl, + bleby spotty CO_3
			83.5		semi-massive py in q + some CO_3 blebs ∨ after ? feld
	sharp contact 73° // S_2		82.8m	sharp	
			81.9	Massive feld-phyric pumice breccia with superb relict ?round-vesicle pumice (v. abundant) in CO_3 spots. This suggests CO_3 pre-S_2 (& probably S_1) & competency prevented modification of pumice fabric. Rock is now mainly alteration rock of CO_3-chl-ser ± q. Primary pumice textures strongly obliterated & attenuated in ser/chl domains. Generally sulphide poor, but up to 5-10% Spgn >py in ser/chl & ser/chl-q rich areas. Some possible stratification in upper part, distinguished by variation in feld xtal content (q after feld).	intense spotty CO_3 (tan weathering). Matrix ser-q at base, grading to chl-ser at top. Superb relict pumice textures in CO_3 - CO_3 pre-S_2. Local q-ser ± veinlets 74-4m overprint CO_3.
			81.5a,b		
			80.6		
80	S_1 10° S_2 78°		80.4		
			78.7		
	S_1 24°		78.2		
			77.2		
			76.2		
	S_2 70°		75.9		
			75.1		
	py, S_1 0°		73.3		(silicification ?overprints CO_3-ser) Pale grey-green, very strong, ser-q-minor fine py alteration, pervasive, feld xtals replaced by q. 1-3% very fine dissem py.
	S_2 80°	10			
70	folded semi-massive py bands // S_1 S_2 axial planar to folds		69.5	thin grey siltst. 3% 0.5-1mm f-phyric lithic. Feld xtals av. 2mm, up to 30%.	gradational change to blotchy-spotted sub-augen textured strong q-ser ≫ CO_3 alteration: Up to 5% Spg-py but overall 1-2% CO_3 spots after feld xtals. Texture comprises q-rich white blotches (augen) with yellow-green-grey-sericite rich anastomosing cleavage domains enclosing them. Qtz rich & blotches are silicified pumice clasts. First stage of mineralization is replacement feld xtals by q-py/gn-sp.
			66.2	sub-augen cleaved, Massive, 10-20% 1-2mm feld-phyric pumice bx. Less feld xtals than parts of interval above. Tube pumice textures faintly visible in white siliceous blotches in many areas but less well preserved than in intense CO_3 & siliceous alteration near ore above!	
			64.5		
60			57.9		
			54.9		
50					

GRAPHIC LOG

Volcanic Resources Ltd

Project: Mt Read Volcanics
Location: Rosebery Mine Northend

☑ Drill hole no. R4452 113
☐ Location no.

Co-ords | RL | Scale 1:200 | Page 3 of 3

Azim | Incl | Diam | Logged by Rod Allen | Date 14.2.96

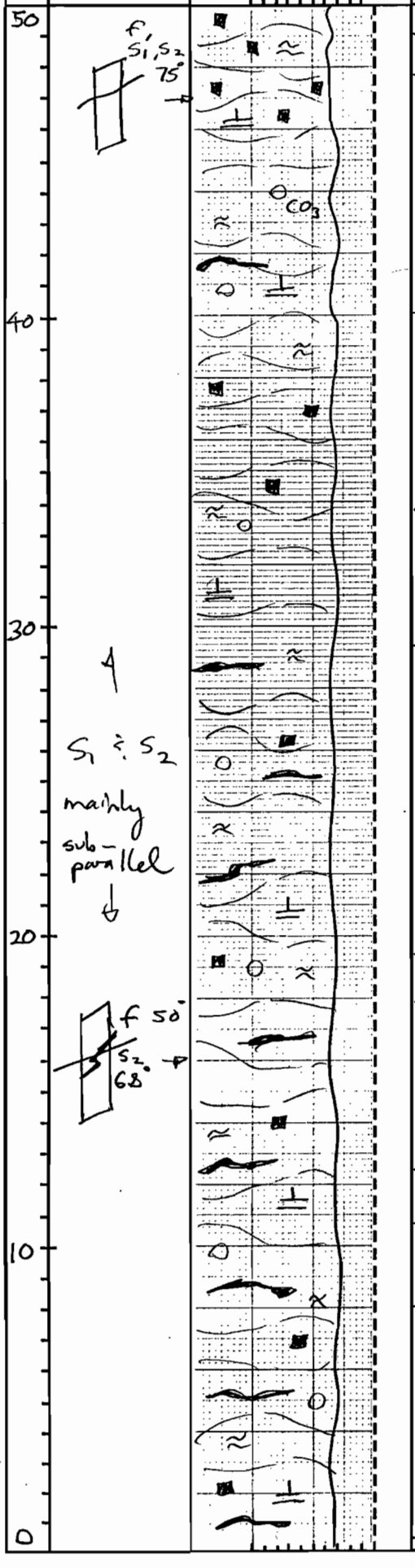

Rock / facies description

homogeneous, 10-20% 1-2mm feld-phyric pumice bx with prominent fiamme texture (dark green chl-ser) and anastomosing S_2 cleavage

Primary texture of pumice clasts (in matrix) and feld xtals poorly preserved.

Fiamme more prominent in chl-altered interval, suggests fiamme may have partly grown during chl-alteration.

Rock texture similar to in ser-q altered intervals above. Chl ± CO_3 relics in the ser-q alteration above suggest that ser-q overprints chl-ser-q (but textures less well preserved in the latter).

Alteration

Feld xtals previously CO_3-ser altered?
Interval has mod. amount of planar to weak folded syn-tect. q > S = $-CO_3$ veins (gradational)

45.7m
medium grey brown weak-moderate q-ser-chl ± biot ± cc comprising anastomosing chl-ser ± biot cleavage enclosing siliceous blotches
Feld xtals CO_3 altered & some larger CO_3 blotches occur.

similar to above 45.7 except less (1-2%) spy replacing feld xtals

32.5m
similar to 45.7-38.5m.

29.5m

medium green-grey, strong chl-ser-q-CO_3 alteration.
Fiamme intense chl-ser enclosing "matrix" pale green chl-ser-q with scattered tan weathering CO_3 blotches (2-5%) in "matrix" 1-2% dissem py.
chl-ser appear strong S_2 cleaved ie are pre- or syn-S_2

weak thin CO_3-q syn-tectonic veining

Appendix: Samples collected for Rosebery north-end alteration study

Drill hole	Depth	Alteration type and stratigraphic unit	Purpose
R4452	0.5 m	Chl with minor carb; footwall pum bx	S, TS, M, A
	8.0 m	Chl with minor carb; footwall pum bx	S, TS
	10.7 m	Chl with minor carb; footwall pum bx	S, TS, M, A
	12.3 m	Chl-ser with minor carb; footwall pum bx	S, TS
	17.8 m	Ser-q-chl; footwall pum bx	S, TS
	19.4 m	Ser-chl-q; footwall pum bx	S, TS, M, A
	29.2 m	Ser-q with minor chl-carb; footwall pum bx	S, TS
	33.7 m	Ser-q-carb; footwall pum bx	S, TS, M, A
	40.0 m	Q-ser-carb; footwall pum bx	S, TS, M, A
	47.5 m	Ser-q-carb; footwall pum bx	S, TS, M, A
	49.0 m	Q-ser with minor carbonate; footwall pum bx	S, TS, M
	54.9 m	Q-ser-py; footwall pum bx	S, TS
	57.9 m	Q-ser-carb; footwall pum bx	S, TS, M, A
	64.5 m	Q-ser; footwall pum bx	S, TS, M, A
	69.5 m	Q-ser-py; footwall pum bx	S, TS, M, A
	73.3 m	Folded py layer in footwall pum bx	S, TS
	75.1 a, b	sp-gn mineralized spotty carb-ser; footwall pum bx	(a) S, TS, M, A (b) S, TS
	75.9 m	Spotty carb in ser with ?S1; footwall pum bx	S, TS, M
	76.2 m	Spotty carb-chl/ser with ?S1; footwall pum bx	S, TS, M, A
	77.2 m	Carb after feldspar phenos; footwall pum bx	S, TS, M, A
	78.2 m	Q-ser-gn-sp + relict pumice texture; footwall	S, TS
	78.7 m	Q-ser zone within carb zone; relict pumice; footwall pum bx	S, TS
	80.4 m	Spotty carb with pumice texture; footwall	S, TS, M
	80.6 m	Spotty carb with pumice texture; footwall	S, TS, M, A
	81.5 a, b	Boundary between q-ser and ser-carb with pumice texture; footwall pum bx	(a) S, TS, M (b) S, TS, M
	81.9 a, b	Spotty carb-chl-ser with pumice texture; footwall pum bx	(a) S, TS, M (b) S, TS, M
	83.2 m	Carb after pum in semi-massive py; footwall	S, TS, M
	83.5 m	Carb after pum in semi-massive py; footwall	S, TS, M
	84.1 m	Spotty carb within semi-massive py-chl; footwall pum bx	S, TS, M
	88.0 m	Q-ser-py with pumice texture; footwall pum bx above ore	S, TS
	88.9 m	Boundary between q-ser and ser-carb; footwall pum bx above ore	S, TS, M
	90.3 m	Folded py layer with S1; footwall pum bx	S, TS
	90.8 m	Ser-q-carb; footwall pum bx with fiamme	S, TS, M
	91.6 a, b	Ser-carb; top of footwall pum bx above ore	S, TS, M, A
	96.0 m	Ser-chl-carb; rhyolite sill	S, TS, M, A
	104.8 m	Ser-q-carb-py-sp; TSV	S, TS, M, A
	108.0 m	Carb impregnated TSV sandstone	S, TS, M
	112.4 m	Ser-q-py-pyrh impregnated TSV sandstone	S, TS, M, A
	117.6 m	Carb-q veins in hangingwall black slate	S, TS, M, A
	119.2 m	Q-carb veins in hangingwall black slate	S, TS, M
65R	3462 ft	weak ser-carb; middle Hangingwall unit 2a	S, TS, M, A
	3488 ft	weak ser-carb; base Hangingwall unit 2a	S, TS, M, A
	3511 ft	Carb veins in hangingwall black slate	S, TS, M, A
	3606 ft	Ser-carb-py; TSV feld crystal sandstone	S, TS, M, A
	3626 ft	Q-ser-py; top of rhyolite sill	S, TS, M, A

(S=thin slab for textural studies, TS=thin section petrography, M=microprobe carbonates ± other minerals, A=chemical analysis

Drill hole	Depth	Alteration type and stratigraphic unit	Purpose
65R cont	3697 ft	Q-ser-chl; rhyolite sill	S, TS, M, A
	3802 ft	Q-ser-chl-carb; rhyolite sill	S, TS, M, A
	3884 ft	Ser-q-carb (bleached); base of rhyolite sill	S, TS, M, A
	3911 ft	Ser-q-carb inter ore zone; top of footwall pum bx	S, TS, M, A
	3926 ft	Q-ser-sulphide; ore zone in footwall pum bx	S, TS, M, A
	3942 ft	Ser-q-carb; footwall pum bx	S, TS, M, A
	4011 ft	Ser-chl-q; footwall pum bx	S, TS, M, A
	4106 a, b	Ser-chl-q; footwall pum bx	S, TS, M, A
	4158 ft	Ser-chl-q-minor carb; footwall pum bx	S, TS, M, A
	4209 ft	Ser-q-carb (bleached) around carb veins; footwall pum bx	S, TS, M, A
	4260 ft	Q-ser(±?biot)-carb; footwall pum bx	S, TS, M, A
84R	576.5 m	weak altered hangingwall mass flow	S, TS, M, A
	622.5 m	weak carb; hangingwall mass flow	S, TS, M, A
	664.0 m	Carb impregnation; hangingwall mass flow	S, TS, M, A
	678.9 m	weak altered hangingwall mass flow	S, TS, M, A
	704.4 m	weak altered hangingwall mass flow	S, TS, M, A
	735.5 m	Carb-ser around veins; hangingwall mass flow	S, TS, M, A
	745.0 m	weak altered hangingwall mass flow unit 2	S, TS, M, A
	773.7 m	Q-carb veins in hangingwall black slate (upper)	S, TS, M, A
	819.7 m	Q-carb veins in hangingwall black slate (lower)	S, TS, M, A
	822.9 m	Carb; upper TSV	S, TS, M, A
	836.4 m	Carb; lower TSV	S, TS, M, A
	843.8 m	Q spots; top of footwall pum bx	S, TS, M, A
	852.1 m	Carb; footwall pum bx	S, TS, M, A
	857.4 m	Carb; footwall pum bx	S, TS, M, A
	875.5 m	Q-ser; footwall pum bx	S, TS, M, A
	877.2 m	Q-carb vein; footwall pum bx	S, TS, M, A
	892.3 m	Q-chl; footwall pum bx	S, TS, M, A
	904.3 m	Q-chl-ser-carb; footwall pum bx	S, TS, M, A
109R	373.9 m	weak altered hangingwall mass flow (matrix)	S, TS, M, A
	392.2 m	weak altered mafic clast in hangingwall	S, TS, M, A
	406.8 m	weak altered hangingwall mass flow (matrix)	S, TS, M, A
	424.0 m	chl-q bx; hangingwall mass flow	S, TS, M
	434.2 m	weak altered hangingwall mass flow (matrix)	S, TS, M, A
	450.3 m	Carb; hangingwall mass flow	S, TS, M, A
	475.0 m	?Silicified limestone clast; hangingwall	S, TS, M
	481.0 m	weak altered hangingwall mass flow (matrix)	S, TS, M, A
	509.2 m	Carb impregnation in hangingwall mass flow	S, TS, M, A
	553.8 m	Hangingwall black slate with limestone layer	S, TS, M, A
	561.5 m	weak altered TSV	S, TS, M, A
	562.6 m	mineralized TSV	S, TS, M, A
	566.8 m	TSV with lithic clast	S, TS, M, A
	573.6 m	Top of footwall pum bx	S, TS, M, A
	590.8 m	silicification; upper footwall pum bx	S, TS, M, A
	620.6 m	silicification; upper footwall pum bx	S, TS, M, A
	638.4 m	silicification; footwall pum bx	S, TS, M, A
	670.6 m	silicification; footwall pum bx	S, TS, M, A
	698.8 m	Q-chl veins; footwall pum bx	S, TS, M
	701.3 m	White carb impregnation; footwall pum bx	S, TS, M, A
	707.8 m	Footwall pum bx	S, TS, M, A

(S=thin slab for textural studies, TS=thin section petrography, M=microprobe carbonates ± other minerals, A=chemical analysis

Drill hole	Depth	Alteration type and stratigraphic unit	Purpose
109R cont	709.7 m	Carb-ser; footwall pum bx	S, TS, M, A
	723.5 m	Carb-ser + carb vein; footwall pum bx	S, TS, M, A
	726.0 m	Feld-chl-ser; footwall pum bx	S, TS, M, A
	741.8 m	Feld-chl-ser; footwall pum bx	S, TS, M, A
	745.9 m	Lithic clast in footwall pum bx	S, TS, M
113RD1	708.3 m	Hangingwall mass flow	S, TS, M, A
	724.3 m	Carb impregnation; hangingwall mass flow	S, TS, M
	732.6 m	Basalt clast in hangingwall	S, TS, M, A (of clast only)
	735.3 m	Minor sp and basalt clast in hangingwall	S, TS, M, A
	736.1 m	Limestone clast in hangingwall mass flow	S, TS, M
	763.7 m	Hangingwall mass flow	S, TS, M, A
	778.9 m	Hangingwall mass flow	S, TS, M
	785.3 m	Carb; Hangingwall mass flow	S, TS, M
	792.3 m	Hangingwall mass flow	S, TS, M, A
	823.1 m	Carb near fault; hangingwall mass flow	S, TS, M, A
	825.9 m	Sp dissem; basalt clast in hangingwall mass flow	S, TS
	847.4 m	Limestone clast in hangingwall mass flow	S, TS, M
	852.8 m	Sp impregnation in hangingwall mass flow	S, TS, M, A
	862.7 m	Limestone clasts in hangingwall mass flow	S, TS, M
	865.4 m	Bleached carb-ser near fault; hangingwall	S, TS, M, A
	871.3 m	Base of hangingwall mass flows	S, TS, M, A
	895.4 m	Q-carb veins in hangingwall black slate	S, TS, M, A
	938.0 m	Q-carb veins in hangingwall black slate	S, TS, M, A
	941.1 m	Q-carb vein	S, TS, M
	947.7 m	?	S, TS, M
	949.7 m	?	S, TS, M, A
	956.4 m	Top of footwall	S, TS, M, A
	973.1 m	Footwall pum bx	S, TS, M, A
	985.9 m	Footwall pum bx	S, TS, M, A
	991.8 m	Footwall pum bx	S, TS, M, A
120R	1068.5 m	Bleached q-ser-carb; hangingwall unit 3	S, TS, M, A
	1083.7 m	Q-ser-dissem sp; hangingwall unit 3	S, TS, M, A
	1094.5 m	Q-ser-dissem sp; hangingwall unit 3	S, TS, M, A
	1100.3 m	Q-carb veins + carb impreg; hangingwall unit 3	S, TS, M, A
	1115.9 m	weak ser-q-leucox; top of hangingwall unit 2a	S, TS, M, A
	1147.8 m	Ser-q±carb; middle of hangingwall unit 2a	S, TS, M, A
	1169.7 m	Chl-carbon-minor carb; base of hangingwall unit 2a	S, TS, M, A
	1184.0 m	Carb veinlets in hangingwall black slate	S, TS, M, A
	1229.3 m	Carb veinlets in hangingwall black slate	S, TS, M, A
	1237.2 m	White carb impreg + q-carb veins; TSV	S, TS, M
	1241.8 m	Q-ser-py; TSV	S, TS, M, A
	1256.0 m	Carb veinlets in black slate	S, TS, M, A
	1265.5 m	Weak ser-q-carb; TSV	S, TS, M, A
	1291.8 m	Ser-q; top of rhyolite sill	S, TS, M, A
	1315.4 m	Weak ser-chl; middle of rhyolite sill	S, TS, M, A
	1353.8 m	Q-ser-minor carb; base of rhyolite sill	S, TS, M, A
	1356.9 m	Massive spotty carb; top footwall pum bx	S, TS, M, A
	1361.4 a, b	Massive spotty carb; top footwall pum bx	S, TS, M, A
	1364.4 a, b	Massive spotty carb; top footwall pum bx	S, TS, M, A

(S=thin slab for textural studies, TS=thin section petrography, M=microprobe carbonates ± other minerals, A=chemical analysis

Drill hole	Depth	Alteration type and stratigraphic unit	Purpose
120R cont	1365.4 a, b	Massive spotty carb + carb vein; top footwall pum bx	S, TS, M, A
	1366.0 m	Massive sp-gn	S
	1378.3 m	Strong q-chl-ser-py; footwall pum bx	S, TS, M, A
	1386.5 m	Strong q-chl-minor carb; footwall pum bx	S, TS, M, A
	1403.3 m	Moderate ser-q-chl-py; footwall pum bx	S, TS, M, A
	1421.8 m	Weak ser-carb; footwall pum bx	S, TS, M, A
	1423.5 m	Lithic clast in footwall pum bx	S, TS
	1436.2 m	Arspy-carb vein with carb selvedge; footwall	S, TS, M
	1440.5 m	Moderate ser-q-chl; footwall pum bx	S, TS, M, A
128RD2	843.5 m	Mt Black dacite	S, TS, A
	864.7 m	?Mt Black dacite	S, TS
	887.4 m	Carb impregnation; hangingwall mass flow	S, TS, M
	887.8 m	Hangingwall unit 3c	S, TS, M, A
	911.4 m	Hangingwall mass flow	S, TS, M, A
	934.6 m	Hangingwall mass flow	S, TS, M, A
	991.3 m	Hangingwall mass flow	S, TS, M, A
	1024.9 m	Limestone clast in hangingwall mass flow	S, TS, M
	1041.2 m	Sp-chl impregnation in hangingwall mass flow	S, TS, M, A
	1046.6 m	Hangingwall unit 2	S, TS, M, A
	1077.0 m	Hangingwall unit 2	S, TS, M, A
	1095.4 m	Sheeted carb veins in black slate	S, TS, M, A
	1098.6 m	Q-carb vein in black slate	S, TS, M
	1108.0 m	Pumice clast in black slate	S
	1110.4 m	Sp impregnation in top of TSV	S, TS, M, A
	1117.0 m	Least altered TSV	S, TS, M, A
	1122.4 m	White carb impregnation in TSV	S, TS, M, A
	1129.1 m	Q-ser-carb-sulphide; TSV	S, TS, M, A
	1142.0 m	Pyritic peperite at margin of rhyolite sill	S, TS
	1148.3 m	Rhyolite sill	S, TS, M, A
	1185.1 m	Q-ser; base of rhyolite sill	S, TS, M, A
	1195.5 m	Carb spots; top of footwall pum bx	S, TS, M, A
	1201.0 m	Carb spots; top of footwall pum bx	S, TS, M, A
	1220.5 m	Footwall pum bx	S, TS, M, A
	1230.4 m	Footwall pum bx	S, TS, M, A
	1259.9 m	Footwall pum bx	S, TS, M, A

(S=thin slab for textural studies, TS=thin section petrography, M=microprobe carbonates ± other minerals, A=chemical analysis

The Darwin Granite-Slate Spur area: Geology, volcanic facies analysis and alteration petrography

Bill Wyman
Centre for Ore Deposit and Exploration Studies, University of Tasmania

INTRODUCTION

The role of granitic magmas in VHMS genesis has been widely debated in the literature, most recently by Large et. al.(in press), and earlier by Stanton (1985, 1990), Sawkins and Kowalik (1981), Stoltz and Large (1992), Large (1977) and Solomon (1976). Many others have argued these issues as well. Two primary schools of thought exist: (1) The granites act as a heat engine driving circulation systems which leach the metals and other components from the overlying volcanic pile by sea-water convection; (2) In addition to heat transfer, the granites supply magmatic components, primarily metals, directly to the ore forming solutions. Magmatic components possibly supplied by the granites include Cu, Au, Mo, Sn, and W. Circulating seawater/magmatic fluids should leave behind textural and/or geochemical signatures in the rocks that may be identifiable. It is the search for this signature that has focused research on the Darwin Granite in this study.

The Darwin granite and Slate Spur area is located approximately 20 km south of Queenstown (Fig. 1). The Darwin granite is interpreted to be a subvolcanic intrusion into the Cambrian Mt Read volcanics. This granite is of particular interest to the alteration study in western Tasmania because of itís apparent association with many small Cu–Au prospects. Small Cu–Au prospects are located along the western margin of the granite and continue northward to form a continuous linear belt through Intercolonial Spur, the Jukes prospect and the Mountain Maid prospect. This is a continuous belt of similar alteration and deposit styles approximately 15 km long and 3 km wide. Alteration assemblages are characterised by three principal minerals: sericite, chlorite and potassium feldspar. These alteration assemblages are characteristic of granite related alteration assemblages found worldwide. Accessory mineral and vein assemblages include hematite/magnetite, tourmaline, minor apatite, pyrite, and chalcopyrite and scheelite. This study is designed to study details of the distribution and character of hydrothermal alteration in and around the Darwin granite, and determine chemical changes in the volcanic host rocks, induced by hydrothermal alteration associated with granitic intrusion.

Results presented in this paper are preliminary. They are the result of twenty days of field work conducted during the summer of 1995–96. Detailed geologic mapping was undertaken in the Slate Spur area, west of Mount Darwin and on and around the Darwin granite itself. Approximately 150 rock samples were collected and are in the process of being prepared for thin sections and geochemistry. Descriptions presented in this paper are based on the results of close examination of field relationships and on detailed examination of selected hand specimens. Facies descriptions and alteration features are presented.

GEOLOGY OF THE MOUNT DARWIN–SLATE SPUR AREA

The Darwin granite and itís surrounding volcanic rocks have been the focus of various studies since Hills in 1914. Numerous other authors, including Solomon, (1960), White, (1975), and Jones, (1993) have worked on various aspects of the area. None, however has focused a study on the alteration in the district, and its association to the various mineral occurrences throughout the region.

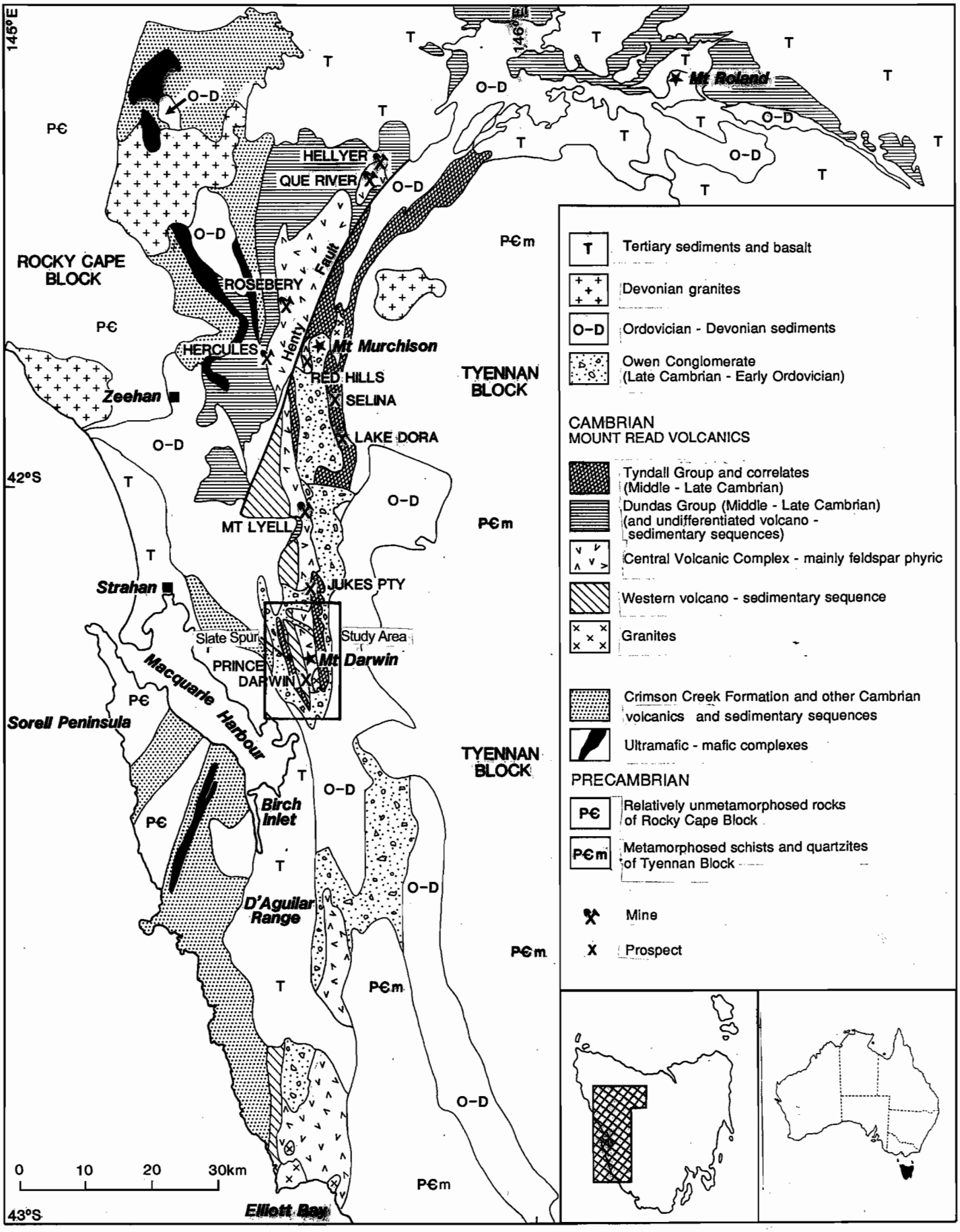

Figure 1: Location Map of the Mt. Darwin - Slate Spur Area

Hills, (1914), described the Darwin granite as "an elongate belt measuring 3 miles long by half a mile wide". Hills, (1914), and later Jones, (1993) described the character of the granite, its phases, and the relationships to surrounding rocks. Solomon (1960), White (1975), and Jones (1993) all speculated on the genetic origin of the granite, and to some extent, itís implications. This paper presents a summary of the current thinking, combined with the results of work conducted this past year.

Figure 2 is a geologic map of the regional geologic setting of the study area. The Mount Read Volcanic belt is dominated by volcaniclastic and mass flow deposits of rhyolitic to dacitic composition. Common, but subordinate to the volcaniclastic facies, are coherent rhyolitic and dacitic lavas. These volcanic facies are intruded by subvolcanic intrusions of granitic composition, as well as andesites and quartz feldspar porphyry rocks. Dating relationships have been primarily based on contact relationships and biostratigraphy. Recently, however new dating techniques have resulted in better control of relationships. Table 1 is a summary of the current geochronology as recorded in the literature.

Darwin granite

The Darwin granite was first studied by Hills (1914), who correctly described the character of two major phases of granite on the Darwin Plateau. Solomon (1960) and later White (1975) also recognised two phases of granite. White (1975) named them the "Pink" and "White" phases, based on their distinct mineralogy. Jones (1993) focused his research on the Darwin granite, mapped it at a scale of 1:5000, and identified and described both the pink and white phases, as well as several other more minor phases. Jones (1993) also described the structure and geochemistry of the granite. Work in this study involved detailed mapping of parts of the Darwin plateau (scale 1:2500), with a focus on understanding the timing relationships of the various phases of granite intrusion to each other, and the granites alteration effects on CVC rocks. As can be seen in Table 1, the dating on the Darwin granite suggests that it is older than volcanic rocks that it clearly intrudes. This suggests problems with the current date of the Darwin granite, and additional well controlled sampling and detailed dating will be required to explain this apparent relationship.

Table 1: Geochronology of the Southern Mount Read Volcanics

Lithology	Dating	Material	Age	Reference
Owen Conglomerate				
Newton Creek Sandstone	Biostrati-graphic	Fossils	Late Cambrian	Jago et al. (1972)
Tyndall Group				
Comstock Tuff	U-Pb	Magmatic Zircons	494.4 + 3.8	Perkins et al. (1993)
Comstock Limestone	Biostrati-graphic	Fossils	Late Middle Cambrian	Jago et al. (1972, 1989)
Volcaniclastic	U-Pb	Igneous Zircons	502.5 ± 3.3	Perkins et al. (1993)
Darwin Granite	U-Pb	Magmatic Zircons	510(+64, -21)	Adams et al. (1985)
Central Volcanic Complex(CVC)		Magmatic Zircons	502.6 ± 3.5	Perkins et al. (1993)

The Darwin granite is a strongly altered, high-K, magnetite series granite following the classification of Ishihara (1981). Both major phases of the Darwin granite are highly fractionated, with SiO_2 contents from 74–78 wt % (Jones, 1993). K_20 contents vary up to 8 wt % and the barium content is anomalously high (up to 3000 ppm). Large et al. (in press), point out that there is a close association between magnetite series granites, and Cu–Au mineralisation. This close association is supported by the alteration and mineralisation around the Darwin granite, and extensions of the alteration and mineralisation to the north.

Presented below is a compilation of petrographic descriptions from research in progress, and support from the literature as necessary.

Darwin Pink Granite(Dpg)

The pink granite as described by Hills (1914), and Jones, (1993), is a coarse equagranular pink-green granite (Plate 1A). Hills, (1914) said "the whole appearance is particularly handsome, the mottled pink, green, white, and black coloring giving the granite quite a distinctive character". Quartz shows marked ìwavy or shadowyî undulose extinction, and in some sections are embayed and partially re-crystallised. Subhedral to anhedral K-feldspar dominates the equagranular granite, and strong cleavage can generally be seen in thin-section. Perthite is common and granophyric texture is locally abundant, Jones, (1993). Feldspars are of two types, dark pink K-Feldspar, and light to dark green sericite/chlorite replaced plagioclase. This gives the rock itís distinctive pink green color. Mica in the granite is wholly biotite, with no muscovite. Primary biotites have suffered intense sericitisation. Accessory minerals include magnetite, zircon, apatite and monozite (Jones, 1993). The coarse equagranular texture is homogeneous throughout the granite body.

Microgranite Dykes

Microgranite, as described by Jones (1993), is restricted to the western half of the Darwin granite. Microgranite forms dykes within the pink granite phase (Plate 1B). Dykes are most abundant close to the contact of the pink granite and the Central Volcanic Complex (CVC). Dykes, observed in this study, are perpendicular to the granite/CVC contact. Jones (1993) reported that microgranite is discontinuous in nature, is in many places in direct contact with the CVC rocks, and may represent a chilled margin to the pink granite. This is disputed by this mapping that clearly shows coarse grained pink granite in direct contact with CVC volcanics. Microgranite dykes are most likely intrusive along parts of the contact where seen by Jones.

Microgranite is fine-grained and holocrystalline. Chilled margins with the pink granite are absent. Dykes weather to high relief with respect to the pink granite. Grain size in individual dykes is zoned, from the edges of the dykes where grain size is 2–3 mm, to the cores where grain size is 1 mm. K-feldspar, plagioclase and quartz predominate with minor opaques and biotite. The mineralogy is remarkably similar to the mineralogy of the pink granite. The microgranite contains modal 48% K-feldspar, 27% plagioclase and 25% quartz (Jones, 1993). K-feldspar is the dominant mineral and perthite is abundant. Crystals of subhedral K-feldspar display post deformation induced sutured contacts with adjacent quartz crystals (Jones, 1993). Albite twinning is visible in the plagioclase, even though it is heavily altered to sericite.

Darwin White Granite(Dwg)

Hills (1914) described the white granite as a "white coarse grained admixture of quartz and feldspar, and there is no greenish discoloration of the feldspar". Jones (1993) used modal analysis to classify the white granite as a granodiorite. For the purposes of this paper, and to stay consistent with the terminology in the literature, the term white granite will be maintained. The white granite is exposed within both the northern and southern parts of the Darwin plateau. The phase is less abundant than the pink granite, and probably makes up less than thirty percent of the total volume.

In fresh samples, there is a distinct visible difference between the pink-green granite and the white granite. The white granite varies from medium to coarse grained with the average grain size between 2–4 mm (Plate 1C). In coarse parts of the white granite, grainsize can approach 6–7 mm and the rock appears porphyritic. This apparent porphyritic texture is due to the homogeneous white appearance of feldspars in the rest of the rock, however close examination reveals that the white feldspars are also of equal grainsize to

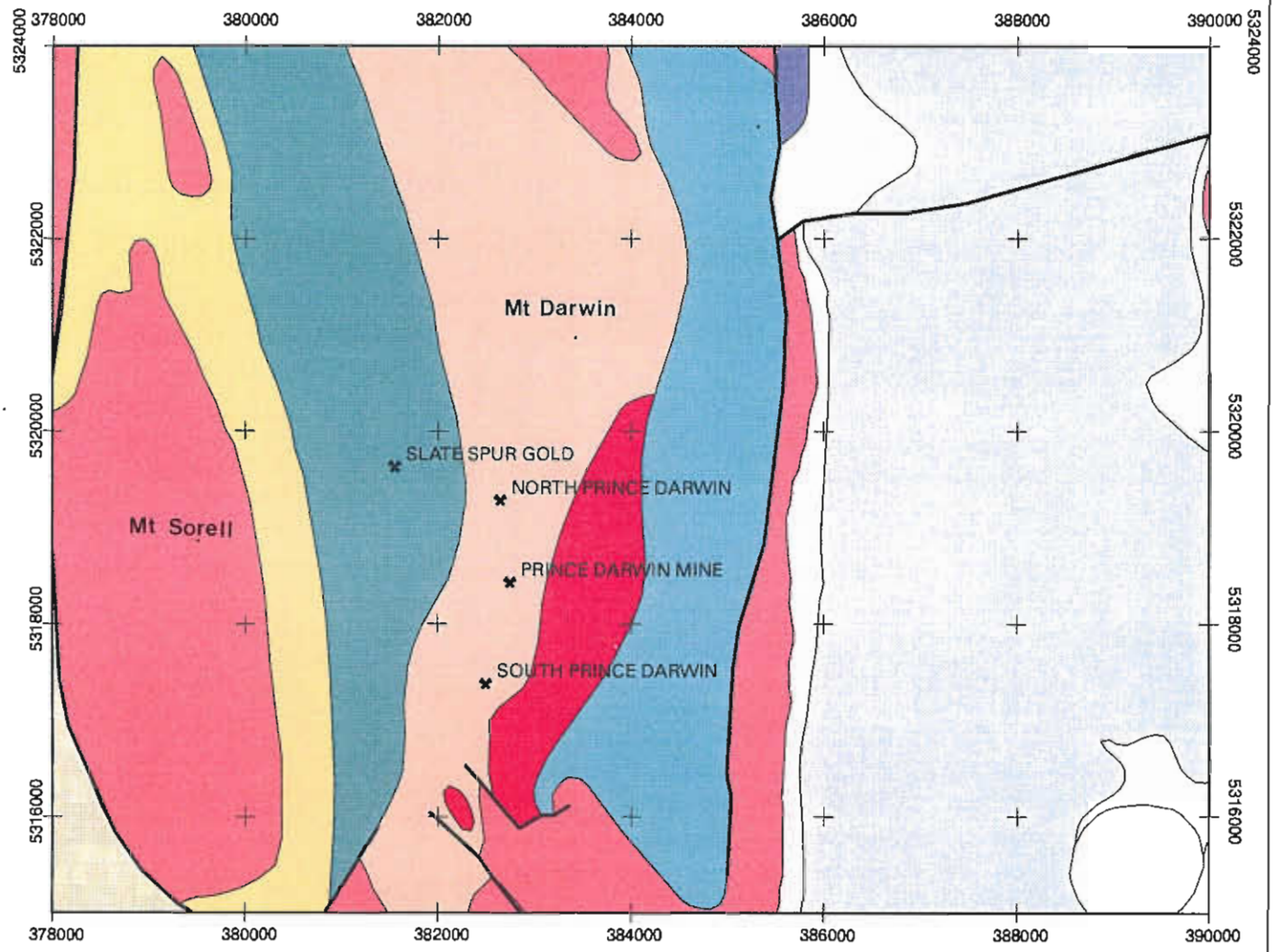

FIGURE 2

DARWIN AREA
Simplified Geology

- Tertiary sediments
- Eldon Group (S-D)
- Silurian sediments
- Gordon Limestone
- Owen Conglomerate
- Tyndall Group
- Tyndall Group conglomerate & sandstone
- CVC feldspar-phyric volcanics
- CVC sedimentary rocks
- Western sequence volcanics & volcaniclastics
- Cambrian granitoids

A: Pink equigranular granite.

B: Microgranite dykes cut sericite/chlorite altered pink equigranular granite. Surface weathering has altered feldspars into clays leaving the less altered microgranite in positive relief.

C: White equigranular granite. Both feldspars are white and biotite is < 1%. This rock is classified by Jones (1993) as a granodiorite. Note the lack of feldspar alteration.

the quartz and the rock is not porphyritic. Modal analysis of the white granite by Jones (1993) gives the following percentages: plagioclase (50%), K-feldspar (27%), quartz (22%) and sericite (1%). Plagioclase is characterised by albite and carlsbad twinning. Extinction angles (18–20°) suggest the more sodic end of the plagioclase spectrum. Jones (1993) agreed with conclusions drawn by Hills (1914), who described the plagioclase as approaching oligoclase. K-feldspar is also white and characterised by carlsbad twinning. Quartz grains are subhedral to anhedral and show evidence of recrystallisation. The mafic mineral biotite constitutes less than 2% of the rock. Although Hills described the white granite as lacking the greenish color, Jones (1993) described sericite alteration on cleavage planes in the plagioclase. In hand specimen and at outcrop scale sericite alteration in the white granite is visible but does not occur throughout the unit.

In several places angular blocks of finer grained equagranular white granite are found in a matrix of coarse grained white granite. These are probably blocks of rapidly cooled white granite along the edges of the magma chamber spalling back into the melt. Although Jones (1993) said that the contact between the pink and white phases of granite was gradational, it is clearly intrusive, and several sharp contacts have been found.

Darwin Quartz Porphyry

Intrusive into both the pink and white granite is a volumetrically minor phase of granite, here called the Darwin quartz porphyry. This granite contains rounded quartz phenocrysts from 5–10 mm in a fine-grained matrix of quartz and white feldspars. The quartz porphyry has blocky weathering. Quartz porphyry appears mineralogically to resemble the white granite phase, and may be genetically related to it. Small tourmaline veins are almost always found within several metres of the contact with intruded phases. Although this phase of granite appears to be volumetrically small in mapped outcrop, it is probably very significant to the overall story of mineralisation. It clearly post dates white granite in age, and has an almost one to one relationship to tourmaline veining within the granite.

Depth of Intrusion

Solomon (1981) and others have argued that the Darwin granite is a high level (2–3 km) subvolcanic intrusion genetically related to the CVC volcanic sequence. This argument is based, in part, on strong evidence that the Darwin granite was emplaced, cooled, uplifted and eroded, all after the deposition of the CVC and before, or simultaneous with, the beginning of Tyndall group deposition. Since little structural evidence (cleavage etc.) exists of a major orogenic event between CVC and Tyndall Group time, the Darwin granite must have been emplaced at a relatively shallow depth. Jones (1993) presented good arguments both for and against the high level emplacement argument, but concludes that the Darwin granite must have been emplaced in the mid to lower epizone (2–4 km).

YOLANDE RIVER SEQUENCE(YRS)

The YRS is the oldest sequence of volcanic rocks in the Mt Read volcanic belt. It generally lies along the western margin of the belt, where it is covered by Silurian age sediments. The Yolande River Sequence is exposed in the north–south Clark Valley and Slate Spur area immediately to the west of Mount Darwin and the south Darwin plateau. Rocks of the CVC are exposed along the eastern part of the valley, and interfinger with rocks of the YRS that are exposed on the floor and western part of the valley. Silurian age sediments are absent from this portion of the southern Mt Reads, and YRS rocks are unconformably overlain by Tyndall Group correlates.

The YRS rocks in the Mt Darwin area were investigated for two reasons. First, an almost continuous uninterrupted stratigraphic sequence apparently exists from the YRS rocks to the west, through a gradational contact and into CVC rocks to the east. The CVC rocks are intruded by the Darwin granite at the top of the east ridge of the Clark Valley. YRS rocks are well exposed along Slate Spur, an east–west saddle at the north end of the Clark Valley and directly west of Mt Darwin. Distal effects of alteration, related to the Darwin granite intrusion, may be able to be measured in the YRS rocks. Second, The Garfield andesite intrudes YRS rocks approximately 5 km north of the Clark Valley. Cu–Au mineralisation, at the

Garfield andesite, appears to have many similarities to Cu–Au mineralisation at the Prince Lyell deposit, at Mt Lyell. Geologic mapping and sampling north of Slate Spur may shed some light on the more regional aspects of alteration around the andesitic intrusions. Results in this paper will stay focused on the alteration effects related to the Darwin granite and alteration around the Garfield Andesite will be the subject of later research.

The YRS is a mixed sequence of quartz-phyric lavas and volcaniclastic rocks, with minor sedimentary facies, including mudstones, sandstones and shales. Quartz-feldspar porphyries and feldspar-phyric units are subordinate. The rocks are easily identified by their clear glassy quartz phenocrysts. Generally they have a pale green, sericitic, foliated groundmass. Volcaniclastic rocks are medium to fine-grained and, due to the well developed cleavage, are not easily distinguishable from coherent lavas.

Fine to medium-grained white lava

The dominant lithology in the YRS, west of Mt Darwin, is fine to medium-grained white lava, intrusives and juvenile volcaniclastics. Generally, cleavage is well developed parallel or subparallel to bedding and flow banding. Quartz phenocrysts are well developed and euhedral to subhedral. Phenocryst size varies from .5–2 mm in diameter. The unit always has well developed light green sericite on cleavage surfaces. Some degree of shearing has occurred along this cleavage surface in almost all of the rocks, giving the rocks a foliated appearance. In the western part of the mapped area, this unit is massive, poorly foliated and may represent a sill.

Volcaniclastic rocks mapped in two areas appear to be autobreccias or hyaloclastites. The rock is dominated by lithic clasts, averaging 5–10 cm, but clasts up to 70 cm are found. Most lithics are partially rounded to sub-rounded, but the larger ones tend to be angular. The lithics appear to be monomictic and are composed of flow-banded quartz-phyric lava. The groundmass is typically quartz-phyric to non-phyric aphanitic rhyolite. The bodies are tens of metres in size and are not mappable along strike for any great distance.

Coarse-grained massive quartz-phyric lava

Coarse grained massive quartz-phyric lava dominates the western part of the YRS in the mapped area. The unit is interbedded with siltstones, sandstones, mudstones and other quartz-phyric rocks. In the coarse-grained massive quartz-phyric lava, quartz phenocrysts average 3 mm but some may be larger. The groundmass is often medium-grained and granular. Foliation and cleavage are poorly developed, but where cleavage is seen, light green sericite is developed along it.

Medium-grained Quartz-feldspar-phyric lava

Medium-grained quartz-feldspar-phyric lava is common in the central part of Slate Spur. Feldspar phenocrysts are preserved although they are typically replaced by light green sericite. This replacement creates a spotted or blotchy appearance to the rock. Quartz phenocrysts are 1–2 mm, and are commonly euhedral to subhedral. In weathered samples, the feldspars are often replaced by iron oxides. Samples shows well developed regional northwest cleavage in the southern portion of the area, but become more massive and coherent to the north and east, with poorly developed cleavage. This unit clearly interfingers with feldspar-phyric rocks of the CVC, The feldspar-phyric rocks of the CVC, represent the first appearance of feldspar-phyric rocks in the lower CVC volcanics in this area.

Quartz-Feldspar-Biotite Porphyry

A quartz-feldspar-biotite porphyry intrudes the YRS stratigraphy near the southern end of the of the sedimentary sequence. The quartz-feldspar-biotite porphyry is medium to dark green massive coherent porphyry containing euhedral phenocrysts of quartz (to 2 mm), feldspar (to 2 mm) and biotite (to 1 mm). In weathered rocks the biotite is altered to iron oxides, but in some fresher rocks the biotite appears to be altered to chlorite. The groundmass is sericitically altered. The dominant northwest regional cleavage is only weakly developed. The unit is clearly intrusive in the southern portion of the mapped area but appears to become more conformable and sill like toward the northwest. It also appears to become quartz-biotite-phyric, and feldspar phenocrysts become less abundant.

Sandstone

Sandstone horizons occur in the YRS along the western side of the Clark Valley–Slate Spur area. Sandstones are medium-grained, light-colored, beige, and may in part be graywackes. Sandstone occurs as thin lenses in the fine to medium-grained white lava sequence. Sandstones are the most common and continuous of the sedimentary rock units mapped and individual horizons may be traceable for up to a kilometer. Sandstone horizons may be up to 50 m thick but are generally thinner. Grading, crossbedding, and other features useful in determining facing direction, are not found, due to poor exposure in the area.

Siltstones and Mudstones

Siltstones and mudstones are difficult to tell apart due to poor exposure and the interbedded nature of the rocks. Samples are fine-grained, thinly-bedded, with light-colored white sericite developed on the cleavage surfaces. Cleavage is parallel to bedding. Individual horizons are often traceable along strike for several hundred metres, and may grade along strike from siltstone, to mudstone, and back again. Individual units are thin, with maximum thickness on the order of ten metres.

Shale

Black shale occurs as a series of thin scattered discontinuous lenses within the sediment rich western part of the YRS. Black shales appear to transition along strike into siltstones and mudstones. The black shales are fine-grained, black to dark green, with well developed slaty cleavage. Disseminated pyrite is a common accessory mineral. Individual units are hard to trace for more than a few metres along strike.

Central Volcanic Complex (CVC)

Feldspar-Phyric Rhyolite

Feldspar-phyric rhyolite is the most common volcanic unit intruded by the Darwin granite. The unit is made up of dominantly feldspar-phyric lavas and volcaniclastic rocks, but can contain minor quartz-feldspar-phyric horizons. This unit is exposed along the entire ridge separating the Darwin plateau from the Clark Valley. This ridge is just west of the western contact with the Darwin granite. Feldspar-phyric rhyolite is locally spherulitic, and contains 10–20% of 1–2 mm size feldspar crystals in a fine-grained groundmass. Relict feldspar-phyric pumice clasts form well developed fiamme-like lenses in one volcaniclastic unit at the summit of Mt Darwin. Undeformed pumice textures are absent. Magnetite and tourmaline veins crosscutting the unit are common, within several hundred metres of the contact with the granite.

CVC units strike generally northwest, but occasional blocks are rotated between fault structures and may locally strike north to slightly northeast. Regional north to northwest cleavage is well developed in rocks with chlorite alteration, but is weakly developed or absent in rocks with intense K-feldspar alteration.

Quartz-feldspar-phyric rhyolite

Quartz-feldspar-phyric rhyolites are abundant, although subordinate to feldspar-phyric rhyolite, along the ridge separating the Darwin plateau from the Clark Valley. Quartz-feldspar-phyric rhyolites interfinger with feldspar -phyric rhyolites throughout the mapped area, but contact relationships are obscured due to intense alteration and lack of outcrop. Crystals are feldspar and quartz and average 10–15%% of the rock. Average crystal size is 1 mm. Groundmass is typically dense and silicified with moderate to intense chlorite or K-feldspar alteration. Primary textures are not uncommon, however frequently they are destroyed due to the intensity of alteration. Quartz-feldspar-phyric rhyolites have well developed regional cleavage. Magnetite and tourmaline veins are commonly found crosscutting the unit.

Tuffaceous-Ash/Sandstone Facies

A tuffaceous-ash/sandstone facies, similar to rocks along Jukes Road, is exposed along the ridge just south of the summit, on Mt Darwin. The tuffaceous-ash/sandstone facies includes thin tuffaceous-ash horizons interbedded with thin tuffaceous-sandstone horizons. The unit is approximately 50 m thick. Graded bedding is not preserved and facing directions can not be interpreted. Regional cleavage is well developed due to the chloritic alteration, and is subparallel or slightly oblique to bedding.

Tyndall Group Correlates

The Tyndall Group and its correlates overlie the CVC throughout the Mt Read volcanics. They are well described by numerous authors, most recently being White, (1996), but including Corbett et al. (1974), McNeill and Corbett, (1992), Corbett, (1992), Corbett et al. (1993) and Jones, (1993). Within the study area, Tyndall Group rocks are exposed to the east of the Darwin granite. Facies identified include: basal conglomerate, volcaniclastic lithic conglomerate, polymictic lithic volcaniclastic sandstone, and feldspar-phyric dacites (Jones, 1993). The basal conglomerate of the Tyndall Group rests unconformably on the Darwin granite, and grading in the basal conglomerate suggests younging to the east (Jones, 1993). This unconformable relationship was confirmed in this study. Tyndall Group rocks in contact with the Darwin granite are medium to coarse-grained polymictic conglomerates containing rounded clasts of sericitically altered coarse-grained pink Darwin granite and other volcanic clasts derived from the CVC. This is taken as unequivocal evidence of a late Cambrian uplift and erosion of the Darwin granite.

Veins

Quartz veins

Quarts veins of two apparent ages occur on the Darwin Plateau. One group is clearly post alteration and intrusion and is of Devonian age. The other group of veins occurs in all rock types and appears to be the same age as mineralisation. Both types of quartz veins are described below.

Devonian Quartz Veins: Devonian age quartz veins occur as single to small groups of discontinuous veins, or en echelon vein sets filling tectonically created openspace. All of the veins have well-developed euhedral quartz crystals growing perpendicular to the side of the vein, with the remaining openspace filled with light-beige clay or chlorite. Characteristic of the Devonian quartz veins, in the Mt Darwin area, is their small size and discontinuity. Sulfides, feldspars, magnetite and other accessory minerals are not seen. Devonian age quartz veins closely align themselves with the dominant regional northwest structural trend

Cambrian Quartz Veins: Quartz veins were recognized by Jones, (1993), but were concluded to all be of Devonian age. Some of the quartz veins are obviously of Devonian age, but others are interpreted to be of Cambrian age, at this time. Quartz veins of probable Cambrian age occur as two types. One is massive white "Bull" quartz veins with various accessory minerals and a habit similar to Cambrian age magnetite and tourmaline veins described below. The other is fine-grained light gray monomineralic ìdrusyî quartz veins. Cambrian age quartz veins in the Mt Darwin area are hosted in both CVC rocks and in the Darwin granite itself.

Massive white "Bull" Quartz Veins: Massive white quartz veins occur in both the CVC and the Darwin Granite. They can occur up to a half kilometer from the granite, however within the granite they are represented by small veins, generally less than a meter wide, and less than 30 m long. They occur infrequently in the pink granite, and are more frequently in the white granite phase. Small white quartz veins are common near the contact between the pink and white phases. Large quartz veins are rare, but a good example is found in the CVC along the ridge west of the CVC/granite contact, in the northern part of the mapped area. A massive white quartz vein up to 3 m wide and over 100 m long is found crosscutting the stratigraphy at a high angle. This vein strikes east–west and has a low angle northerly dip, similar to the magnetite veins described below. This quartz vein contains accessory magnetite, K-feldspar, and pyrite. It has numerous branches and offshooting networks of veinlets, snaking out into the country rock, in much the same manner as the magnetite and tourmaline veins. These fractures were likely created by hydrostatic overpressure of fluids, during emplacement of the vein. White quartz veins are characterised by their crosscutting relationships to regional structural trends, and inclusion of accessory minerals such as feldspar and pyrite.

Fine-grained Drusy Quartz Veins: Fine-grained drusy quartz veins occur as described above but are uncommon. They are usually found within the granite,

and are found in close association to a small barite vein described below. Fine-grained drusy quartz veins are 2–15 cm wide and rarely longer than 10 m. Accessory minerals and openspace are completely absent. Grain size is < 1 mm.

Magnetite-Hematite-Specular Hematite-Quartz Veins

Several distinct types of magnetite veins have been recognised in rocks around Mt Darwin: Magnetite ±hematite ± specular hematite, quartz veins are commonly referred to as simply: magnetite veins. Three distinct types recognised are: magnetite + hematite + quartz veins, magnetite + specular hematite + quartz veins, and specular hematite + quartz veins. Magnetite veins also frequently contain tourmaline. Magnetite veins containing tourmaline are discussed below in the section on tourmaline veins. Magnetite veins containing tourmaline are always <10 cm in width, and larger magnetite veins do not appear to contain tourmaline. Magnetite veins occur both within the pink phase of the Darwin granite and in all facies of CVC rocks. Magnetite veins are not seen in the white granite nor in YRS rocks. Occurrences of magnetite veins within the pink granite are not common, and are always small and discontinuous (Plate 2A). Magnetite veins are common in the CVC rocks, and occur up to a kilometer or more away from the granite. Magnetite veins vary in width from <1 cm to >5 m in width (Plate 2B). Individual veins are typically <5 cm in width, and are irregular in length. Typically, veins can expand from a few centimetres in width, to over a meter wide, and back to < 1 cm, along only a few metres of strike length. The larger veins are on the order of 10s of metres long. Smaller veins have more random network like habits in their orientation with respect to the host rocks. Large veins with widths > 1 m show a definite preferred east–west orientation and low angle northerly dip. Large magnetite veins crosscut stratigraphy in the CVC rocks, and appear to be subparallel to the current top of the Darwin granite. Large veins have broad networks of progressively smaller and smaller veins, radiating randomly outward into the host volcanics, and the larger the vein, the further the small network veins radiate in continuously decreasing size. One 5 m wide vein, on the south side of Mt Darwin, has small magnetite veins radiating outward for over 50 m.

Magnetite, silica, hematite, and specular hematite, appear to be intergrown. Frequently, brown metallic hematite dominates the vein mineralogy, over magnetite, to the degree that the veins are only weakly magnetic. In hand specimen, without the use of a magnet, the two vein types appear nearly identical. High silica content, and hardness of magnetite/hematite, create a positive erosion feature to the veins. Magnetite breccia veins, containing blocks of altered volcanics in a magnetite/hematite matrix, are common. Breccia veins are small in size but appear identical to similar breccias found at Intercolonial Spur (C. Gadaloff, pers. comm) and at the Jukes Prospect. In larger magnetite veins, angular blocks of altered volcanic rocks appear to be spalling off the wall of the vein into the magnetite matrix, even though the cores of these veins may have few to no lithic clasts, and may even have a banded appearance.

Barite Veins

Two small flesh to white barite veins occur parallel to a sericitically altered and sheared zone, within the pink phase of the Darwin granite. The barite veins contains massive coarsely crystalline barite, as well as minor quartz and minor hematite (Jones, 1993). Barite veins are not associated with either tourmaline or magnetite veins. One barite vein is up to 30 cm wide and has distinct augen-like structure along its strike. The second vein is smaller and parallel to the first. Both barite veins, and the sericitised shear are parallel to the regional cleavage developed in the granite. Sulfur isotope signatures, from the barite vein, give $\delta^{34}S$ values of +29.01‰ (Jones, 1993). This is suggestive of a seawater source for the sulfur, and indicates that seawater probably circulated into the granite during collapse of the hydrothermal system (Jones, 1993).

Tourmaline Veins

Tourmaline veins occur throughout both the pink granite phase of the Darwin granite and CVC rocks. Several varieties of tourmaline veins have been recognised on Mt Darwin. They are: tourmaline + quartz veins, tourmaline + magnetite + quartz veins, and tourmaline + magnetite + quartz + specular hematite veins. Tourmaline veins are generally < 5 cm wide, but occasionally reach 10 cm. Tourmaline veins are discontinuous in nature, and frequently contain

rock fragments and rock dust derived from the host rocks. Plate 2C shows a typical tourmaline vein cutting CVC rocks. Tourmaline is always black and microcrystalline, and veins frequently have bleached alteration halos along their edges. Small tourmaline veins are frequently found within several metres of the contact with the quartz porphyry phase of the white granite. This apparent relationship is believed to be significant to the overall story of mineralisation. Tourmaline veins are closely related in timing to the magnetite veining, as evidenced by the combination of mineralogies within the veins. Tourmaline veins have been found both cutting, and being cut by, magnetite veins. Some tourmaline/magnetite veins appear to be crudely zoned, with tourmaline rich outer rims, and magnetite/hematite rich cores.

Discussion of veins

Ten vein types have been identified on Mt Darwin and the Darwin plateau. They are summarised below in Table 2.

Table 2—Vein Types Found on Mt Darwin

1**	Quartz veins with chlorite and no other accessory minerals, ladder-like structure
2	Massive white "Bull" quartz veins with various accessory minerals
3	Fine-grained light gray monomineralic "drusy" quartz veins
4	Barite veins with accessory quartz and minor hematite
5*	Magnetite + hematite + quartz, strongly magnetic
6	Magnetite + specular hematite + quartz, weakly magnetic
7	Specular hematite + quartz, non-magnetic
8*	Tourmaline + quartz, non-magnetic
9	Tourmaline + magnetite + quartz, strong to weakly magnetic, zoned
10	Tourmaline + magnetite + quartz + specular hematite, weakly magnetic

* Cambrian and most common

** Devonian and common

Clearly some of the veins found on the Darwin plateau are of Devonian age. These veins will not be the subject of any further research. Cambrian veins are of significance and understanding their timing and mineralogy is important in understanding the alteration and mineralisation around the Darwin granite and its surrounding volcanics.

Magnetite and tourmaline veins are clearly of Cambrian age and will be the focus of further work. Magnetite and tourmaline veins are important because of the information that they can reveal regarding the chemistry of the granite and possible ore bearing fluids exolved from it. Polished section petrography, microprobe analysis, and mineral separate geochemistry are planned.

STRUCTURE

The structural history of the area has been the subject of considerable work by numerous authors. Among them are Seymour (1980), Solomon and Griffiths (1974), Corbett and Lees (1987), Berry and Keele (1992) and Jones (1993). Without specific reference, the structural history of the Southern Mt Reads can be divided into at least four definite stages.

- 1st Stage: Mid to late Cambrian uplift and erosion of the Darwin granite, CVC and YRS rocks. Evidence includes clasts of all rock types in the basal conglomerate of the late Cambrian Tyndall Group, some with an earlier developed cleavage.
- 2nd Stage: Early Ordovician deformational event, corresponding to the Jukesian Orogeny. Evidence includes abrupt change in provenance of source materials, and development of an angular unconformity between Mt Read volcanic units and the Ordovician Owen Conglomerate.
- 3rd and 4th Stages: Major deformation occurred after deposition of the Owen Conglomerate, and can be correlated to two stages of deformation, recognised in the Tabberabberan Orogeny, elsewhere in the Mt Read Volcanics. These events produced the dominant N–S and NW–SE fault and cleavage trends within the CVC and Tyndall Groups.

Tabberabberan-related deformation structures clearly dominate the structure of the southern Mt Read Volcanics, in the area around the Darwin granite. Features associated with this event have created a strongly developed cleavage in many of the altered

A: Small magnetite veins fill minor joint sets in the pink granite.

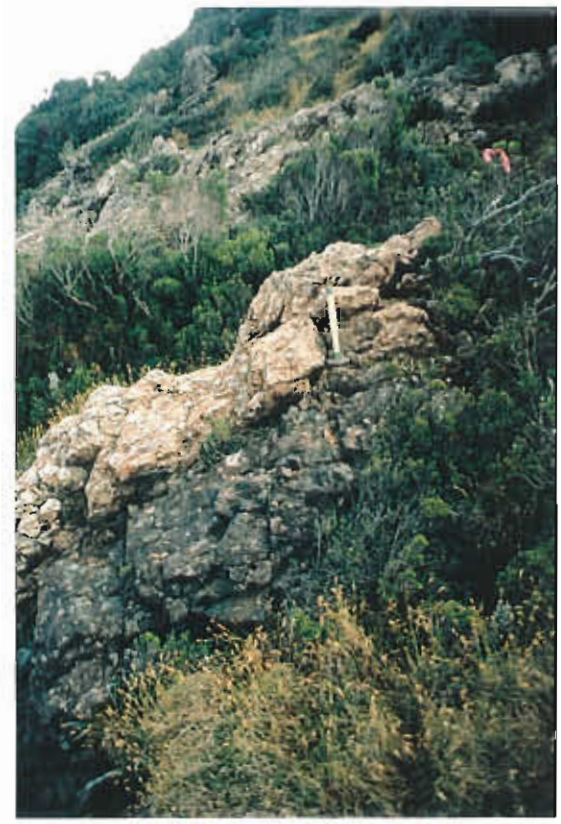

B: Large magnetite vein cutting the CVC. The vein has a shallow northerly dip, and a well developed network of smaller magnetite veins radiating outward from it. Notice, also, the large number of small angular lithic clasts scattered throughout.

C: Typical tourmaline vein cutting the CVC volcanics west of the Darwin granite. Notice the small angular lithic fragments of altered volcanic rock being incorporated into the vein, and the bleached alteration halo around the vein.

volcanic rocks, obscuring original preserved textural relationships. The Tabberabberan-related deformation also created openspace for Devonian veins, and remobilised and concentrated sulfides along these structures. Clearly, recognition and removal this of Devonian overprint from any study of Cambrian alteration and mineralisation, in the area, will be important.

ALTERATION

Alteration, in and around the Darwin granite, has many characteristics of alteration found in and around other mineralised granite systems worldwide. Alteration assemblages are dominated by K-feldspar, chlorite, sericite, and silica with lesser amounts of carbonate, pyrite magnetite and other accessory minerals. Lack of outcrop restricts the amount of geologic mapping that can be done, and in most places it is difficult to accurately define distinct zones. Crude zoning is seen, however, on Mt Darwin and the ridge south from Mt Darwin to the contact with the Darwin granite. Described below are the megascopic characteristics of alteration in the various units mapped during this past field season, combined with petrographic descriptions from Jones (1993).

Alteration in the Darwin Granite

Alteration in Pink Granite

Alteration in the pink granite has been recognised by Hills (1914), Solomon (1960), White (1975) and Jones (1993). Although recognised, only Jones (1993) made any real attempt to characterise and describe the alteration. Feldspars are of two types, dark pink K-Feldspar and light to dark green sericite/chlorite replaced plagioclase, giving the rock itís distinctive pink-green color. Mica in the granite is wholly biotite, with no muscovite. Primary biotites have suffered intense sericitisation. In detailed mapping, this sericite/chlorite alteration is found in most, but not all, of the pink granite phase. Intensity of alteration within the plagioclase varies from weak to moderate. Phenocryst shapes are typically obscured, and alteration is confined to plagioclase feldspars and biotite. Fluid movement responsible for sericite alteration in the pink granite was controlled by fracture density and porosity (Plate 3A). Sericite alteration becomes progressively more diffuse away from fractures. Altered fractures are parallel to the major joint sets in the pink granite phase, suggesting that the pink granite had already created cooling related joint sets, prior to alteration.

Alteration in the microgranite

Alteration assemblages in the microgranite are the same as in the pink granite. Plagioclase is intensely altered to sericite/chlorite, and biotite is intensely sericitised (Jones, 1993). Microgranite found in this study, does not appear to be as altered as that found by Jones (1993). The Microgranite found in this study appears to be only weakly altered by sericite, and the biotite appears to be unaltered. Microgranite, intruding along the contact between the CVC and the pink Darwin granite, was not observed, and may be more intensely altered.

Alteration in the White Granite

Hills (1914) described the white granite as lacking the greenish color. Jones, (1993) described sericite alteration on cleavage planes in the plagioclase. In hand specimen, and at outcrop scale, sericite alteration in the white granite is visible only locally.

Intrusion, of both the white granite, and the quartz-porphyry phase of the white granite, appear to be almost contemporaneous. Intrusion of these phases probably provided the hydrothermal fluids responsible for altering the pink phase of granite, as well as fluids responsible for the magnetite and tourmaline veins.

Alteration in CVC

Alteration, within the CVC, is dominated by K-feldspar/chlorite/silica assemblages of variable intensities and combinations. Chlorite overprints K-Feld. and K-Feld. overprints chlorite. Intensities range from intense chlorite (Plate 3B), with few, if any accessory minerals and almost total textural destruction, to intense K-feldspar assemblages (Plate 3C), with only large quartz phenocrysts preserved. Multiple overprinting alteration phases are suggested. Quartz (silica) and sericite are common. Silica

alteration can be locally intense, with subordinate K-feldspar and chlorite. Most samples contain minor magnetite, with the highest abundanceís in the more chloritically altered rocks. Chlorite is frequently found selectively replacing feldspar phenocrysts in rocks with K-feldspar rich groundmasses.

Alteration, at the summit of Mt Darwin, is dominated by locally weak, but typically intense, K-feldspar and silica alteration, with almost total textural destruction. Alteration intensity was apparently controlled by primary rock porosity. One unit mapped is a welded pumiceous volcaniclastic with only weak alteration and virtually no textural destruction. Several metres away, rocks that are clearly different, compositionally and texturally, are almost totally replaced with K-feldspar and silica. These rocks were probably not welded and had higher porosities. Magnetite, tourmaline and quartz veins are small but not uncommon.

Along the ridge, extending south from the summit of Mt Darwin, distinct alteration zoning can be documented. Rocks are generally striking north to NNE and then turn to the northwest. Dips are steeply west or southwesterly. Rocks at the top of the ridge are intensely K-feldspar and silica altered, with almost total textural destruction. Traversing down the ridge, there is a definite change from a K-feldspar dominated regime, to one dominated by silica and lesser chlorite. Farther down the ridge, chlorite then replaces silica as the dominant alteration mineral. Continuing, southward along the ridge, toward the granite, the alteration changes again to chlorite dominant, with moderate silica and weak K-feldspar. Frequently K-feldspar is absent. The rocks in this area are also cut by two large magnetite veins, and a network of smaller magnetite veins. Textural destruction is frequently total. This chlorite dominant zone of alteration continues for almost half a kilometre, until it transitions into a zone of moderate chlorite, moderate K-feldspar and weak silica alteration. This zone of moderate chlorite, moderate K-feldspar and weak silica alteration, dominates the western boundary of the Darwin granite, in the region within 400–500 m from the mapped contact. Only a few local scattered areas of more intense chlorite or K-feldspar alteration are found

Intense silica alteration, in the CVC, appears to be confined to approximately 400–800 m above the projected granite contact. Only weak silica alteration is found in rocks along the west side of the granite, as described above. Intense K-feldspar alteration is typically most common over 600 m above the projected granite contact, and is only typically moderate closer to the granite, where occurs with moderate chlorite alteration. It appears that the most intense alteration assemblages, of all styles, are found in the cupola region above the granite, and along the sides of the granite, to the west, alteration intensities change to weak sericite assemblages over a short distance.

Roof pendants within the Darwin granite show strong chloritic ± silica alteration assemblages, with pyrite and chalcopyrite as accessory minerals. Some of the rocks appear hornfelsed, and silica and chlorite ± pyrite is the dominant alteration style in the rocks.

Alteration in YRS Rocks

YRS rocks come to within 1–1.5 km of the granite contact, on the ridge east of Clark Valley. K-feldspar alteration, chlorite alteration, and magnetite or tourmaline veining, were not observed in YRS rocks. Alteration is typically sericitic, with intensities ranging from weak to moderate. If hydrothermal alteration, related to the Darwin granite, has affected the YRS rocks in the Clark Valley, the effects may only be detected using geochemical means. For this reason several geochemical traverses were conducted across the Clark Valley perpendicular to the strike of the granite contact with surrounding rocks. Locations are shown on Figure 3.

Discussion of Alteration

The Darwin granite is interpreted as plunging to the north under the CVC rocks (Leaman and Richardson, 1989; Payne, 1991). K-feldspar and chlorite alteration assemblages are dominant, and magnetite, and even barite veins, occur along the entire projected northward trend of the granite, 15 km to the north. These alteration assemblages, combined with geophysical evidence from Leaman and Richardson (1989) and Payne, (1991), appear to be strong evidence that there is a buried granite, at least as far north as

A: Fracture controlled diffuse sericite alteration in the pink phase of the Darwin granite.

B: Intense K-feldspar alteration in a quartz-feldspar-phyric volcanic from west of the Darwin granite. The only remaining texture is relict quartz phenocrysts, all others are destroyed.

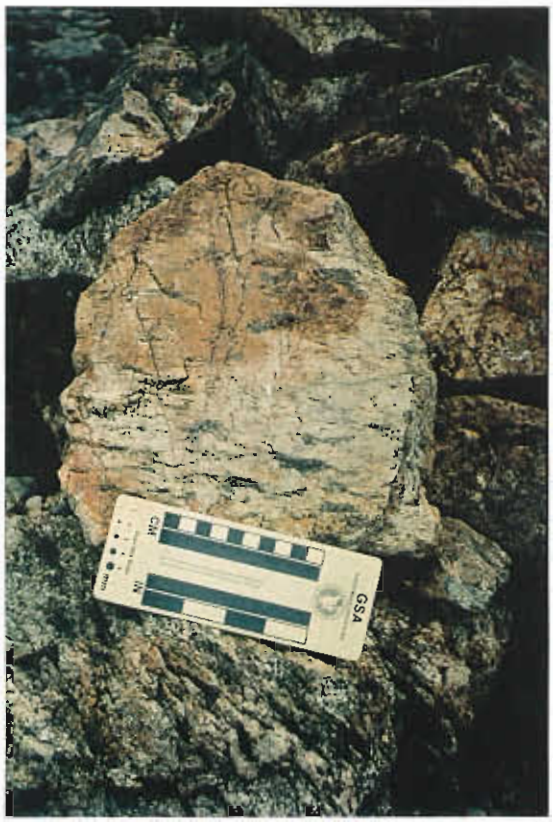

C: Pumice breccia from the summit of Mt. Darwin. Notice the fiamme like pumice with relict spherulites preserved.

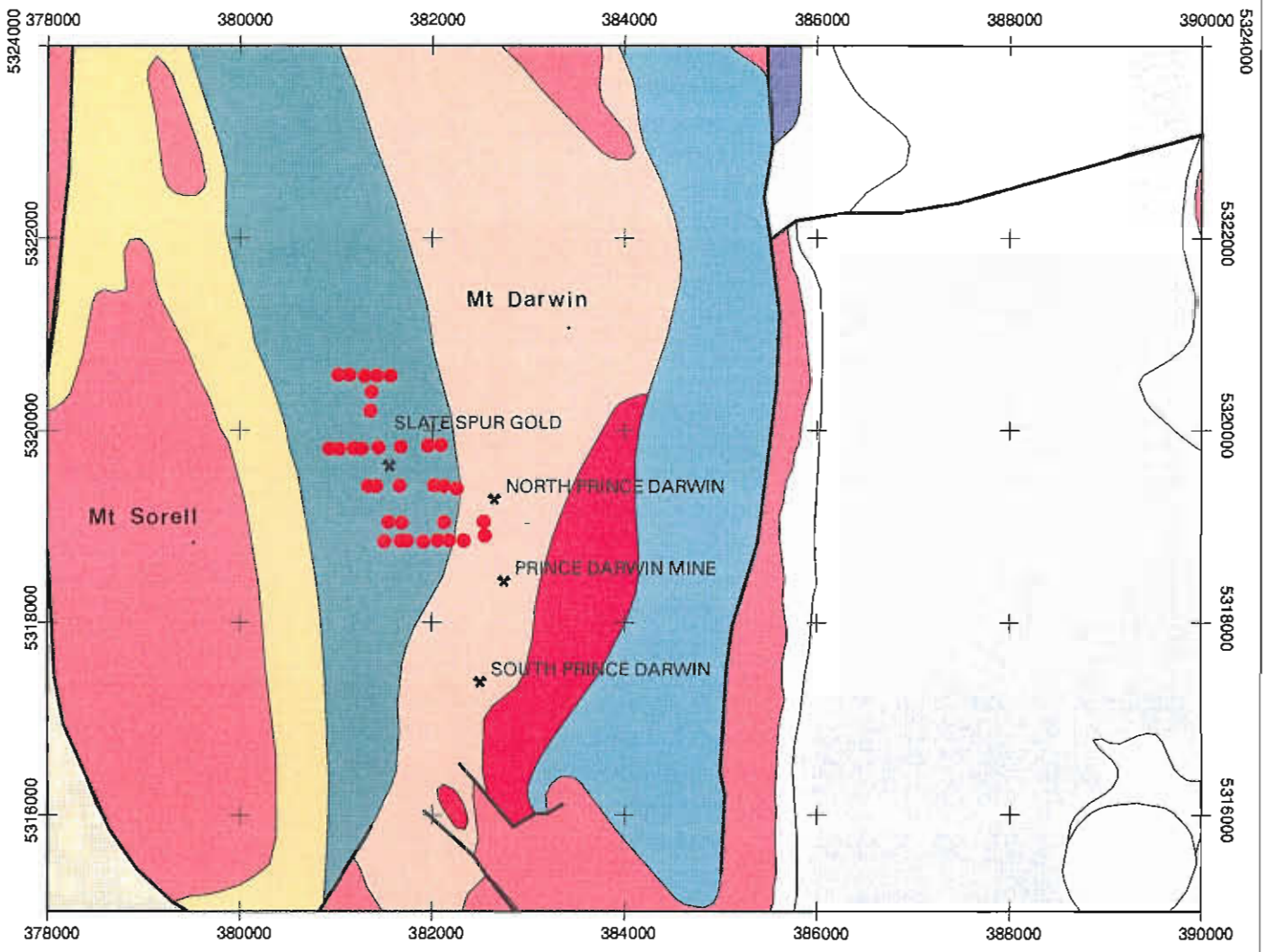

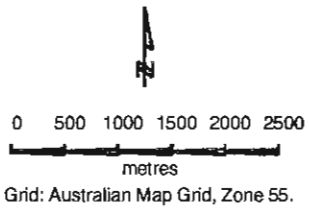

FIGURE 3

DARWIN AREA
Simplified Geology
& Slate Spur
Geochemical Sample Locations

- Tertiary sediments
- Eldon Group (S-D)
- Silurian sediments
- Gordon Limestone
- Owen Conglomerate
- Tyndall Group
- Tyndall Group conglomerate & sandstone
- CVC feldspar-phyric volcanics
- CVC sedimentary rocks
- Western sequence volcanics & volcaniclastics
- Cambrian granitoids

Mountain Maid. Also this is strong evidence that alteration is most intense and widespread in the cupola region of the granite, and although there is intense alteration along the sides of the granite, it is confined to less than 1 km.

DISCUSSION

The Darwin granite is a highly fractionated granite of the magnetite series. A well documented close association exists between magnetite series granites and Cu–Au mineralisation. Alteration assemblages, in and around the Darwin granite, resemble alteration assemblages found in other granite related hydrothermal systems throughout the world. Alteration assemblages are dominated by K-feldspar, chlorite, silica and sericite in various combinations and intensities. Accessory minerals include pyrite, magnetite, tourmaline, barite and chalcopyrite. Alteration assemblages appear to be most intense and widespread in the cupola region of the granite, and appear to drop off rapidly along the sides. Mineralisation and alteration appear to be related to the late stage intrusion of the white equagranular granite and the porphyritic white granite phase. Magnetite and tourmaline veining also appears to be related to this phase of granitic intrusion. Hydrofracturing of the cupola region, above the granite, resulted in emplacement of the alteration assemblages, veins and mineralisation.

PLANNED FUTURE WORK

This study is designed to investigate details of the distribution and character of hydrothermal alteration in and around the Darwin granite, and determine the chemical changes in volcanic host rocks, induced by hydrothermal alteration associated with granitic intrusion. Results presented in this paper are preliminary. They are the result of twenty days of field work conducted during the summer of 1995–96. Detailed geologic mapping was undertaken in the Slate Spur area, west of Mount Darwin, and on and around the Darwin granite itself. Approximately 150 rock samples were collected, and are in the process of being prepared for petrography and geochemistry. Research over the winter will focus on completing a compilation of the geologic mapping, in an attempt understand the spatial distribution of alteration in the Mt Darwin to Slate Spur area. The current focus will be on alteration effects related to the Darwin granite, and results will be presented in future papers.

REFERENCES

Adams, C.J., Black, L.P., Corbett, K.D. and Green, G.R., 1985. Reconnaissance isotopic studies bearing on the tectonothermal history of the Early Palaeozoic and Late Proterozoic sequences in western Tasmania. Aust. Jour. Earth. Sci. 32: 7–36.

Berry, R.F. and Keele, R., 1992. Structural studies in mineralised areas. In Master of Economic Geology Course Work Manual 6. CODES, University of Tasmania.

Corbett, K.D., 1992. Stratigraphic-volcanic setting of massive sulfide deposits in the Cambrian mount Read Volcanics, Tasmania. Econ. Geol. 87: 564–586.

Corbett, K.D. and Lees, T.C., 1987. Stratigraphic and structural relationships and evidence for Cambrian deformation at the western margin of the Mt Read Volcanics, Tasmania. Aust. J. Earth Sci. 34(1): 45–67.

Corbett, K.D., Pemberton, J. and Vicary, M.J., 1993. Map 13. Geology of the Mt Jukes – Mt Darwin area. Scale 1:25000. Geol. Surv. Tasm.

Corbett, K.D., Reid, K.O., Corbett, E.B., Green, G.R., Wells, K. and Sheppard, N.W., 1974. The Mount Read volcanics and Cambrian-Ordovician relationships at Queenstown, Tasmania. J. Geol. Soc. Aust. 21: 173–186.

Crawford, A.J., Corbett, K.D. and Everard, J.L., 1992. Geochemistry of the Cambrian volcanic - hosted massive sulfide - rich Mount Read Volcanics, Tasmania, and some tectonic implications: Economic Geology 87: 597–619

Doyle, M.G., 1990. The geology of the Jukes Proprietary prospect, Mt Read Volcanics: Unpubl. Honours Thesis, Univ. Tas.: 114 pp.

Hills, C.L., 1914. The Jukes–Darwin mining field. Bull. Geol. Surv. Tasm. 16.

Ishihara, S., 1981. The granitoid series and mineralization. Econ. Geol. 75th Anniv. Vol.: 458–484.

Jago, J.B., Reid, K.O., Quilty, P.G., Green, G.R., and Daly, B., 1972. Fossiliferous Cambrian limestone from within the Mt Read Volcanics, Mt Lyell Mine area, Tasmania. J. Geol. Soc. Aust. 19: 379–382.

Jones, A.T., 1993. The geology, geochemistry and structure of the Mt Darwin – South Darwin Peak area, western Tasmania. Unpupl. Honours Thesis, Univ. Tas., 120 pp.

Large, R.R., 1977. Chemical evolution and zonation of massive sulfide deposits in volcanic terrainís: Economic Geology 72: 549–572.

Large, Ross R., 1992. Australian Volcanic-Hosted Massive Sulfide Deposits: Features, Styles, and Genetic Models: Economic Geology 87: 471–510

Large, R.R., Doyle, M., Raymond, O., Cooke, D., Jones, A., and Heasman, L.,1995. Evaluation of the Role of Cambrian Granites in the Genesis of World Class VHMS Deposits in Tasmania: In Press, Ore Geology Reviews.

Leaman, D.E., and Richardson, R.G., 1989., The granites of west and North-west Tasmania, a geophysical interpretation: Geological Survey Bulletin 66. Tas. Dept. Mines, Hobart: 146 pp.

McNeill, A.W. and Corbett, K.D., 1988. Geology of the Tullah – Mt Block area: Tasmania Dept of Mines, Mt Read Volcanics Proj. Geol. Rep. 2: 19 pp.

Payne, B., 1991. Geophysical interpretation of the Mt Sedgewick – Red Hills area, western Tasmania. Unpupl. Honours Thesis, Univ. Tas.: 107 pp.

Perkins, C. and Walshe, J.L., 1993. Geochronology of the Mt Read Volcanics, Tasmania, Australia. Econ. Geol. 88: 1176–1197.

Sawkins, F.J., and Kowalik, J., 1981. The source of ore metals at Bucans: Magmatic versus leaching models: Geol. Assoc. Canada Spec. Pap. 22: 255–267.

Seymour, D.B., 1980. The Tabberabberan Orogeny in northwestern Tasmania. Unpubl. Ph.D. Thesis, Univ. Tas.

Solomon, M., 1960. The Dundas group in the Queenstown area. Pap. Proc. R Soc. Tasm. 94: 33–49.

Solomon, M., 1976. Volcanic massive sulfide deposits and their host rocks - a review and an explanation: In: K. A. Wolf (Editor), Handbook of strata-bound and stratiform ore deposits: II Regional studies and specific deposits. Amsterdam. Elsevier: 231–250.

Solomon, M., 1981. An introduction to the geology and metallic ore deposits of Tasmania. Econ. Geol. 76: 194–208.

Solomon, M. and Griffiths, J.R., 1974. Aspects of the early history of the Tasman Orogenic Zone. In Denmead, A.K., Tweedale, G. W. and Wilson, A. F. (Eds.) The Tasman Geosyncline. A Symposium. Geol. Soc. Aust. (Qld. Div.), Brisbane: 19–39.

Stanton, R.L., 1985, Stratiform ores and geological processes: Roy. Soc. N.S.W. 118: 77–100.

Stanton, R.L., 1990. Magmatic Evolution and the ore type-lava type affiliations of volcanic exhalative ores. Austral. Inst. Min. Met. Monog. 15: 101–107.

Stoltz, A.J. and Large, R.R., 1992. Evolution of the source rock control on precious metal grades in volcanic-hosted massive sulfide deposits from western Tasmania: Economic Geology 87: 720–738.

White, N.C., 1975. Cambrian volcanism and mineralisation, SW Tasmania: Unpubl. Ph.D. Thesis, Univ. Tas.

White, M., 1996. Volcanic facies correlations in the Tyndall Group. Unpubl. Ph.D. Thesis, Univ. Tas.

Volcanic facies relationships and hydrothermal modification of primary volcanic textures, Thalanga

Anthea P. Hill
Centre for Ore Deposit and Exploration Studies, Geology Department, University of Tasmania

The Thalanga Zn–Pb–Cu–Ag–Au deposit is located at the contact between rhyolitic volcanics of the Mount Windsor Formation, and the overlying dacitic to andesitic volcanics and volcaniclastics of the Trooper Creek Formation in the Cambrian to Ordovician Mount Windsor Volcanics, northern Queensland. The ore and enclosing volcanics are locally strongly deformed and metamorphosed to upper greenschist facies. Bedding is now subvertical and the ore horizon has been divided into four main lenses by post-tectonic normal faults: West, Central, and East Thalanga and the Vomacka Zone (Fig. 1).

Sulfide mineralisation at Thalanga is spatially, and probably genetically associated with subaqueous felsic intrusions and mass-flow deposits, that together constitute the ore horizon. The main ore minerals are sphalerite, chalcopyrite, pyrite and galena, and in most places the sulfides are coarse-grained with annealed grain boundaries. Banding in the massive sulfide lenses is interpreted to be mainly tectonic in origin. Chalcopyrite, and to a lesser degree, sphalerite and galena have been remobilised during deformation and now occupy fault zones and sites of dilation. Metal zonation is erratic and mainly reflects the widespread remobilisation of sulfides at Thalanga, although there is a general variation from pyrite–chalcopyrite-rich sulfides at the base of the ore horizon, to sphalerite–galena ± barite towards the stratigraphic top of the ore horizon. Quartz–magnetite lenses along strike from the massive sulfides are interpreted as distal, low temperature exhalites contemporaneous with sulfide mineralisation (Duhig et al., 1992).

Rhyolites (Rhyolitic Volcanics) with both coherent and clastic textures are present in the footwall at Thalanga. However, variable quartz ± sericite ± chlorite ± pyrite alteration makes identification of facies relationships difficult. The least altered coherent rhyolite at Thalanga is feldspar- and quartz-phyric with microcrystalline quartzo-feldspathic groundmass, and is present down dip and along strike from the sulfide lenses. Rare spherulites and perlitic fractures demonstrate that the groundmass was originally glassy.

Perlitic fractures in the altered rhyolites are replaced by fine grained white mica (sericite), and the kernels are replaced by recrystallised quartz. With increasing quartz–sericite±pyrite alteration, a network of sericite envelopes circular or polygonal quartz kernels. Textures comprising isolated kernels of recrystallised quartz in pervasive sericite may result from intense alteration of perlite.

Monomict rhyolitic breccias that have gradational contacts with coherent rhyolite were probably generated by autoclastic (quenching, flow fragmentation) processes. Single flow-banded rhyolite clasts in pervasive quartz ± sericite ± chlorite ± pyrite alteration are possibly relicts of rhyolitic hyaloclastite or autobreccia. In intensely altered parts of the footwall, textural domains comprising abundant, irregularly distributed, poorly sorted quartz crystals are interpreted as originally volcaniclastic, whereas domains of evenly distributed, well sorted quartz crystals are interpreted as altered coherent rhyolite.

Syn-volcanic quartz–feldspar–porphyry (QFP) sills, with peperitic contacts with enclosing siltstones, are present within the ore horizon in East Thalanga. QFP sills also occur at the ore horizon position in the Thalanga Range to the northwest of the deposit. The QFP sills are coarsely porphyritic and contain 25–35% distinctive rounded and embayed blue quartz (maximum = 8 mm) and white feldspar (maximum =

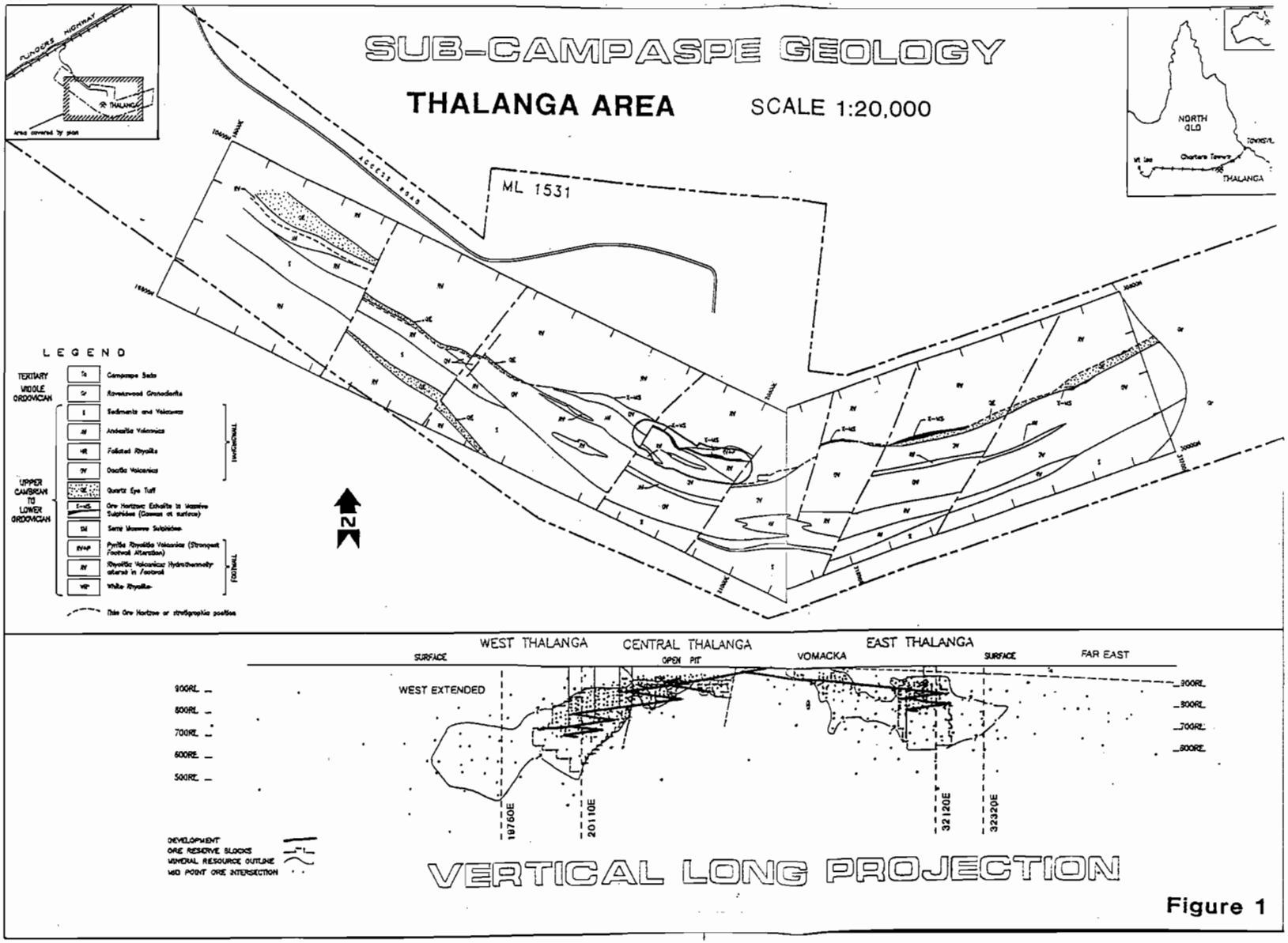
SUB-CAMPASPE GEOLOGY
THALANGA AREA
SCALE 1:20,000
TUNGOR'S HIGHWAY
THALANGA
Area covered by plan
ACCESS ROAD
ML 1531
NORTH QLD
TOWNSVILLE
Charters Towers
Mt Isa
THALANGA
LEGEND
TERTIARY
Campaspe Beds
ORDOVICIAN
Rowesswood Granodiorite
Sediments and Volcanics
Andesitic Volcanics
Foliated Rhyolite
Dacitic Volcanics
UPPER CAMBRIAN TO LOWER ORDOVICIAN
Quartz Eye Tuff
Ore Horizon: Exhalite to Massive Sulphides (Caravan at surface)
Semi Massive Sulphides
Pyritic Rhyolite Volcanics (Stronyest Footwall Alteration)
Rhyolitic Volcanics: Hydrothermally altered in Footwall
White Rhyolite
Thin Ore Horizon at stratigraphic position
HANGINGWALL
FOOTWALL
N
WEST THALANGA
CENTRAL THALANGA
EAST THALANGA
SURFACE
OPEN PIT
VOMACKA
SURFACE
FAR EAST
WEST EXTENDED
900RL
800RL
700RL
600RL
500RL
19760E
20110E
32120E
32320E
DEVELOPMENT
ORE RESERVE BLOCKS
MINERAL RESOURCE OUTLINE
MID POINT ORE INTERSECTION
VERTICAL LONG PROJECTION

Figure 1

4 mm) phenocrysts. Typically, the groundmass is composed of fine grained, recrystallised equant quartz, with minor sericite. Mega-clasts of QFP (>20 m) in Central Thalanga contain recrystallised spherulites, indicating that the microcrystalline, sericite-rich groundmass was formerly glassy.

Poorly sorted, polymict, normally graded quartz crystal-rich breccias (locally, quartz 'eye' volcaniclastics; QEV) occur in both West and East Thalanga, and rarely in Central Thalanga. Components of the QEV are listed in Table 1. The blue quartz crystals, feldspar crystals, and crystal fragments in the QEV have no glassy selvages. QFP clasts are non-vesicular and are the largest and most abundant clasts in the QEV, suggesting proximity to source. Rare QFP clasts with sericite-rich groundmass and wispy terminations may be altered pumice.

The abundant coarse quartz and feldspar crystals in the QEV are interpreted to have been liberated from of a highly porphyritic QFP magma by explosive eruption. The small volume of clasts interpreted as altered pumice or glass shards suggests that some of the pumiceous fraction produced by such an explosive eruption was separated from the crystals during eruption and/or transportation. The site of eruption is poorly constrained, but was probably located in shallow water (≤ 1 km deep; cf. McBirney, 1963) or in a subaerial environment at the basin margin. The internal organisation of units of the QEV is consistent with transport to the site of final deposition by subaqueous mass flows (cf. Cas, 1983). The mass flows collected clasts from the substrata, including clasts from massive sulfide lenses which must have been exposed on the seafloor.

Large, angular to blocky QFP clasts are more common at the base of the QEV, and apparently grade into coherent QFP in East Thalanga. Non-vesicular QFP magma is interpreted to have been emplaced as shallow sills while the QEV was wet and unconsolidated, resulting in blocky peperite comprising QFP clasts in QEV matrix. In West Thalanga, where QFP sills are absent, the QEV may include clasts generated by quench-fragmentation of QFP clasts. Perhaps QFP intrusions broke through the seafloor, quenched and fragmented, and the resulting hyaloclastite was incorporated by subsequent crystal-rich mass flows.

The Hanging Wall Fragmental (HWF) has sharp, depositional contacts with the underlying QEV and massive sulfides, and is composed of multiple beds of unaltered, graded to massive siltstones and sandy siltstones, with fresh feldspar crystal fragments. Perlitic dacite clasts are dispersed through the siltstones, and minor rhyolite clasts are common at

Table 1 Components of the Quartz 'Eye' Volcaniclastic deposit

Components	Size Range	Shape	Abundance
Quartz crystals and crystal fragments – blue to grey	<1 mm to 12 mm, average = 6 mm	rounded crystals to angular fragments	variable, up to 60%, common towards top of QEV
Feldspar crystals – partly albitised plagioclase, minor K-feldspar crystals	<1 mm to 4 mm	subhedral crystals to angular fragments	variable, absent in places, common towards stratigraphic top
QFP clasts	1 cm to 5 m, commonly 10–20 cm	angular and blocky, irregular, to rounded	common, up to 80% of QEV in places
Rhyolite clasts– siliceous, quartz-phyric	<1 cm to 60 cm, commonly 5–10 cm	rounded to blocky and cuspate in places	minor component, overall <10% of QEV
Chloritic wisps – patches of chlorite	< 1 cm	angular to wispy, elongate parallel to	patchy distribution, about 5–10% of QEV (after biotite) cleavage
Sericitic streaky wisps – quartz-phyric with intergrown quartz-sericite groundmass	<5 cm	wispy, irregular clasts	patchy distribution about 5–10 % of QEV
Massive sulfide clasts – massive py to sp–gn±cp	<10 cm, possibly up to 1 m	rounded to elongate parallel to cleavage	rare
Quartz–magnetite clasts	up to 30 cm	blocky to rounded and irregular	rare

the base of graded beds. Dacite clasts in the HWF are more common in East and Central Thalanga, where the HWF is up to 18 m thick, compared to West Thalanga where the HWF is <2 m thick.

Coherent dacite overlies the HWF in all parts of the Thalanga deposit, with sparsely (2–5%) feldspar-phyric dacite common in East Thalanga, and 5–8% feldspar-phyric dacite present in West Thalanga. The basal contact varies from sharp and planar, to disrupted and peperitic with clasts of perlitic sparsely feldspar-phyric dacite within the HWF. Perlitic fractures are present towards the stratigraphic top of the dacite. The dacite has gradational contacts with overlying poorly sorted dacite breccia thought to be in situ hyaloclastite. The dacite is interpreted to have flowed over and foundered into partly consolidated HWF.

A gradational contact occurs between the in situ dacite hyaloclastite and overlying, normally graded, poorly-sorted dacite breccias. White, siliceous dacite clasts with angular to cuspate margins are the most abundant clast-type in this breccia, and are interpreted as resedimented dacite hyaloclastite. Coherent andesite overlies and partly intrudes the resedimented dacite hyaloclastite in Central Thalanga. Elsewhere, either dacite or andesite overlie the resedimented hyaloclastite.

Massive sulfide lenses in West Thalanga are interpreted to partly replace carbonate- and chlorite-rich alteration that is restricted to a narrow interval (<30 m thick) at the stratigraphic top of the Rhyolitic Volcanics. The QEV overlies the massive sulfides in West Thalanga. In Central Thalanga and the Vomacka Zone, a single lens of massive sulfides, interpreted as exhalative in origin, directly overlies the Rhyolitic Volcanics. QEV and QFP do not occur in the Vomacka Zone, but pods of QEV and QFP are present in the western parts of Central Thalanga. Two main ore lenses are present in East Thalanga, the footwall lens and the hangingwall lens, and each is interpreted to be exhalative and to represent a seafloor position. The QEV and QFP sills occur between the ore lenses, and are interpreted to have been synchronous with mineralisation, interrupting but also preserving the ore lenses.

References

Cas, R.A.F., 1983. Submarine 'crystal tuffs': their origin using a Lower devonian example from southeastern Australia. *Geological Magazine* 120: 471–486.

Duhig, N.C., Stolz, J., Davidson, G.J., and Large, R.R., 1992. Cambrian microbial and silica gel textures in silica iron exhalites from the Mount Windsor volcanic belt, Australia: their petrography, chemistry, and origin. *Economic Geology* 87: 764–784.

McBirney, A.R., 1963. Factors governing the nature of submarine volcanism. *Bulletin Volcanologique* 26: 455–469.

Facies architecture, alteration and metamorphism of the volcanic host rock sequence at the Thalanga massive sulphide deposit, north Queensland, Australia

Holger Paulick
Centre for Ore Deposit and Exploration Studies, University of Tasmania

Introduction

The Thalanga base metal mine is located approximately 180 km west of Townsville (north Queensland) and has been in operation since 1990. The ore body consists of several semi connected, stratabound massive sulphide lenses totalling 6.35 Mt @ 12.3% Zn, 2.2% Cu, 3.9% Pb, 0.6 g/t Au and 99 g/t Ag (Gregory et al., 1990). It is hosted within the subvertical, south-facing, Cambro-Ordovician Mount Windsor Subprovince. The mineralisation occurs at the stratigraphic contact between regional extensive rhyolites (Mount Windsor Formation) in the footwall and a sequence of dacites, andesites and sediments (Trooper Creek Formation) in the hangingwall. The host rocks experienced variable degrees of hydrothermal alteration and have been deformed and metamorphosed under upper greenschist facies conditions.

The geological and structural features of the deposit have been described by several authors, including Wills (1985), Berry (1989), Gregory et al. (1990), Hill (1991), Berry et al. (1992) and Herrmann (1995). A study of the rhyolitic footwall sequence has been presented by Herrmann (1994) addressing alteration-related geochemical changes and mass-balances with a strong emphasis on interpretation of abundances of immobile elements such as Ti and Zr. Furthermore, an ongoing PhD project by A.P. Hill is concerned with the structural setting of the ore body and the geology of the ore horizon.

Building on results of these previous studies, this project will integrate volcanic facies analysis with geochemical and petrological studies. The principal aims of the project are to :

- define the facies architecture of the host sequence (focused on the footwall and hangingwall to avoid overlap with A.P. Hill's project)
- determine the sequence and geological implications (P, T, fluid composition) of mineral reactions related to hydrothermal alteration and metamorphism
- examine the relationship between volcanic facies and alteration facies
- find vectors to mineralisation (e.g. volcanic facies association, metamorphic mineral assemblages, mineral phase composition, oxygen isotopes).

Comparison of mineralised and strongly altered cross-sections with unmineralised and less altered cross-sections through the Thalanga host rock sequence will be essential in achieving these goals.

Progress to date

During the field season of 1995 three cross sections in the western part of the Thalanga deposit have been examined (Fig.1). As most of the mine area is covered by thick Tertiary alluvial deposits this involved almost exclusively logging of drill core. Diamond drill holes have been selected in order to cover a maximum of stratigraphic thickness and vertical extend. About 8500 core metres from 18 diamond drill holes (6 per section) have been logged.

Analytical work included petrographic examination of 175 thin sections and the compilation of XRF whole rock geochemical data. This data set contains 57 samples taken in 1995 which have been analysed at the XRF facility at the Department of Geology (University of Tasmania). Additional data of samples from logged drill cores was sourced from Wills (1985), Herrmann (1994), Stolz (1991) and A.P. Hill (pers. comm.).

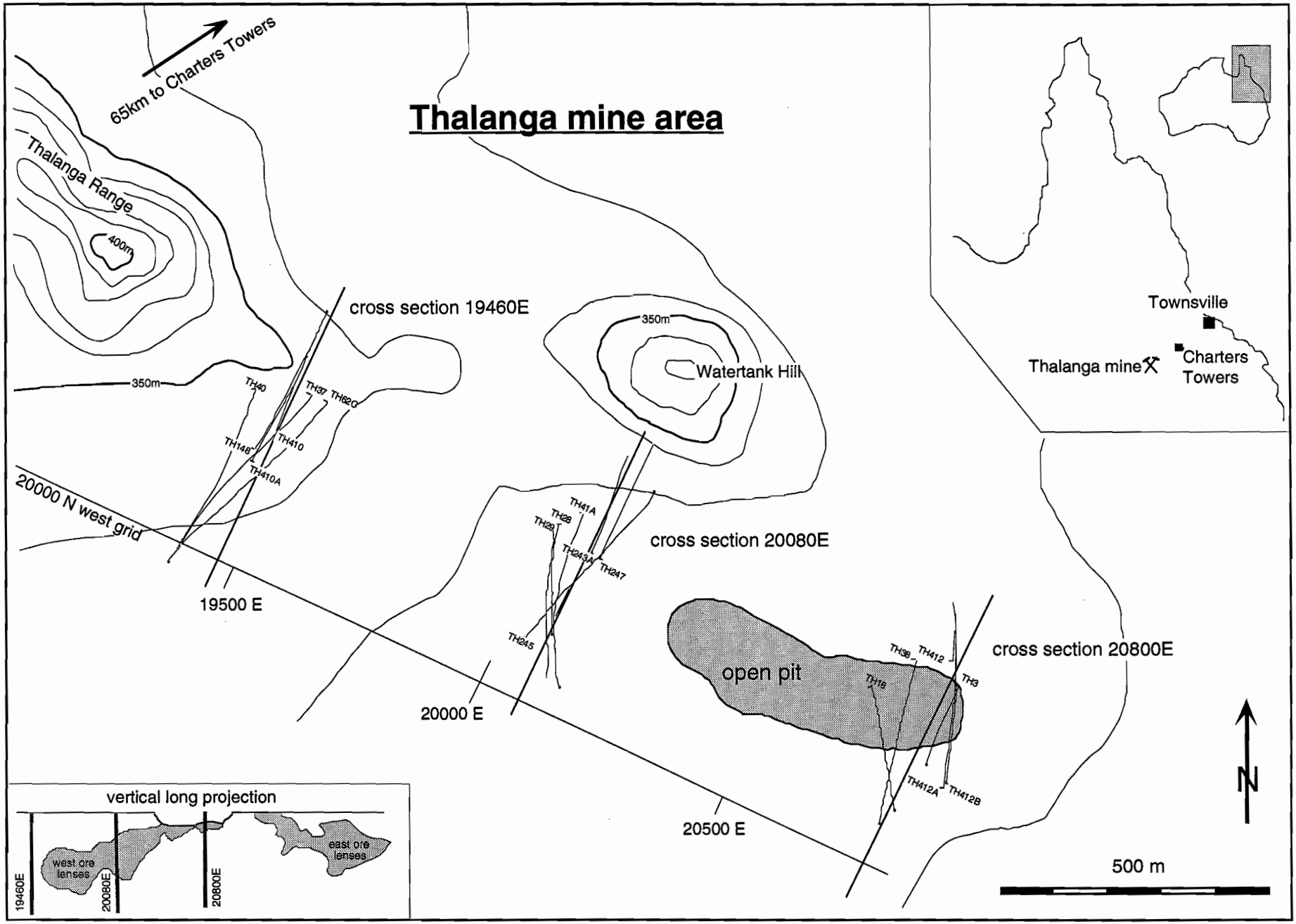

Fig. 1: Map of the Thalanga mine area showing the location of cross-sections and the surface traces of the diamond drill holes examined in this study.

Stratigraphy

The principal stratigraphic components of the Thalanga mine sequence can be summarised as follows (Fig. 2). In the footwall weakly to strongly altered, moderately quartz (-feldspar)-phyric, medium to fine rhyolites dominate over monomict rhyolitic volcaniclastic deposits. However, positive discrimination between clastic and coherent volcanic facies is a challenging task in altered parts of the sequence. A number of thin sections from the footwall rhyolites contain relict or well preserved perlitic textures which are outlined by fine arcuate, sericite domains encircling siliceous kernels.

The ore hosting stratigraphic position — topping the footwall rhyolites — is commonly refered to as the favourable horizon. It contains a laterally variable succession of volcaniclastic sediment, coarse, quartz-rich rhyolites, mudstones, massive sulphides, carbonate–tremolite–chlorite rocks and massive barite and quartz–magnetite of possible exhalative origin. The most intriguing characteristic of the volcaniclastic deposits is the abundance of large quartz crystals (up to 12 mm in diameter) that are commonly blue in colour. This feature led to the introduction of the terms 'quartz eye volcaniclastics' (QEV) and 'quartz feldspar porphyry' (QFP) at the Thalanga mine. A detailed account of the composition and significance of the 'QEV' and 'QFP' units in the favourable horizon has been presented by Hill (1995).

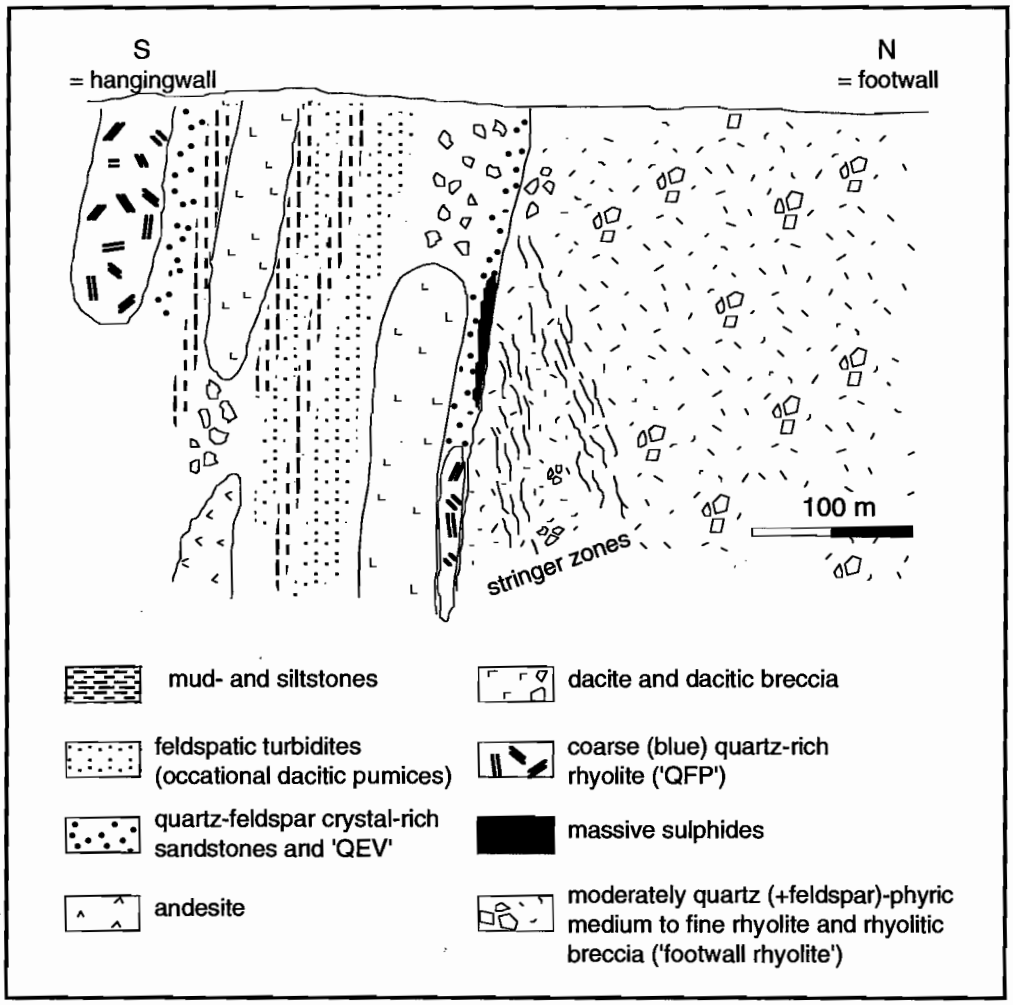

Fig. 2: Sketch map of the principal geological components of the Thalanga mine stratigraphy in an idealised cross -section.

A variable succession of coherent volcanics and sedimentary deposits forms the hangingwall sequence on top of the favourable horizon. The sedimentary facies comprises dark grey or dark green laminated mudstones to siltstones, massive to normal graded turbiditic deposits with feldspar crystals and quartz - feldspar crystal-rich, volcaniclastic sandstones. Scoria and dacitic tube pumice clasts have been identified in thin sections of turbidites.

Non-graded, matrix supported, locally feldspar-rich sedimentary units with dacitic clasts ('dacitic breccia') may be interpreted as peperitic intervals or genuinely sedimentary deposits. Textural examination of the respective drill core intervals did not provide unambiguous evidence.

The coherent facies in the hanging wall includes two types of dacites (medium and fine feldspar-phyric varieties), feldspar–pyroxene–phyric andesites and a highly blue quartz -feldspar phyric, coarse rhyolite ('QFP'). The top contacts of these units can be characteristic of intrusive or extrusive emplacement but in several cases the textural features are not conclusive.

The most important findings during the last field season are the quartz-feldspar crystal-rich volcaniclastic sandstones and the coarse, blue-quartz-rich rhyolite in the hangingwall. These units show very similar textural characteristics to the 'QEV' and 'QFP' units of the favourable horizon. These 're-discoveries' may have a considerable bearing on exploration for further base metal mineralisation as a genetic relationship between 'QFP' emplacement in the favourable horizon and mineralisation has been suggested (R.A. Sainty, pers. comm.).

Alteration

The host rocks of the Thalanga massive sulphide deposit have been affected by variable types and styles of alteration. These may be subdivided into five facies according to the main mineral phases present (Table 1). In the footwall rhyolites phyllosilicate-rich assemblages with variable amounts of sericite, chlorite and biotite constitute the most wide spread alteration facies. While sericite and chlorite are common products of hydrothermal alteration in VHMS systems the biotite is most likely of metamorphic origin. The relative abundances of these phyllosilicates vary between strongly sericite-dominated assemblages and nearly equal amounts of these three phases in samples with low total phyllosilicate contents. Phyllosilicate-rich alteration is pervasive in foliated-schistose samples, but can

Table 1: Subdivision of alteration facies and summary of their styles and distribution in footwall rhyolites and hangingwall dacites.

Alteration type:	style and distribution in:	
	FW rhyolites	HW dacites
phyllosilicate-rich (sericite– chlorite–biotite)	networks, domains or pervasive in foliated samples	networks
white silica flooding	patchy to pervasive	not observed
green staining (epidote alteration)	rare	common, patches and along veins
red staining (albite ? alteration)	rare	common , patches and along veins
carbonate–calc-silicate alteration	locally prominent (close to favourable horizon)	common but usually weak

also be confined to domains giving rise to pseudoclastic textures as described by Allen (1988).

In the hangingwall this alteration facies is considerably less prominent with phyllosilicate (dominantly biotite) forming interconnected networks. This texture suggests that cracks or pre-existing zones of weakness formed the pathways for fluids which reacted with the surrounding feldspar-rich dacitic groundmass.

The second most prominent alteration facies in the footwall can be described as 'white silica flooding' and occurs as patches or occupies intervals of 1–3m in drill core. These white, siliceous domains have gradational contacts and contain the same amount of quartz phenocrysts as adjacent phyllosilicate-rich rhyolite. Hence, these white, siliceous areas represent a domainal silica enrichment alteration phase within the coherent rhyolites. This alteration style has not been observed in the hangingwall dacites.

A very typical alteration feature of the dacites are irregularly distributed spots and patches (cm size range) of red and green staining of the volcanic groundmass. These alteration styles had been considered to be exclusive to the hangingwall but could be observed in the footwall rhyolite (DDH TH410) during the 1995 field season. While petrographic examination clearly showed that green staining correlates with fine, dispersed epidote crystals, the causes for red staining — which has been inferred to be related to albite alteration (Stolz, 1991) — are not apparent in thin sections. It seem likely that fine hematite crystals could be the dying agents but further study is required to confirm this proposition.

Carbonate alteration refers to the occurrences of calc-silicate phases (mostly tremolite–actinolite and epidote–zoisite) and carbonates. These phases may occur as minor constituents in rhyolites and dacites or form distinctive massive carbonaceous rocks such as the carbonate–tremolite–chlorite rocks examined by Herrmann (1994). These carbonate-rich assemblages are abundant close to and within the favourable horizon in the western part of the Thalanga ore body. It is inferred, that the carbonates are related to hydrothermal alteration and that the calc-silicate phases formed during metamorphism.

Geochemistry

The geochemical changes associated with the hydrothermal alteration in the footwall have been examined by Herrmann (1994). He concluded that Ti, Zr and Al remained chemically immobile during alteration and subsequent metamorphism and that large gains of silica, iron, sulphur and loss of sodium characterise the zone of most intense footwall alteration. Furthermore Herrmann (1994) demonstrated that footwall rhyolites occupy a very limited range of Ti/Zr ratios restricted to values between 3 and 6. Dacites have Ti/Zr values varying between 10 and 20 while 'QFP' analyses range between 8 and 20 (Herrmann, 1994, Fig. 9a).

Some new conclusions may be drawn from a plot of Ti/Zr ratio vs. SiO_2 for the analyses compiled for the present study (Fig.3). In accordance with the outlined previous findings nearly all analyses of footwall rhyolite samples plot on a trend parallel to the x-axis with Ti/Zr ratios strongly concentrated between 3 and 5. This indicates that variation in SiO_2 contents (61–83 wt%) is not related to magmatic differentiation but to alteration processes that did not affect the Ti/Zr ratios.

The coarse, blue quartz-rich rhyolites ('QFP') from the favourable horizon and the hangingwall have very distinctive Ti/Zr ratios. Samples from the favourable horizon have values between 4 and 7 – slightly higher than the majority of footwall rhyolites. The 'QFP' sample from the hangingwall has Ti/Zr ratios of 19 (Wills, 1985) and 16 (this study). Hence, two petrogenetical unrelated 'QFP' rock suits are distinguishable in the Thalanga mine area.

The hangingwall dacites have Ti/Zr ratios between 10 and 20 with two clusters of analyses following a x-axis parallel trend at Ti/Zr values of about 18.5 and 11. These trends are most likely due to SiO_2 addition during alteration. The distribution of dacite samples with Ti/Zr ratios intermediate to these 'alteration lines' suggest that the dacites are genetically related and evolved by magmatic differentiation resulting in a decrease in Ti/Zr ratios from about 19 to 10 and a SiO_2 increase from about 68 wt% to 76 wt%.

Significant compositional differences between white silica and phyllosilicate-rich assemblages in the footwall rhyolites could be detected. In diamond drill hole TH410 three samples, each about 20 cm

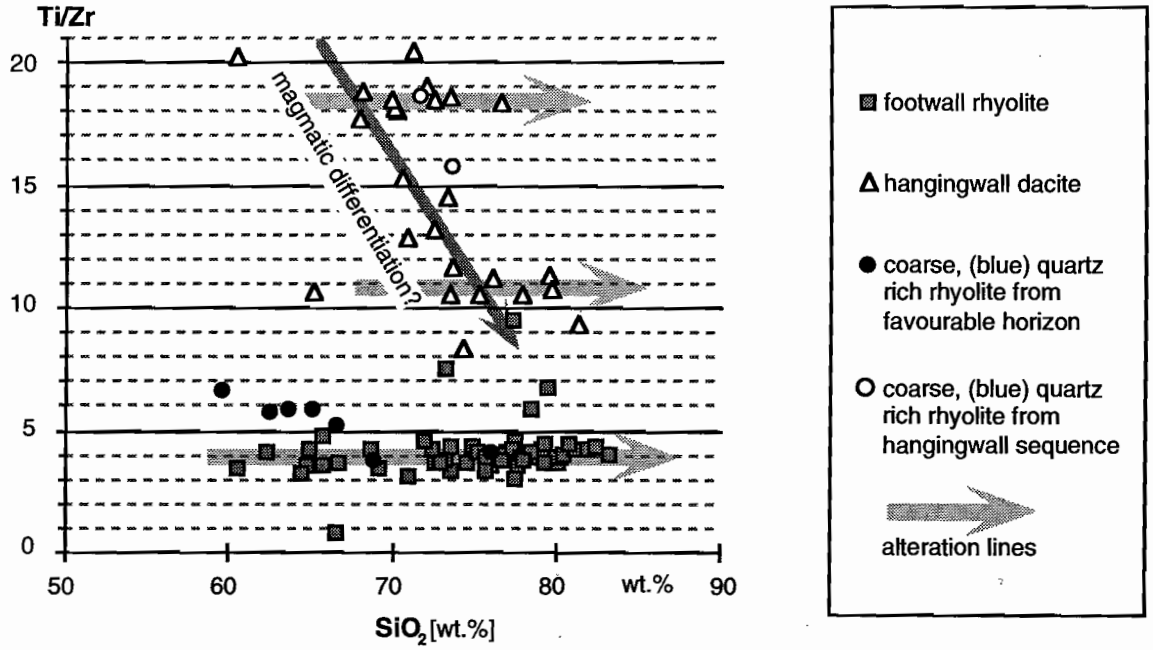

Fig. 3: Ti/Zr ratios vs. SiO_2 for footwall rhyolites, 'QFP' and hangingwall dacites (from data base compiled in this study).

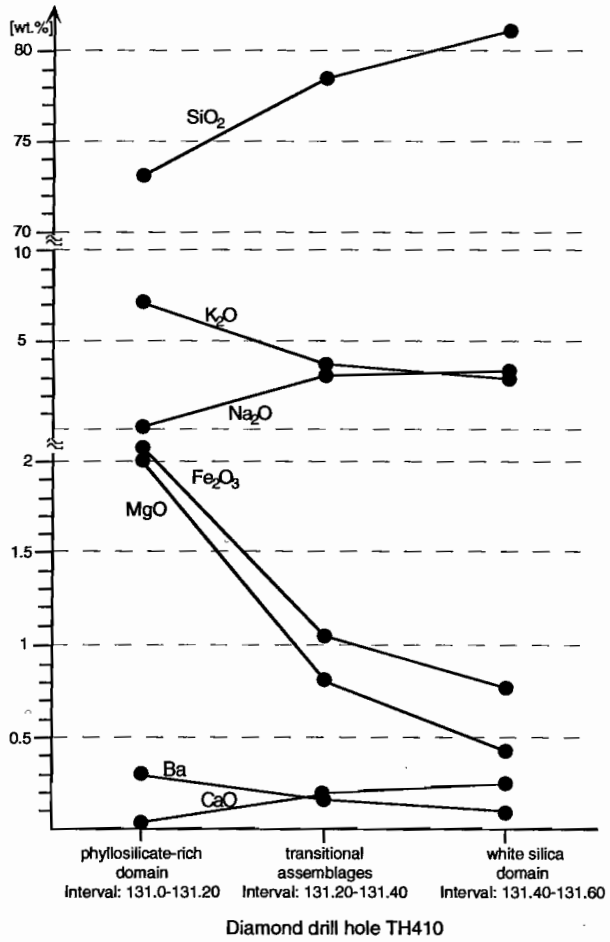

Fig.4: Systematic changes in SiO_2, K_2O, Na_2O, Fe_2O_3, MgO, CaO and Ba content of coherent footwall rhyolite across the contact of pervasive phyllosilicate alterationand white silica 'flooding' (DDH TH410 interval: 131.0m to 131.60m).

long, have been collected over a contact of these alteration types and systematic changes in chemical composition of the rhyolite are apparent (Fig.4). The increase in SiO_2 from the phyllosilcate-rich domain into the silica-rich domain correlates with a substantial increase in CaO and Na_2O. However, K_2O, MgO, Fe_2O_3 and Ba show a pronounced negative correlation with SiO_2 increase. These relationships suggest that the 'silica flooding' alteration took place before the passage of the Ba- (and base metal?)-rich hydrothermal fluids which were responsible for the Na-depletion typical for phyllosilicate altered parts of the footwall rhyolites.

These findings contradict the positive correlation between silica addition and increase in iron and sulphur coupled with the loss of sodium referred to by Herrmann (1994) to be characteristic of the most intense footwall alteration. Rather it may be suggested that silica enrichment is an independent process and that phyllosilicate alteration alone correlates with sodium depletion and increases in iron and sulphur (hence pyrite) contents.

Metamorphism

The most abundant metamorphic mineral in the Thalanga host rock sequence is biotite. It is most likely a product of a continuous reaction involving sericite, chlorite and K-feldspar under greenschist facies conditions. This interpretation is supported by the presence of tremolite–actinolite, epidote–zoisite and — less abundant — garnets. Other metamorphic minerals are rare and include stilpnomelane and diopside (in meta calc-silicates), cordierite (in a phlogopite–Mg-chlorite–sericite assemblage) and andalusite.

The occurrences of garnet are locally restricted to chlorite-rich (± biotite) domains and microprobe analyses showed that they are rich in MnO (A.P. Hill, pers. comm.). These observations are in agreement with the major control of bulk rock composition on the garnet isograd (Spears, 1991). In pelitic schists with high MnO contents the first appearance of garnet+chlorite can occur at temperatures of 440°–470°C. Given the relative scarcity of the garnet occurrences at Thalanga it seem unlikely that peak metamorphic conditions exceeded 500°C.

Future study

- compile comprehensive logs and stratigraphic interpretations of the three examined cross-sections
- include alteration assemblage in graphic logs to examine the relationships between volcanic facies and alteration facies.
- clarify the geochemical effects of the defined alteration assemblages
- examine the variations in pleochroism of chlorites and biotites in accordance with volcanic and alteration facies

References

Allen, R.L., 1988. False pyroclastic textures in altered silicic lavas, with implications for volcanic-associated mineralisation. *Economic Geology* 83: 1424–1446.

Berry, R.F. 1991. Structure of the Mount Windsor Sub-province. *In* Geological controls on VMS mineralisation in the Mt Windsor Volcanic Belt (Eds.: J. Pongratz & R.R. Large). Mount Windsor Project Research Report 2. CODES, University of Tasmania: 23–83..

Berry, R.F., Huston, D.L., Stolz, A.J., Hill, A.P., Beams, S.D., Kuronen, U. & Taube, A., 1992. Stratigraphy, structure and volcanic hosted mineralisation of the Mt. Windsor Subprovince, North Queensland, Australia. *Economic Geology* 87: 739–763.

Gregory, P.W., Hartley, J.S. & Wills, K.J.A., 1990. Thalanga zinc-lead-copper-silver deposit. *In* F.E. Hughes (Ed.): Geology of the mineral deposits of Australia and Papua-New Guinea AusIMM, Melbourne: 1527–1537.

Herrmann, W., 1994. Immobile element geochemistry of altered Volcanics and Exhalites at the Thalanga Deposit, North Queensland. Unpublished, M.Econ.Geol. thesis, University of Tasmania, Tasmania.

Herrmann, W., 1995. Geochemical aspects of the Thalanga massive sulphide deposit, Mt Windsor Subprovince. *In* Beams (Ed.): Mineral Deposits of Northeast Queensland: Geology and Geochemistry, EGRU contribution 52. International Geochemical Exploration Symposium, Townsville, Australia: 17.

Hill, A.P., 1991. Structure and metal zonation of the Thalanga Zn–Pb–Cu deposit. *In* Geological controls on VMS mineralisation in the Mt Windsor Volcanic Belt (Eds.: J. Pongratz & R.R. Large). Mount Windsor Project Research Report 2. CODES, University of Tasmania: 147–169.

Hill, A.P., 1995. Volcanic facies relationships and hydrothermal modification of primary volcanic textures at the Thalanga deposit. *In* Studies on VHMS-related alteration-geochemical and mineralogical vectors to ore. AMIRA project P439 Report 1: 143–146.

Spear, F.S., 1993. Metamorphic phase equilibria and pressure–temperature–time paths. Monograph. Mineralogical Society of America.

Stolz, A. 1991. Stratigraphy and geochemistry of the Mt Windsor volcanics and associated Exhalites. *In* Geological controls on VMS mineralisation in the Mt Windsor Volcanic Belt (Eds.: J. Pongratz & R.R. Large). Mount Windsor Project Research Report 2. CODES, University of Tasmania: 23–83.

Wills, K.J.A., 1985. Thalanga Comprehensive Study – Final Report. Pennaroya (Australia) P/L, unpublished report No: 1551/10.

Gossan Hill alteration: Styles and distributions

Robina Sharpe
Centre for Ore Deposit and Exploration Studies, University of Tasmania

Introduction

Gossan Hill is an Archean (2.8 to 3.0 Ga; Pidgeon et al., 1994) Cu–Zn massive sulphide deposit located in the Yilgarn Block of Western Australia. Studies of the Gossan Hill deposit are part of a PhD project on the mineralisation, alteration and structure of the Gossan Hill Cu–Zn VHMS deposit, supported by the Murchison Zinc Company. Investigations of hydrothermal alteration enveloping the Gossan Hill deposit form a case study as part of the AMIRA alteration project. Aspects of the alteration study include; alteration styles, textures, spatial distributions and geochemistry of alteration types and minerals. The following report documents progress of the alteration study and briefly summarises host lithology, alteration types, distributions and textural investigations made to date. A brief overview of the deposit setting, lithology, styles of mineralisation and thus context of the alteration will be covered.

The Gossan Hill deposit

The Gossan Hill deposit is located in the Murchison Province granite–greenstone terrane, Western Australia; 500 km NNE of Perth and 140 km east of Geraldton (Fig. 1). Distinguishing features which make the Gossan Hill deposit unique for an Australian massive sulphide deposit include:

- a host package of volcaniclastics (100–400 m thickness)
- magnetite alteration and massive magnetite associated with Cu- rich zones
- Au-rich massive sphalerite
- stratigraphic separation of zinc and copper-rich zones (stacked system)

Gossan Hill has many of the characteristics ascribed to a Mattabi-style of mineralisation as defined by Morton and Franklin (1987) in their classification of Archean deposits. Mattabi-type deposits generally show abundant felsic fragmental volcanic rock in the footwall and diffuse, poorly defined alteration zones that are broadly zoned. Examples of similar styles of mineralisation to Gossan Hill include the Mattabi deposit (Franklin et al., 1975) and the New Brunswick deposits (Fyffe, 1995). However, Gossan Hill differs in style and form to polymetallic VHMS deposits hosted in the Mt. Windsors and Mt. Read Volcanic Belts.

Status of Gossan Hill

Gossanous outcrop at Gossan Hill was discovered in 1971 (Pitt, 1990) and delineation of the Cu–Fe–Zn-rich deposit was carried out between 1972 and 1976. However preliminary feasibility studies demonstrated that the ore resource could not be economically exploited at that time. Discovery of Zn–Cu mineralisation at Scuddles 4 km north of Gossan Hill was made in 1979 (Mill, 1990) and the Scuddles deposit is currently being mined. A feasibility study is presently being undertaken on the mineralisation at Gossan Hill by means of an exploration decline. The decline will access footwall units, from which ore delineation drilling of the deposit will commence. This drilling commenced in May 1996. The current inferred underground resource of Gossan Hill is 7.7 m.t at 3.7% Cu and 2.4 m.t. at 12% Zn. In addition a gold and copper supergene zones exist overlying the zinc and copper orebodies respectively. The copper supergene zone has a resource of 2 m.t. at >2% Cu and the gold zone of 1 m.t. in excess of 3 g/t.

Two major studies have been completed in the region. Frater (1983) completed mineralogical and

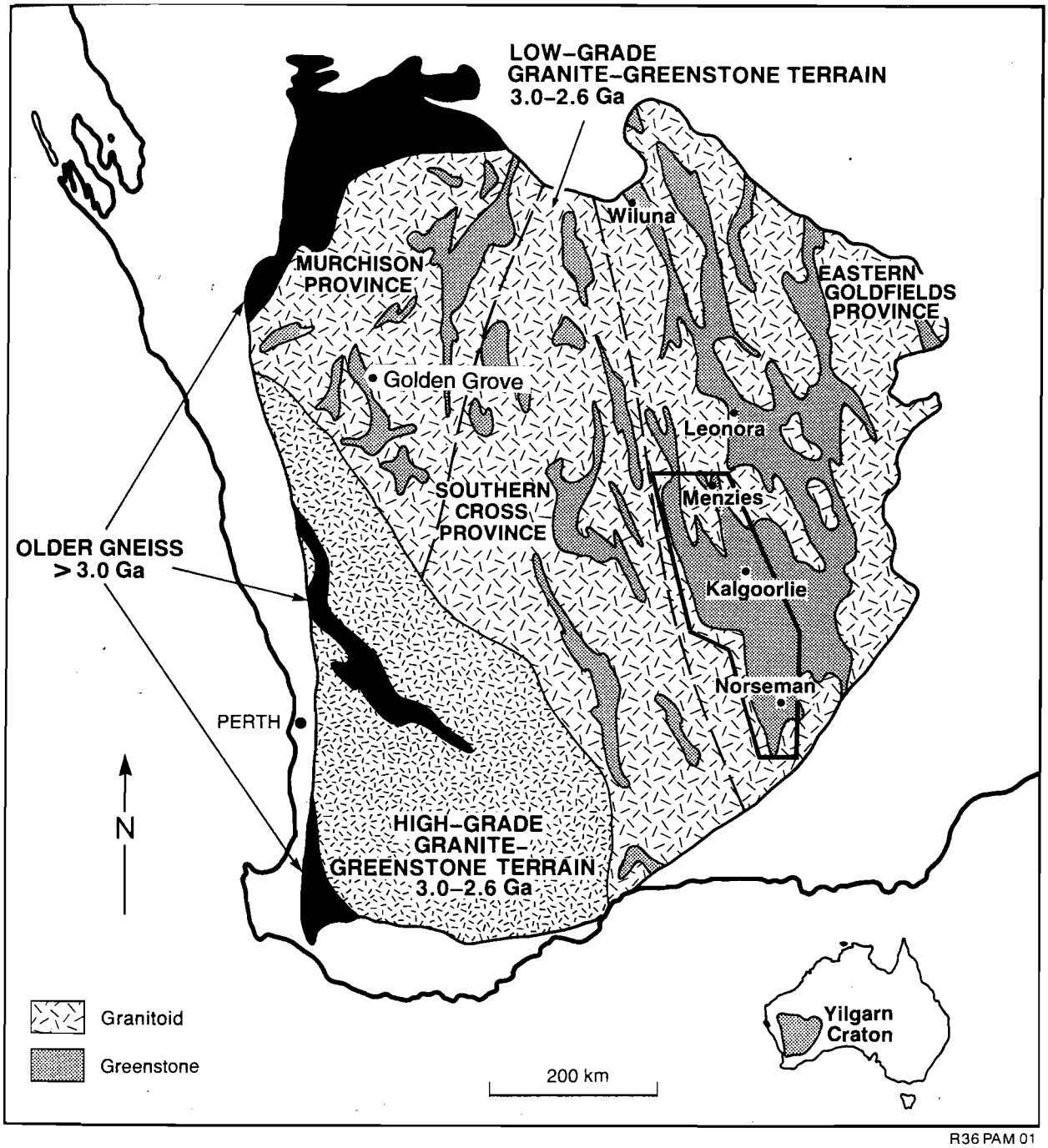

Figure 1 Locality map of the Golden Grove District, hosting mineralisation at Gossan Hill and Scuddles (from Morris, 1992)

textural studies on Gossan Hill mineralisation and Clifford (1992), completed a PhD on facies and palaeoenvironment analyses of the volcanic-sedimentary succession hosting base metal mineralisation in the Golden Grove Domain.

Golden Grove Domain

Mineralisation at both Gossan Hill and Scuddles occurs at the same stratigraphic interval within the Golden Grove Domain. The Golden Grove domain is located on the northeast flank of the Warriedar Fold Belt (Fig. 2), on the western limb of a north trending, subvertically plunging F3 anticline. The Golden Grove Domain is a coherent stratigraphic succession of felsic to intermediate volcaniclastics, lavas and breccias, as well as minor chemical ('exhalite') horizons. The depositional setting is inferred to be deep subaqueous, indicated by the subaqueous mass-flow style of sedimentation of the host units (Clifford, 1992). Regional metamorphism is greenschist to lower greenschist facies as indicated by the chlorite–sericite–quartz–carbonate assemblage (Watkins and Hickman, 1990).

The stratigraphy of the Golden Grove Domain is divided into three groups, the Gossan Hill, Thundalara and Minjar Groups. Mineralisation occurs within the west facing, steeply dipping Gossan Hill Group; which is composed of five formations. Of these formations, mineralisation at Gossan Hill is hosted within Golden Grove Formation (GGF). GGF is a package of volcanolithic sediments with minor coherent lavas. Lavas, breccias and minor volcaniclastic constituents of the Scuddles Formation form the hangingwall volcanics to massive sulphide mineralisation. The stratigraphic framework of the Golden Grove and Scuddles Formation is presented in Figure 3.

Stratigraphy

Gossan Hill mineralisation straddles three separate stratigraphic members of the Golden Grove Formation as defined by Clifford (1992); namely GG4, GG5 and GG6 (Fig. 3). A schematic facies variation diagram is presented as Figure 4. Of these three members, zinc mineralisation is almost exclusively hosted within GG6, and copper mineralisation within GG4 (refer Figs 4, 5). Low grade copper mineralisation occurs below the zinc mineralisation within the lower stratigraphic portions of GG6.

GG6

The GG6 Member is host to massive zinc-rich sulphide and associated stringer mineralisation. GG6 predominantly consists of a thinly bedded sequence of fine grained sandstones to siltstones but also includes interbedded polymict, poorly sorted, open framework cobble and pebble breccias. Clifford (1992) classifies GG6 as Mixed Provenance Litharenite Facies that was deposited as an ambient background sedimentation.

Sandstones generally show a granular nature with abundant well rounded quartz grains. Normal grading is frequently observed in sandstones and cobble/pebble breccia units. Bedforms may show wavy, undulose basal contacts indicative of locally erosional basal contacts. Hand specimen scale syn-depositional normal faulting of sedimentary layers is also observed. Thinly bedded units show generally intense silicification and minor chlorite alteration. In zones where silicification is no original textures remain. Silicification does, however, preserve stratification. In chlorite altered beds, chlorite forms fine grained interlocking arrays which generally show higher modal proportions of disseminated sulphides. The abundance of sulphides in GG6 is variable, occurring as sulphide veining through the host grading to massive sulphide.

Pebble breccias are moderately to poorly sorted, matrix supported, open framework breccias. Lithic constituents generally comprise <50% modal abundance and are sediment clasts which often contain relict quartz grains and host microcrystalline quartz alteration. Silicified lithics indicate that silicification was prior to incorporation of the pebble breccia and are most likely derived locally from underlying GG6 strata. Matrix constituents of these pebble breccias are chloritoid and fine grained chlorite.

GG5

GG5 units are grey massive, well sorted, thickly bedded quartz pumiceous sandstone. Gradational, interbedded, upper contacts with GG6 and conformable lower contact with GG4 Member units are

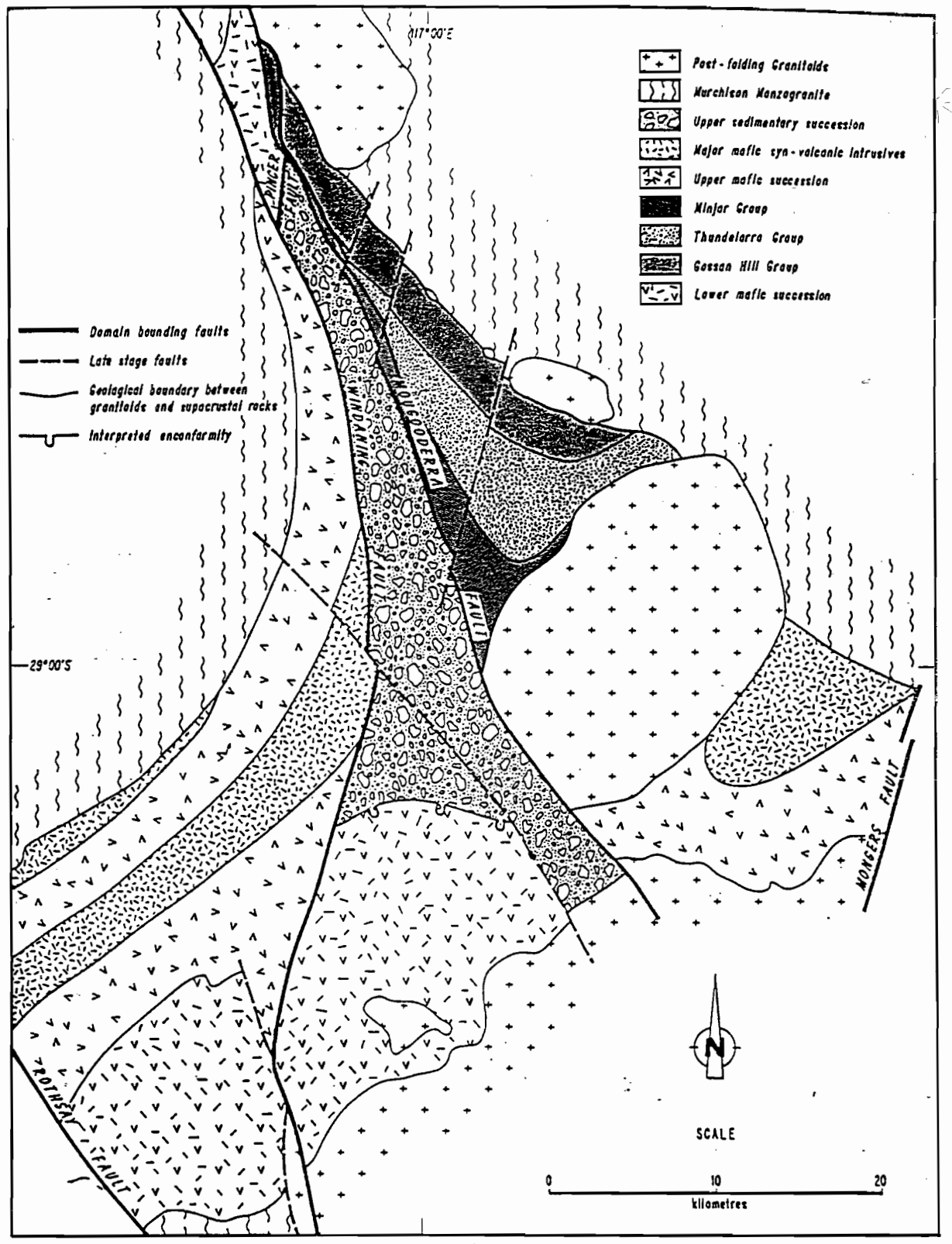

Figure 2 Stratigraphic components of the Warriedar Fold Belt (from Clifford, 1992)

observed. Minor thin interbeds (<10 cm thick) of open framework, poorly sorted, normally graded pebble breccias are present. GG5 is relatively massive and uniform with few bedding indicators. Strong, pervasive, fine grained chlorite alteration of the matrix material is common. Minor opaque phases may be present; mainly magnetite (± ilmenite) grains disseminated throughout the chlorite altered matrix. Massive sulphide mineralisation is absent from the GG5 Member which separates the lower copper zone from the upper zinc zone.

GG4

Clifford (1992) stated that GG4 contains both Mixed Provenance Litharenite Facies and tuffaceous volcaniclastic debris. Lithofacies ascribed to the GG4 Member are sandstone and siltstone and contain high modal abundances of volcanic quartz and pumice. Sandstones are massive and thickly bedded to thinly bedded. Quartz grains may form up to 40% modal and are angular and fragmented volcanic grains. The matrix of these sandstones and siltstones is generally strongly chlorite altered, however relict textures indicate the matrix to have been glassy. Chloritic alteration of the GG4 units is ubiquitous and texturally destructive. However, in all but the most intense alteration, relict quartz grains are visible.

GG4 is subdivided into two lithologies on the basis of constituents. The upper portions of GG4 show units of polymict, lithic, pebble breccias to sandstones and siltstones. Lithic constituents include thinly bedded to laminated siltstones fragments and tube pumice fragments. Pebble breccia units are poorly sorted, clast supported tube pumice breccias that are strongly chlorite altered. Tube pumice shows alteration of the pumice walls to quartz and tube vesicles filled by chlorite. Siltstone lithics show a variable size up to 0.6 cm in length and are generally angular and elongate . Quartz is less abundant in the upper zone of GG4 and is present as irregular, angular quartz fragments or elongate grains scattered sparsely throughout the matrix. The elongate quartz grains likely represent non-welded glass shards recrystallised to quartz.

Lower stratigraphic portions of GG4 are composed of thinly bedded to thickly bedded quartz crystal-rich sandstone to pumiceous siltstone. The contact between upper and lower portions of GG4 is a sharp transition, depicted by a marked contrast in the quartz crystal morphologies and abundances. Quartz grains are up to 1.5 mm and angular. Quartz may also be present as well rounded grains to cuspate angular fragments that likely represent relict bubble wall shards. Volcanic quartz grains are poorly sorted and may show insitu disaggregation along fractures indicated by the jigsaw fit and aligned extinction of quartz grain fragments. GG4 siltstone units are thinly bedded and variably very fine grained (quartz grains <0.5 mm) to medium grained (quartz crystal <1–2mm). Thinly bedded zones are chlorite altered and may represent finer resedimented glassy debris with lower crystal abundances and occasional shard textures. The glass shard textures shows cuspate to curviplanar narrow elongate forms. The diagnostic feature of the tuffaceous component of GG4, is the crystal-rich nature comprising angular, broken volcanic quartz grains in an open framework. Matrix material is variably chlorite–pyrrhotite–magnetite altered. Bedding and sorting of the quartz grains in sandstone units and associated interbedding of the crystal-rich component with mixed provenance material are interpreted as the result of epiclastic processes; reworking and resedimentation of pyroclastic material.

Hangingwall Volcanics (Scuddles Formation)

Two dominant facies form the hangingwall position to zinc-rich massive sulphides: A quartz-feldspar phyric rhyodacite lava (VRDA) is present in the hangingwall position immediately overlying GG6 and may be in direct contact with massive sulphide mineralisation. This unit is classified as Scuddles Formation Member 2 (SC2) after Clifford (1992). VRDA is a massive, cream to grey quartz-phyric to quartz porphyritic ± feldspar unit, showing large rounded quartz grains (up to 8mm diameter).

Stratigraphically overlying VRDA are dacites, also classified as the SC2 Member of the Scuddles Formation (Clifford, 1992). These dacites are massive grey feldspar ± quartz (<1.5mm size) that may show irregular shaped inclusions of devitrified glass. Small quartz grains are sparsely distributed throughout groundmass and feldspars are abundant but variably chlorite ± carbonate altered. North of C zone, a rapid facies variation is observed where the VRDA unit is absent and dacite units are present.

1. Epiclastic facies

(a) Quartz Arenite Facies: Poorly sorted, quartzo-feldspathic, fine to coarse sandstones, minor interbedded pelite. Eroding gneissic/granitic source terrain. Facies lensoidal when interbedded with other epiclastic or volcanic facies. Distribution limited: Shadow Well and Gossan Valley Formation Member 1 (Chapter 4).

(b) Mixed Provenance Litharenite Facies: Moderate to poorly sorted, polymict-lithic, fine sandstones to cobble breccias; the breccias being subordinate. Source area dominated by eroding andesitic volcanics, with subordinate plutonic, dacitic, basaltic and ultramafic volcanic sources. Bedded cms to 15m, partial Bouma sequences and scoured bases. The facies is lensoidal when interdigitating with volcanic facies. Stratigraphic distribution: upper four formations of the Gossan Hill Group (Chapter 4).

(c) Tuffaceous Volcaniclastic Facies Associations: Poorly sorted breccias composed of resedimented juvenile magmatic and phreatomagmatic tuffaceous debris. Massive to bedded, depositional units cms to 9m, massive to crudely graded (A2A3 Bouma sequences), and scoured bases. Individual facies are laterally continuous on a scale of kilometres. Stratigraphic distribution: Golden Grove Formation (Chapter 6).

2. Volcanic facies

(a) Coherent Basalt Facies: Thin laterally discontinuous, aphyric, amygdaloidal, coherent basalt flows and some associated syn-volcanic intrusives. Stratigraphic distribution: Gossan Valley and Cattle Well Formations (Chapter 5).

(b) Andesite Facies Association: Three related facies are defined, the *Coherent Andesite, Massive Andesite Breccia* and *Stratified Andesite Breccia Facies*. All facies are weakly porphyritic, amygdaloidal, laterally discontinuous and together form a genetically related facies group. Stratigraphic distribution: Golden Grove Formation, Member 2 (Chapter 5).

(c) Dacite Facies Association: Three facies, the *Coherent Dacite, Massive Dacite Breccia* and *Stratified Dacite Sandstone and Breccia Facies*, are defined within this facies association. Six distinct eruptives have been identified (Dacite 1-6). These vary from aphyric to quartz-feldspar porphyritic and are locally amygdaloidal. Stratigraphic distribution: Gossan Valley Formation Member 2, Scuddles Formation Members 1-4 (Chapter 5).

(d) Rhyodacite Facies Association: Three facies, the *Coherent Rhyodacite, Massive Rhyodacite Breccia* and *Stratified Rhyodacite Breccia Facies*, are defined within this facies association. Three distinct eruptives have been identified (Rhyodacite 1-3), all being quartz-feldspar porphyritic and locally amygdaloidal. Stratigraphic distribution:Golden Grove Formation Member 2, Scuddles Formation Member 2 & 4 (Chapter 5).

(e) Rhyolite Facies Association: Three facies, the *Coherent Rhyolite, Massive Rhyolite Breccia* and *Stratified Pebbly Rhyolite Sandstone Facies*, are defined within this facies association. The association includes a single eruptive, which is quartz-feldspar porphyritic and restricted in stratigraphic distribution to Gossan Valley Formation, Member 3 (Chapter 5).

3. Chemical sediment facies

(a) Chert Facies: Fine grained silica, commonly with finely disseminated carbonate, sulphide and oxide impurities, defining delicate laminations. Geometry of facies is thin (≤5m) lensoidal occurrences of limited (≤200m) lateral continuity. Isolated occurrences known, but most abundant as a lateral equivalent of, or in the hanging wall to, significant *Massive Sulphide Facies* occurrences. Most stratigraphically widespread chemical sedimentary facies: Golden Grove and lower Scuddles Formation (Chapter 4).

(b) Massive Oxide Facies: The facies has two end-member varieties. Variety 1 - coarse grained (1-2mm) subhedral magnetite, beds of ≤2cm interbedded with *Chert Facies*. Variety 2 - fine grained (≤0.01mm) magnetite, massive stratiform lenses of ≤10m thickness and ≤80m lateral continuity overlying epigenetic magnetite stockwork, footwall to significant massive sulphide facies. Stratigraphic distribution: Golden Grove and lower Scuddles Formation (var. 1) and Golden Grove Formation, Member 4 (var. 2) (Chapter 4).

(c) Massive Sulphide Facies: Primary and recrystallized Fe, Zn, Cu, Pb sulphides. Geometry varies from thin (≤2cm) lensoidal occurrences interbedded with chert and massive magnetite, through to stratiform massive sulphide lenses ≤40m thick, with lateral dimension of ≤400m. Major occurrences exhibit zoned metal distributions and underlying well developed epigenetic stockwork. Stratigraphic distribution: Golden Grove Formation Members 4 and 6 and Scuddles Formation Member 3 (Chapter 4).

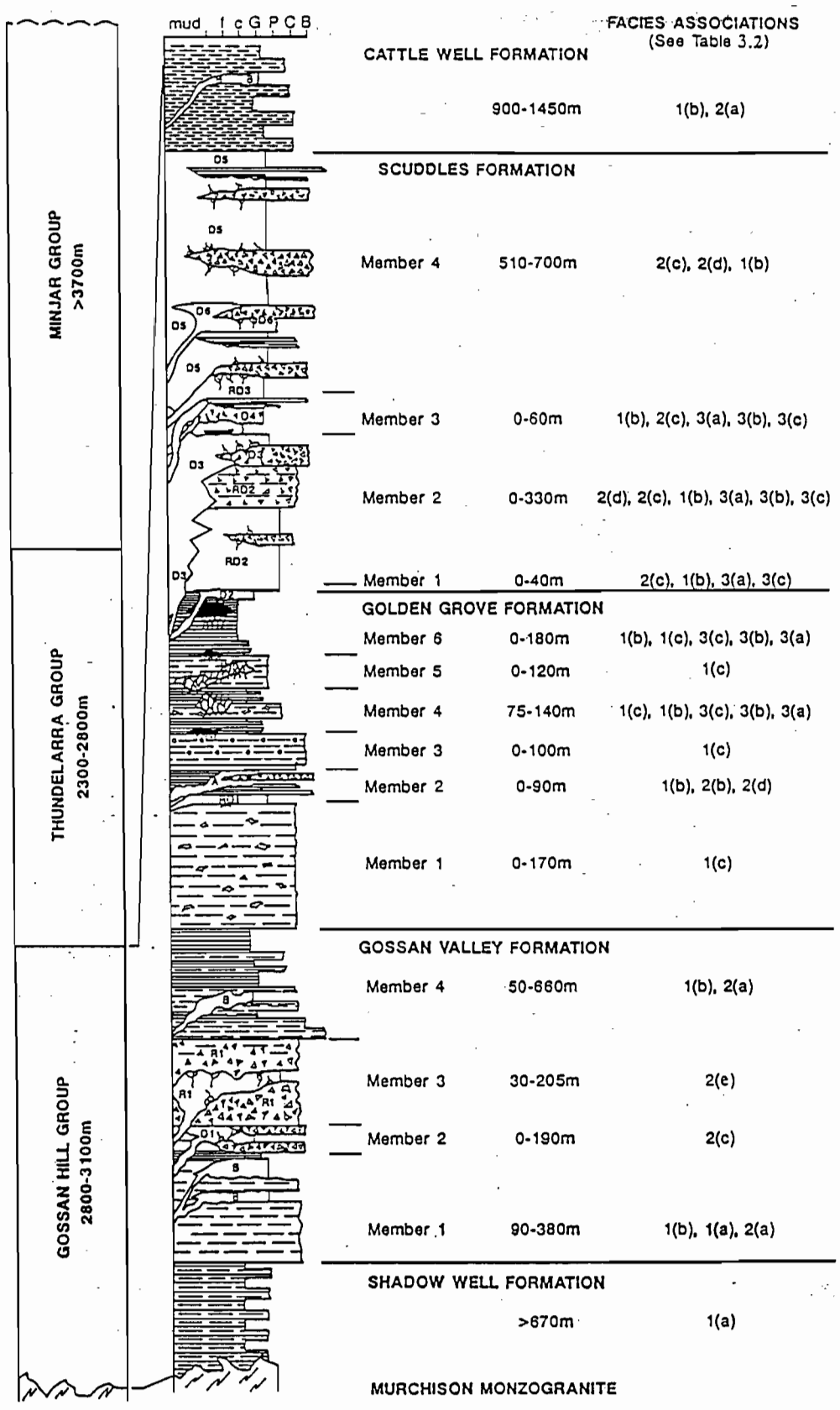

Figure 3 Stratigraphic framework of the Golden Grove Domain (from Clifford, 1992)

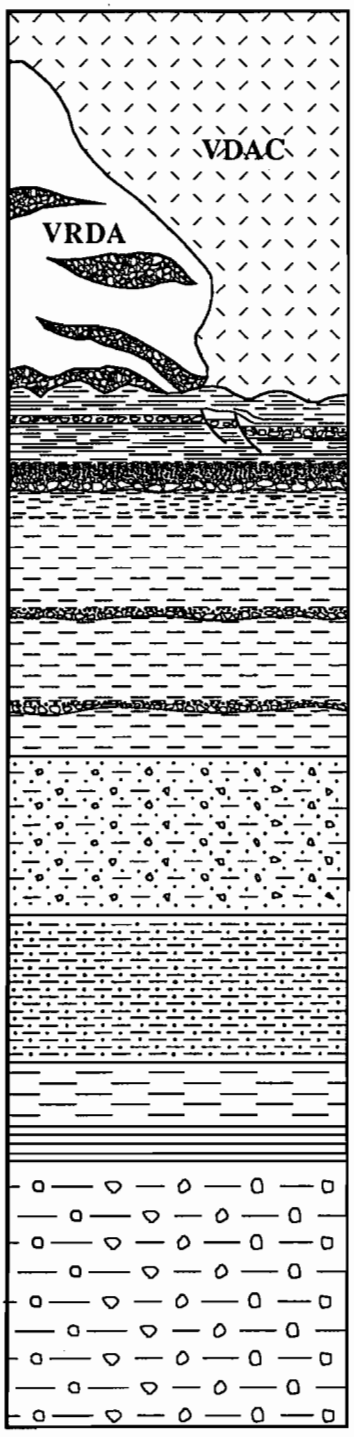

Clifford (1992) Stratigraphic Subdivision	1994 Field Work Observation
VDAC = SC2 RD2	Interfingering quartz feldspar phyric rhyolite lavas and feldspar quartz phyric dacite lavas
VRDA = SC2 (D3)	Rhyolite lava hosts 'rafts' of breccia. Breccia sourced from underlying GG6 sediments and incorporated to coherent rholite. Erosional base to dacite and rhyolite. Breccia margins developed at base of rhyolite
GG6	Laminated to thinly bedded sediments Normal Grading and syndepositional faulting
	Gradational contact between GG5 and GG6
GG5	Thickly bedded sandstone to siltstone showing minor interbeds of coarse grained polymict cobble breccias with normal grading and erosional bases
GG4	GG4 Upper : Lithic rich pumiceous volcaniclastic with angular broken vitric quartz.
	GG4 Lower : Thinly bedded, pumiceous, glassy angular broken vitric quartz volcaniclastics
GG3	Not observed
GG2	Not observed
GG1	Lithic pumiceous breccias with minor broken vitric quartz debris

NOT TO SCALE

Figure 4 Gossan Hill stratigraphy : Facies variation diagram

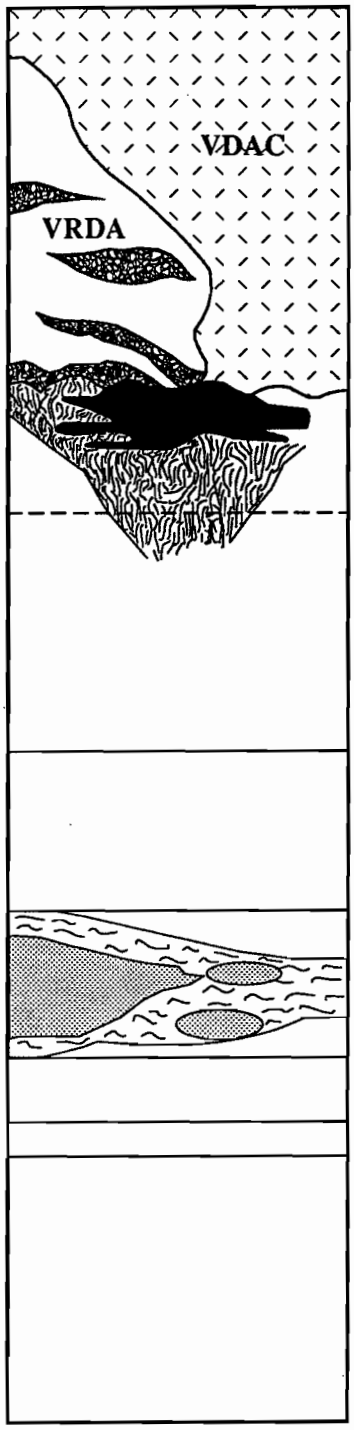

Clifford (1992) Stratigraphic Subdivision

1994 Field Work Observation

VDAC = SC2
RD2

VRDA = SC2
(D3)

Clasts of sulphide hosted within hangingwall breccias

GG6

Layer parallel and stockwork stringer veins.

Semi conformable stringer development into GG5 underlying C Panel

GG5

GG4

Gradational contacts between massive sulphides/oxides and altered host rocks

GG3 Not observed

GG2 Not observed

GG1

LEGEND

Massive zinc mineralisation

Massive pyrite and/or magnetite copper - rich mineralisation

Zinc - rich stringer sulphides including stockwork and layer parallel veinsets

Diffuse pyrite - rich sulphide + oxide + chlorite mineralised alteration

NOT TO SCALE

Figure 5 Schematic distribution of alteration within the host lithologies at Gossan Hill

VRDA shows a consistent stratigraphic occurrence at the hangingwall GG6 contact. In these contact zones, a thin veneer of polymict breccia of 2–3 m thickness may be observed. These breccias contain clasts of GG6 in a rhyodacitic quartz-phyric matrix. Fragment populations include thinly bedded to laminated silica altered GG6 volcaniclastic clasts as well as fragments of zinc-rich massive sulphides. Soft sediment deformation of volcaniclastic clasts is observed and strong development of hydrothermal alteration (chlorite–silica–sulphides.) is present. Sediment rafts within the massive rhyodacite are suggestive of incorporation of underlying unconsolidated GG6 volcaniclastics and are most abundant in basal portions of the lava. A discordant contact is interpreted between GG6 and VRDA, with local erosion of underlying unlithified GG6 sediments by rhyodacite.

Dacite units consistently overly the massive VRDA where it is present. Overlying C zone massive sulphides, dacite units show various stratigraphic associations with both GG6 and VRDA. In this area dacites show an intrusive contact to VRDA, with massive dacite in direct contact with GG6 and massive sulphides. This dacite is interpreted to be syn- to post- sulphide formation. Difficulties arise in ascertaining the spatial distribution of the dacite units due to conflicting temporal associations. The crux of the problem lies in the inability to differentiate between certain dacite units, which may include post folding dacite intrusives. As a result, 'dacite hangingwall' units have been categorised as such irrespectively. Future lithofacies work and immobile element geochemistry are required to resolve these problems.

Zinc mineralisation

Massive zinc sulphides are hosted by volcanogenic sediments of GG6 (Fig. 5). Sulphides are predominantly sphalerite and pyrite with lesser occurrences of chalcopyrite, galena, pyrrhotite, magnetite, tetrahedrite, arsenopyrite, cobaltite, cassiterite, native silver and electrum. Zinc mineralisation at Gossan Hill forms three presently discrete zones; A, B and C. Mineralisation has a strike extent of 550 m and a dip extent in excess of 450 m. Spatial associations between zinc zones and hydrothermal alteration, indicate zinc mineralisation to have formed an elongate, continuous, narrow sheet of sulphides that thickened to the north (toward C zone). Drill section interpretations indicate that the present deformed state and apparent spatial separation of A, B and C zone massive sulphides is an artefact induced specifically by the post-folding intrusive dolerite sills and dykes and contributed to by other late intrusive phases and late brittle faulting. Stringer mineralisation is associated with each of the three zones, but is extensively developed at C zone.

The M1 marker

A distinctive horizon comprising thinly interbedded chert and fine grained volcanogenic sediments overlies the mineralisation at Scuddles. This chert-lithic unit is termed the M1 Marker unit (Ashley et al., 1988; Clifford, 1992). The distinctive nature of the M1 Marker unit is the result of interbedded white quartz bands and chlorite-altered lithic bands; the later is host to disseminated magnetite. This unit is interpreted to represent a mixed hydrothermal ('exhalite')-epiclastic horizon similar in occurrence and style to those observed in association with other VHMS deposits (e.g. Kalogeropoulos and Scott, 1983, Duhig et al., 1992). Observations at Gossan Hill indicate a similar unit to the M1 Marker at Scuddles is present in the hangingwall GG6 units at Gossan Hill. M1-type equivalents at Gossan Hill occur in C zone and show lower gradational contacts to silicified thinly bedded GG6. A comparative investigation was undertaken between identified M1 Marker units and those similar units observed at Gossan Hill, to determine textural and mineralogical similarities for stratigraphic correlation.

The lateral distribution of the M1 Marker unit at Scuddles is discontinuous and lensoidal (Rayner, pers. com.). Similar conclusions can be made for the M1-type unit at Gossan Hill, where it is only observed overlying C zone and at A and B zone. It is possible that the M1-type unit at Gossan Hill may have been removed during deposition of the massive hangingwall rhyodacites/dacites, or that it was not deposited at all.

Textural similarities between M1 Marker unit at Scuddles and Gossan Hill supports the conclusion that the two units are of a similar origin. Such a conclusion requires the substantiation of geochemical

data. It is imperative that future analytical investigations compare and contrast the two M1-type units geochemically as well as address the possibility that the 'quartz' portions may be hydrothermal precipitates. No evidence, at present suggests a precursive lithology for the quartz bands, indicating that either a hydrothermal origin be invoked or they have resulted from preferential replacement of a former horizon during intense silicification associated with the mineralising event.

Copper mineralisation

Copper mineralisation occurs in lower stratigraphic portions of GG4 (Fig. 6), north of zinc mineralisation. Thinly bedded quartz crystal-rich sandstone and siltstone hosts the copper mineralisation. Low grade copper mineralisation also occurs in the lower portions of GG6 and is interpreted to represent chlorite + pyrite ± pyrrhotite ± chalcopyrite ± magnetite ± carbonate veins within GG4-type lithologies in basal portions of GG6. Copper mineralisation forms an irregular and discontinuous zone. In the copper zone, sulphides and oxides form an anastomosing stockwork vein system that grades through sub massive sulphide and/or magnetite to massive sulphide and/or massive magnetite. Chalcopyrite is disseminated throughout massive pyrite and massive magnetite zones. Variable proportions of pyrrhotite occur and chlorite ± talc ± carbonate (siderite) are the major gangue constituents. Ore contacts are generally gradational in the footwall and hangingwall over metres, but may also be sharp.

Footwall aAlteration

Three dominant stringer-footwall alteration assemblages occur at Gossan Hill. These are; silica, chlorite and carbonate alteration with each alteration assemblage representing end members of a broad spectrum (Fig. 6). Lithological-stratigraphic alteration associations are also observed. Descriptions of alteration styles are based on hand specimen and thin section descriptions of selected samples typifying alteration end members. The following section examines spatial associations, distributions and textures of the alteration end members.

Silica aAlteration

Two silica alteration styles occur. Intense, pervasive siliceous alteration forms a stratabound zone that is host to massive zinc sulphide mineralisation. This silicification is the dominant alteration phase throughout GG6. Nodular silica alteration is does not form an alteration zone, but is disseminated throughout GG4 lithologies.

Pervasive silica alteration

Pervasive silica alteration is developed as interlocking meshworks of microcrystalline quartz. Where siliceous alteration is intensely developed, few textural indicators of the original host remain. Silicification is not ubiquitously developed throughout GG6 footwall units. Pebble breccia units of mixed provenance generally show poorly developed silicification, but may contain fragments that are strongly silicified. Units which indicate a tuffaceous component (including pumice fragments, glass shards and volcanic angular quartz grains) do not contain siliceous alteration but pervasive chloritic alteration. Relict textural and lithologic elements of the host are generally confined to those units where siliceous alteration is less well developed; primarily the coarser grained sandstone bands or pebble breccia units. GG6 units at A and B zone are relatively thinly developed and show stratabound pervasive siliceous alteration. Siliceous alteration is observed at C zone but becomes gradationally chlorite-rich with depth into the footwall.

At Gossan Hill, the degree of silicification in the GG6 host strata to zinc mineralisation is intense, with finely laminated to thinly bedded units entirely composed of microcrystalline quartz. The chert nature of these GG6 units is best developed in upper stratigraphic portions adjacent to or encompassing zinc mineralised zones. Away from mineralisation in footwall GG6 units, the intensity of silicification decreases. Comparatively, GG5 and GG4 units rarely show intense pervasive silicification. As a consequence, the intensely developed pervasive silicification is associated with the zinc mineralising system.

Nodular silica alteration

Nodular silica alteration is observed in GG4-type units. Silica nodules are up to 2mm diameter and uniformly disseminated throughout the GG4 host.

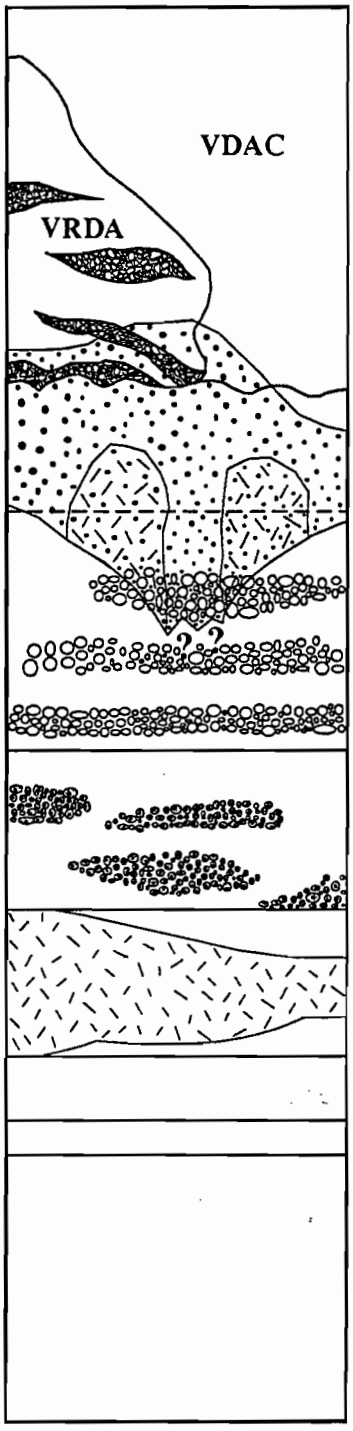

Clifford (1992) Stratigraphic Subdivision	1994 Field Work Observation
VDAC = SC2 RD2	
VRDA = SC2 (D3)	
	Silica alteration developed locally in hangingwall lavas and breccias
GG6	Intense to strong pervisive silica alteration showing chlorite overprint
GG5	Silica alteration overprints nodular carbonate altered GG5 units : indicating carbonate nodular development is pre - to syn - silica alteration Carbonate nodular alteration developed as zone likely reflecting specific beds in the GG5 stratigraphy
GG4	Nodular silica alteration developed in beds in GG4 upper, likely reflecting more pumiceous units (?) Pervasive intense chlorite alteration
GG3	Not observed
GG2	Not observed
GG1	

LEGEND

- Intense silica alteration
- Intense chlorite alteration
- Carbonate nodular alteration + silica
- Nodular silica alteration
- Chlorite + silica alteration

NOT TO SCALE

Figure 6 Stratigraphic distribution diagram of zinc and copper-rich sulphide mineralisation

Silica nodules comprise rounded patches of microcrystalline quartz, some of which show relict volcanic quartz grains at the core.

Chlorite alteration

Pervasive chlorite alteration

Pervasive chlorite alteration is developed throughout GG4 and intensely developed in copper-rich zones. This alteration forms a broad stratabound zone. Based on their textural associations to sulphides and other gangue constituents, at least two generations of chlorite are present. Early chlorite is Mg-rich and occurs as variably sized, interlocking laths of well formed chlorite. The second chlorite is interpreted as a late stage chlorite, acicular in form and overprints most sulphide and gangue mineral phases.

Chlorite alteration also hosts magnetite ± ilmenite needles. These needles rarely exceed 0.5 mm and are associated with units containing andalusite and chloritoid. The needles may represent primary acicular hematite precipitates that have been replaced or metamorphosed, however, no relict hematite mineral phase remains. Alternatively, the acicular magnetite ± ilmenite needles may reflect a pseudomorphing origin after devitrified glass shards in the sandstones. Disseminated magnetite is frequently associated with chlorite alteration and contains ilmenite lamella. The magnetite ± ilmenite association represents a changing oxidation state, ilmenite produced as a result of comparatively increased reducing conditions compared to that of magnetite development.

Chlorite ± silica (± copper) association

The development of chlorite ± silica (± copper) alteration is confined largely to the lower stratigraphic portions of C zone. The chlorite ± silica (± copper) association is not present in A zone and is observed only from limited drill intercepts through B zone. At C zone this chlorite alteration is an overprint to silica alteration of the host sediments and is associated with pyrite ± pyrrhotite ± magnetite ± sphalerite ± chalcopyrite ± carbonate ± chlorite veining of the host.

Chlorite spotted textures

Arrays of chlorite 'spots' occur within pervasive silica altered sandstones to siltstone of GG6. The chlorite spots form irregular millimetre sized zones with diffuse and may contain euhedral, tabular chloritoid laths. The enclosing silica alteration is pervasive and intense.

Chlorite spots represent relict patches of pervasive to patchy chlorite alteration that has been overprinted by siliceous alteration in the form of microcrystalline quartz. The chlorite spotted texture is interpreted to form an integral part of the ore deposition process due to its consistent occurrence in upper portions of A and B zone and its occurrence as clasts in pebble breccia units. This texture represents a replacement texture of an original laminated to thinly bedded host lithology, by alteration and sulphide assemblages associated with the zinc mineralisation. The formation of the chlorite spots does not appear to be the result of preferential chlorite deposition, but the culmination of a silica ± sulphide alteration overprinting a chlorite alteration.

Carbonate alteration

Pervasive carbonate alteration

Fine grained, pervasive, calcite alteration is observed in GG5 units and in massive dacite units. In GG5 units, carbonate alteration is generally associated with fine grained sericite and chlorite. Dacites have moderate to intense calcite alteration of feldspars together with a pervasive calcite–sericite alteration of the groundmass. In all of these examples, pervasive calcite development is late stage and likely associated with regional metamorphism and associated deformation.

Nodular carbonate alteration

Nodular carbonate alteration is a sporadically developed as narrow zones in footwall GG5 volcaniclastic units underlying A and B zone. At C zone the presence of this distinct alteration phase is poorly developed (or alternatively poorly preserved). It is unclear how the distribution of the nodular carbonate alteration relates to bedding within GG5, but may be preferentially developed in some beds within GG5 strata.

Nodular carbonates are an alteration feature frequently documented in footwall hydrothermal

alteration associated with VHMS deposits. Examples include; Hellyer (Gemmell and Large, 1992), Hercules and Rosebery (Zaw, 1991), Thalanga and Koongie Park (Hill and Orth, 1995) and Scuddles. At Gossan Hill, the nodular carbonate is dolomite. Carbonate nodules are generally rounded and show irregular gradational margins to chlorite-altered GG5 host. They may be overprinted by chlorite and coarser grained carbonate. Carbonate in these nodules does not form euhedral or well formed grains but occurs as a drusy fine grained carbonate mosaic. Nodules may coalesce to form anastomosing 10 cm to 1 m wide zones. Some nodular structures contain quartz in central portions of nodules. The occurrence of the carbonate nodular alteration is interpreted to be an overprint of earlier nodular silica alteration as evidence by dolomite replacement of microcrystalline quartz in many of the nodules. Direct comparison may be made between the carbonate and silica alteration textures.

Unusual alteration minerals

Andalusite

Large, well formed, prismatic, variably altered laths of andalusite are observed in intensely chlorite altered GG4 units. Chloritoid also observed and is syn- to post-andalusite formation. Andalusite grains show a spectrum of textures. In least altered lithologies, andalusite occurs as well developed isolated tabular laths up to 3–4 mm. In strongly altered lithologies, relict andalusite laths consist of blocky tabular jigsaw-fit pieces. Andalusite laths and those consisting of blocky fragments are enclosed by pyrrhotite ± sphalerite ± magnetite ± pyrite rims. Textural associations of sulphide and oxide rims enclosing andalusite grains suggest these opaque phases formed post andalusite ± chloritoid development. Deformation in andalusite is reported by Ribbe (1982) to be common via gliding parallel to (001) and the (100) cleavage directions. Blocky andalusite aggregates observed at Gossan Hill are consistent with this type of deformation. Opaque phases are interpreted to have developed along these preferred orientations to form rims around, and through, andalusite grains.

Andalusite appears to have formed early in the alteration-mineralisation history of Gossan Hill. Andalusites show overprint by chlorite and all opaque phases associated with alteration and mineralisation. The formation of andalusite is not ascribed to localised post-folding intrusive phases and is inferred to have developed as a result of either contact metamorphism due to granitoid intrusion pre- /syn-mineralisation or as a result of hydrothermal processes associated with mineralisation. The occurrence of andalusite ± chloritoid is rare and likely dependant on the composition of specific host units; being confined to beds rich in Al and Si. This occurrence corresponds to andalusite forming in GG4-type units that host constituents including resedimented glassy pyroclastic debris. As the andalusite is confined to discreet beds within the footwall sedimentary strata, its presence may reflect the original composition of those specific units.

Chloritoid

The occurrence of chloritoid at Gossan Hill is not as well constrained as the andalusite. Chloritoid is variably developed at Gossan Hill throughout GG6 strata as well as laterally distributed in host units to A, B and C zone. Chloritoid occurs as isolated well formed tabular grains and may also form 'bow tie' or 'fan tail' morphologies characteristic to chloritoid (Bearley, 1988; Agnew et al., unpub.) or interpenetrating, radiating to interlocking grain aggregates. Grain size rarely exceeds 1–2 mm, with grains hosted by fine grained chlorite. Chloritoid laths generally show random orientations in the host matrix. Evidence of brittle deformation includes grain dislocation structures that are well developed in zones of strong foliation. Ragged margins to well formed grains are indicative of chlorite replacement. Infrequently, chloritoid occurs hosted within andalusite grains suggestive of a pre- to syn-andalusite formation. Chloritoid also shows pseudomorphic replacement by microcrystalline silica, indicating silicification post chloritoid development.

Chloritoid laths have a spatial association with disseminated magnetite–ilmenite grains throughout the chlorite matrix. This association is observed by chloritoid laths rimmed or partially replaced along grain boundaries, cleavage planes and fractures by pyrrhotite ± magnetite ± ilmenite. Where such replacement occurs, replacement along twinning and cleavage planes in chloritoid aggregates forms a 'pseudo-dendritic' array of irregularly developed,

differentially oriented needle shaped grains of pyrrhotite ± magnetite. The random orientation and subsequent 'dendritic' appearance is a result of the original orientation of the chloritoid grains. Some chloritoid grains are preferentially replaced by pyrrhotite ± magnetite ± ilmenite phases and chlorite, which suggests preferential alteration due to compositional variations.

Chloritoid is commonly associated with regionally metamorphosed rocks, but may also form within contact metamorphic aureoles (Deer et al., 1992; Ribbe, 1982). Chloritoid associated with alteration systems of massive sulphide deposits has been reported by Franklin et al. (1975), Morton and Nebel (1984) and Agnew et al. (unpub). At Teutonic Bore, chloritoid (Fe-rich) alteration forms a discreet inner core portion of the inferred feeder zone (Agnew et al., unpub.), its development is correlated specifically to the original high alumina contents of host epiclastics. Similar occurrences of chloritoid ± andalusite are reported at the Mattabi massive sulphide deposit (Franklin et al., 1975), where both andalusite and chloritoid occur in the footwall alteration zone and are interpreted to represent metamorphic reactions involving Fe chlorite and hydrous aluminium silicate mineral (pyrophylite?) (Morton and Franklin, 1987).

Studies of chloritoid indicate its formation and stability have a strong dependence on the bulk composition of the original pelitic host (La Tour, 1980). Chloritoid will form in units whose bulk compositions meet the following criteria:

- comparatively high Al_2O_3 content
- low abundance of alkalis and CaO
- high $FeO^t/(FeO^t+MgO)$ ratio

At Gossan Hill the occurrence of chloritoid ± andalusite is interpreted to be in units containing at least some detritus of glassy and/or pumiceous nature. This is consistent with the observations and conclusions of LaTour (1980), who concluded that chloritoid (and andalusite) shows preferential development in units of comparatively elevated Al_2O_3 and low alkalis contents.

Summary

A, B and C zone represent a continuous zone of massive sphalerite–pyrite mineralisation hosted within a sandstone/siltstone package of GG6. Footwall rocks to zinc mineralisation contain hydrothermal siliceous alteration which is stratabound at A and B zones and crosscutting at C zone. The development and style of the alteration reflects not only intensity of the system, but the differential composition of the specific host unit interacting with the hydrothermal fluid. This is exemplified by glassy units which are preferentially chlorite altered as compared to fine grained, well sorted, volcanogenic siltstones and sandstones which are silica altered. Lateral migration of zinc-rich hydrothermal fluids via bedding parallel stringer veins at A and B zones selectively replaces apparently coarser (more permeable) thinly bedded horizons. Chlorite alteration is ubiqutously developed through GG4 and is host to copper-rich mineralisation. Pyrite–magnetite copper-rich zones represent a poorly constrained stockwork stringer zone.

Strong lithological control on the distribution of hydrothermal alteration is indicated by the stratabound nature of the altered and mineralised GG4 and GG6 members, as well as their apparent separation by comparatively less altered GG5 units. GG5 units contain a distinct carbonate nodular alteration style which is interpreted to have formed pre to syn silicification of the GG6 Member. In addition to the stratabound nature of the alteration and mineralisation, a spatial mineralogical zonation is evident. Siliceous alteration is associated with zinc mineralisation in the GG6 Member, whilst chlorite alteration dominates copper mineralised zones and oxides lenses of the GG4 Member.

References

Agnew, P. W., Clough, B. J. & Vaughn, J. P., unpublished. Stratigraphy and wallrock alteration of the Teutonic Bore Cu–Zn–Pb–Ag Deposit, Western Australia.

Ashley, P. M., Dudley, R. J., Lesh, R. H., Marr, J. M. & Ryall, A. W., 1988. The Scuddles Cu–Zn prospect, an Archean volcanogenic massive sulfide deposit, Golden Grove District, Western Australia. *Economic Geology* 83: 918–951.

Bearley, A. J., 1988. Chloritoid from low-grade pelitic rocks in North Wales. *Mineralogical Magazine* 52: 396.

Clifford, B. A., 1992. Facies and palaeoenvironment analysis of the Archean volcanic-sedimentary succession hosting the Golden Grove Cu-Zn massive sulphide deposits, Western Australia. Unpubl. PhD thesis, Department of Earth Sciences, Monash University.

Deer, W. A., Howie, R. A. & Zussman, J., 1992. *AN INTRODUCTION TO ROCK-FORMING MINERALS (second edition).* Longman, Hong Kong.

Duhig, N. C., Stoltz, J., Davidson, G. J. & Large, R.R., 1992. Cambrian microbial and silica gel textures in silica iron exhalites from the Mount Windsor volcanic belt, Australia: Their petrography, chemistry, and origin. *Economic Geology*, 87:764–784.

Franklin, J. M., Kasarda, J. & Poulsen, K. H., 1975. Petrology and chemistry of the alteration zone of the Mattabi massive sulfide deposit. *Economic Geology* 70: 63–73.

Frater, K. M., 1983. Geology of the Golden Grove prospect, Western Australia: a volcanogenic massive sulfide-magnetite deposit. *Economic Geology* 78: 875–919.

Fyffe, L. R., 1995. Regional geology and lithogeochemistry, in the vicinity of the Chester VMS deposit, Big Bald Mountain area, New Brunswick, Canada. *Exploration Mining Journal* 4(2): 153–173.

Gemmell, J. B. & Large, R.R., 1992. Stringer system and alteration zones underlying the Hellyer volcanic-hosted massive sulfide deposit, Tasmania, Australia. *Economic Geology* 87(3): 620–649.

Hill, A. & Orth, K., 1995. Textures and origins of carbonate associated with the volcanic-hosted massive sulfide deposit at Rosebery, Tasmania *In* Studies of VHMS-related alteration: geochemical and mineralogical vectors to ore. AMIRA/ARC Project P439 Rep. 1. Centre for Ore Deposit and Exploration Studies, University of Tasmania: 129–141.

Kalogeropoulos, S. I. & Scott, S. D., 1983. Mineralogy and geochemistry of tuffaceous exhalites (Tetsusekiei) of the Fukazawa Mine, Hokuroku district, Japan. *In* H. Ohmoto & B. J. Skinner (Eds.), *The Kuroko and related volcanogenic massive sulphide deposits, Economic Geology Mon.* 5: 412–432.

LaTour, T. E., Kerrich, R., Hodder, R. W. & Barnett, R. L., 1980. Chloritoid stability in very iron-rich altered pillow lavas. *Cont. Mineral. Petrol.* 74: 165–173.

Mill, J. H. A., 1990. The Scuddles base metal deposit: an exploration case history. *In* K. R. Glasson & J. H. Rattigan (Eds.), *Geological Aspects of the discovery of some important mineral deposits in Australia.* AusIMM Mon. Ser: 211–218.

Morton, R. L., & Franklin, J. M. (1987). Two fold classification of Archean volcanic associated massive sulfide deposits. *Economic Geology* 82: 1057–1063.

Morton, R. L., & Nebel, M. L., 1984. Hydrothermal alteration of felsic volcanic rocks at the Helen siderite deposit, Wawa, Ontario. *Economic Geology* 79: 1319–1333.

Pidgeon, R. T., Furfaro, D., & Clifford, B. A., 1994. Investigation of the age and rate of deposition of part of the Gossan Hill Group, Golden Grove using conventional single grain zircon U–Pb geochronolgy. *In* Geoscience Australia 1994 and beyond, 12th AGC, Perth: University of Western Australia 37: 346.

Pitt, J., 1990. The Gossan Hill deposit. *In* K. R. Glasson & J. H. Rattigan (Eds.), *Geological aspects of the discovery of some important mineral deposits in Australia* AusIMM Mon. Ser.: 103–106.

Ribbe, P. H., 1982. Kyanite, andalusite and other aluminium silicates *In P.H. Ribbe, Orthosilicates. Reviews in mineralogy,* 5(2nd edition), 189–214.

Watkins, K. P., & Hickman, A. H., 1990. Geological evolution and mineralization of the Murchison Province, Western Australia. *Geological Survey of Western Australia Bulletin* 137: 260–267.

Zaw, K., 1991. The effect of Devonian metamorphism on the mineralogy and geochemistry of the Cambrian VMS deposits in the Rosebery–Hercules district, western Tasmania. Unpubl. PhD thesis, University of Tasmania.

PIMA-II Spectral analysis of alteration associated with the Hellyer VHMS deposit: Preliminary results

Kai Yang, J. Bruce Gemmell and Russell Fulton
Mineral Mapping Technologies Group, CSIRO Exploration & Mining;
Centre for Ore Deposit and Exploration Studies, University of Tasmania

INTRODUCTION

AMIRA project P435 "Mineral Mapping with Field Spectroscopy for Exploration" (Project leader Jon Hunnington) is a multi-disciplinary research project focusing on the development of new, operational, field spectroscopic techniques for mapping mineral, soil and rock composition during exploration. The field portable spectrometer (PIMA-II) has brought the opportunity of applying this technology routinely to exploration programs. For example, the PIMA-II can easily map, in situ, hematite, geothite, smectite varieties, kaolinite, dickite, halloysite, sericite/illite varieties, gibbsite, jarosite, alunite, gypsum, pyrophyllite, amphiboles, opaline silica, carbonate species, epidote, talc, tremolite, chlorite varieties, phlogopite, and biotite.

As part of this project P435 several case histories of well documented alteration zones around selected mineral deposits are being undertaken. One of these case histories is the Hellyer VHMS deposit in Tasmania as the footwall alteration zonation (Gemmell and Large, 1992) and the hangingwall alteration (Jack, 1989) is well developed and preserved. AMIRA projects P435 and P439 started at roughly the same time and several companies are sponsors of both projects. These companies suggested that as the alteration at Hellyer was being investigated by both projects that we should collaborate. Both sponsor groups were approached and it was decided to combine research efforts to compare the spectral data from the PIMA-II generated from P435 with the detailed mineral chemistry and whole rock chemistry obtained from P439. From March 27–30 Kai Yang visited CODES and worked with Bruce Gemmell and Russell Fulton to obtain spectral data from selected drill core and rock pulps, previously used for whole rock analyses, from Hellyer. This paper reports some preliminary results from the study of the Hellyer material.

SAMPLES AND METHODS

Samples from 10 diamond drill-holes, comprising 293 pulverised composite samples (most representing a 10-metre interval) and 21 core splits (Table 1), were measured with the PIMA II portable infrared spectrometer. For each powder sample, one spectrum was collected; for each peace of core sample, two to four spectra, depending on the degree of heterogeneity of the sample as can be visually recognised, were obtained.

Table 1. Sample list

drill-hole	sample type	sample #	number of samples
HL 14	Pulp	333969 to 333977	14
HL 28	Pulp	334195 to 334206	12
HL 55	Core	334010 to 334033*	21
HL 57	Pulp	334207 to 334216	10
HL 306	Pulp	209598 to 209647	49
HL 840	Pulp	626260 to 626313	53
HL 841B	Pulp	626324 to 626419	80
HL 850	Pulp	629017 to 629045	27
MAC 19	Pulp	430563 to 430604	42
MAC 19	Pulp	622213 to 622219**	6

* not consecutive. ** 622214 missing.

Processing of raw reflectance spectra (e.g., smoothing spectra, generating hull quotient (HQ) and second-derivative spectra, and gaussian deconvolution) and extraction of various spectral parameters (e.g. wavelengths and intensities of absorption features) were carried out automatically by the software package XSPECTRA, which is developed by the Division of Exploration and Mining of CSIRO. Mineralogical interpretation of the SWIR spectra was made manually with reference to USGS Spectral Library and CSIRO spectral collections.

In the Hellyer samples only phyllosilicates and, in some cases, carbonate minerals were interpreted from the PIMA spectra. Other minerals that may be also present in the samples, such as plagioclase, quartz and sulphides, are not considered, as they show either very weak or no absorption features in the PIMA II wavelength region (1300–2500 nm).

For many of the samples, geochemical data were made available by Aberfoyle Resources Ltd and CODES. These data were used as references for the spectrally extracted (semi)quantitative mineralogical data (e.g. relative mineral abundances). To check the spectral data, additional mineral chemistry (by electron microprobe) and whole-rock potassium content (by gamma-ray spectrometry) were analysed in this study at the Division of Exploration and Mining, CSIRO.

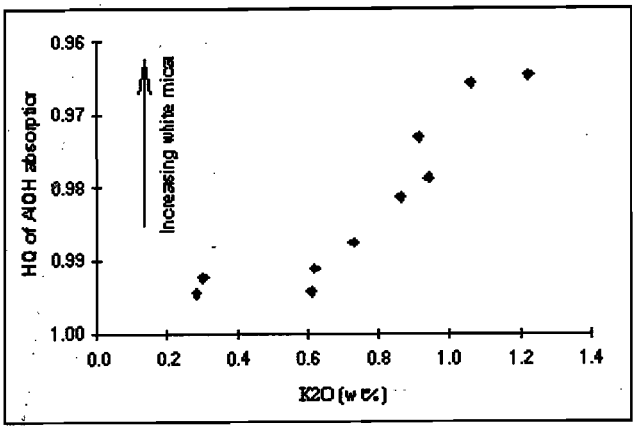

Fig. 1. Correlation between whole-rock K2O and hull quotient (HQ) of AlOH absorption for HL 28 hangingwall basalt samples. Lower HQ corresponds to higher AlOH intensity.

SUMMARY OF RESULTS

White mica

Intensity of mica AlOH absorption is a good index for mica abundance in the altered volcanics, as confirmed by the correlation between AlOH intensity and whole-rock K content (Fig. 1). Therefore, the AlOH intensity is a reliable parameter for mapping out the white mica content in the alteration zones.

Variable wavelength of the AlOH absorption of white mica indicates a wide range of cation substitution between Al and Fe, Mg and Cr in the octahedral site. Compositionally, white mica at Hellyer ranges from ordinary muscovite (represented by short-wavelength AlOH, 2200–2210 nm) towards phengite (represented by long-wavelength AlOH, > 2220 nm). In many samples, two populations of white mica, with short- and long-AlOH respectively, are evident.

Different types of mica composition, in relation to alteration zoning, have been observed at Hellyer:

1. In some drill-holes (e.g. HL 841B), the mica with long-wavelength AlOH (phengitic) tends to occur in the footwall alteration zones, and the trend of wavelength change is roughly in accordance with change in alteration intensity, especially in the hangingwall basalt (Fig. 2).

2. In others, however, the trend is not evident and phengitic muscovite is also observed in the hangingwall basalts (Fig. 3).

3. It appears that white mica with very short AlOH wavelength (< 2200 nm) formed preferentially in basaltic volcanics with high Cr content (e.g. Hellyer basalt).

4. Muscovites within the stringer zone may be more phengitic than those in the surrounding altered volcanics (e.g. HL 840, Fig. 4).

5. Within an alteration pipe (e.g. HL 306), the AlOH wavelength may change significantly but without any correlation with depth (Fig. 5).

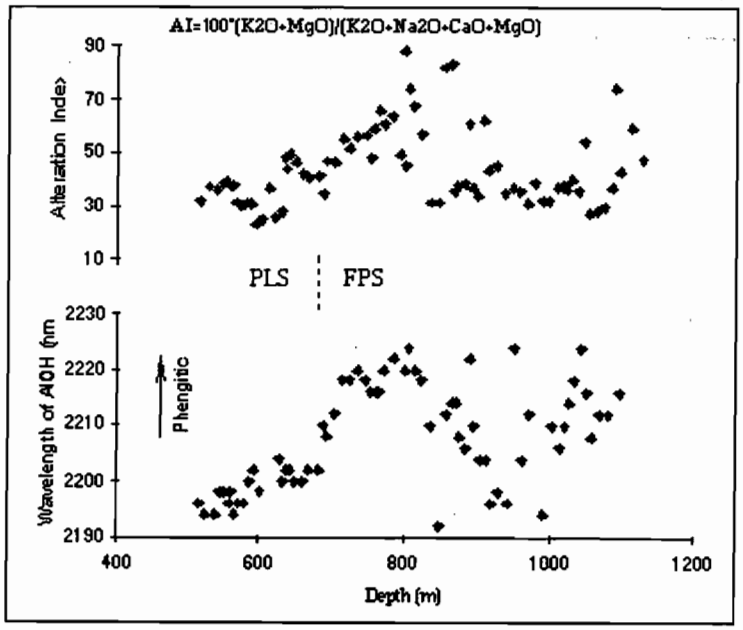

Fig. 2. Variation in wavelength of white mica AlOH absorption and Alteration Index through HL 841B. (PLS = Hellyer basalt-pillow lava sequence in the hangingwall, FPS = feldparphyric andesite in the footwall)

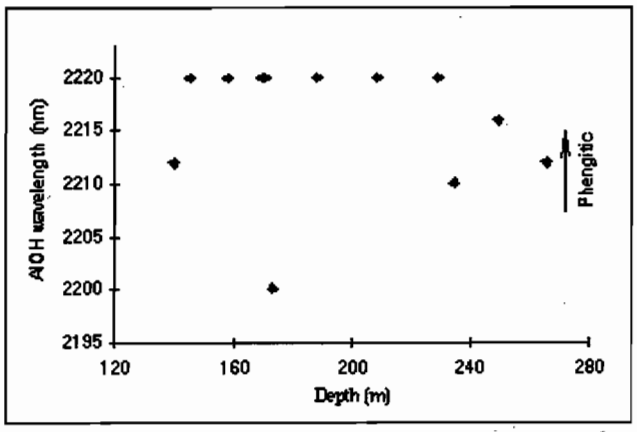

Fig. 3. Wavelength variation of white mica AlOH in Hellyer basalt from HL 28 samples.

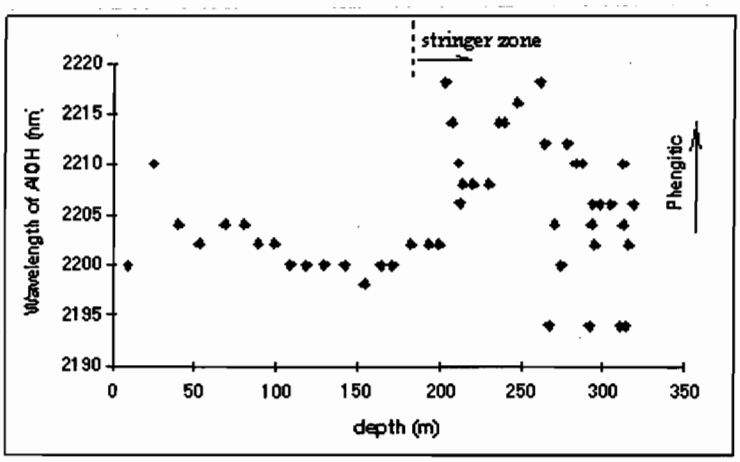

Fig. 4. Wavelength variation for white mica AlOH absorption through HL 840.

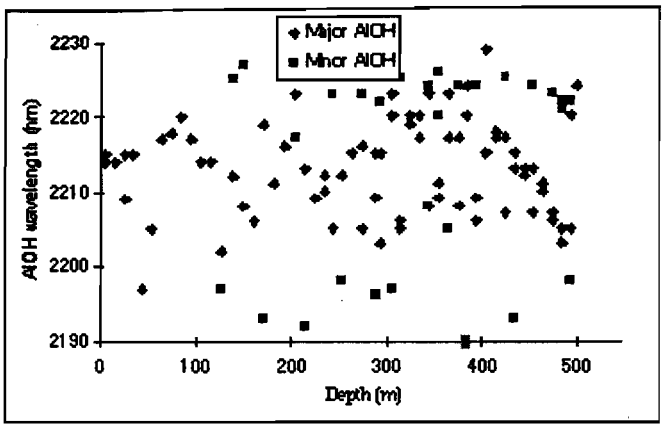

Fig. 5. Wavelengths of AlOH absorption in white mica from HL 306. The major and minor AlOH data points designate coexisting major and minor mica species.

Judged from the data obtained so far, there does not appear to be an unique, well-established relationship between mica composition (i.e. AlOH wavelength) and alteration zoning, although white mica in stringer zones and footwall andesites can be more Fe (and/or Mg)-rich than that in altered rocks outside the stringer zone and in hangingwall basalts, respectively.

In the hangingwall alteration plume at Hellyer a bright "granny smith apple green" mica, nominally called fuchsite, is very common. It has not been clearly demonstrated how the substitution of Cr for octahedral Al affects the wavelength of AlOH absorption. Limited microprobe analyses show minor Cr_2O_3 (< 1 wt%) present in many muscovites, and the AlOH wavelength of these mica is usually > 2210 nm. Therefore, the so-called phengitic muscovite as determined by the PIMA-II may include Cr-bearing species. Further research is ongoing to accurately separate the Cr-rich white micas from other species of white mica.

In summary, mapping the intensity and the wavelength of AlOH absorption is an effective way of delineating semi-quantitatively spatial distribution of white mica (abundance and composition). Mica composition varies widely in alteration systems. Although the variation may not be related to VHMS alteration zoning in a simple way at Hellyer, longer-AlOH mica (Fe and/or Mg-rich) tends to occur in more intensely altered parts. More work is underway to study this association.

Chlorite

Chlorite is another important mineral in the VHMS alteration systems. Chlorite abundance can be semi-quantitatively indexed by the intensity of the FeOH absorption minimum in the 2250–2265 nm region. Since no other coexisting phases absorb in this wavelength region, the FeOH intensity is ideal for mapping out chlorite in the alteration zones. As an example, Fig. 6 shows the change in relative abundance between mica and chlorite in drill-hole HL 306. In this drill-hole, the 270 m depth marks a significant change from silica and mica-dominated (above) to a chlorite-dominated assemblage (below). Visually this boundary has been put at approximately 350m (Gemmell and Large, 1992). The reliability of the FeOH intensity as the parameter for chlorite content is verified by whole-rock MgO data (Fig. 7).

Chlorite composition varies considerably in the Hellyer alteration system with depth as illustrated by the HL 306 samples. Firstly, the FeOH wavelength of chlorite (within the chlorite-rich zone) decreases with depth, indicating an increase in Mg#, whereas the chlorite in the upper muscovite-silica zone varies markedly in composition but without an obvious trend (Fig. 8). Secondly, with regard to interzonal changes, chlorite in the stringer zone may contains higher in Fe than that in the surrounding rocks (Fig. 9). Both modes of variation appear to suggest that in the footwall rocks relatively Fe-rich chlorite is proximal to the massive sulfide deposit. In the altered hangingwall Hellyer basalts, it was also observed that chlorite of lower Mg# tends to develop in the more intensely altered part (Fig. 10).

In summary, variations in both the abundance and the composition of chlorite are related to alteration intensity and zoning. Therefore, spectrally mapping out the FeOH feature (intensity and wavelength) can be of value to exploration.

K-feldspar

Although potassium feldspar alteration has been reported in the footwall at Que River (McGoldrick and Large, 1992) little has been reported of hydrothermal K-feldspar in the alteration systems at Hellyer. In this study, a K-feldspar enriched zone was found

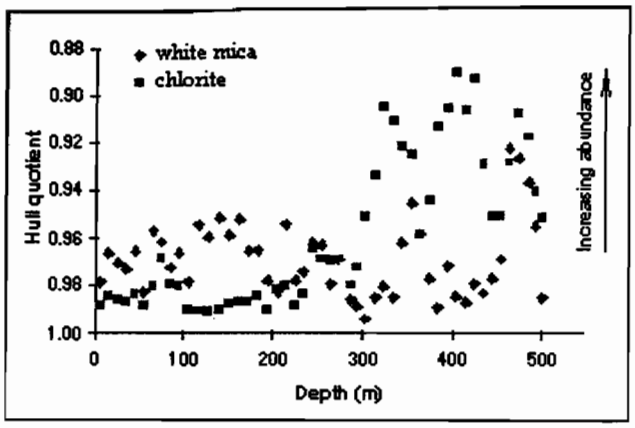

Fig. 6. Abundance variation of white mica and chlorite through HL 306. Notice the change at around 270 m depth from mica-domination to chlorite-domination. There are two narrow sections within the lower chlorite zone, where muscovite content sharply increases.

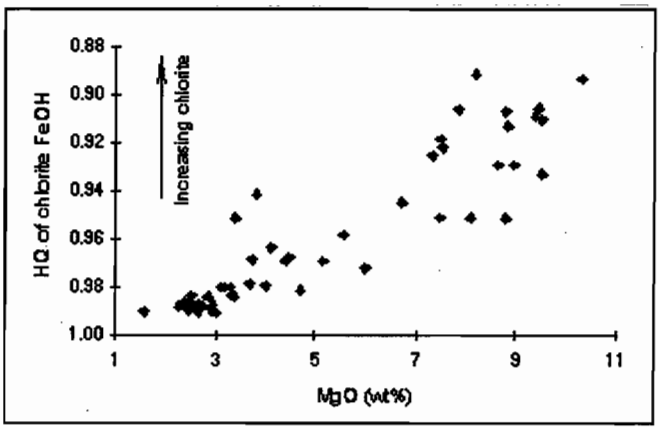

Fig. 7. Correlation between whole-rock MgO content and hull quotient (HQ) of chlorite FeOH absorption for samples from HL 306. Lower HQ value indicates higher chlorite content.

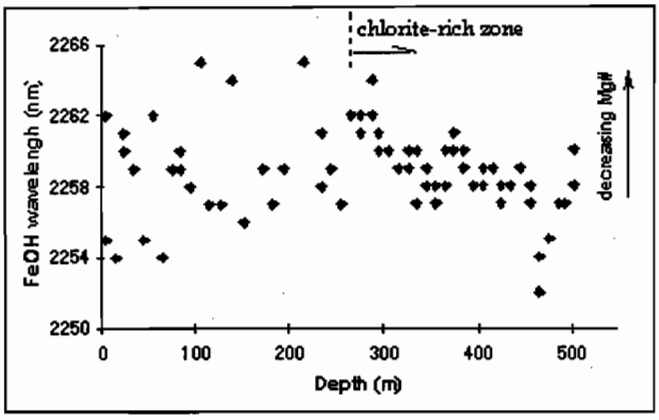

Fig. 8. Wavelength variation of FeOH absorption through HL 306. The chlorite-rich zone is defined based on the data presented in Fig. 6.

in the altered footwall in both HL 841B (at 741–870.3 m depth) and HL 840 (at 142–247 m depth). Although K-feldspar could not be directly identified by PIMA (absorptions not in the PIMA wavelength range), the potassium deficiency found by comparing the spectral mica abundance with whole-rock K content suggests presence of additional K-bearing phase in this interval (Fig. 11). Analysis by electron microprobe resulted in abundant secondary K-feldspar in selected samples. Texturally, the K-feldspar is associated with muscovite, chlorite, albite or quartz. Microprobe analysis of the K-feldspar has shown up to 1.36 wt% BaO, a feature common for hydrothermal K-feldspar in this type of environment. Host rocks of the K-feldspar-rich interval range from andesitic to basaltic (with minor dacite), and from lava, volcaniclastic to polymict. The nature and significance of secondary K-feldspar will to be further investigated.

Carbonates

Due to the problem of overlapping with both chlorite and mica spectra, carbonates are not the emphasis of this study. According to our limited spectral and probe data, calcite and dolomite-ankerite series are the main carbonate minerals in both the footwall and hangingwall volcanics.

Dickite

In one hangingwall basalt sample (HL 841B, 595.4 m) abundant dickite found as sub-rounded aggregates and appears to be of hydrothermal origin.

Prehnite

In all samples studied, the metamorphic mineral prehnite was spectrally evident only in one HL 55 sample. The scarcity of metamorphic minerals in the altered volcanics confirms that the altered rocks at Hellyer have only been weakly affected by later regional metamorphism. The grade of the metamorphism in the Que–Hellyer area is prehnite-pumpellyite (Gemmell and Large, 1992).

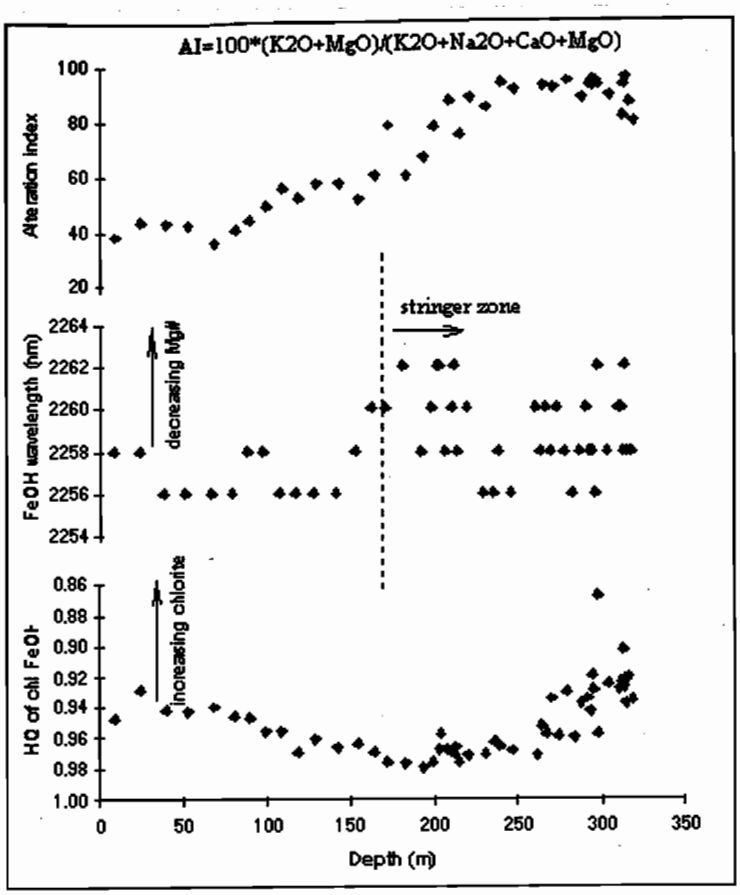

Fig. 9. Variations in wavelength and hull quotient (HQ) of chlorite FeOH absorption in drillhole HL 840. For comparison, change in alteration index (AI) through the hole is shown. Chlorite with higher Fe occurs in the stringer zone.

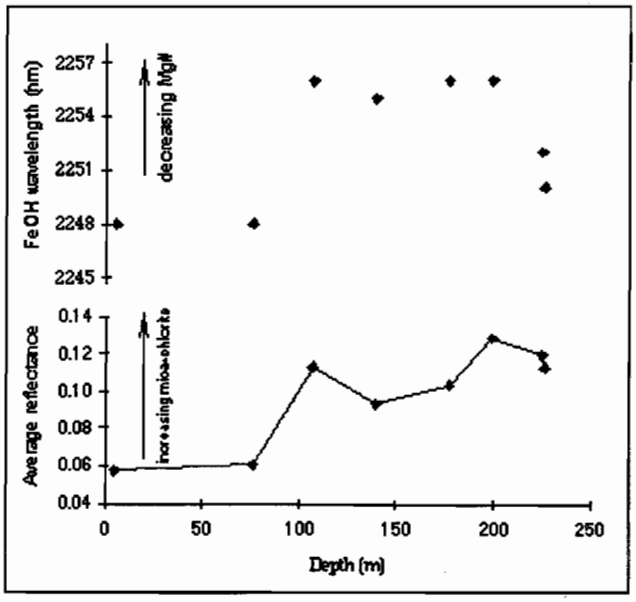

Fig. 10. Variation in wavelength of chlorite FeOH and average reflectance (relative to gold) of bulk-sample of the Hellyer basalt through HL 14. Increase in average reflectance is due mainly to increased phyllosilicate content.

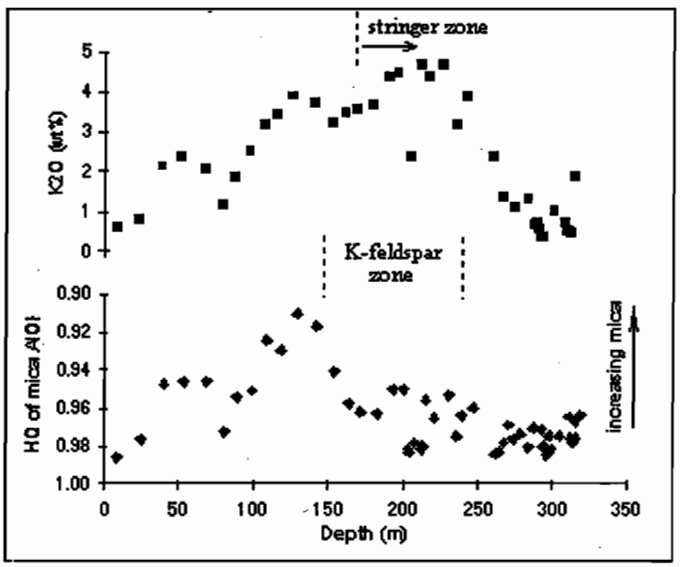

Fig. 11. Variations in whole-rock K (upper) and mica content (lower) in the footwall feldspar-phyric andesite in HL 840. The K-feldspar zone occurs in the interval where the trend of mica abundance does not match that of whole-rock K content.

References

Gemmell, J B and Large, R R, 1992, Stringer system and alteration zones underlying the Hellyer volcanogenic massive sulphide deposit, Tasmania, Australia, *Economic Geology* 87: 620–649.

Jack, D.J., 1989, Hellyer host rock alteration: Unpub. Masters thesis, University of Tasmania. 182 p.

Large, R R, 1992. Australian volcanic-hosted massive sulphide deposits: features, styles and genetic models, *Economic Geology* 87:471–510.

McGoldrick, P J and Large, R R, 1992. Geologic and geochemical controls on gold-rich stringer mineralisation in the Que River deposit, Tasmania, *Economic Geology* 87:667–685.

Database update

Nathan Duhig
Centre for Ore Deposit and Exploration Studies, University of Tasmania

Progress on the database has been slow since the last report (Duhig 1995). The main development has been to combine our database with the publicly released ISM data. This has resulted in a database of over 2100 records. As expected there were many samples that appeared in each database; these were weeded out prior to integration. Oddly, some replicated samples contained slightly different analyses for the same sample and every effort was made to ensure that the integrity of the data was maintained.

The database that was donated by Pasminco Exploration has undergone some manipulation but has not been integrated with the other databases for two reasons. Firstly, descriptive information is lacking for about half the data and that which is present is coded at a fairly basic level, limiting its usefulness. Secondly, it was predicted by Pasminco that about 90% of it was open file, and as such will (eventually) be released by the Mines Department.

A preliminary interpretation of the database is given by Stolz et al. (this volume) and Large et al. (this volume).

Duhig, N., 1995 *GIS Report.* AMIRA/ARC Project P439, Report No. 1, Nov. 1995. pp29-38.

Progress report on the utilisation of the Mount Read Volcanics database

Joe Stolz, Ross Large and Nathan Duhig
Centre for Ore Deposit and Exploration Studies, University of Tasmania

Aims and Strategy

The geochemical database for the Mount Read Volcanics has been compiled to enable evaluation of all the available data for the volcanic belt from a variety of sources in order to assess the geochemical variability that has developed in response to a range of process, but particularly different styles of hydrothermal alteration.

The ultimate aim of the project is to assess the Mount Read database in conjunction with our control dataset derived from the regional traverses. Information about mineralogy, alteration style, and degree of alteration that we will have for the traverse samples is essential to fully understand and interpret the geochemical variability. Although this information is not available for the MRV database, we have undertaken a preliminary examination of the database to assess the gross variability in the geochemical data and to determine to what extent it reflects:

- primary magmatic variations
- variability due to relatively low temperature seafloor alteration, and
- variability resulting from different styles of relatively high temperature hydrothermal alteration related either to seafloor massive sulphide hydrotheral systems or granitoid-related fluids.

Primary Magmatic Variations

A direct comparison with a modern analogue of the MRV belt is not possible due to the scarcity of data that is available for calcalkaline volcanics presently being erupted in submarine settings. Sites of current back-arc basin formation on continental lithosphere such as the Okinawa Trough may be a good analogue of the setting in which the MRV were developed, but only very limited geochemical data are available for the volcanics hosting massive sulphides in this basin.

Many workers in the MRV have observed that the volcanics have chemical characteristics most similar to volcanics from mature island arc and continental margin arc settings, athough Berry and Crawford (1988) and Crawford et al. (1992) argued that the actual tectonic setting in which they were erupted was a post-collisional intracratonic rift. Regardless of the precise eruption setting, a comparison with modern arc volcanics provides a useful means of assessing the likely magnitude of the primary variations, and to what extent these have been preserved in the MRV despite the potential for modification by interaction with seawater, and subsequent regional metamorphism.

A large database for modern arcs is available for this purpose and several plots of major elements as functions of SiO_2 are shown in Figures 1-6 to demonstrate the chemical variation that may have characterised the Mt Read arc at the time of eruption. The plots principally employ data for very fresh modern volcanics spanning a wide range of silica contents from both oceanic and continental margin arcs. The plots have been restricted to include only the Sunda, Scotia, Aleutian and Andean arcs, although similar plots including data for other arcs show essentially the same patterns. The subduction-related character of arc rocks (and also the MRV) is depicted by the relatively low TiO_2 (generally < 1.5 wt.%; Fig. 1) and Nb contents of the most mafic eruptives compared with intraplate and mid-oceanic ridge volcanics. Of more importance with regard to alteration effects is the quite clear cut-offs in the range of Na_2O contents

for modern arc volcanics. There are few volcanics with less than 2 wt.% Na_2O (Fig. 4), and these are principally K-rich alkaline volcanics from the Sunda arc, whereas the maximum upper Na_2O content is ~ 5.5–6.0 wt.%. Variation of K_2O in modern arcs is much more pronounced, particularly for the Sunda arc. A plot of K_2O vs. SiO_2 (Fig. 3) shows the very large range in K contents for both the basic and silicic rocks. Many of the K-rich basic rocks are shoshonitic and potassic alkaline rocks with similarities to the Hellyer hangingwall basalts. This demonstrates the potential primary variability upon which alteration effects may have been superimposed.

In contrast some of the other major elements display very coherent chemical variations (e.g. SiO_2 vs Al_2O_3, CaO and MgO; Figs 2, 5, 6) which reflect the limited range of compositions that are produced by partial melting in the upper mantle, coupled with controls by crstal-liquid driven differentiation. However, these coherent trends would not be expected to survive most types of alteration. A plot of SiO_2 versus the Alteration Index of Ishikawa et al. (1976) (Fig. 7; Alteration Index = $(100(K_2O+MgO)/(K_2O+MgO+Na_2O+CaO))$ for the unaltered arc rocks indicates that the bulk of these volcanics fall in a very restricted field with values <40–50. The slight increase in alteration index at lower silica contents seems to reflect the quite primitive (Mg-rich) potassic alkaline rocks which despite relatively high CaO also have low Na_2O. The increase in alteration index at the higher silica contents also seems to reflect K-rich rhyolitic rocks with relatively low CaO and Na_2O. Plots of Na_2O and K_2O as functions of Alteration Index (Figs 8, 9) also show very tight groupings with the great majority of samples having Na_2O of 2–6 wt.% and Alteration Indices of 20–50. For the same range of Alteration Indices the same volcanics have K_2O contents of 0.1–5 wt.%.

Although data for the base metals (Cu, Zn and Pb) are only available for a portion of the modern arc database, the upper limits of the concentrations of these elements in these volcanics (Figs 10, 11, 12) provide a useful indication of the thresholds above which base metal concentrations may be regarded as anomalous. Zinc concentrations increase slightly from the basic to intermediate rocks reaching a maximum of about 150 ppm Zn and decreasing systematically to values of 10–50 ppm in the most silicic volcanics. The Cu data are much more scattered, particularly for the intermediate rocks, although some individual data sets show more coherent variations which are similar to Zn. Cu concentrations of the silicic rocks are generally <10–20 ppm. Pb concentrations in the mafic rocks are generally < 1-2 ppm and increase to a maxima of about 25–30 ppm in the silicic variants.

The MRV Database

In this preliminary examination of the MRV database, the analyses have been grouped on the basis of the major formation in which they occur (i.e. Que–Hellyer — equivalent to the Mt Charter Group, CVC, Tyndall and Eastern Quartz-Phyric Sequence). No attempt has been made to filter the data on the basis of whether the rocks are coherent or volcaniclastic as both are likely to demonstrate broadly similar geochemical variability. However, other sedimentary rocks and unusual compositions such as the ultramafics etc have been removed.

As expected, in plots similar to those for the unaltered arc rocks (Figs 13–17), the MRV data generally show much greater variability reflecting the different styles and degrees of alteration. This is perhaps best illustrated in the plots of Na_2O and K_2O versus Alteration Index (Figs 19, 20) where rocks with very high A.I. values (>70–80) and high K_2O represent strongly sericite altered volcanics. Samples with similar A.I. values but low K_2O most likely represent strongly chlorite altered material, and there appears to be a continuum of compositions between these extremes. On the other hand volcanics with A.I. values < 20, coupled with high Na_2O and low K_2O most likely represent albite altered samples, and samples with intermediate A.I. values but very low Na_2O contents are probably dominantly carbonate altered.

Base metal concentrations display no strong correlation with the Alteration Index (Figs 21, 22, 23), although the highest Cu concentrations occur in the rocks with the highest A.I. values, and many samples with A.I. values in the 'unaltered' range have significantly higher Zn and Pb concentrations than the modern arc suites. Somewhat surprising is the large number of samples with high A.I. values but relatively low Cu, Zn and Pb concentrations. Some of

these may represent leached footwall rocks peripheral to major fluid conduits.

Summary

A preliminary examination of the MRV database has been undertaken to assess the gross chemical variability in the data set and the likely causes of this variability. Comparisons with a large database for modern unaltered volcanics from both oceanic and continental margin arc settings provides useful constraints on the likely variability in the MRV database that could be due to primary magmatic compositions. The modern unaltered volcanics display a very limited range of values for the traditional Alteration Index (20–50) compared with the MRV database. Samples with A.I. values <20 appear to be characterised by albitic alteration, whereas the Ca and Na depletion which accompanies feldspar breakdown and development of sericite and chlorite results in the characteristic high A.I. values (>80). Samples with substantial carbonate alteration commonly have values for the A.I. in the range of unaltered volcanics. Minimum Na_2O contents of about 2 wt.% prior to alteration typify most arc volcanics except for unusual K-rich alkaline varieties. The unaltered island arc suites also indicate the very restricted ranges expected for base metal concentrations over a range of whole-rock compositions.

References

Berry, R.F. and Crawford, A.J., 1988. The tectonic significance of Cambrian allochthonous mafic-ultramafic complexes in Tasmania. *Australian Journal of Earth Sciences* 35: 523–533.

Crawford, A.J., Corbett, K.D. and Everard, J.L., 1992. Geochemistry of the Cambrian volcanic-hosted massive sulfide-rich Mount Read volcanics, Tasmania and some tectonic implications. *Economic Geology* 87: 597–619.

Ishikawa, Y., Sawaguchi, T., Iwaya, S. and Horiachi, M., 1976. Delineation of prospecting targets for Kuroko deposits based on modes of volcanism of underlying dacite and alteration halos. *Mining Geology* 26: 105–117.

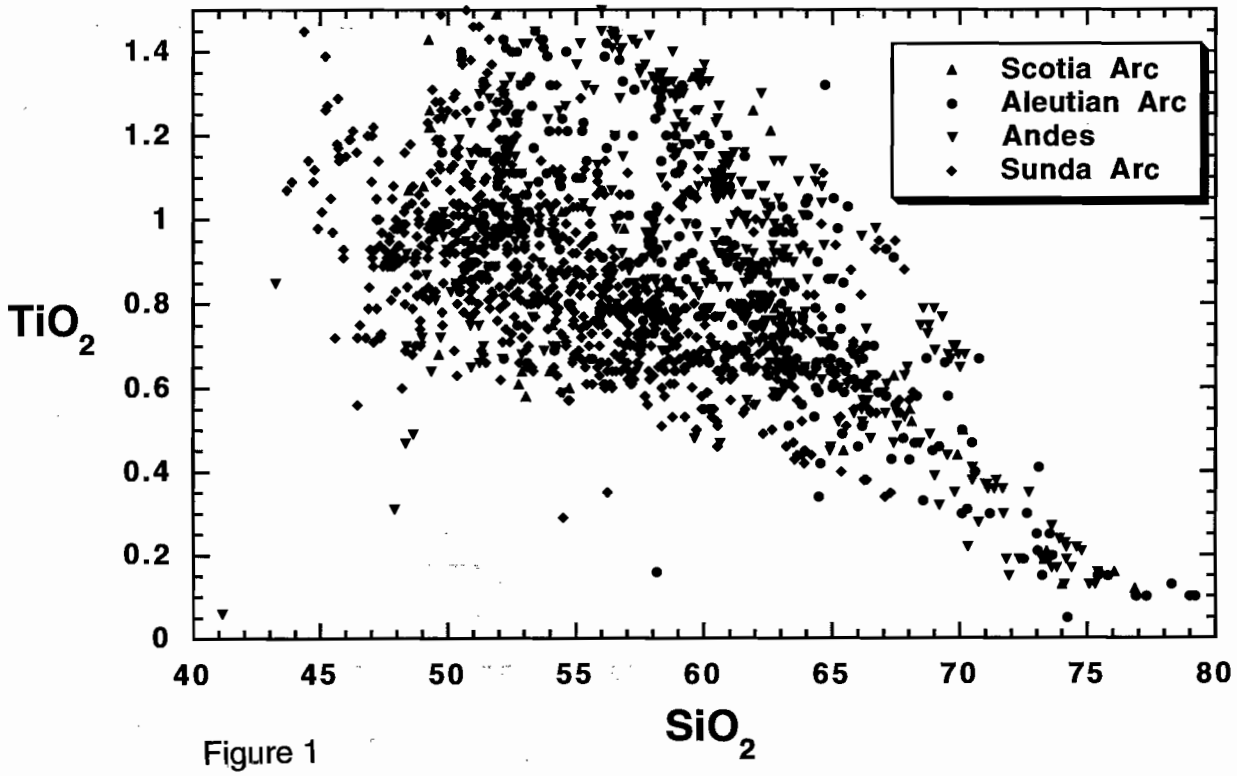

Figure 1

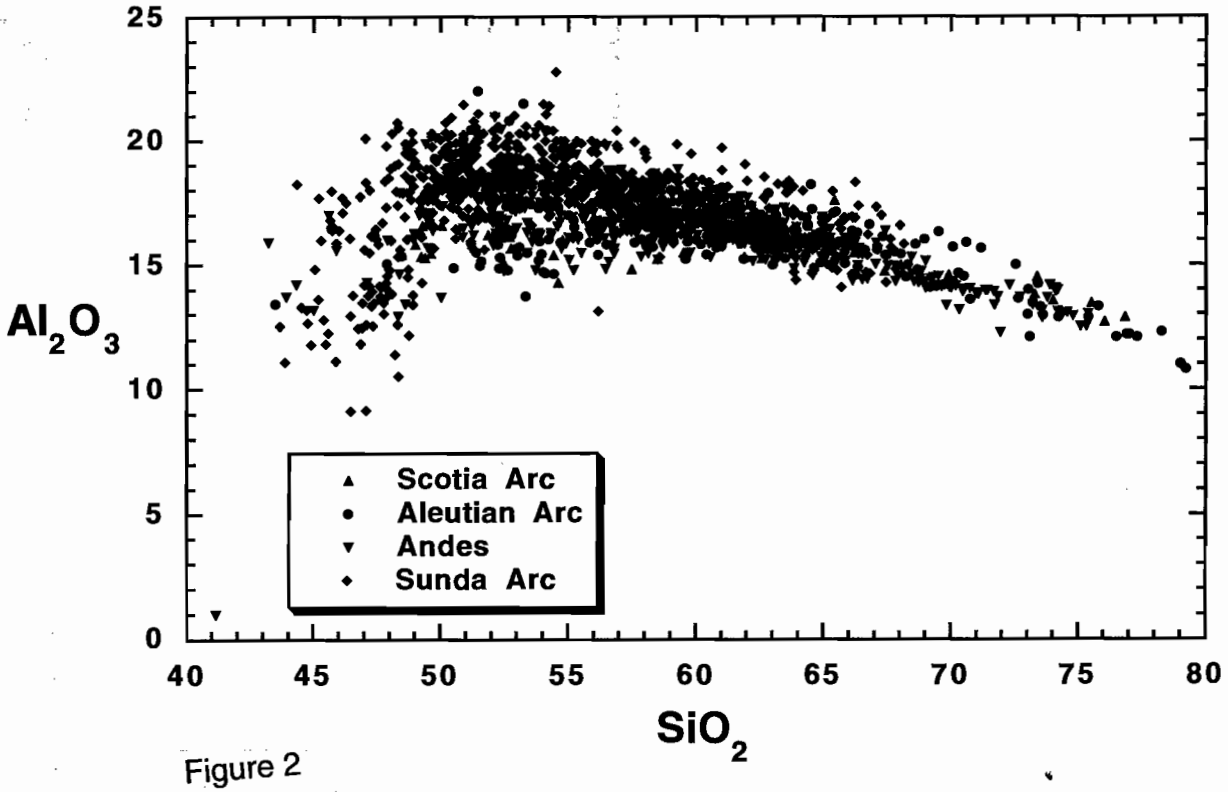

Figure 2

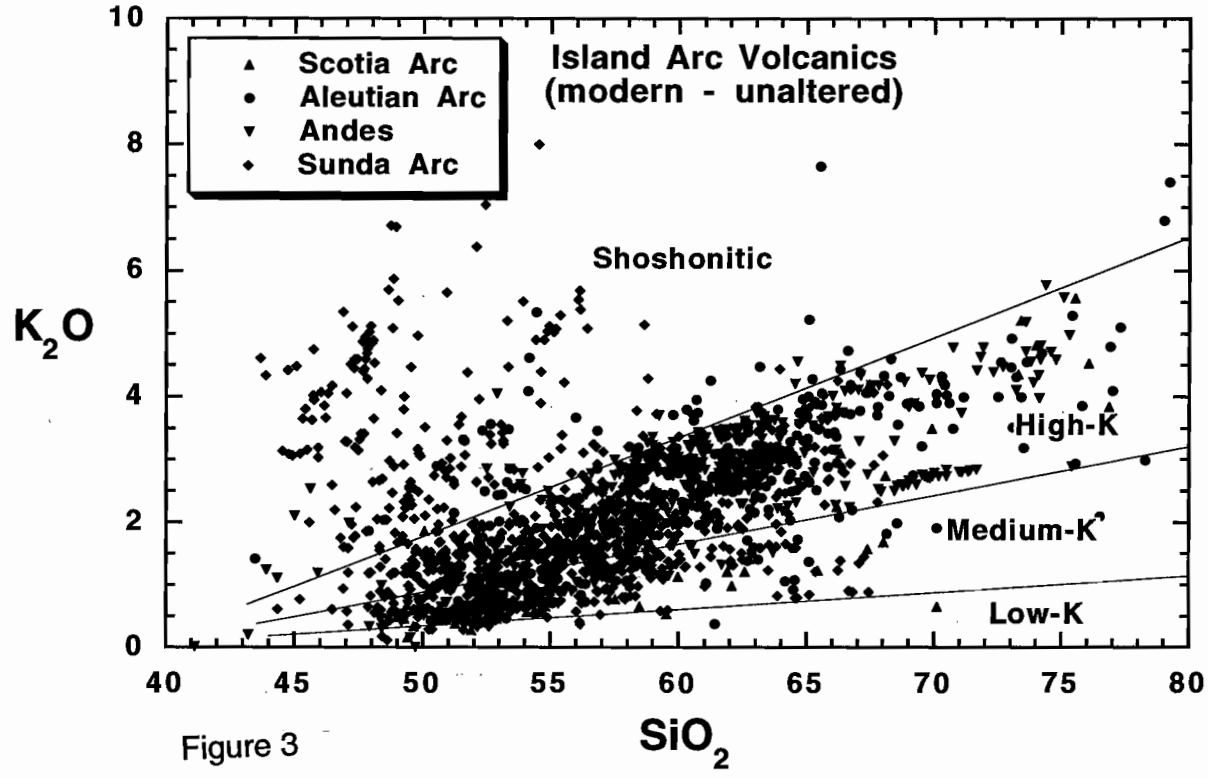

Figure 3

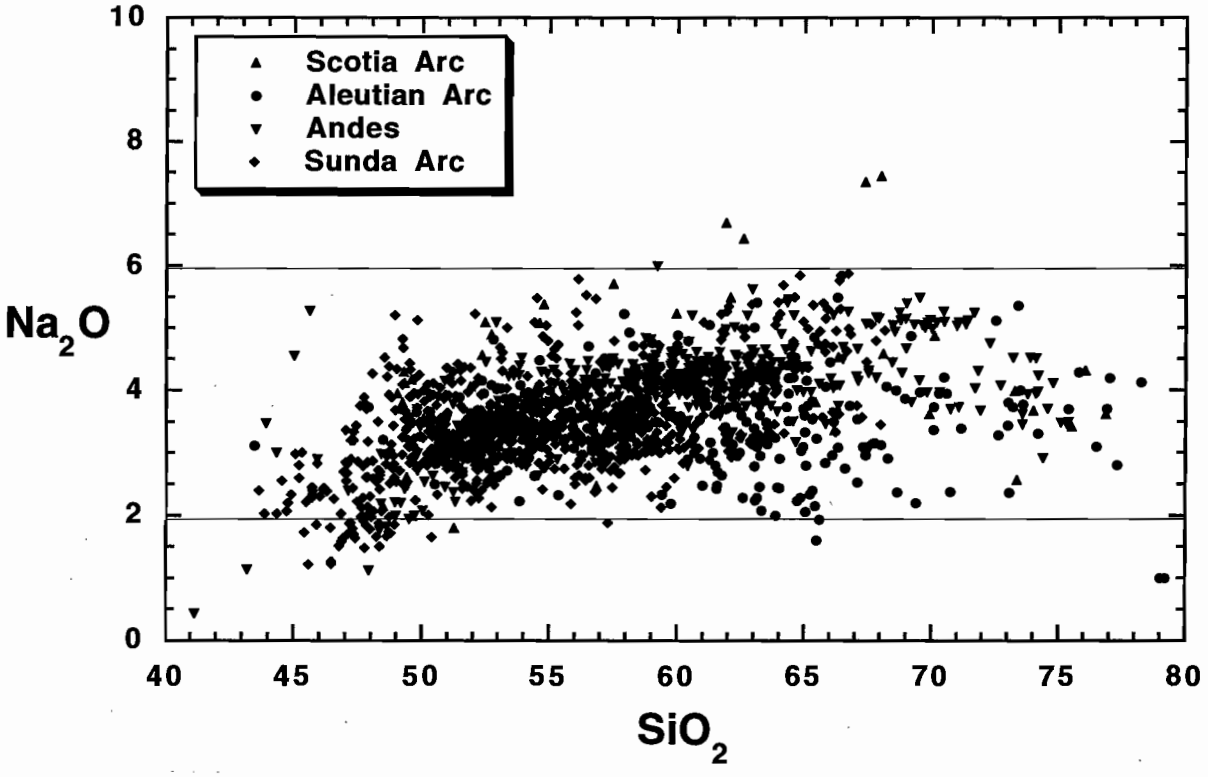

Figure 4

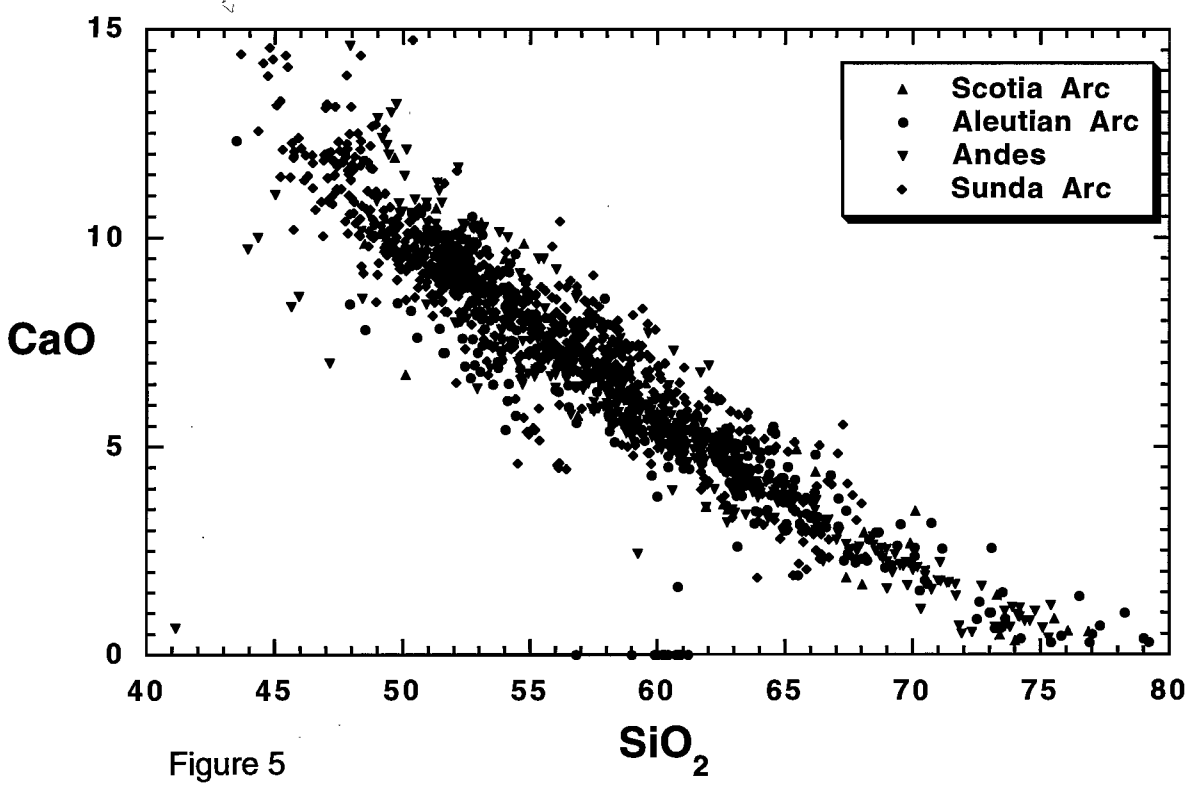

Figure 5

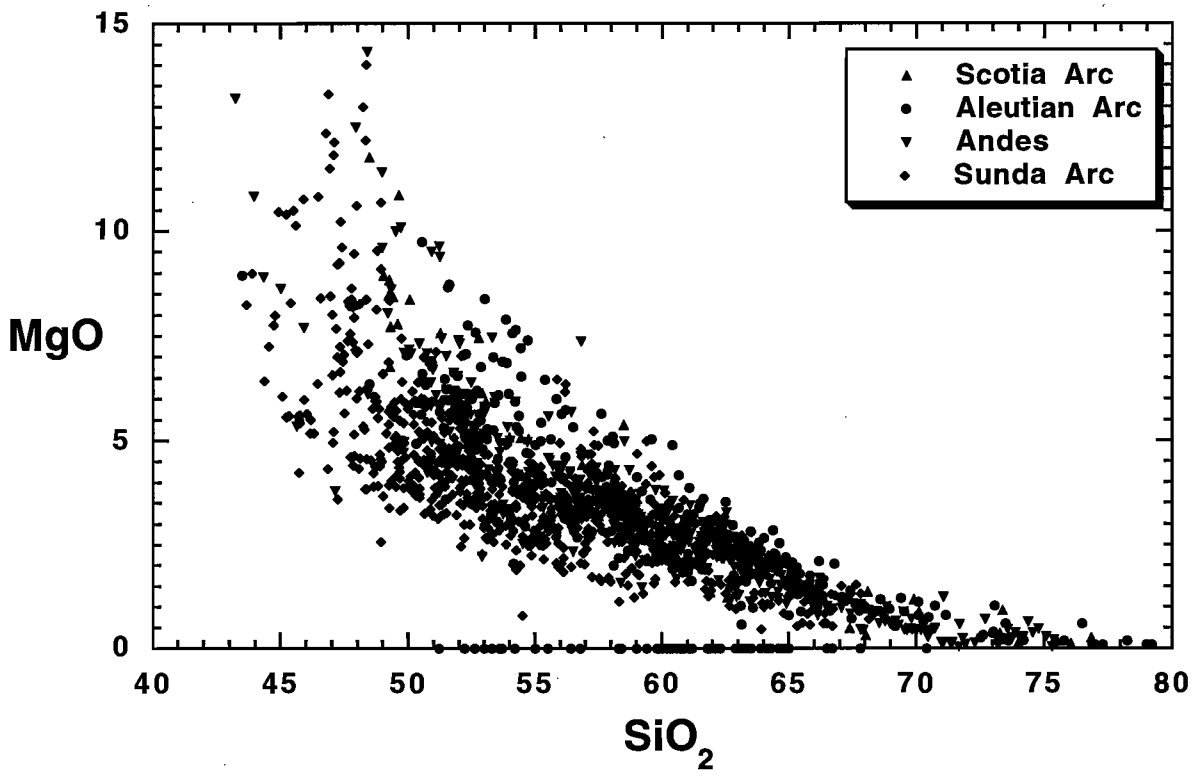

Figure 6

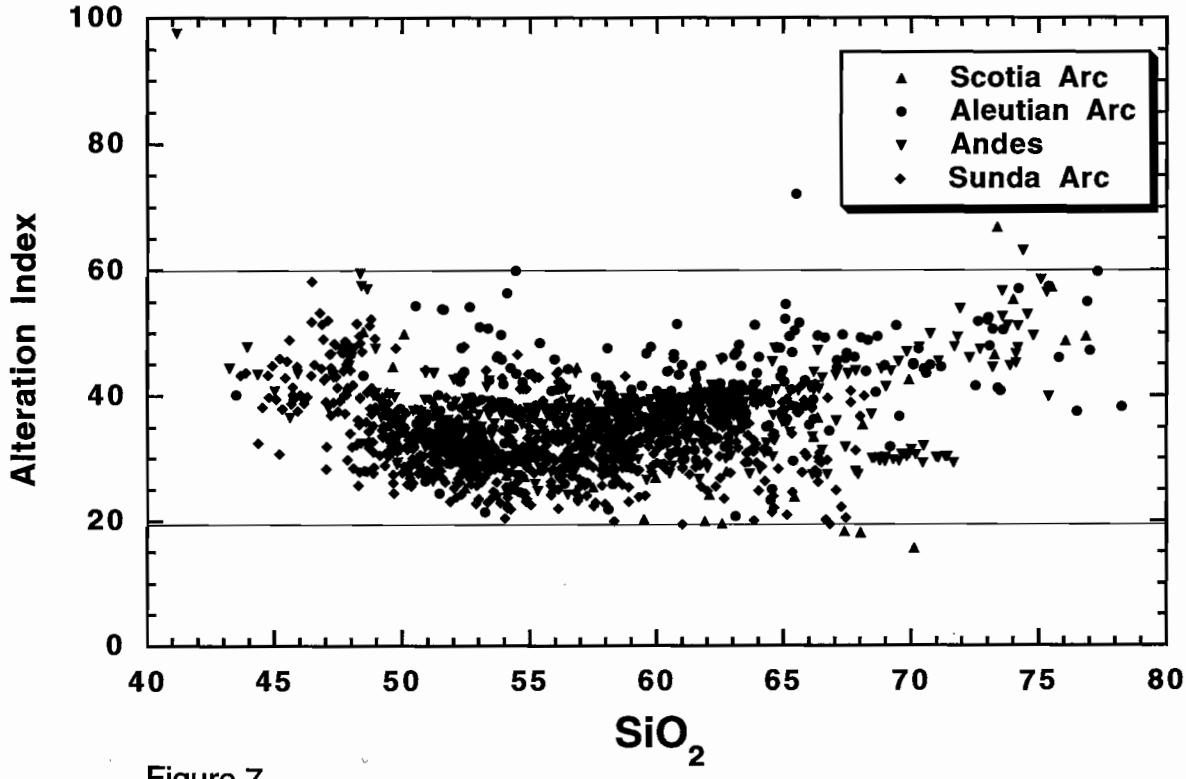
Alteration Index
100
80
60
40
20
0
40
45
50
55
60
65
70
75
80
SiO_2
Scotia Arc
Aleutian Arc
Andes
Sunda Arc

Figure 7

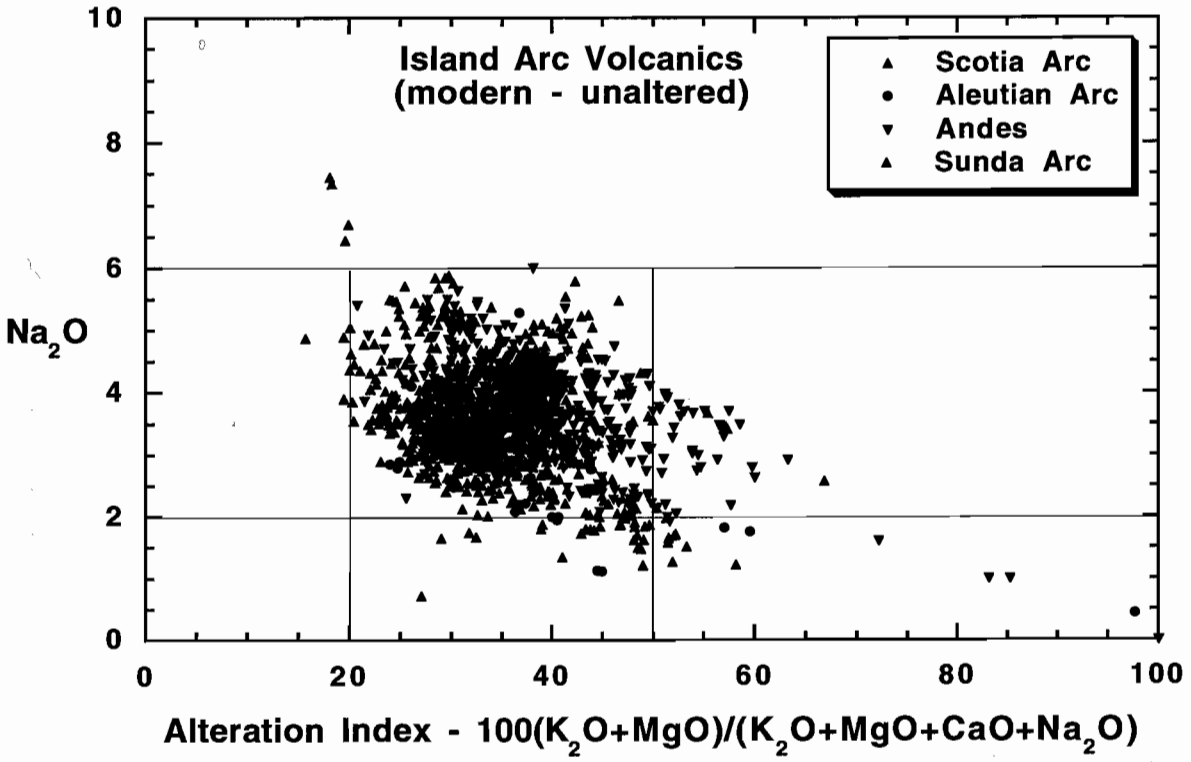

Figure 8

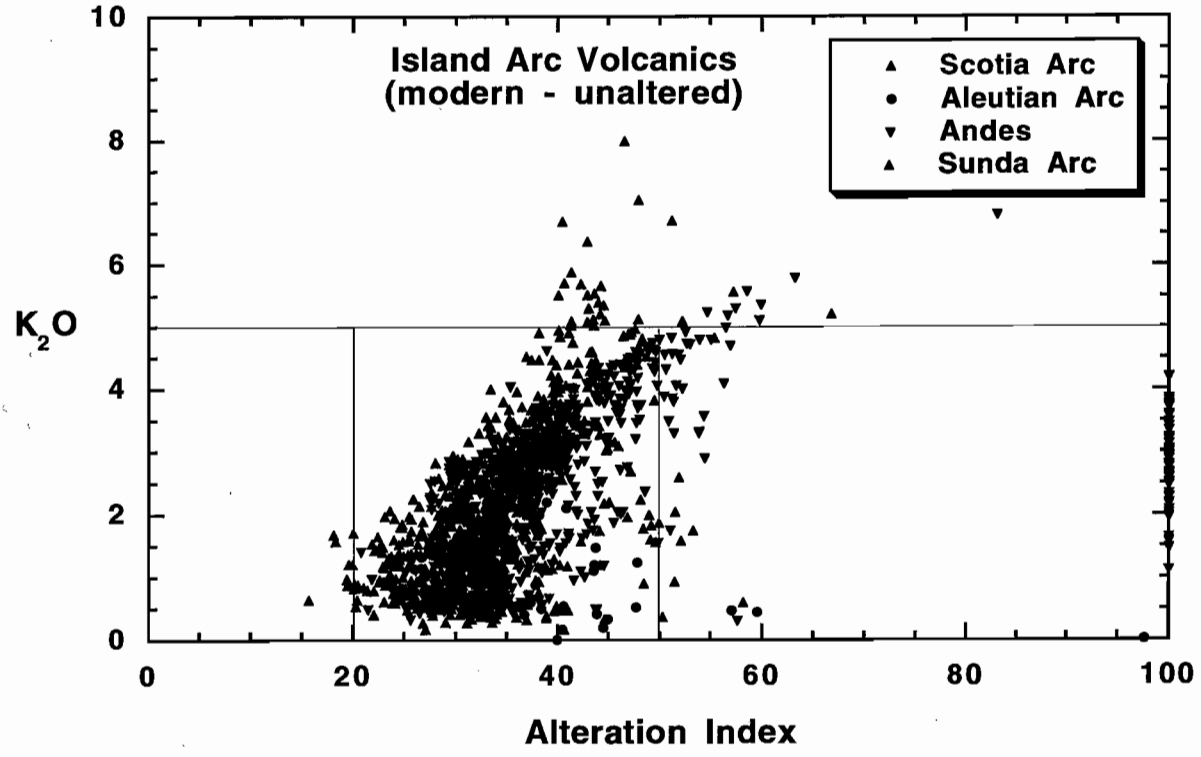

Figure 9

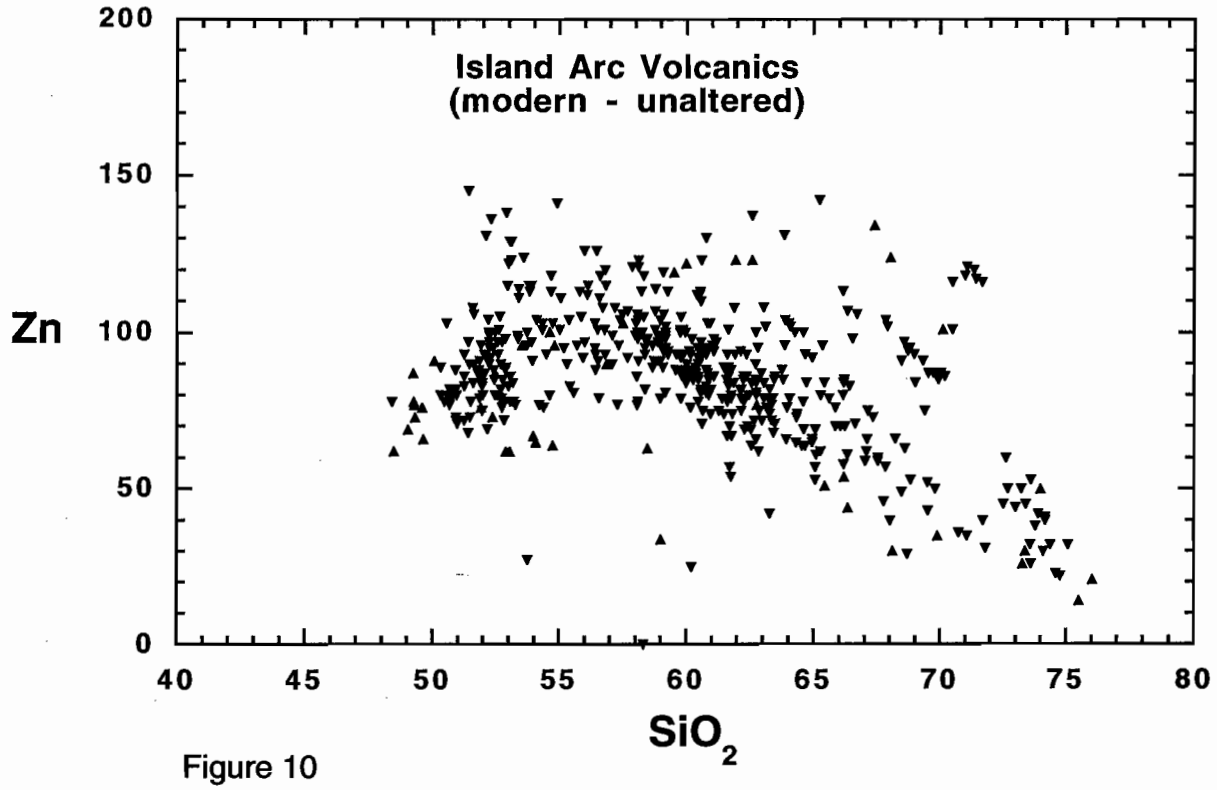

Figure 10

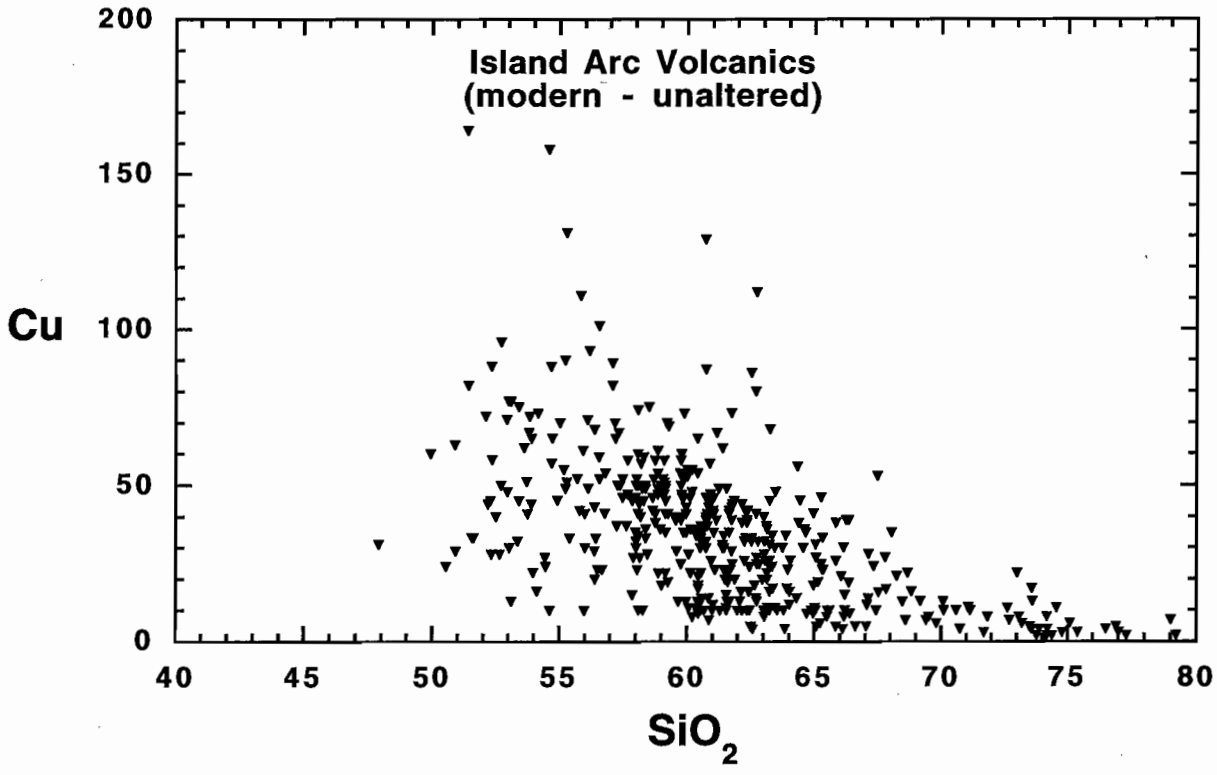

Figure 11

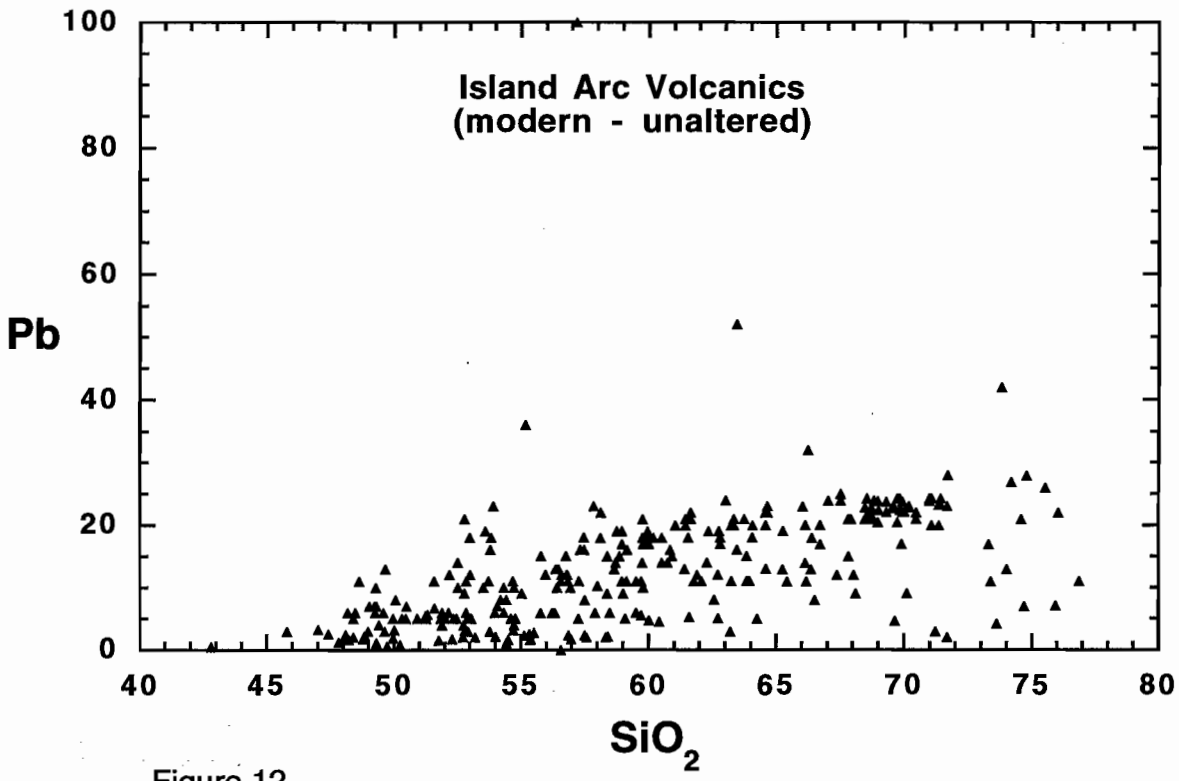
Island Arc Volcanics
(modern - unaltered)
Pb
100
80
60
40
20
0
40
45
50
55
60
65
70
75
80
SiO2

Figure 12

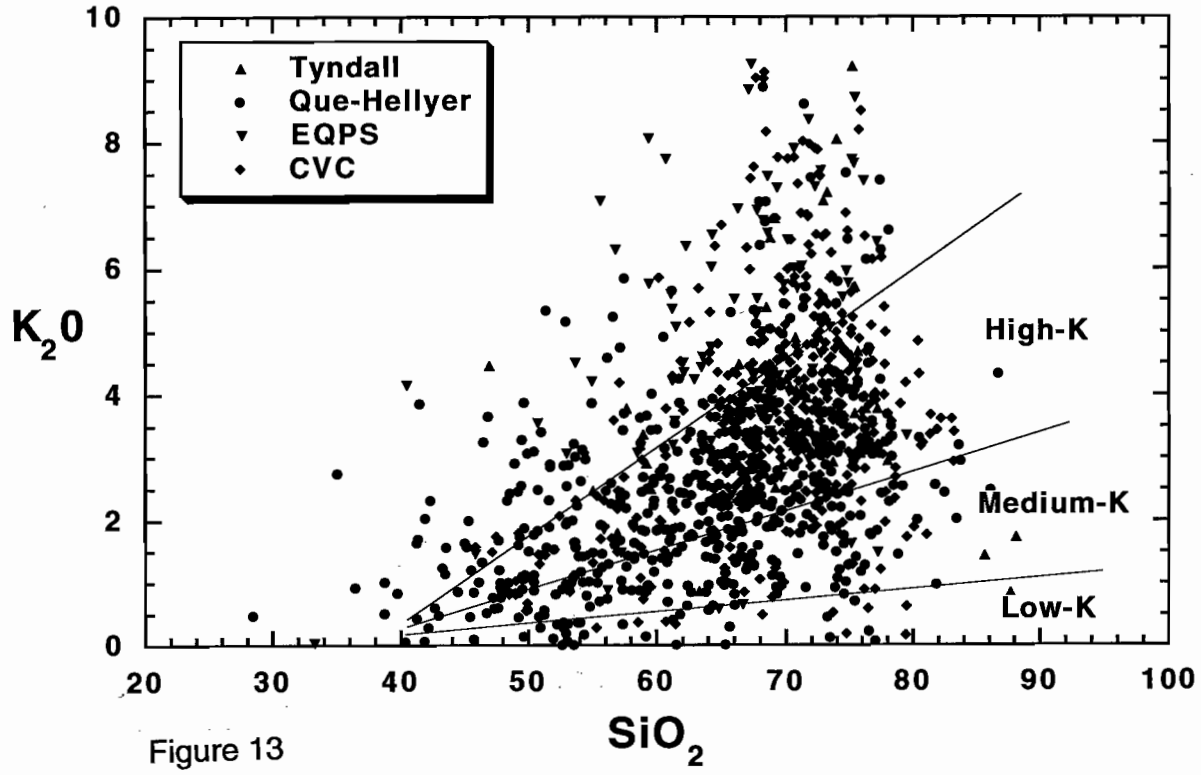

Figure 13

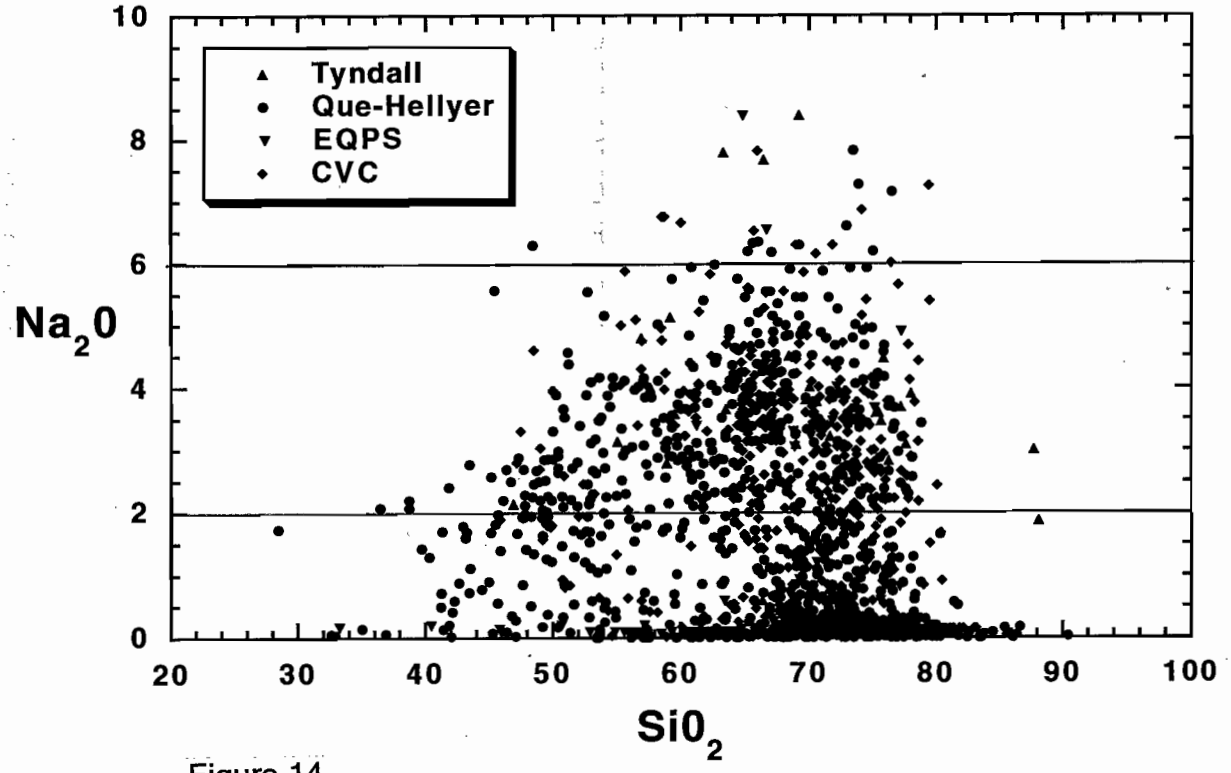

Figure 14

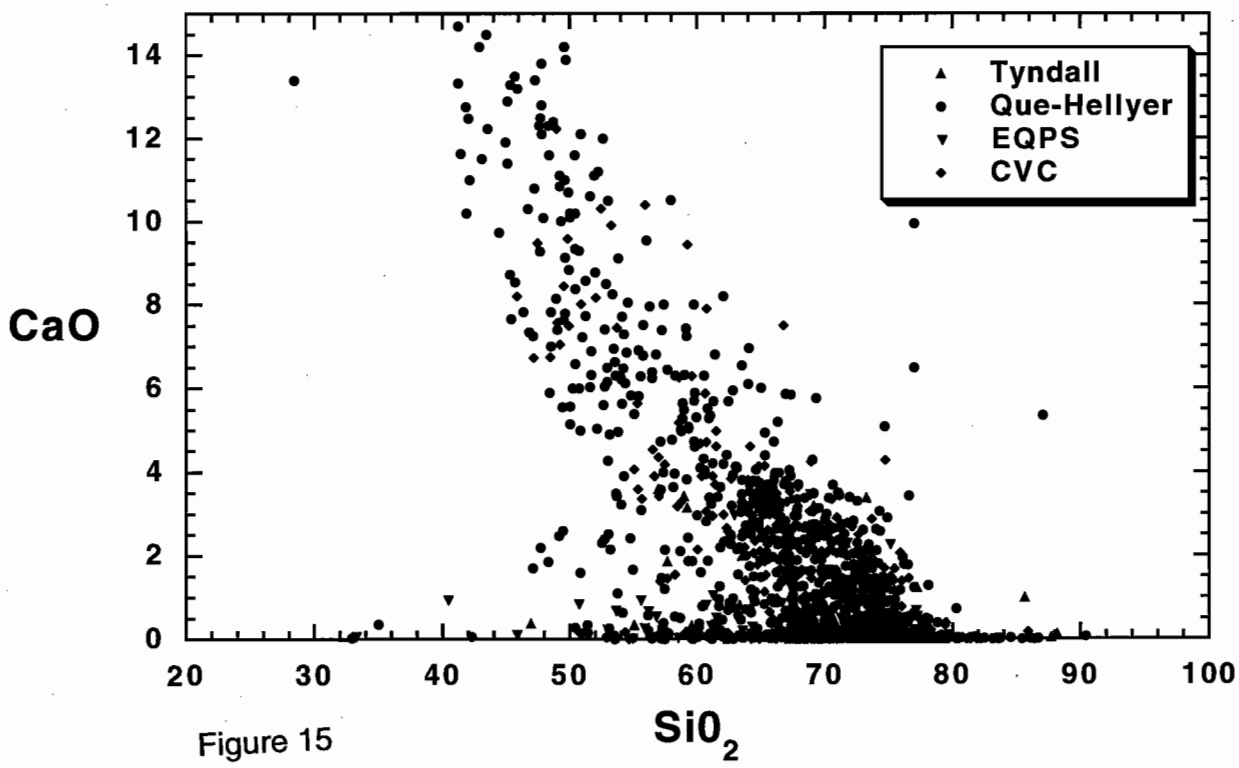

Figure 15

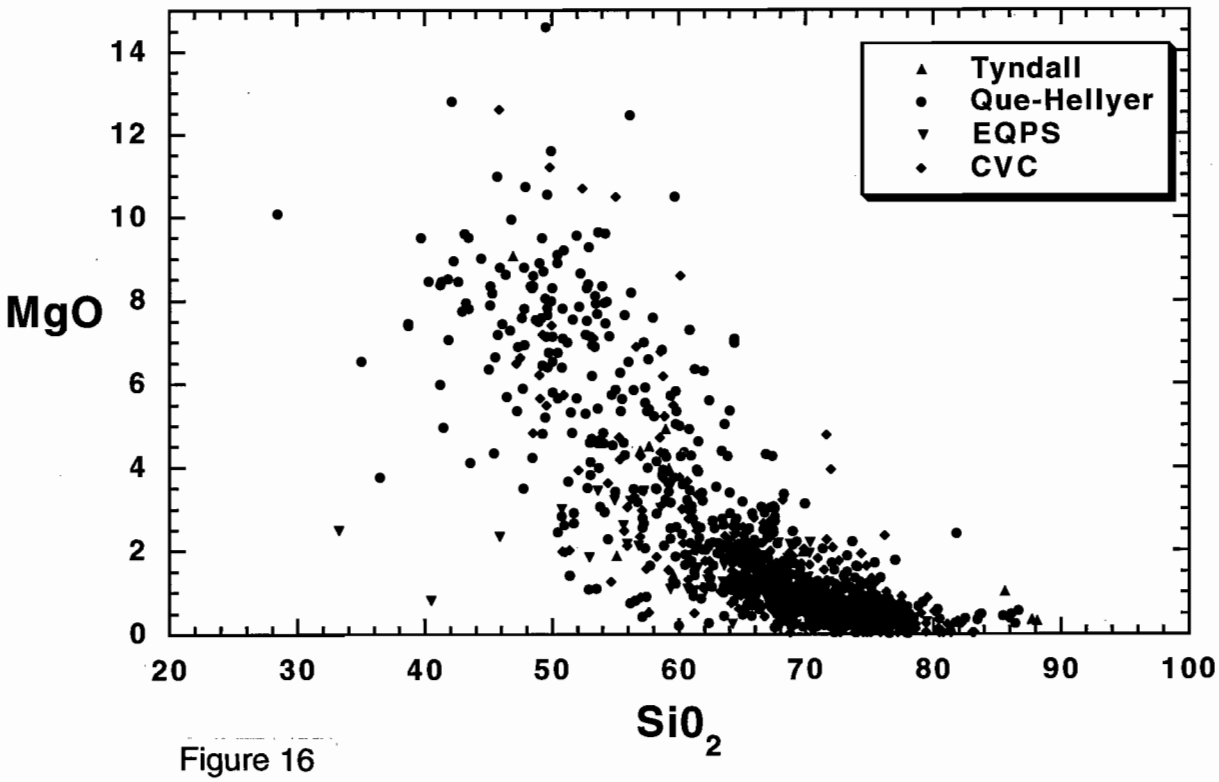

Figure 16

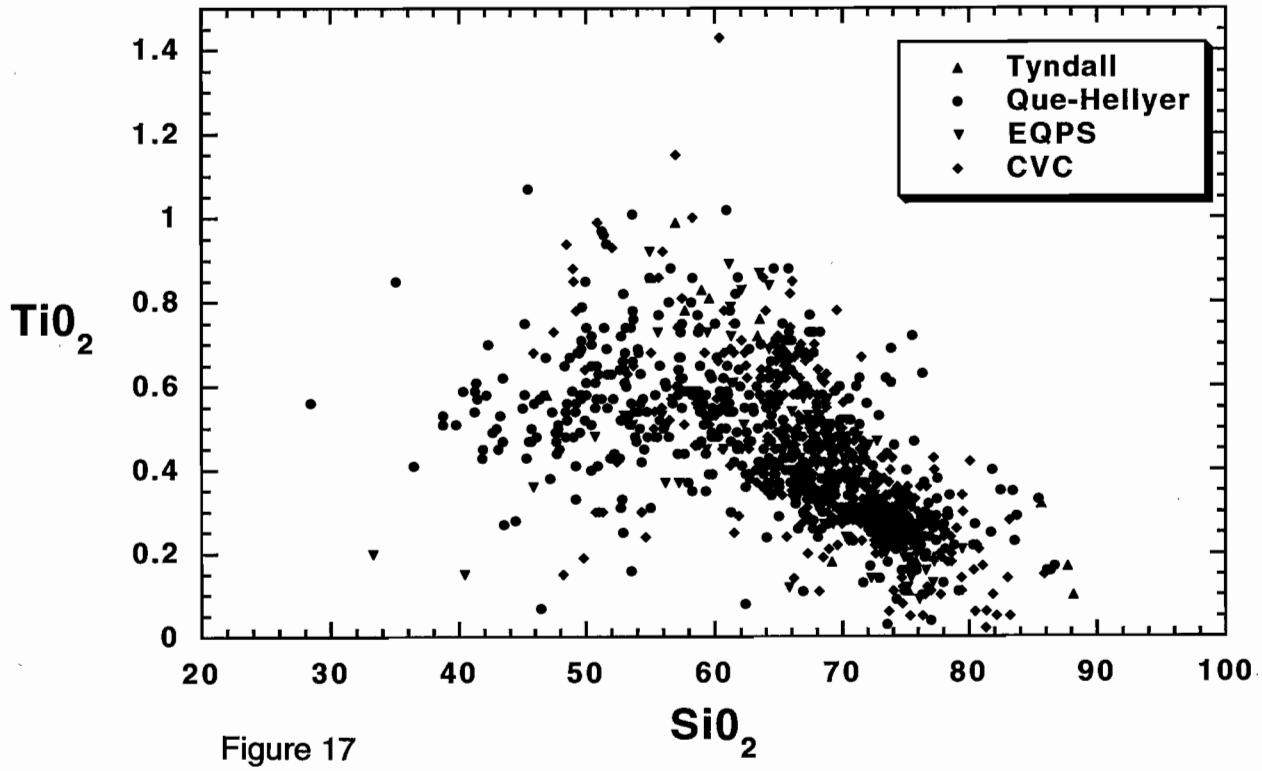

Figure 17

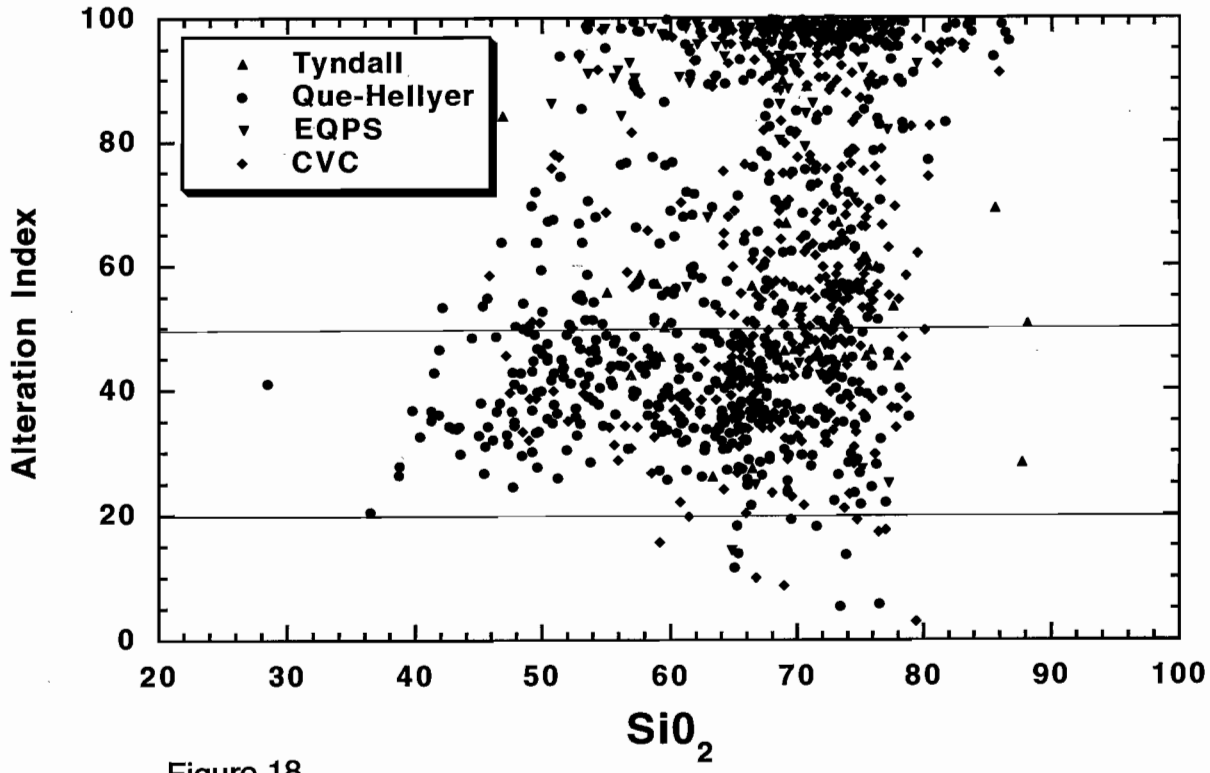

Figure 18

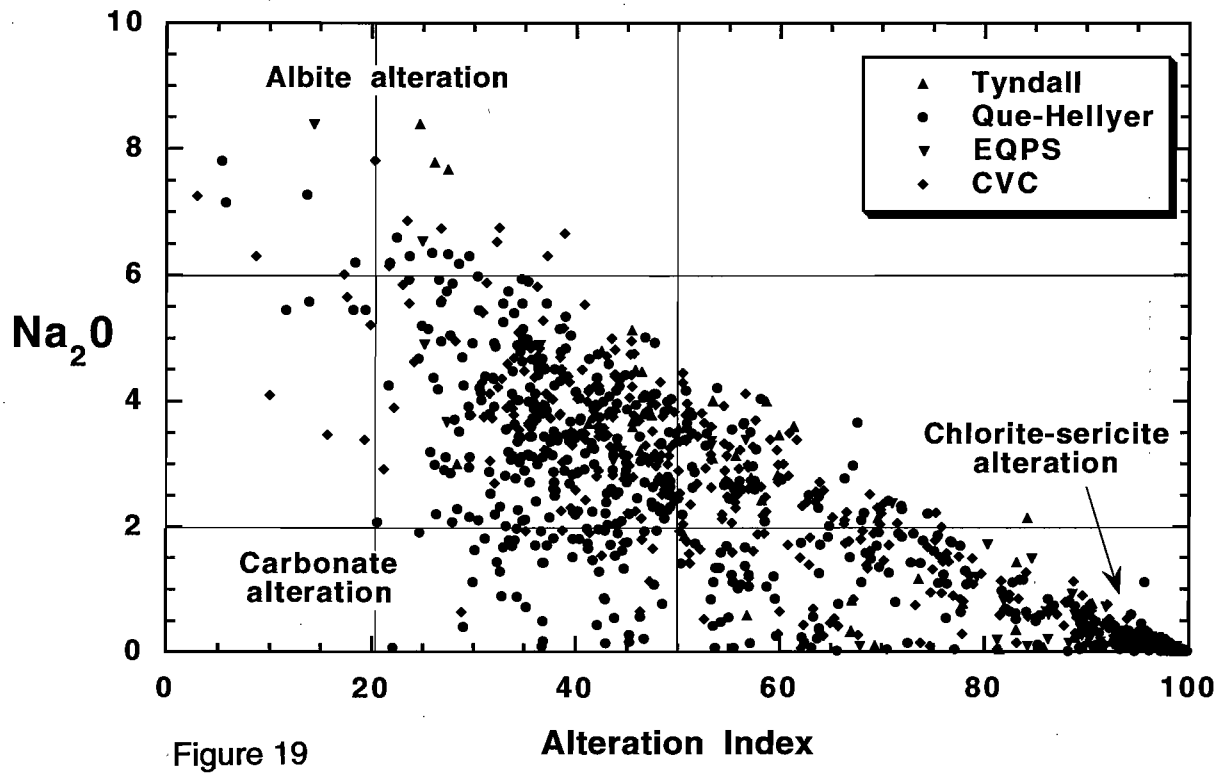

Figure 19

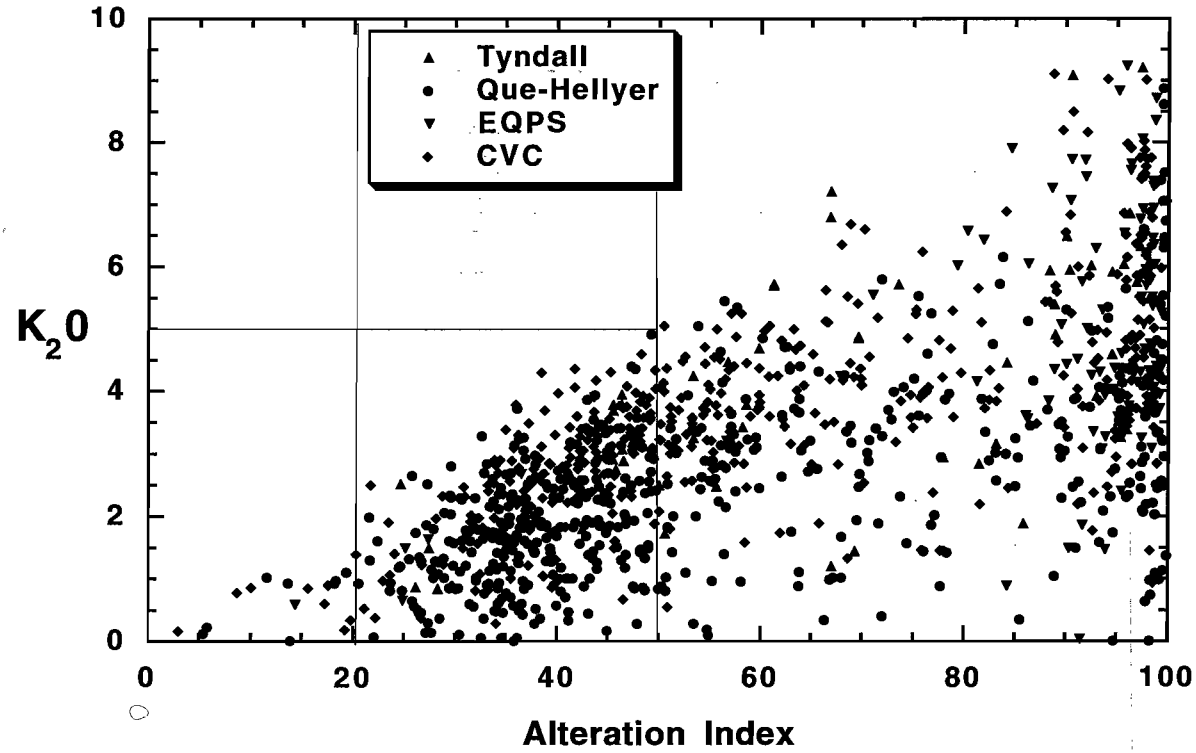

Figure 20

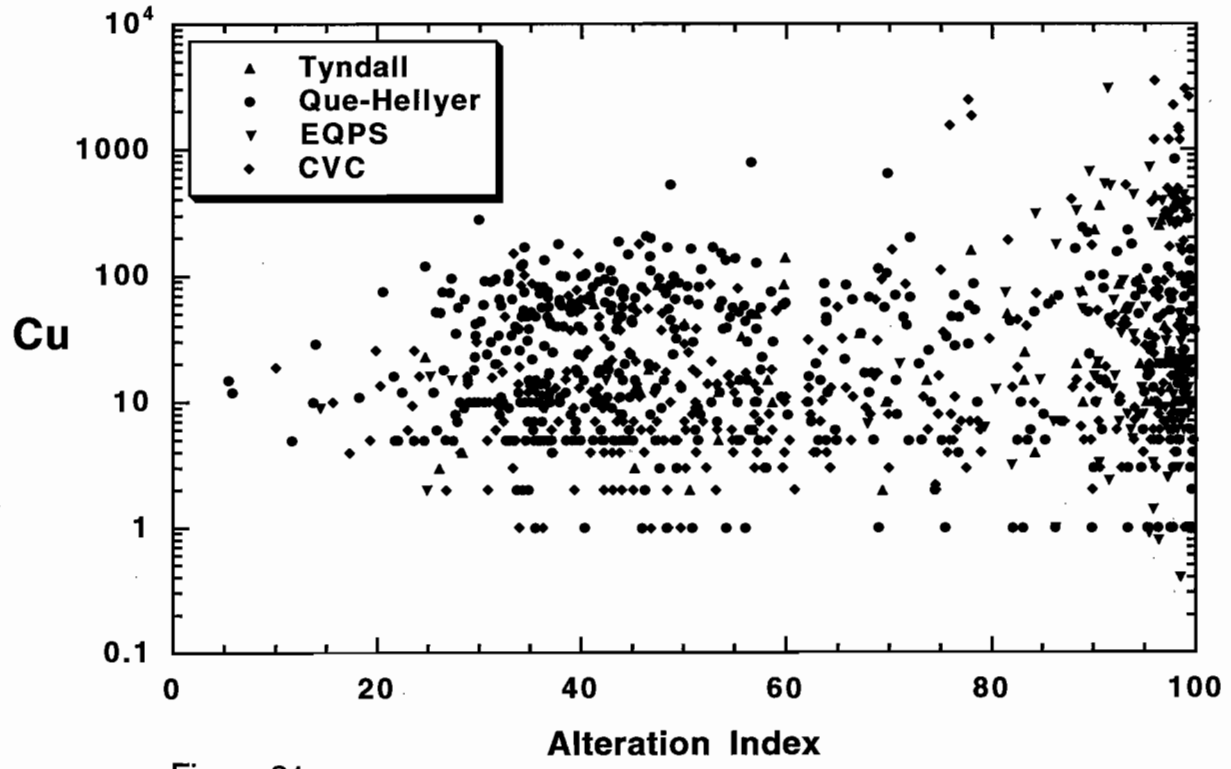

Figure 21

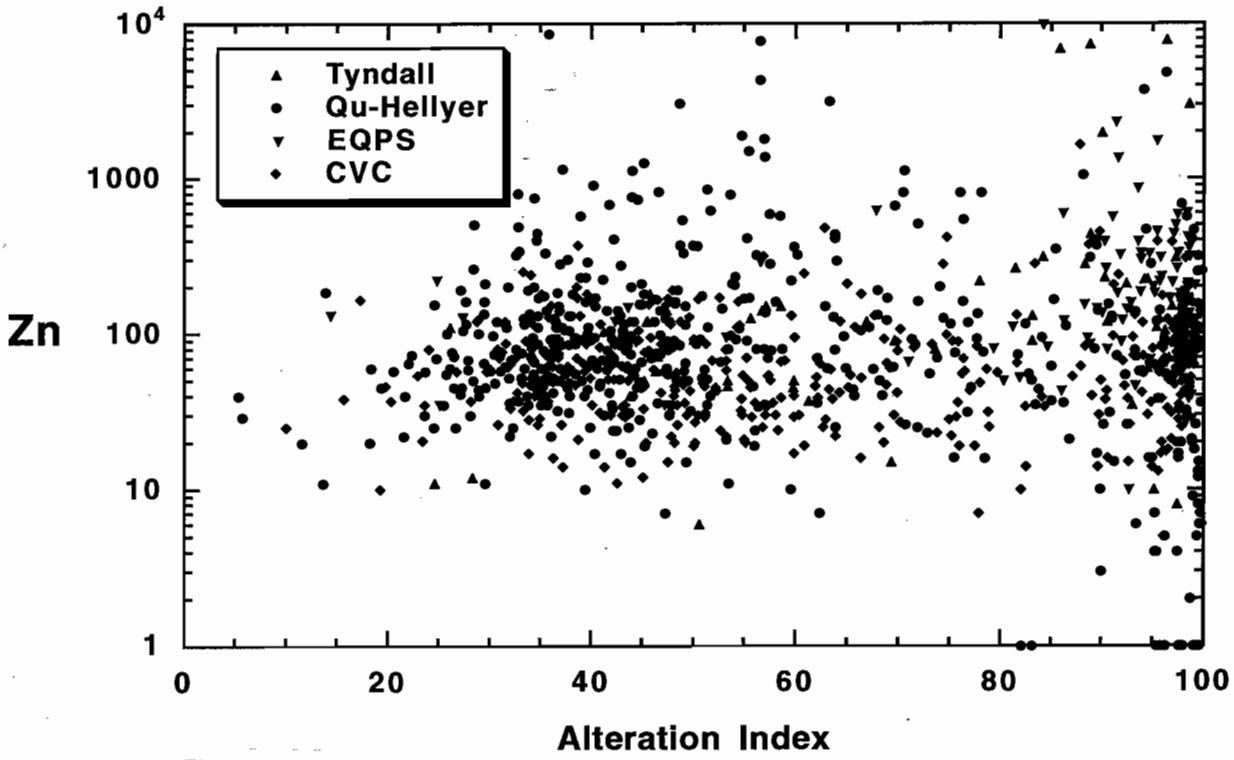

Figure 22

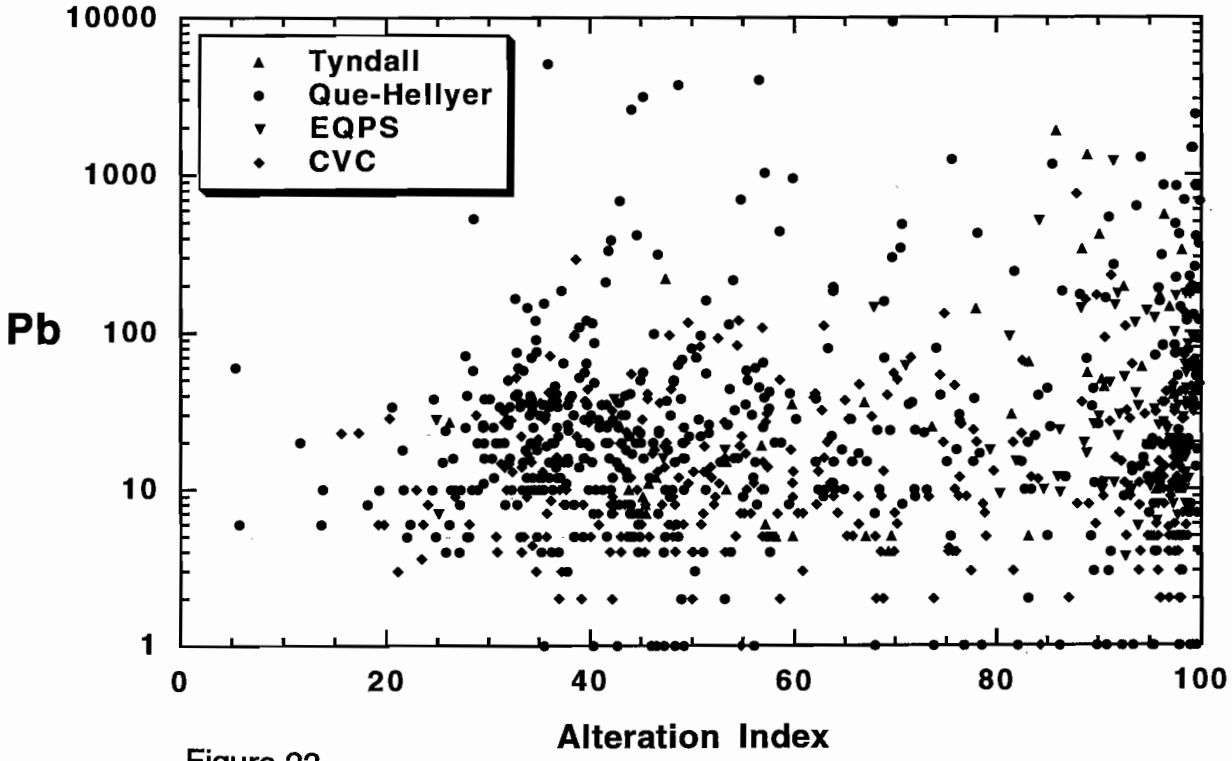
Tyndall
Que-Hellyer
EQPS
CVC
Pb
10000
1000
100
10
1
0
20
40
60
80
100
Alteration Index

Figure 23

Preliminary assessment of MRV geochemical database in terms of possible vectors to ore

Ross R Large, Joe Stolz and Nathan Duhig
Centre for Ore Deposit and Exploration Studies, University of Tasmania

Introduction

This brief report outlines a preliminary assessment of the potential of the recently compiled Mt Read Volcanics (MRV) geochemical database to be used in the development of whole-rock and trace element geochemical vectors to VHMS mineralisation. It needs to be stressed that the database is not yet complete and may contain entry errors and other bugs that are yet to be removed. When completed, the database will include analyses from the regional traverses and ore deposit case studies (Hellyer, Rosebery, Henty) thus enabling a full evaluation of whole-rock and trace element geochemical vectors to ore. This preliminary assessment therefore represents a first pass, which will be further developed as the AMIRA project and data collection progresses.

Approach taken

Only data from the Central Volcanic Complex (CVC; 495 samples) and the Mt Charter Group (Que–Hellyer Volcanics; 1220 samples) have been evaluated in this preliminary study. The data from these groups has been plotted on a series of x–y scatter diagrams, concentrating on the use of the Ishikawa Alteration Index (AI), and evaluating major element trends against this index. Other potentially useful indices (major element ratios), including a chlorite index and Mn–carbonate index, have been devised and compared to the Ishikawa alteration index.

Ishikawa Alteration Index

$$AI = \frac{100(K_2O + MgO)}{(K_2O + MgO + Na_2O + CaO)}$$

This index was defined by Ishikawa et al. (1976) to quantify the intensity of sericite/chlorite alteration that occurs proximal to VHMS deposits. The key reactions measured by the index involve the breakdown of feldspars and its replacement by sericite and chlorite.

(1) $NaAlSi_3O_8 \rightarrow$ albite

$CaAl_2Si_2O_8 \rightarrow$ anorthite

$KAl_3Si_3O_{10}(OH)_4$ sericite

(2) $NaAlSi_3O_8 \rightarrow$ plagioclase

$CaAl_2Si_2O_8$

$(Fe,Mg)_5Si_3Al_2O_{10}(OH)_8$ chlorite

These reactions involve Na_2O, CaO loss and K_2O, MgO, FeO gain. The index varies from values of 20 to 50 for unaltered rocks, and between 50 and 100 for altered rocks, with AI = 100 representing complete replacement of feldspars by chlorite ± sericite. The index has been shown to be particularly useful in defining the intensity of footwall alteration related to VHMS, increasing to maximum values in the footwall alteration pipe below the deposit. An example from the Hellyer deposit (Gemmell & Large, 1992) is shown in Figure 1, where AI is shown to increase from 35 to 95 through the various zones of the footwall alteration pipe, from the outside to the centre.

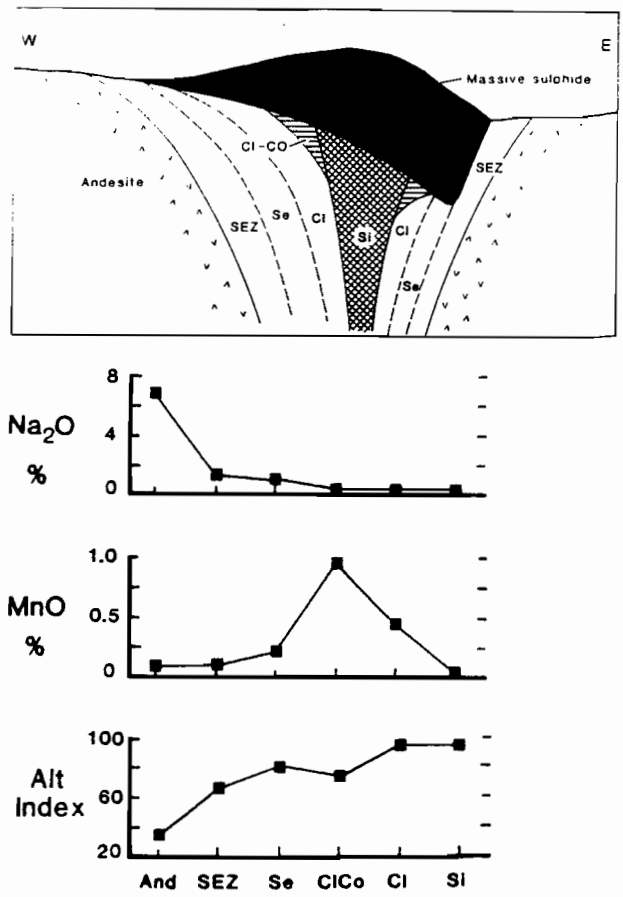

Figure 1: Idealised cross section of the Hellyer VHMS deposit showing the zoned footwall alteration system. Mean values of Na_2O, MnO and Ishikawa AI are shown for the various alteration zones from margin to centre of the pipe. Abbreviations: SEZ = Sericite>quartz, Se = sericite>chlorite>quartz; Cl = chlorite>quartz, ClCo = chlorite>dolomite; Si = quartz/ sericite (from Gemmell & Large, 1992).

In Figure 2, the AI values of the MRV database are plotted against Na_2O for the CVC and Que–Hellyer (H–Q) groupings. The dominating effect of Na_2O loss is shown in this figure, with the highly altered rocks (AI = 80–100) showing values of less than 1.5 wt %.

The majority of the "unaltered" volcanics plot in a roughly circular pattern in the centre of this diagram with AI = 30–60 and Na_2O = 1.5–5.0 wt %. This grouping includes both felsic and mafic volcanics. The unaltered arc volcanics selected by Stolz et al. (this volume) show a similar distribution of AI and Na_2O values.

Although the Ishikawa AI has proved very useful, two key limitations of the index are that (a) it does not distinguish sericite from chlorite alteration, and (b(carbonate alteration results in a decrease in the index. These problems will be addressed in the following discussion.

Patterns of AI for the MRV database

For the purposes of this discussion the combined CVC and Q–H datasets have been divided into three groups based on Na_2O content:

Group 1: $Na_2O < 1.5$ wt % "hydrothermally altered volcanics"

Group 2: Na_2O = 1.5 to 5.0 wt % "unaltered volcanics"

Group 3: $Na_2O > 5.0$ wt % "albitised volcanics"

In this preliminary assessment the exact boundaries (Na_2O values) between the three groups were chosen arbitrarily and may need to be refined when petrographic data is available from the regional traverses. It is likely that some samples within the "unaltered group" are in fact weakly altered.

AI vs Na_2O

Figure 3 shows the AI vs Na_2O plot with samples in the three groups depicted by different symbols. The data is constrained below a line joining the chlorite/ sericite endmember (AI = 100, Na_2O = 0) and the albite endmember (AI = 3, Na_2O = 11.0 wt %)

Note that a significant number of the "altered" volcanics, with $Na_2O < 1.5$ wt %, extend away from the chlorite/sericite endmember toward the dolomite/ankerite endmembers, with AI values varying from 40 to 80. This demonstrates a major weakness in the Ishikawa alteration index, when carbonate alteration is associated with VHMS mineralisation.

AI vs K_2O (Fig. 4)

In this figure the position of FeMg–chlorite, sericite (phengite) and K-feldspar endmembers are plotted on the K_2O axis. This shows that the majority of data

is constrained within the albite–chlorite–sericite triangle, and gives a clear distinction between chlorite-rich samples and sericite-rich samples including an estimate of the sericite/chlorite ratio (provided the samples do not contain K-feldspar). Very few samples plot in the K-feldspar–sericite–albite triangle even though the dataset includes samples from the Jukes Road which contain K-feldspar alteration (Wyman et al., this volume). This anomaly requires further study.

Al vs CaO (Fig. 5)

This figure enables an estimate of the significance of carbonate alteration in the dataset. A weakly ferroan dolomite (Deer, Howie & Zussman, 1966: 474) has been plotted as an endmember, forming a triangular field with albite and chlorite at the other apices. The majority of the data is confined to this triangle. Previous work indicates that carbonate alteration in the MRV includes dolomite, ankerite, siderite, calcite and various Mn-carbonates, indicating that the use of dolomite as an endmember is a gross over-simplification. This will be refined with further microprobe work on regional traverse and case study samples. However, at this stage, the CaO content of altered volcanics ($Na_2O < 1.5$ wt %) can be used as a rough estimate of carbonate alteration (excluding siderite).

Al vs MgO (Fig. 6)

This diagram allows a split between the sericite–chlorite–dolomite–albite endmembers. Altered samples contain up to a maximum of 15 wt % MgO with two groups suggested by the data; (1) MgO variation along the sericite–chlorite join, and (2) MgO variation along the sericite–dolomite join.

Chlorite Index (Fig. 7)

Chlorite alteration is typically developed close to VHMS deposits and it is therefore important to develop geochemical criteria to clearly distinguish samples with elevated chlorite content, within the "altered" dataset. The following index is suggested for this purpose:

$$\text{Chlorite Index} = \frac{100(MgO + FeO)}{(MgO + FeO + Na_2O + K_2O}$$

In the plot of chlorite index against alteration index (Figs 7, 8) the major alteration endmember minerals are clearly separated (chlorite + pyrite, dolomite, calcite, sericite, K-feldspar and albite). Samples containing pyrite, magnetite or haematite will also plot with a high chlorite index, which will cause problems when interpreting mineralised samples. This problem will be addressed in a further report.

Mn–Carbonate index

Manganese-bearing carbonates have previously been reported as an alteration phase in proximity to the Rosebery and Hercules deposits (Dixon, 1980; Khin Zaw & Large, 1992). A case study at Rosebery (Allen et al., this volume) is designed to determine the composition and spatial patterns of Mn around one of the northern ore lenses. In view of the importance of potential Mn halos associated with VHMS deposits, an attempt has been made to develop an Mn–carbonate index to apply to the MRV database. Due to the fact that Mn is commonly hosted by calcium carbonate minerals (dolomite, ankerite, calcite), then it was considered that CaO content should be a key factor in the index. A plot of CaO versus MnO for the MRV dataset compared with the unaltered modern arc volcanic database of Stolz (this volume) is shown in Figure 9. A similar trend of increasing MnO with increasing CaO is shown for both the "unaltered" MRV data and the unaltered modern arcs. Background MnO values in the unaltered volcanics of both datasets are generally below 0.2 wt % MnO. However, the "altered" MRV dataset shows a spread of values up to 1.4 wt % MnO. Based on these observations, and the need to give MnO a heavy weighting in the index, the following is proposed:

$$\text{Mn-carbonate Index} = \frac{100(CaO + 10MnO)}{(CaO + 10MnO + Na_2O + K_2O)}$$

This index is based on the premise that (a) carbonate alteration of plagioclase in the volcanics is accompanied by albite depletion and sericite (± chlorite) enrichment, and (b) Mn is preferentially hosted by carbonate minerals.

Plots of alteration index against Mn–carbonate index are shown in Figures 10 and 11. The background "unaltered" volcanics have a Mn–carbonate index varying from 0 to 95 with the majority of the data in the 0 to 50 range. No distinct pattern is present in the "unaltered" dataset. However, the "altered" (Na_2O < 1.5 wt %) dataset shows two clear trends across the diagram; firstly a group of data at high alteration index values (AI > 85) which trends between the sericite–Mn–chlorite join; and secondly, a group of data varying from AI = 100–30 which trends across the diagram between the sericite and Mn–dolomite join. The albitised volcanics show lower Mn–carbonate index values than the "altered" and "unaltered" groups.

Further studies will need to be undertaken to determine how the Mn–carbonate group and Mn–chlorite group relate to proximity to mineralisation in the regional or local sense.

Zinc content of altered samples

A plot of zinc content versus alteration index is shown for the three groups of samples; unaltered, altered and albitised in Figure 12. Surprisingly, there is no correlation between alteration index and zinc. The majority of the "unaltered" volcanics fall in the range 10–200 ppm Zn, however, many of the samples with AI = 30–60 show elevated zinc content from 200 to 10,000 ppm. In contrast, the "altered" volcanics show a spread from abnormally(?) low values 1–10 ppm, probably representing leached samples, through the normal background (10–200 ppm) to include some high values, although less than expected. The albite altered rocks generally show background Zn levels.

Conclusions

Preliminary assessment of the MRV geochemical database allows a division of the CVC and Que–Hellyer volcanics into three groups based on Na_2O content; "altered" (Na_2O < 1.5 wt %), "unaltered" (Na_2O = 1.5–5.0 wt %), and "albitised" (Na_2O > 5.0 wt%). Using these three groups, and the Ishikawa alteration index, it is possible to plot a series of diagrams to show the relationship between the major alteration mineral endmembers (sericite, chlorite, K-feldspar, dolomite and albite) and the alteration index variation. Two new indices have been developed and tested on the database; a chlorite index and a Mn–carbonate index. The latter index shows potential for use as a vector to VHMS mineralisation, however, considerable more work is required to evaluate, refine and test the index. By combining the three indices in various graphs, it is possible to obtain a rapid visual estimate of the spread of alteration mineral assemblages in the MRV database.

References

Date, J., Watanabe, Y. & Saeki, Y., 1983: Zonal alteration around the Fukazawa Kuroko Deposits, Akita Prefecture, Northern Japan. *Economic Geology, Monograph* 5: 365–386.

Deer, W.A., Howie, R.A. & Zussman, J., 1966: *AN INTRODUCTION TO THE ROCK FORMING MINERALS*. Longmans, London: 529 pp.

Dixon, G.H., 1980: Geological, geochemical and stable isotope studies of the carbonates at Rosebery. Unpubl. Honours thesis, University of Tasmania: 173 pp.

Ishikawa, Y., Sawaguchi, T., Iwaya, S & Horiachi, M., 1976: Delineation of prospecting targets for Kuroko deposits based on modes of volcanism of underlying dacite and alteration halos. *Mining Geology* 26: 105–117 (in Japanese with English abstract)

Gemmell, J.B. & Large, R.R., 1992: Stringer system and alteration zones underlying the Hellyer volcanogenic massive sulphide deposit, Tasmania. *Economic Geology* 87: 620–649.

Khin Zaw & Large, R.R., 1992: The precious metal-rich south Hercules mineralisation, western Tasmania: a possible subsea-floor replacement VHMS. *Economic Geology* 89: 931–952.

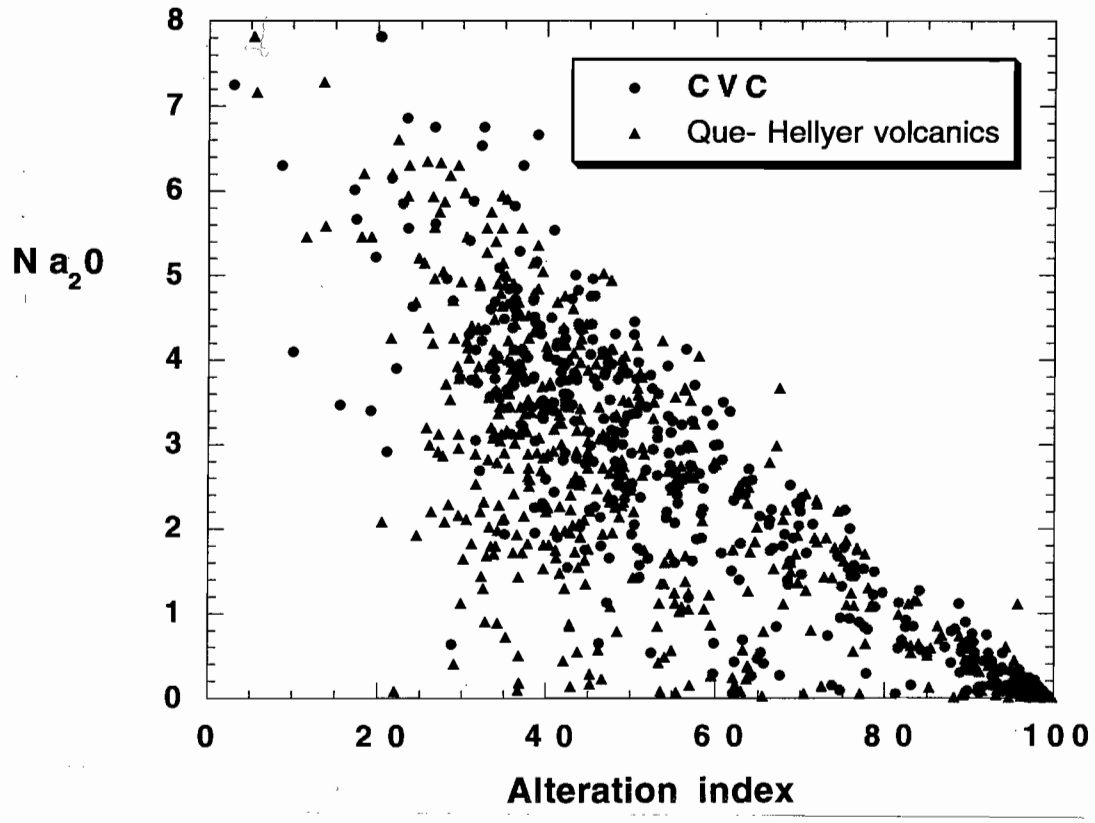

Figure 2: Alteration index versus Na_2O for the MRV dataset; CVC and Que–Hellyer samples only. Note that the background, unaltered volcanics concentrate between AI = 30 to 60 and Na_2O = 1.5 to 5.0 wt %.

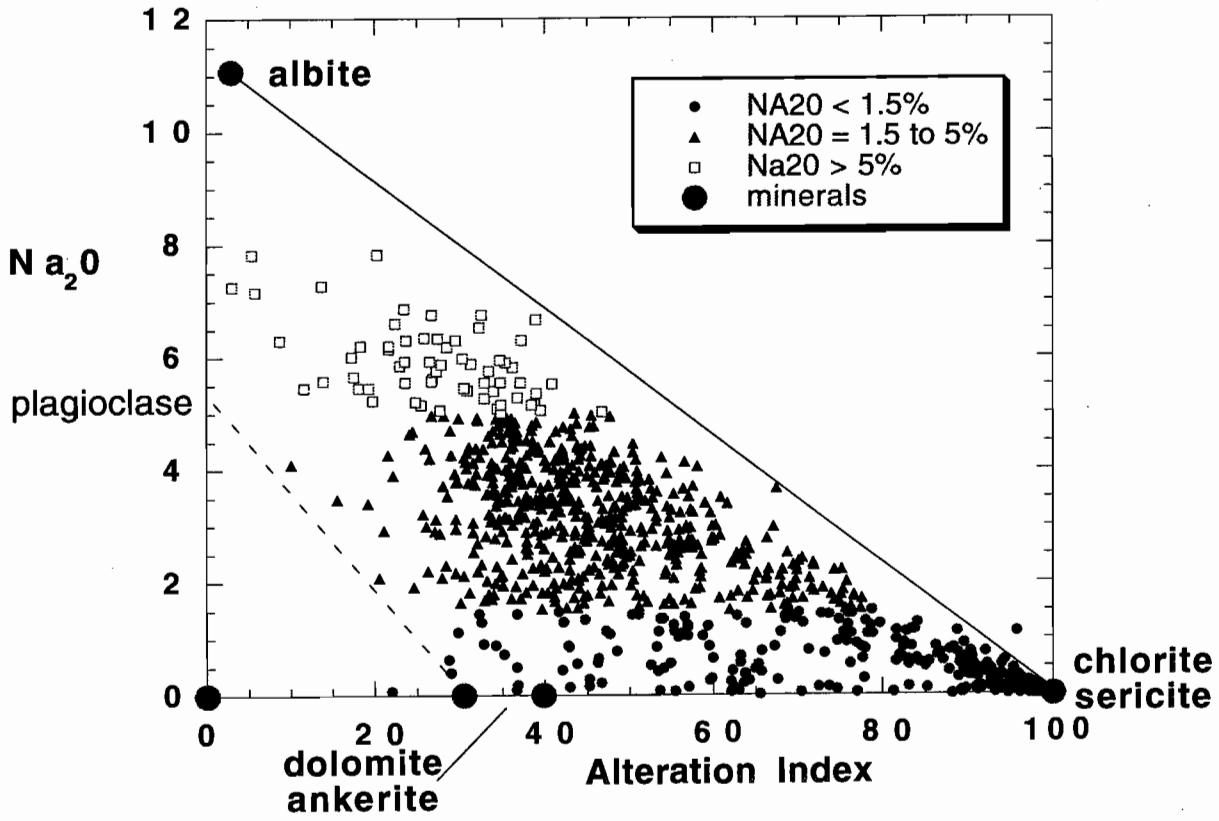

Figure 3: MRV dataset (CVC and Que–Hellyer Volcanics) divided into three groups based on Na_2O content. Chlorite and sericite alteration of albite drives the data to the bottom right hand corner of the diagram.

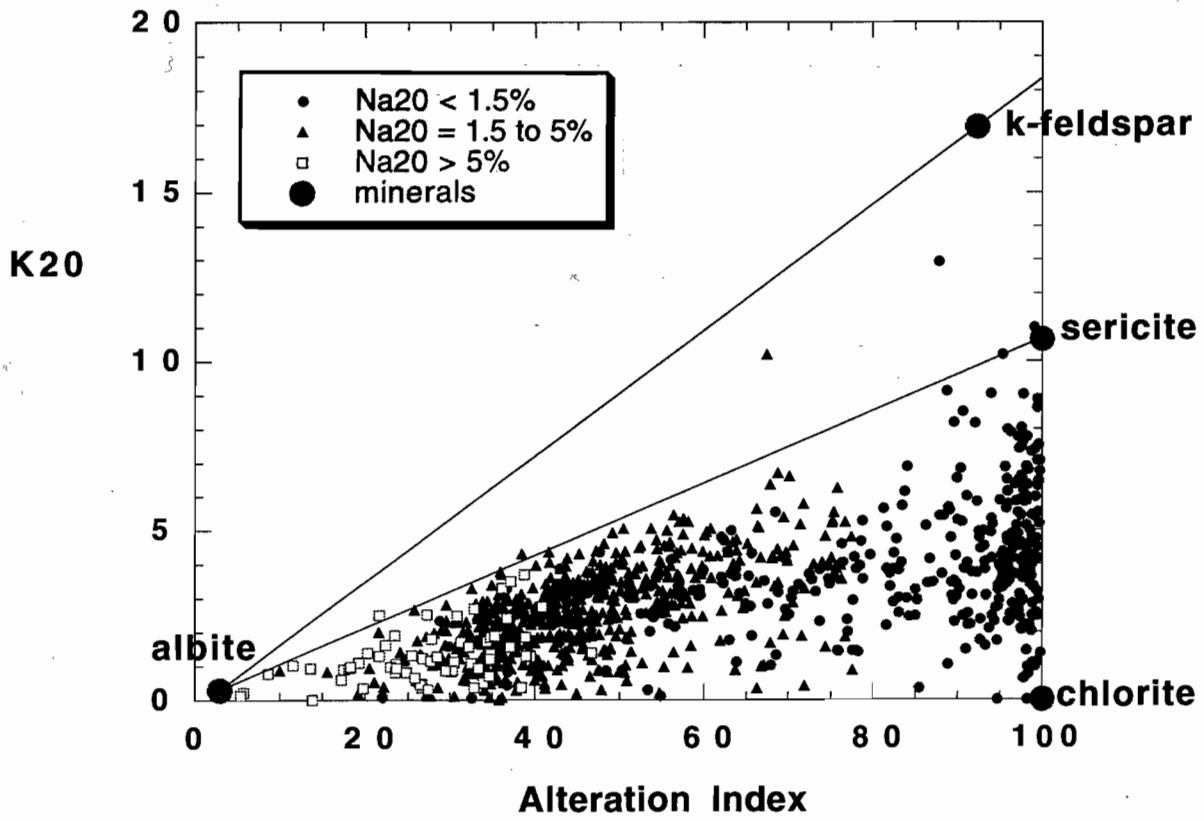

Figure 4: Alteration index versus K_2O. Most of the "altered" volcanics form a group between the chlorite and sericite endmembers.

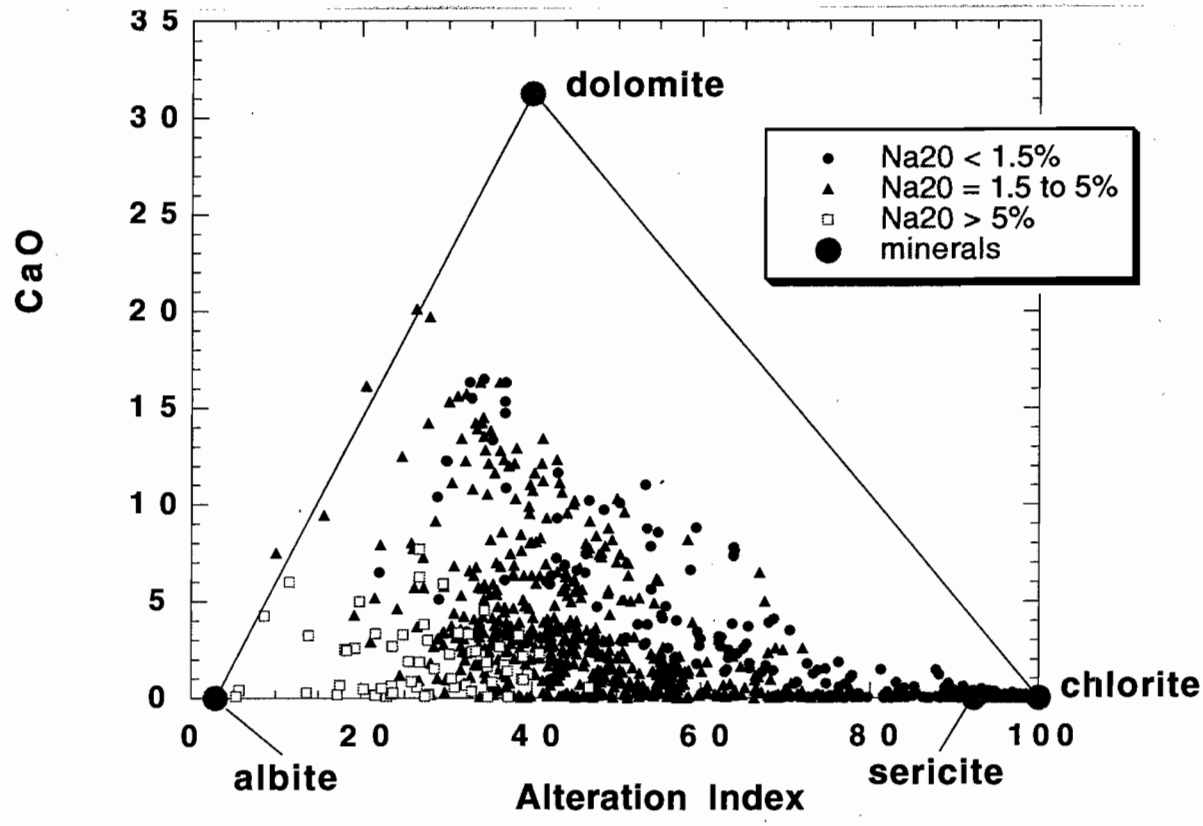

Figure 5: Alteration index versus CaO. This plot allows the carbonate altered samples to be identified as those approaching the dolomite apex.

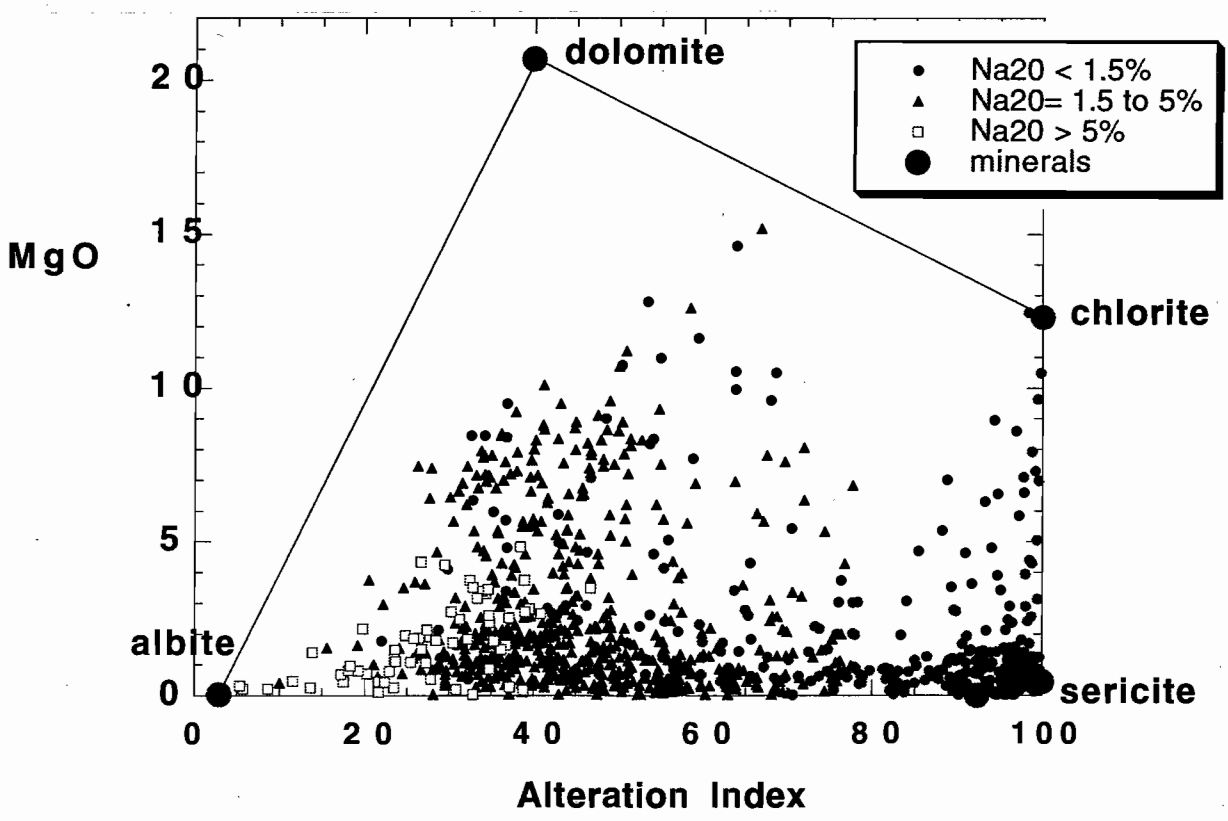

Figure 6: Alteration index versus MgO. This plot enables samples to be interpreted in terms of sericite, chlorite, dolomite and albite endmembers.

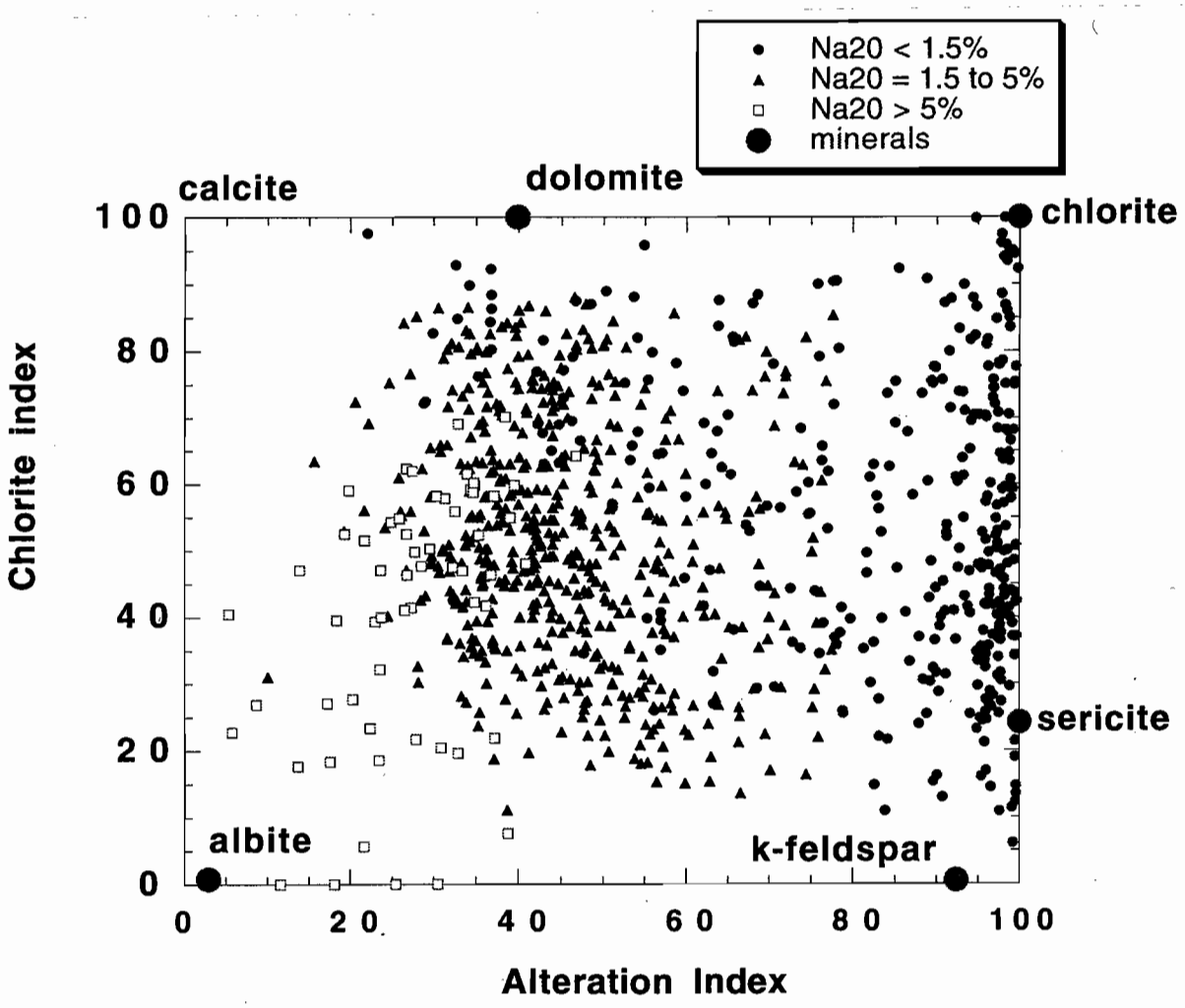

Figure 7: The chlorite index is defined as:

$$\text{Chlorite Index} = \frac{100(FeO + MgO)}{(FeO + MgO + Na_2O + K_2O)}$$

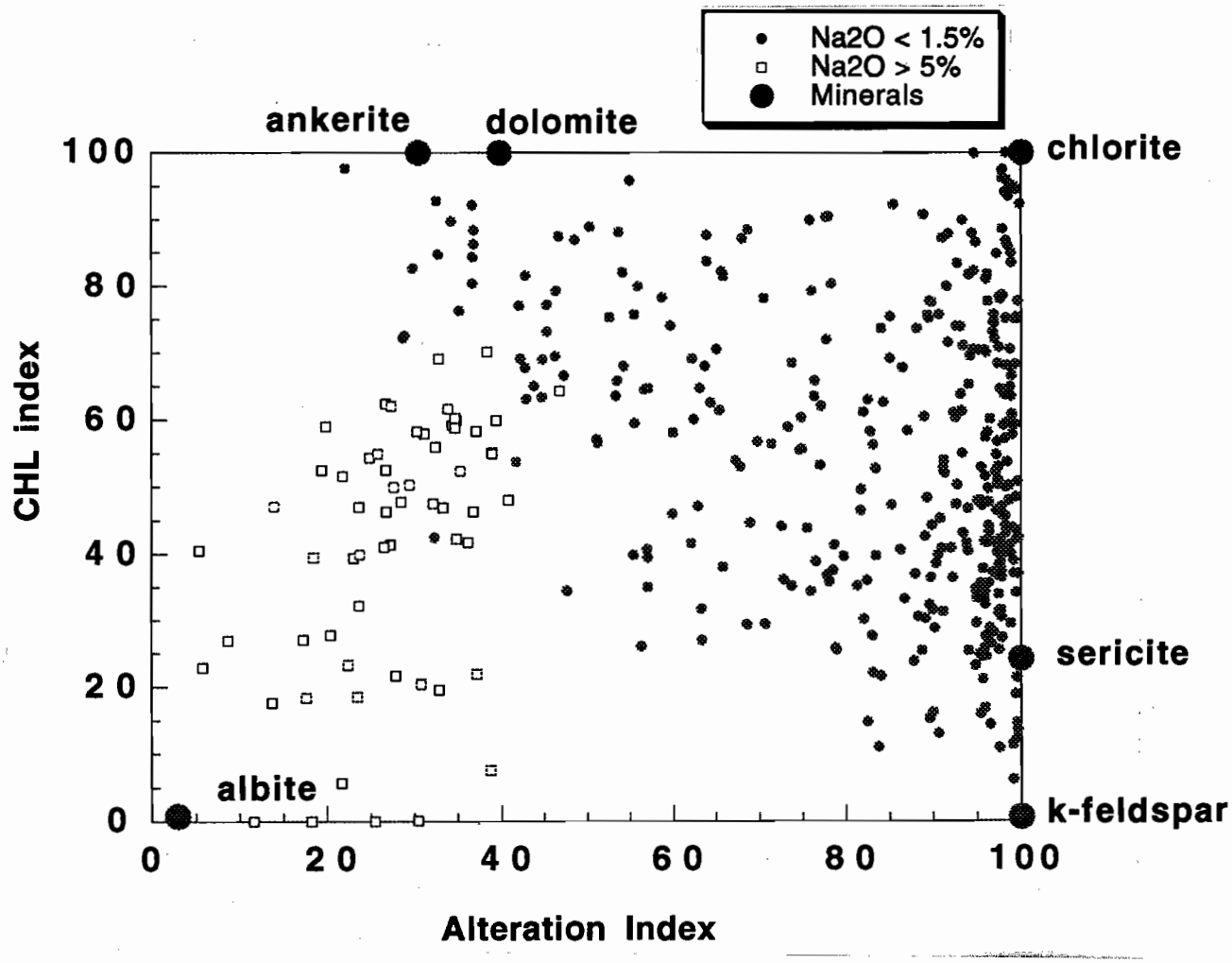

Figure 8: Chlorite index versus alteration index for the "altered" volcanics (Na_2O < 1.5 wt %) and the albitised volcanics (Na_2O > 5.0 wt %). Most of the "altered" samples plot within the carbonate–chlorite–sericite triangle.

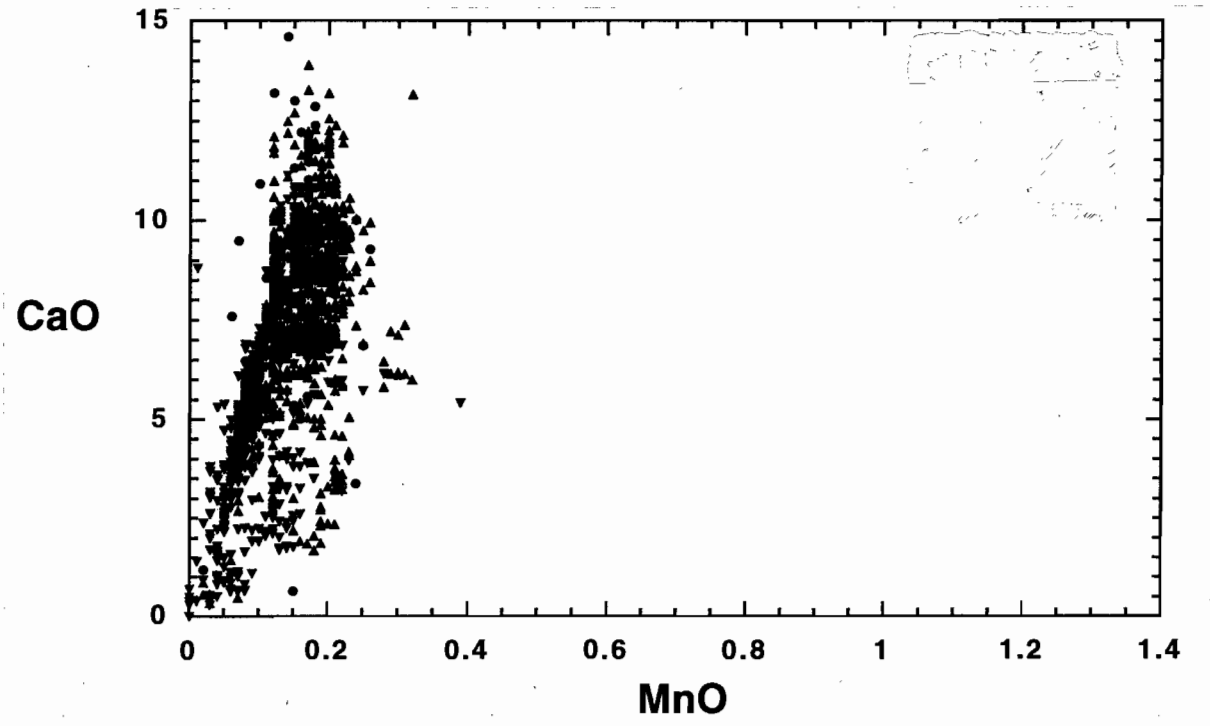

Figure 9a: CaO versus MnO for modern unaltered arc volcanics (Stolz, this volume).

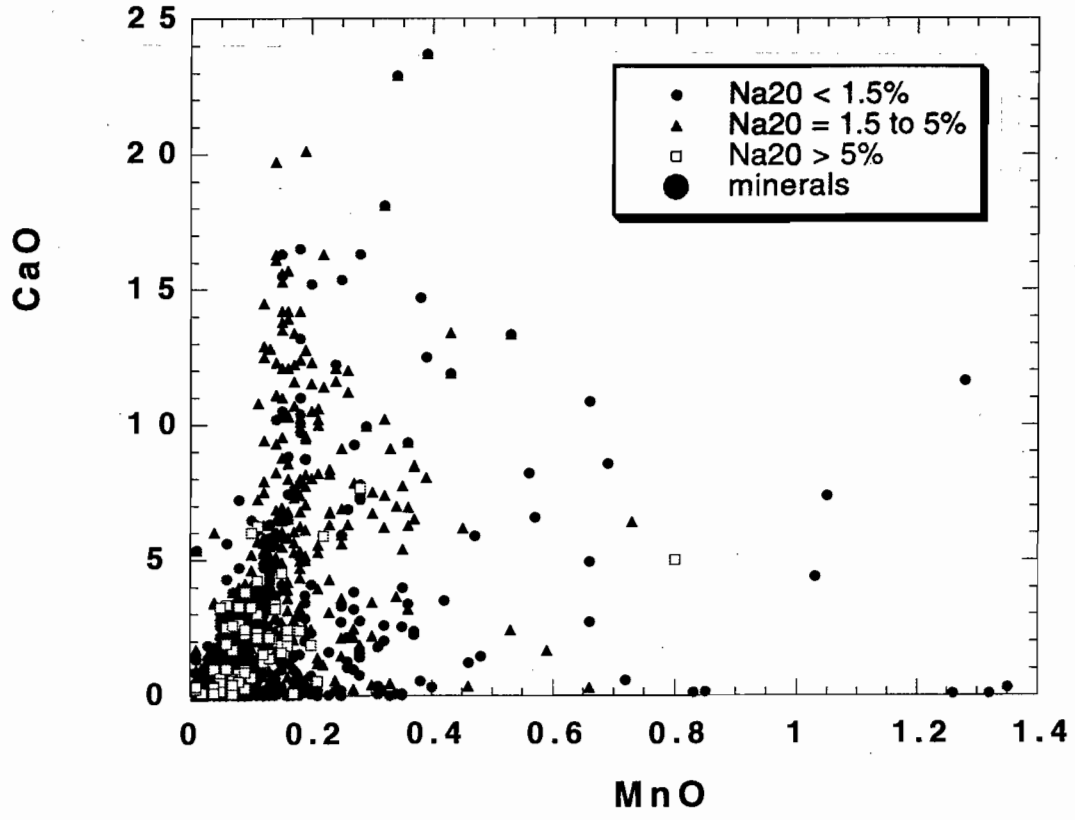

Figure 9b: CaO versus MnO for the MRV database, showing a spread to anomalous MnO values of 0.2 to 1.4 wt % MnO.

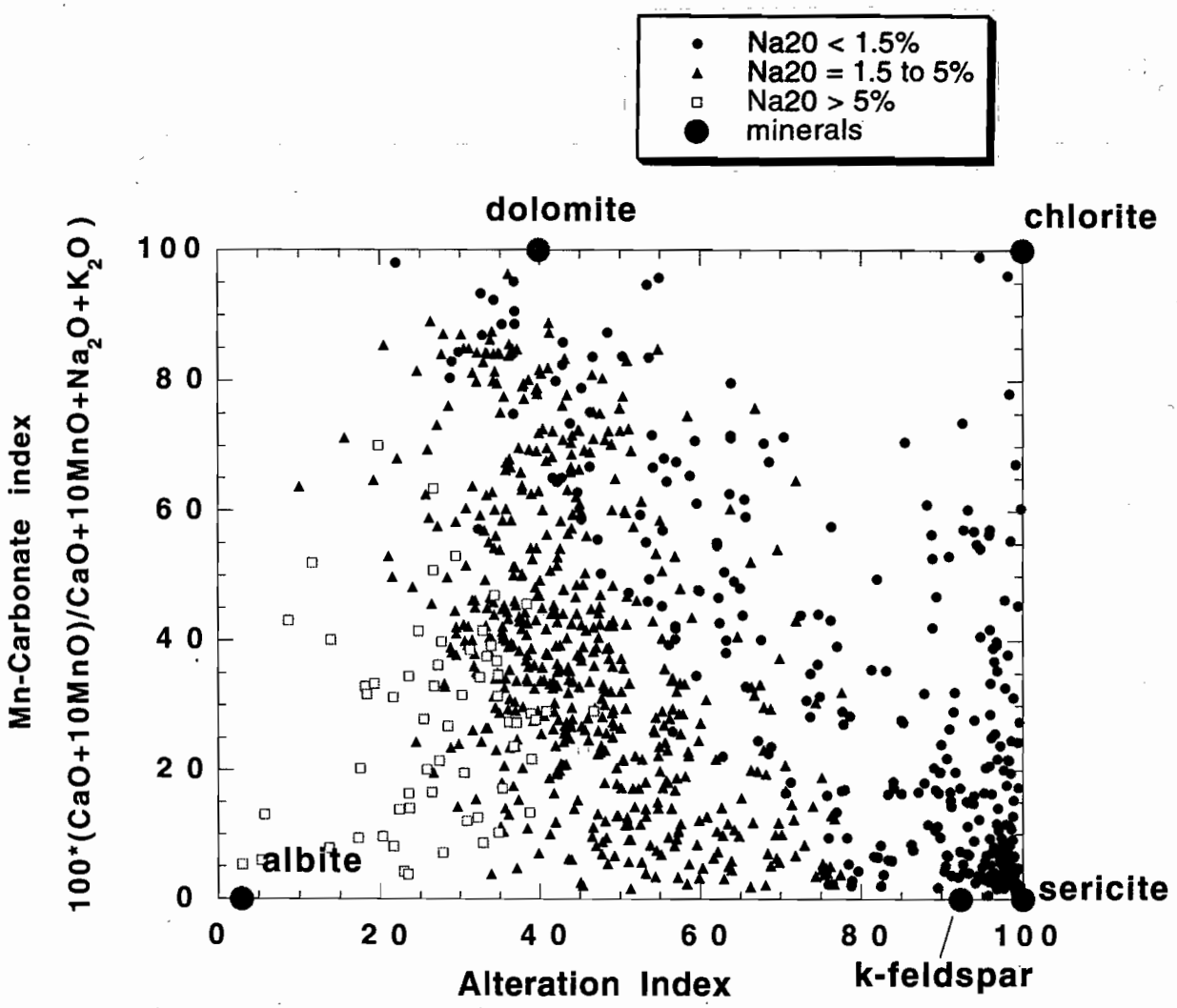

Figure 10: Mn–carbonate index versus alteration index for the complete dataset.

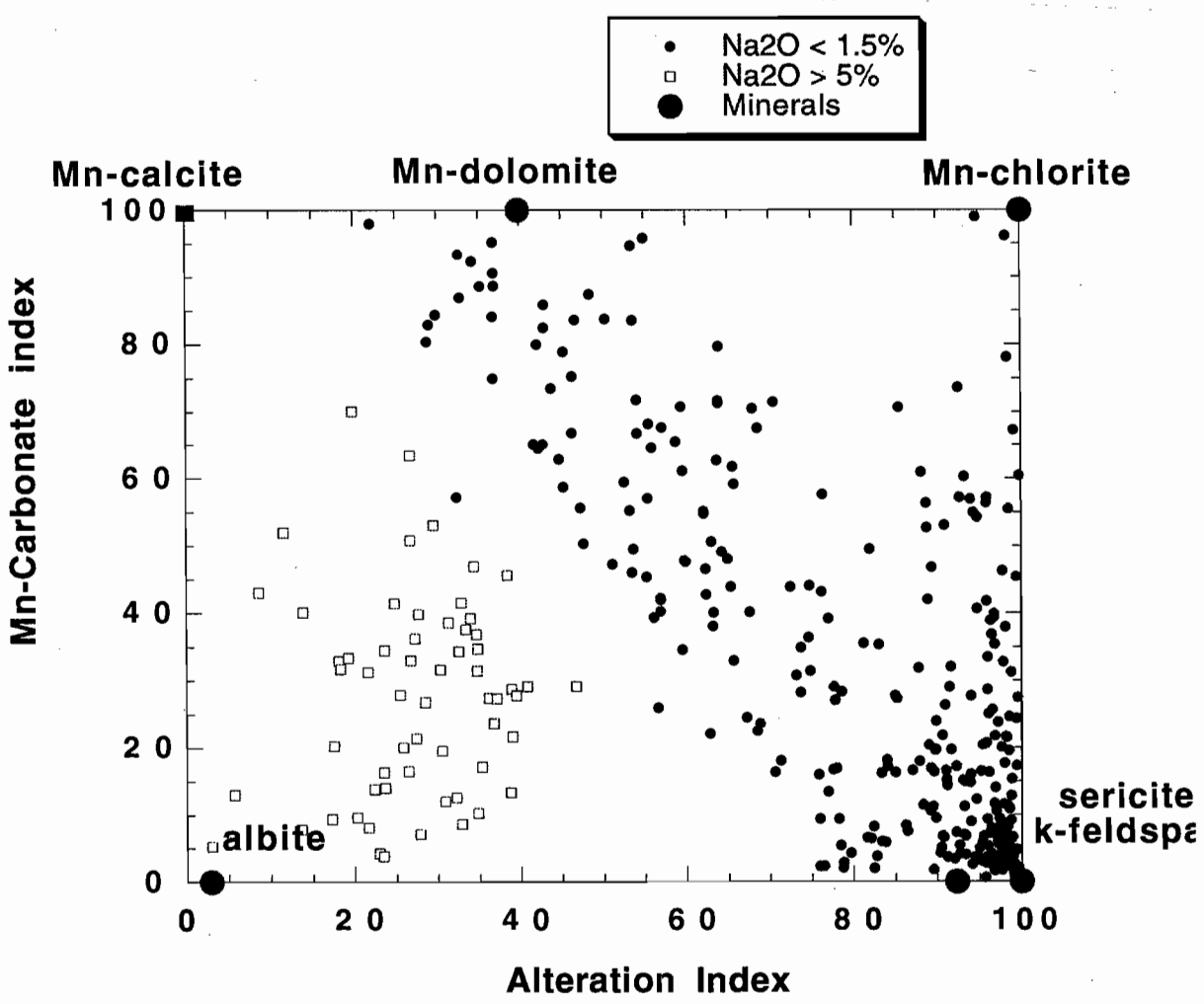

Figure 11: Mn–carbonate index versus alteration index for the altered volcanics and albitised volcanics. The trends of Mn enrichment in chlorite and Mn enrichment in dolomite are clearly shown on the plot.

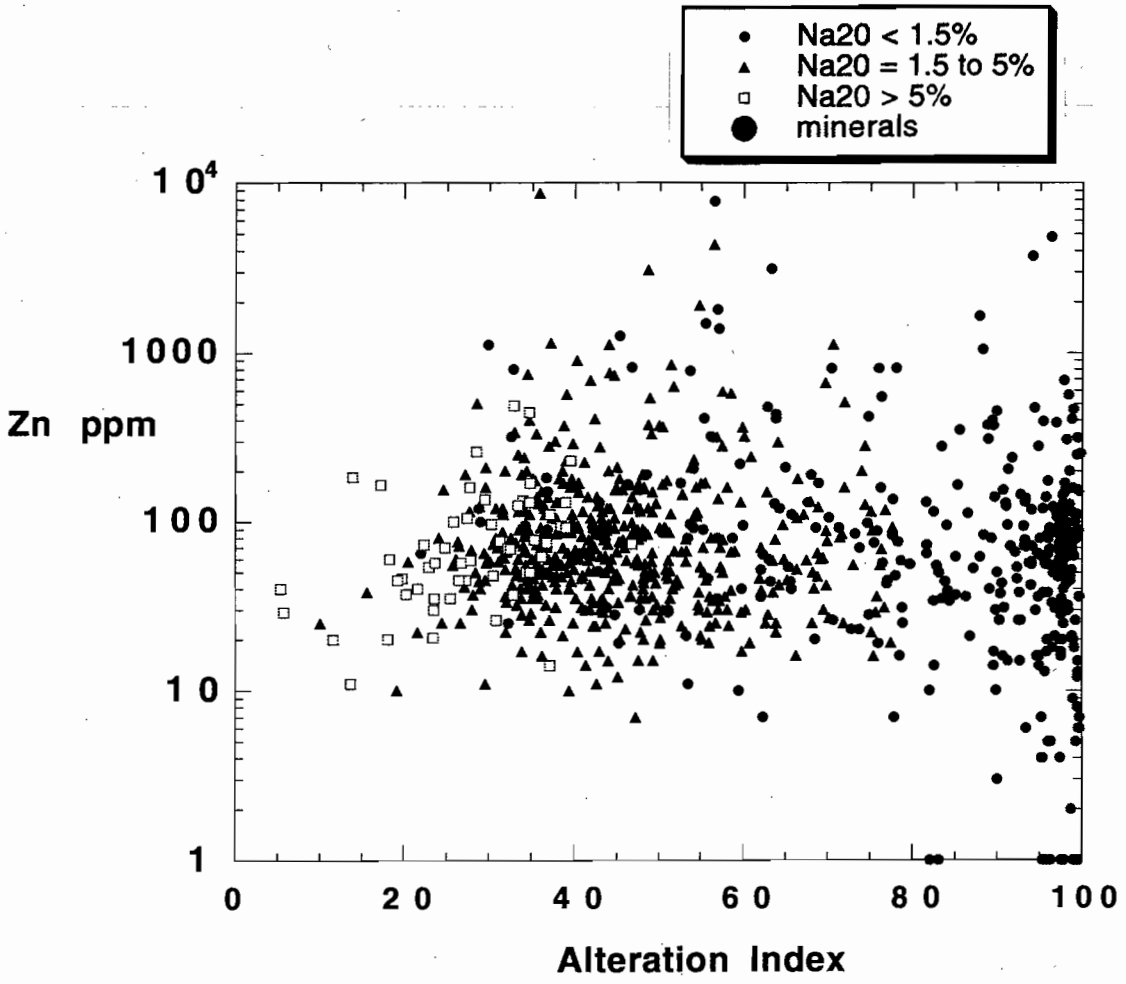

Figure 12: Alteration index versus zinc for the three groups of MRV data. The background zinc content varies 10 to 200 ppm. However, samples with anomalous zinc (200 – 10,000 ppm) occur in both the "unaltered" and the "altered" groups.